UNIVERZITA KARLOVA V PRAZE

Matematicko-fyzikální fakulta

Non-equilibrium complex systems

Habilitační práce
ve smyslu §72 odst. 3 b) zákona 111/1998 Sb., v platném znění

Autor: *František Slanina*

Fyzikální ústav AVČR, v.v.i.
Na Slovance 2, 18221 Praha

2013

Contents

Preface

Už je to tady - už je to tady,
jsem jako drak!
Nechytit se rychle stolu
ulétnu do oblak!

Jan Haubert

This habilitation thesis is the commented collection of 14 of my papers published in the period from 1998 to 2012. Ten of them are authored only by myself, the rest was created in collaboration with various co-authors. Where considered appropriate, I mention specifically the part of the joint work I am responsible for.

The common denominator of all the presented works is the concept of complexity, in its various manifestations. Although not new, the word *complexity* continues to carry a sensational flavour, at least for general audience. This atmosphere helps selling the results and getting funds for continued research but simultaneously burdens the researcher by false expectations and mass media confusions. Nonetheless, I consider the science of complexity one of most topical fields of science now. Let me briefly sketch its general relevance by mentioning its roots and ramifications.

Very often the discussions on complexity begin and eventually end at the definition of the very notion of "complexity". There are good reasons to avoid these terminological battles as they rarely produce any progress in understanding real phenomena. Yet I wish to mention at least one formulation, due to Giorgio Parisi [1]: "A system is complex if its behaviour crucially depends on the details of the system."

Indeed, the way in which various theories treat the details of the system in question may be their distinctive feature. After the 17th century breakthroughs the analytical mechanics assumed its more or less definitive form a century later. At that time it was constantly repeated that having infinite (God-like) intellectual capacities implies predicting, with infinite accuracy, the behaviour of the Universe to its tiniest parts. The epistemological optimism of the era of Enlightenment took it for granted that we can approach that ideal infinitely, much like an infinite series approaches its limit.

However, the realm of Infinity showed to be much less domesticated than the 18th century scientific giants ever thought. Bolzano, Cantor, Russel and their followers released the dragons of the mathematic set theory, which the general public is perhaps less prepared to assimilate than the wonders of the general relativity. The stories of J. L. Borges (El Aleph, Funes el memorioso, etc.) try to get feeling of the abyss: "The Aleph's diameter was probably little more than an inch, but all space was there, actual and undiminished. (...) I saw the Aleph from every point and angle, and in

the Aleph I saw the earth and in the earth the Aleph and in the Aleph the earth; I saw my own face and my own bowels; I saw your face; and I felt dizzy and wept, for my eyes had seen that secret and conjectured object whose name is common to all men but which no man has looked upon – the unimaginable universe. I felt infinite wonder, infinite pity." The foundations of the optimistic world-view were irreparably shattered, but the shock was yet to be felt within physics.

Indeed, a classic says: "more is different" [2], and dealing with infinity of particles or infinity of time or infinite requirements as to precision represents a qualitative jump with respect to the physics of small assemblies of bodies the classical mechanics was initially designed for. Even worse, all everyday objects we have to live with (including our bodies) are composed of very large number of particles; and "very large" may be much more difficult than "infinite" as it implies we must investigate not only the infinity itself but infinity of ways the infinity is reached. That is the thermodynamic limit, if taken properly. Let us look at some of the beasts infinity set free, to make the life of a scientist more adventurous.

The gradualist idea of completing the picture of the world by adding the details of the system one by one, as Euler did with his perturbation treatment of the Solar system, was burned instantly by the first rays of rising deterministic chaos in the works of H. Poincaré. If anything could be called a paradigm shift after the Galileo's relativity principle, surely it is the idea of deterministic chaos. From now on all minuscule details in the initial conditions were equally important, every indiscernible perturbation equally disastrous. Any effort to approach the truth about trajectories by pouring more precision into the formula is nothing more than a child's occupation: pouring the water out of the Ocean with a shell in hand.

Now, how do we renounce the precise predictions of bodies' movements and retain scientific rigour of our discourse? The answer lies in the use of the language of chance. Indeed, we cannot predict the location of a tagged molecule in a gas container, but still we can predict at which temperature the gas starts condensing, within a prescribed expectancy range. We made virtue out of necessity, introducing probabilistic approaches of statistical mechanics. Treating the physical systems as ensembles of particles' collections, differing by small details, we loose the possibility to predict the detailed evolution of each member of the ensemble, but gain the insight into the generic features of the system behaviour. Indeed, it would be foolish to attribute the same relevance to the question about the position of a single molecule and the question whether the system is liquid or solid. Too much knowledge obscures understanding; therefore the gains from the statistical approach were much larger than the apparent losses.

Statistical mechanics was indeed extremely successful branch of physics since its establishment by Maxwell, Boltzmann and Gibbs at the end of the 19th century. Once again, it seemed that a machinery to predict every substance's phase diagram is at hand. Such prediction, however, showed completely illusory when the attention turned to living beings.

New experimental techniques and advances in handling extremely large amounts of data made it possible to investigate in detail the tiny building blocks of life: proteins, nucleic acids, cytoskeletons etc. As every single protein molecule is significant for the cell structure, there may not be statistical mechanics of cell proteins. Every single detail of the protein makeup and placement makes huge difference. We are facing similar difficulty as with the deterministic chaos: any minuscule change in the Hamiltonian of a given system results in tremendous consequences. Adding a single extra particle into an information molecule changes the message completely. Here we come to a situation which is typical to what is commonly called *complexity*.

Yet it is not something new nor unexpected. Adding a single neutron to an atomic nucleus makes a big difference in the spectrum of nuclear energy levels. To calculate precisely the energy levels of an iron nucleus starting from the Standard model of particle physics is a daunting task. But even if someone succeeds, using the biggest supercomputers, and lists a very long collection of numbers, what could we learn from that result? Does it bear any significance that the 154th level assumes this or that value? Stated differently, we could possess an answer but still lack the question.

The science of complexity provides a clue: while we do not underestimate the detailed and precise treatment of a system, with all details included, we look for generic features of our systems, using again the language of probability. Thus, the study of complexity does not yield predictions about the outcome of each realisation of the complex system, but shows, which features are to be expected, decides, what is common to all proteins and what is a specific feature of the one we are studying just now.

For example, complexity studies may tell us, what is the generic distribution of level spacings within any nucleus, be it vanadium or nickel, while precise placement of the levels may remain unknown. The science of complexity may reveal, how long a protein must be, in order to be useful as an enzyme, but specific function of a specific protein still needs to be determined. The "conventional" physics should go hand in hand with physics of complexity. The former calculating conductivity or infrared spectra of a substance, the latter saying what is trivial, what is typical and what is surprising. The former providing useful knowledge, the latter understanding.

While perceived as something (relatively) new, complexity science relies on many quite old achievements, assembling them into a systematic framework. Therefore, I do not think complexity marks any kind of revolution in physics; rather, it is like a growing plant, which suddenly develops a blossom. It might be stunning for a visitor, but not for a gardener who has watched day after day the preparations.

Still I do believe there is an immense resource of good, hard and exciting problems in the realm of the complex. As a teacher, I am trying my best to bring the students' attention to it. An example: who would not like to understand life? Studying *artificial life* is one of the promising tracks. But where to go, if neither the direction nor the thing itself is known? The word "life" seems to make so much confusion that its meaning draws to naught. "Go there, I do not know where, find that, I do not know what." This is the typical situation a complexity scientist faces: the question itself is to be established in the course of the research. But, quoting again Parisi [1]: "I am convinced that in the next century a much more deep understanding of life will come from this approach." I invite you to share his optimism. A. M. D. G.

Prague, October 2013 *František Slanina*

Chapter 1

Commentary

1.1 Introduction: Non-equilibrium and complexity

There is a broad variety of complex systems studied in physics in the last couple of decades. Second order phase transitions belong perhaps to the oldest ones. Still today, the *critical phenomena* related to second order transitions are textbook examples of a complex behaviour. Opening a textbook again, we find the classical phase diagram of water, with the line of liquid/vapour equilibrium ending in a mysterious point. Measuring optical properties close to it we discover critical opalescence, one of the handful of phenomena which lead Einstein to his breakthroughs.

Now, what is complex about the critical opalescence? To make it short, it is the absence of a typical length scale. There are always some thermal fluctuations around (provided atoms of finite size exist, which is what Einstein showed). The characteristic size of the fluctuations is measured by the correlation length ξ. Close to the critical point the correlation length diverges as a (negative) power of the distance from the critical point. The power is a special function with respect to the change of the units of measurement: if we change the scale, the functional form does not change. The opposite is also true: if a function is scale-invariant, it must be a power.

Important thing about the critical point is that not only the correlation length diverges as a power, but also the correlation function itself behaves as a power, and many other quantities, including thermal capacity and susceptibility, have power-law singularities. This fact marks an important observation: at the critical point the system is scale-free, i.e. it is invariant with respect to change of the units of measurement.

Concentrating on a single typical scale of length, time, or energy is a widespread approach in physics. We neglect gravity when dealing with semiconductors and we forget quarks in civil engineering. There is a deep reason for it: nature does separate phenomena in different energy bins and we rarely need to jump from one bin to another. Things are changing, however, in recent years, with systematic use of multiple-scale modelling. For example, somebody may use ab-initio quantum-mechanical calculations for atoms adsorbed on a surface and pass the resulting energy barriers to somebody else, who makes Monte Carlo simulations of diffusion of many such atoms. Or, in a unified study of crack propagation the microscopic core of the crack is treated quantum-mechanically, the surrounding cluster by molecular dynamics and the rest of the body by conventional elasticity theory.

These powerful methods mark a significant progress, but still they are rather like conglomerates of heterogeneous approaches glued together by ingeniously designed interfaces. Going back

to critical phenomena, we face a more serious problem of being able to cover all length scales by unique approach. To be sure, we cannot investigate all features of the system at once; reductionist paradigm is still in force, but it is applied along different axis. We do not proceed from a "fundamental scale" microscopic level and build our theories upon them. This would be a bottom-up advance, selecting a smaller scale as more basic and larger scales as derived ones. Instead, we should select "fundamental fluctuations", spanning all length scales. All other fluctuations are projected out or taken into account as corrections. The problem with this approach is, that there is no a priori criterion as to what are the fundamental fluctuations, while the fundamental scale is obvious: the smaller, the more basic it is, at least according to the reductionist orthodoxy.

To overcome this problem, *renormalisation group* theory [3, 4] was developed since early 1970s. The RG machinery selects automatically the proper fluctuations which contribute to the critical behaviour. The RG operation defines a flow in the space of Hamiltonians and the investigation of critical behaviour is reduced to the study of the properties of the fixed points of the flow. The first reduction comes from the linearisation of the flow around fixed points. This screens out fluctuations which are relevant only far off the critical point. Moreover, unstable and stable directions define relevant and irrelevant parameters in the Hamiltonian. This way, the flow is effectively reduced to a few-dimensional problem.

As there are many more irrelevant than relevant parameters, many systems with different Hamiltonians must share the same flow diagram. This fact implies natural grouping of physical systems into *universality classes* characterised by unique values of critical exponents. People are dreaming about full classification of all possible universality classes; however, a major breakthrough would be indispensable to achieve that, and besides the two-dimensional case, where the conformal field theory provides nearly full information, it is beyond the capacities of current theoretical tools. I used the renormalisation-group techniques once, when investigating the effect of impurities on a growing surface [5].

It became a common wisdom to attribute scale-free properties to fractals and vice versa. Algorithmic creation of fractals via recursive formulae is a straightforward tool. It is doubtful, though, that nature uses the same tools in making so abundant fractals around us. One possible exception are the plant shapes, like the fern leaves. In this case, the Lindenmayer L-systems based on recursive automata may be biologically plausible [6].

In most cases, other mechanisms are involved. One of them was already hinted in the above discussion of critical phenomena. Indeed, the power-law behaviour at the critical point is the manifestation of emergent fractality, which can be verified by analysing the shape of domains in spin systems on lattices or connected components in bond percolation.

Another bunch of mechanisms is related to the dynamics and non-equilibrium nature of many physical systems. Take for example the bushy aggregates many people admire in showcases at mineralogy departments. Usually they are deposited from hot and very dilute solutions of various minerals. We may idealise the situation as the movement of sticky Brownian particles, which are released one by one from a large distance. We start with one such particle already stuck at one point and let the newcomer particle walk until it sticks to one of the already immobilised particles. Important point is that the new particle is injected only after the preceding one sticks. This corresponds to the limit of negligible concentration and infinitely strong inter-particle bonding, preventing any diffusion within the aggregate. The model we just described is called the *diffusion limited aggregation* (DLA) and for many years it was the paradigmatic model of fractal growth [7].

Another model, introduced in 1986, deals also with particles attaching on a surface. More specifically, it describes a surface growing by the molecular-beam epitaxy. Particles are sent from above onto a plane substrate and attach when they hit the already deposited layer. Diffusion over the surface is prohibited. On a very large scale, the discreteness of the atomic structure of the material can be neglected and the deposition process is described by time evolution of a real function of a continuous coordinate. The prominent model of this process is described by the *Kardar-Parisi Zhang (KPZ) equation* [8], perhaps the most studied stochastic non-linear partial differential equation. The surface grown in this way has fractal properties with non-trivial scaling exponents. The model is exactly solvable in 1 spatial dimension, using replica Bethe-ansatz method [9]. There is also ingenious dynamical renormalisation group treatment, which gives exact values of the critical exponents in 1 dimension [10].

Even broader and largely unexplored is the area of lattice models. It is believed (and confirmed by ample numerical evidence) that restricted solid-on-solid growth model, where particles of finite size are attached on the surface, while the slope of the surface is restricted to fixed bound, belongs to the KPZ universality class. In fact, exact solution of this discrete problem was found in 1 dimension, again using Bethe ansatz, which gives the same set of exponents as continuous KPZ [11].

It is believed that many more very different models belong to the KPZ universality class. Indeed, the range of various problems related to this simple equation is astonishing. Remaining within continuous space description, besides the surface growth it was proved that KPZ equation can be exactly mapped to the problem of directed polymers in random media [12] and to a simplified model of turbulence, described by Burgers equation. I contributed to this field by the papers [5, 13, 14] which analyse the effect of impurities on the growing surface and the growth of a two-component material.

The scale-free nature is palpable in visible spatial structures such as fractal aggregates. There is a much more subtle way the complexity is generated, which is at work in strongly frustrated spin systems, like *spin glasses*. In reality, they are diluted alloys of a magnetic substance in a non-magnetic metal. The paradigmatic model of a spin glass introduced by Edwards and Anderson in 1975 remains as a kind of a mystery up to the present time [15]. There is a beautiful and comprehensive solution of its mean-field variant, called the Sherrington-Kirkpatrick model [16], which was obtained by Parisi in early 1980s [17]. The peculiar beauty of this solution consists in the structure of pure states in the spin-glass phase. To assess the novelty, let us compare the situation with textbook examples. The low-temperature phase of the Ising model has just two pure states related by the global reflection symmetry. The pure states of the classical Heisenberg model form a sphere, therefore the set of pure states can be mapped on a Lie group coinciding with the group of global rotational symmetries of the Hamiltonian.

On the contrary, it was found that spin glasses exhibit multitude of pure states which are not related by any symmetry, yet they are not random, but organised in a very peculiar hierarchical manner. Introducing overlaps between states as a measure of distance, it was shown that the set of pure states is an *ultrametric space*. This fact provides, among others, a straightforward explanation of extremely slow relaxation processes and ageing observed in spin glasses experimentally. The "fractality" of spin glasses is not manifest in their external appearance, neither in a spatial geometry. It is rather a property of the state space, which assumes a "scale-free" or "fractal" feature due to the ultrametric structure of pure states. Moreover, unlike the usual magnetic systems showing critical behaviour close to a unique critical point, spin glasses are, in a certain well-defined

sense, explanation of which we skip here, critical at all temperatures and magnetic fields beyond the so-called de Almeida-Thouless line.

It was realised very soon that the physics of spin glasses and the nature of Parisi's solution reveals connectedness of many seemingly unrelated subjects, like models of neural networks [18], combinatorial optimisation [19], simulated annealing methods [20], directed polymers (already mentioned in the context of the KPZ equation, [12]), error-correcting codes [21], and, indeed, the theory of structural glasses, namely the so-called colloid glasses [22, 23]. The hierarchical classification of species in biology was also interpreted as a manifestation of the same combination of frustration and disorder, that is responsible for the complexity of spin glasses [24]. In short, spin glasses became one of the typical examples of complex systems in general. I contributed to this field by articles [25–28] dealing with learning in neural networks, finite-size effects in spin glasses, and non-perturbative effects in directed polymers.

At the end of 1980s there were a handful of well-defined models with non-trivial critical behaviour. These might have been considered as prototypes of fractal generators. However, quite soon the area was thrown into a state of much confusion by a burst of new, unexpected, and puzzling models. The event was marked by the appearance of the concept of *self-organised criticality* (SOC) which emerged in the works of Per Bak and others [29]. The basic mechanism was built upon a dynamical process in an open dissipative system, where the attractor of the dynamics is a state manifesting certain crucial features of (static) critical states. The most important of them is the power-law decay of correlation functions and power-law distribution of "events" (what an event is, depends on the specific model in question) described mainly as "avalanches".

The first and pedagogically most appealing is the *sandpile model*: grains of sand are dropped one by one onto a two-dimensional table, until a heap is built and if a threshold slope is reached, a toppling occurs, distributing the excess grains onto neighbours. The neighbours may in turn surpass the threshold as well, topple, send some grains to their neighbours and the process may continue until a new equilibrium is reached. The origin of the concept of avalanche is then evident. Important feature and indeed a (once thought infallible) fingerprint of self-organised critical state is the power-law probability distribution for avalanche sizes.

The idea seemed so brilliant that many people hoped a kind of a "Theory of everything" is imminent, spanning virtually all fields of human curiosity, from pulsars to solar eruptions to global terrestrial geology to biological evolution to brain function and social movements [30]. Indeed, there was a hope to grasp all emergent fractals (and power laws) in nature within a single framework. The most important and repeatedly stressed feature is that the critical state emerges naturally without any fine-tuning of any state parameters, like temperature or density. To put the things in a right perspective, it became clear quite soon that SOC cannot constitute any universal theory for the appearance of fractals. The years that separate us from Per Bak's promises to finally understand "How nature works", taught us that SOC is a useful concept in specific phenomena, like domain-wall movement, but covers only a narrow segment of nature's works. Nevertheless, it is still fruitful to look at some self-organised critical models.

Let us make a few general remarks concerning the theory of SOC as a whole. More thorough investigations showed that the idea of no tunable parameters in SOC is only partially true. It was established that the tunable quantity is the order parameter itself, being tuned to value zero by the definition of the model dynamics. It is therefore clear that nothing else than critical point can emerge as an attractor. Stated differently, the self-organisation towards the critical state arises from *infinitely slow driving*. From this perspective, the older representatives of growing fractals,

namely diffusion-limited aggregation and the KPZ equation, are the early examples of what was later named self-organised criticality.

On the other hand, slow driving can be also understood as infinitesimal concentration of elementary excitations created by thermal noise. This marks the connection of SOC to a very rich field of *zero-temperature physics*. Indeed, one-dimensional dynamical Ising model at $T = 0$ exhibits power-law distributed avalanches and may be considered as the simplest model of SOC.

Perhaps the richest and practically most relevant example of a zero-temperature system is a *granular medium*, i.e. an assembly of a large number of small but macroscopic beads interacting by contact forces. Despite much effort in the last two decades many fundamental questions remain unsolved. Let us mention only one of them. It is well known that the most dense packing of spheres is achieved by one of the (infinity of) equivalent fcc/hcp packings. This was conjectured first by Kepler in his treatise De nive sexangula (1611) and included as 18th item to the Hilbert's list of problems. Full mathematical proof was completed in 1998 by T. Hales and S. P. Ferguson with a heavy use of computers. On the other hand, dense random packings have densities distributed consistently around certain value which is well below the fcc/hcp value. Does it mean there is certain "ideal random packing" with specific density and geometry? Most probably the techniques necessary to answer this question still await for their discovery.

The phenomenon called self-organised criticality can be viewed from yet another perspective, as related to *absorbing-state phase transitions*. Indeed, in an open system the dynamics can alter not only the configuration but also the control parameter, such as the particle density, until an absorbing state is reached and everything stops. Then, addition of a single particle excites the system and simultaneously increases the control parameter. The dynamics continues until an absorbing state is reached again. Therefore, the control parameter is tuned to the critical value separating the absorbing phase from the phase in which the dynamics lasts forever. By such a recipe, any system with absorbing-state phase transition can be turned into a SOC model. My own contribution to the field of SOC consists of papers [Slanina99], [Slanina99a], [Slanina02], and [SlaKot00], which make part of this thesis and will be discussed later.

Among various ramifications of SOC, there is one which brings us further to new themes. There is a puzzling phenomenon in biological evolution called *punctuated equilibrium*, first noticed by J. S. Gould in 1972 [31]. The point is that evolution of species does not proceed gradually, as Darwin originally supposed, but exhibits alternation of very slow and very rapid phases. In fossil record it looks like quasi-instantaneous extinctions of entire ecosystems and equally fast bursts of new species. The dinosaurs' extinction 65 millions years (not very long!) ago is just the best known of these events. The discussions on the causes of this mass extinction continue and perhaps will continue further. On the other hand lots of similar extinction events are documented in the fossil record and the statistics of their sizes obeys relatively well a power law [32]. So, the SOC was called on for help and soon a model emerged, now known as the *Bak-Sneppen model* of biological evolution [33]. Unfortunately, the model, while qualitatively right, failed to reproduce quantitatively the exponent in the power law, despite several modifications and efforts for improvement. It was found that the problem lies in the over-simplified treatment of the network of relations between species. The Bak-Sneppen model and its variants considered static network with linear or hypercubic geometry, or fully connected networks. Using a network with evolves in parallel to the evolution of species improves greatly the thing. My contribution to this field is contained in the paper [SlaKot00] (to be discussed later) and papers [34] and [35].

This brings us to another big theme which makes part of the current studies in complex systems. It is the theory of *complex networks*. We have just mentioned the complexity of the ecological networks representing the relationships between species in an ecosystem. This is just a single example of the vast area which covers as much physics as biology, engineering, economy and sociology. As a mathematical discipline, it belongs to the graph theory. Already in 1950s Hungarian mathematicians Pál Erdős and Alfred Rényi developed the theory of random graphs [36] which serves as a basis and a starting point for all studies in complex networks up to now [37]. In parallel to the mathematical studies there were investigations on a purely empirical basis. The notion of "six degrees of separation" was coined by Milgram, as a result of his study in which letters had to be delivered to predefined destination through a chain of personal acquaintances [38]. It was found that the average length of such chains was about 6, hence the conclusion that arbitrarily chosen inhabitants of the USA are separated by about six steps of personal relationships. This is very few compared with the number of people and vast geographical areas covered. Such apparent paradox was then called the *small-world effect*. It took some time before this phenomenon started to be taken seriously within a mathematical model introduced by Watts and Strogatz [39]. By that time, the boom of social network studies already started. Perhaps the best known pioneer is A.-L. Barabási, who contributed by groundbreaking empirical studies on the network structure of the WWW [40]. The most striking finding was the power-law distribution of degrees in the WWW network. Barabási himself, with his student R. Albert, devised a model, now called the Barabási-Albert (BA) model, which beautifully explained the power law on a basis of the preferential attachment principle: vertices in the network receive new edges with probability growing linearly with the degree of the vertex. Therefore, the degrees evolve according to a kind of a multiplicative-additive process, which is a well-known and rather trivial generator of power-law distributions [41]. As such, the WWW is an empirical example of a complex system endowed with power-law distribution of its characteristics, but with no connection to critical phenomena. Let us recall that the apparent absence of parameter tuning in SOC was unveiled to be a slow self-tuning to a critical point. In the BA model, any reference to criticality is gone.

The complexity in network structure demonstrated by power-law distributions was, on one hand, discovered in many other real systems; on the other hand, it was found that it has numerous consequences for systems which are placed on such a networks [42–45]. For example, the percolation threshold is absent, therefore the networks are in principle very robust with respect to failure. On the other hand, there are other weak points, for example virus spreading on such networks is extremely fast.

Let us mention just one purely physical system in which complex networks are relevant. We have already said that granular materials are examples of zero-temperature physics, in which the complexity arises due to absence of thermal (and quantum) fluctuations. Here we note another feature. If we put a granular medium under pressure, stress is not distributed smoothly as in an elastic continuum or regular lattice of elastic elements. The irregularity of random packing leads to the appearance of *force chains*, i.e. networks of contacts between the beads which carry most of the load. Majority of the material is rather loose or does nor bear any load at all. These force chains can be easily visualised by polarised light and they are vital for mechanical properties of sands and powders. Moreover, they make the transmission of sound through granular medium rather unusual [46]. For example, there may be localised vibrational modes in the medium, which is a phenomenon which resembles Anderson localisation of electrons in disordered metals [47].

However, due to the complex network structure, this effect poses many more difficulties. This area is still largely open.

However, this topic has direct interdisciplinary ramifications. In fact, one of the most studied problems in the theory of complex networks consists in partitioning the networks into clusters so that connections between clusters are rare, while connections within clusters are dense. As we notice, such a definition is very vague and hardly can serve as a firm basis for a computation. The complexity of the problem consists in the fact that both the formulation of the task and its mathematical solution is to be found. As a result, many different approaches to network clustering appeared [48]. One of the methods is based on spectral properties of the adjacency matrix encoding the structure of the network. Relevant eigenvectors are either located at the extreme edges of the spectrum (largest and second largest eigenvalues) or they are identified as localised states (inverse participation ratio being the quantitative measure of localisation). Here we recover the connection to the sound propagation along force chains in granular medium. I contributed to this field by the articles [SlaKon10], [Slanina11], and [Slanina12] which make part of this thesis and will be discussed later. Besides that, I also participated in a project which studied dynamical topological phase transitions in complex networks [49, 50] and in a few other investigations concerning complex networks [51–53].

Among all sciences, physics is unique in its perpetual and recurrent attempts to constitute a "Theory of everything". Indeed, if physics is to be a coherent aggregate of knowledge, it must comprise all physical existence, not just selected pieces of it. It comes as a kind of paradox that the current "theories of everything", like the string theory, are the most special, rather than universal, disciplines and instead of providing a firm basis for further deductions, their own empirical justification is still awaited. This does not mean these theories are less relevant. They are just too difficult, as everybody knows. We leave aside the philosophical considerations on the chances that human brain ever penetrates all the tangled mathematical schemes. Instead, we try to explore other ways physics may help to unite separate sciences into a more compact whole. Indeed, however exaggerated it may seem, physics does constitute the explanation of all chemistry and large part of biology, as a classic said [54]. But if physics successfully describes complex behaviour of single proteins [55], why not extend the description to protein complexes, cells, bacteria, green hydra, ants, apes, humans? Where is the limit to stop? Speculations do not help. A scientist must raise a hypothesis and then make an experiment and see. A large part of complexity studies and about a half of this thesis is devoted to the attempts to transfer physical tools, ideas and models to areas classically covered by social sciences. This is the aim of the discipline now called *sociophysics*. (See [56] for a personal testimony of S. Galam, one of the founders of sociophysics.) To make our cause stronger, let us make first a very brief historical overview, without claims of being systematic.

There is an often forgotten event that played a decisive role in the transfer of the ideas and language of physics into other branches of human knowledge. A conference was scheduled to take place in Moscow from 1 to 5 July 1974. Scientists both from the West and from the USSR were invited to discuss implications of physics in other fields, including social sciences and humanities. The organising committee included people like Kenneth Arrow, a Nobel laureate in economics, and Hans Bethe, a Nobel laureate in physics. However, the communist leaders found the subject of the meeting incompatible with the ruling ideology. The conference was banned, most of the Russian participants were arrested and a majority of them eventually left USSR, mainly to Israel. But many drafts scheduled for the conference talks were successfully smuggled from the USSR

to the West, and eventually were published in a proceedings volume [57]. A tiny portion of it appeared in [58].

But the history of interdisciplinary physics did not start with the Moscow non-event. Just before his mysterious disappearance, Ettore Majorana wrote a paper on consequences of quantum mechanics for the studies of human society [59]. Certainly we could find more physicists who shared similar views. But let us go further into history. There were always people who thought that social phenomena can be described as completely as physical ones if only we knew the right set of laws and we were smart enough to do the calculations involved. Auguste Comte [60, 61] was the first prophet of this belief, in the early 19th century. Comte coined the term "social physics" as an explicit reference to the success of the Newtonian mechanics. Though Comte himself abandoned the term social physics, it was called to life again by his successors, most notably Adolphe Quételet [62], and it has survived in various disguises up to the present time.

There were other pioneers of the use of physics in social phenomena, but let us only mention the south-Bohemian nobleman Georg Graf von Buquoy, the Count of Nové Hrady [63, 64], and the swiss-italian engineer Vilfredo Pareto [65]. These attempts were not quite successful. Of course, the Pareto law does describe the distribution of wealth in society, but any presumed connection to physics was illusory. In the second half of the 20th century the situation started to change. One of the inspiration for Mandelbrot's fractal geometry was his study of cotton price fluctuations [66]. It was found that the price fluctuations are not Gaussian, i.e. the price does nor follow a random walk. Instead, Mandelbrot suggested that *Lévy walks* might be appropriate. They are characterised by power-law tails in the distribution of displacements and this is just what Mandelbrot observed empirically. In 1991, the journal Physica A published a paper [67] by R. N. Mantegna, who applied the Lévy walks to the fluctuations of prices at Milan stock exchange. Nowadays, this event is considered to mark the birth of a new discipline called *econophysics*. Meanwhile, the study of economy in a wider context of the theory of complex systems was promoted at the Santa Fe Institute. Among the leading personalities we find people like P. W. Anderson and D. Pines [68]. Since the beginning of the 1990s, the use of physics in economics started to be taken very seriously. Among the physical concepts which found a fertile ground in economics we name for example scaling, universality, percolation, turbulence, spin glasses, reaction-diffusion processes, random matrix theory, and we could mention many more [69–71]. Note also that the ideas of self-organised criticality [72] and complex networks [73] find their use in econophysics, thus connecting the fields we are discussing here. In some sense, econophysics should be considered as a part of sociophysics, because economy is only a narrow segment of the social life. But we have no intention to argue on names, so let us leave econophysics and sociophysics separate. I contributed to both sociophysics and econophysics by a certain number of papers (there is no need of listing them all here). Among them, I chose for this thesis the papers [Slanina01], [SlaLav03], [SlaSznPrz08], and [Slanina11a] as representatives of my results in sociophysics and [Slanina04], [Slanina01a], and [Slanina08] as representatives concerning econophysics. Besides these papers I would dare to mention also my chapter "Social Processes, Physical Models of" in the *Springer Encyclopedia of Complexity and Systems Science* [74], and the chapter on the minority game in the book *Oder, disorder, and criticality, vol. 3* [75]. A book of mine, entitled "Essentials of Econophysics Modelling" is now being processed with the publisher and should appear in a few months [71].

The field of the science of complexity is very vast and the topics covered by my own work are by no means representative for the whole discipline. Nevertheless I believe the reader can

understand that complexity studies are not a marginal segment of physics, but it is, quite the contrary, an important development of the physics of many-particle and/or non-equilibrium systems.

1.2 Overview of the problems solved

My own work contained in this thesis is divided into four sets. Thematically, there are a few overlaps between them. The first set contains three papers devoted to the study of self-organised criticality and investigates strongly non-linear mechanical systems. As temperature plays no role, they can also be classified as zero-temperature physics. The second set contains four papers related to the theory of complex networks. At the same time, the first one of the four takes inspiration from SOC and therefore makes a bridge between the first and second set. The third set contains four papers which use physical models to describe social phenomena, i.e. they belong to the field of sociophysics. In fact, already the second paper of the second set was inspired by sociophysical problems, meaning that there is a link between the second and third set too. The fourth set contains three papers belonging to the field of econophysics. As economy is just a part of a social life, these three papers may be considered as a special focus within the sociophysics field and in particular a special ramification of the themes covered in the third set of papers. Therefore, I feel the papers make a weakly tied, yet coherent ensemble.

1.2.1 Self-organised criticality

What is it about?

Here I describe my contributions to the field of self-organised criticality (SOC). All of them belong to the study of avalanche phenomena. The point is that the systems are out of equilibrium, but infinitely close to it. Usually, such situation is physics is described by the linear response theory (LRT). Here, LRT is not applicable for two reasons. First, the system is non-linear as the response is never proportional to the cause. Second, LRT assumes perturbation around a well-defined and unique equilibrium. In the models investigated in the three articles discussed in this section, absorbing states play the role of equilibrium states, and there is a large number of these absorbing states. After an infinitesimal instantaneous perturbation, the dynamics brings the system from an absorbing state to another, instead of returning it back to the same equilibrium state, as happens in LRT. The transition between two absorbing states is an avalanche. If we insisted on using the concept of avalanche in LRT, it would correspond to the exponential relaxation. If we perturb several times a system subject to LRT, we observe each time the same unique rate of relaxation. Therefore, if avalanches do have any meaning in LRT systems, all avalanches have the same typical time scale. On the contrary, SOC systems exhibit power-law distribution of avalanche durations, thus no typical avalanche duration can be identified. The set of avalanche durations is scale free. The same holds also for other characteristics of avalanches, like their size etc.

Before going to the three original articles making part of this thesis, let us demonstrate the idea of SOC more formally on a trivial example. Imagine an Ising model on a finite linear chain of length L, with open boundary conditions. The configuration of spins can be equivalently described by the position of domain walls, i.e. links joining spins of opposite sign. The model is endowed with parallel zero-temperature dynamics. In terms of the domain walls, it means that at each time step each of the walls can jump one lattice position left or right with equal probability. If two walls

happen to be at the same position, they annihilate each other. Therefore, the dynamics is equivalent to the dynamics of a set of annihilating random walkers on a finite one-dimensional chain. With probability one, an absorbing state is reached in a finite time.

There are two absorbing states in the model. Both of them are characterised by the absence of domain walls, i.e. all the spins have the same sign. In the spirit of SOC, we perturb the absorbing state infinitesimally by flipping one randomly chosen spin. A pair of domain walls (i.e. random walkers) is created at the distance of one lattice spacing. Then, the walkers are left to walk until they meet and annihilate. The time elapsed until the walkers meet determines the duration of the avalanche. The problem is equivalent to the study of first return times of a random walker to the origin. This is a well-known exercise in probability theory. It can be easily found that the generation function of the distribution of first return times is

$$\widehat{P}_{\text{first return}}(z) = 1 - \sqrt{1 - z^2} \tag{1.1}$$

and from here we obtain for the distribution of avalanche durations

$$P_{\text{dur}}(t) = \frac{(2t)!}{2^{2t+1}\, t!\, (t+1)!} \, . \tag{1.2}$$

For large t, the Stirling formula gives

$$P_{\text{dur}}(t) \sim t^{-3/2} \, . \tag{1.3}$$

Therefore, we obtain exactly the power-law tail in the avalanche distribution. This example is not a mere toy, but provides a typical example of SOC behaviour in many more models. Indeed, very often the behaviour of SOC systems can be, in this or that means, mapped on a random walker returning to the origin. In many other cases, as we shall see in the paper [Slanina02], the mapping is not exact but provides a very good approximation. In many cases, such approximation has the flavour of a "mean field" approach, so that the exponent $3/2$ found in (1.3) is considered a mean-field value of the avalanche exponent, much like the Landau theory of phase transitions provides the mean-field set of critical exponents for equilibrium critical points.

Friction

Now I will proceed to my own work. In the paper [Slanina99] I introduced a model of mechanical friction [76]. The complexity of friction consists in the fact that the apparently flat surfaces are in contact at many tiny irregularities of the surface shapes. These individual contacts are called asperities. Several approaches are possible. One of them is a mechanical analogy, considering the system of asperities as solid balls connected by springs and moving in a periodic (e.g. cosine) potential. This is called the Frenkel-Kontorova model [77]. Another approach concentrates on a single asperity and takes the rest as a kind of an effective medium [78]. Many more examples can be found in Ref. [76]. My model is based on the mechanism of *extremal dynamics* which proved useful in description of avalanche phenomena in dislocation movement [79]. (We shall return to the extremal dynamics once more later, discussing the article [SlaKot00].)

The idea is based on an idealisation of the system of asperities, as illustrated in Fig. 1.1. There are two types of asperities. Some of them are in touch with the substrate and some not. Those in touch store certain amount of elastic energy, while those which are not in touch are free. In an

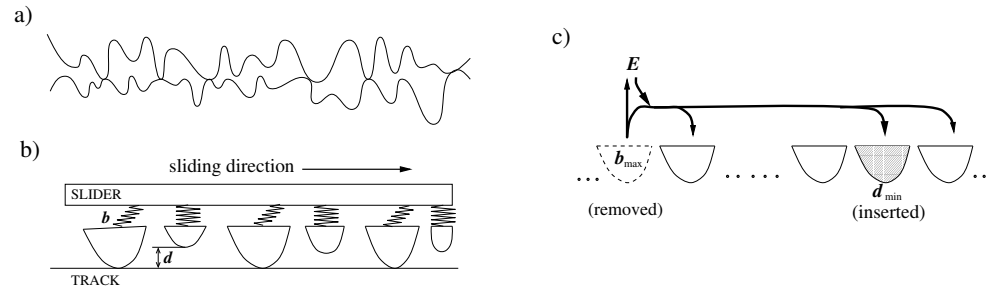

Figure 1.1: Illustration of the model. A schematic drawing of two sliding interfaces in contact is given in a), the idealisation of the situation used in our model is depicted in b). The elastic energy stored in the asperity is described by the quantity b, the slot between potential asperity and the track is d. In c), the redistribution in one step of extremal dynamics is shown schematically.

idealised scheme, each lattice point hosts one asperity in touch and one free. Those in touch are characterised by a dynamical variable b measuring the elastic energy stored in the asperity. Those not in touch are characterised by their distance d from the substrate.

The dynamics proceeds by alternating slow and fast episodes. We can describe it also as a stick-slip movement. During the fast regime (a slip) the entire body moves a macroscopic distance, until it sticks. We suppose that all slips have the same typical length. After a slip, all values of b and d are completely random. Then, the slow movement starts. In each step, the asperity with highest stress b is updated (hence the name extremal dynamics). This means that it is detached from the surface. In order to keep the number of touching asperities constant, a new position is found at the site with lowest d and the old asperity is "moved" to the new position. Meanwhile, the released stress b is redistributed among neighbouring asperities and partially transferred to an external energy reservoir, which can be interpreted as a big spring pushing the whole body. A slip occurs when the energy stored in the reservoir exceeds certain threshold.

If the threshold is infinitely large, the system exhibits self-organised critical behaviour. At the same time, the velocity of the movement is zero, as there are no slips. If we diminish the threshold, the stick-slip movement starts. Hence we obtain the dependence of the friction force on velocity v. It can be well fitted on the formula

$$F_{\mathrm{fric}} = F_0\Big(1 - \exp\big(-\frac{A}{v}\big)\Big) \tag{1.4}$$

where F_0 and A are constants. This velocity dependence of the friction force is the main result of the article.

Cracking

In the second paper of this set [Slanina99a], I looked at slow internal failure of a heap of fragile beads. One might think of a pile of eggs on which a foolish cook sits. How many of the eggs will survive? Surprisingly, quite a lot.

It is well known that in a granular medium (sand, powder, etc.) under external load stress is distributed in a very inhomogeneous way. Force chains are formed where the stress is localised, and these chains form arches carrying the load, much like the arches in a Gothic cathedral carry all the weight of the stone blocks, leaving free space to windows illuminating the interior. This arching

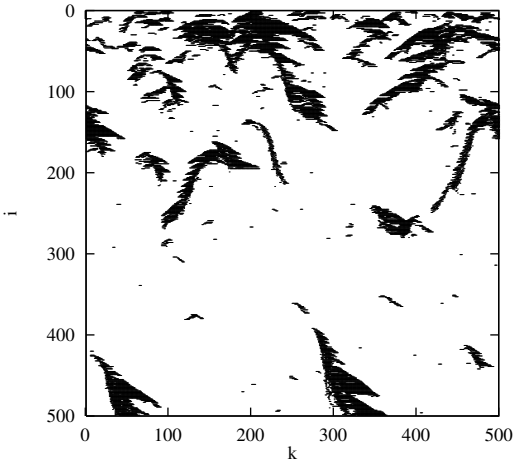

Figure 1.2: An example of the morphology of cracked areas. Every cracked grain is depicted by a black dot.

phenomenon has, for example, a paradoxical consequence that the stress exerted on a flat support by a conical heap of sand has a minimum just below the top of the heap. The first experimental evidence if this fact is due to the Czechs J. Šmíd and J. Novosad [80] and it was explained a decade later by a model of stress propagation [81]. The model I use assumes that the stress tensor can be replaced by a scalar, namely the diagonal element of the stress tensor along the vertical axis. The stress is transferred from upper layers of the granular material to the lower ones stochastically. We can also view it as an evolution of a stress configuration within a layer, if the vertical coordinate is interpreted as time, directed to the bottom. Then, going from the top, stress develops so that in each step the stress on a bead is redistributed randomly to its neighbours in the layer below. What I have just sketched is the so-called q-model of stress fluctuations [82].

For the purpose of studying the cracking of beads, I define a threshold above which the stress on a single bead leads to a collapse. Collapsed bead cannot bear as much load as before, which means that the stress it carried before the collapse is partially redistributed to its horizontal neighbours. But as a result thereof, these beads can also collapse and the collapses propagate through the heap as an avalanche. After the avalanche stops, the system is "excited" again by increasing the external load from above, until a bead is found where the stress reaches the threshold. This marks the beginning of another avalanche. It was found that the cracked areas are localised along arches, much like the force chains. This is of course something that should have been expected. Less expected is that, depending on the parameters of the model, most of the cracked beads can be found either on the top or on the bottom of the heap. An example of the morphology of cracked regions is shown in Fig. 1.2. Moreover, it was proved that the distribution of avalanche sizes follows a power law, thus confirming the self-organised critical state.

Ricepiles

In the third paper [Slanina02] I investigated rather special variant of the original BTW sandpile [29] The model was inspired by experiments in which grains of rice were thrown into a slot between two parallel vertical perspex plates [83], where power-law distribution of avalanches was verified. (A nice demonstration was given by Mária Markošová at a miniworkshop in the Center

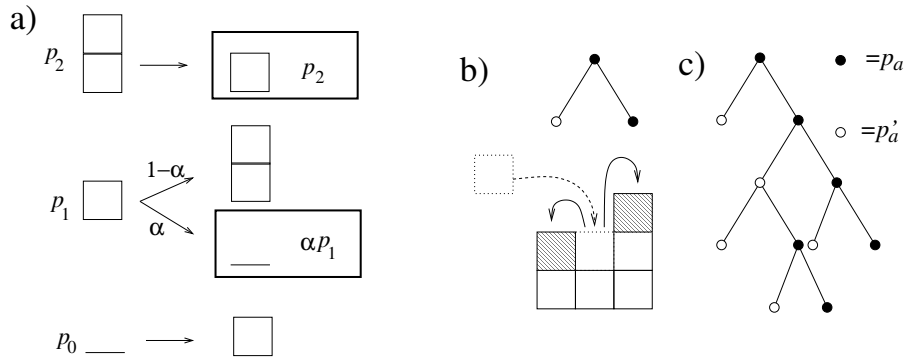

Figure 1.3: Illustration of the one-dimensional ricepile. In the panel a) we show the events happening after adding a grain. In b) the toppling is represented as a branching event, in c) we show an example realisation of the resulting branching process. Branching probabilities are different for the nodes resulting from the left and the right branch.

of Theoretical Studies in Prague, 1997.) The model of this situation [84, 85] is a one-dimensional cellular automaton. At each site, there may be 0, 1, or 2 grains. A new grain is dropped always at the first site from the left. If a site with a grains receives a new grain, it topples (i.e. sends one grain to both left and right neighbour) with probability q_a. We have $q_0 = 0$, $q_1 = \alpha \in [0, 1]$, and $q_2 = 1$. Numerical simulations found a power-law distribution of avalanche sizes with exponent $\tau \simeq 1.55$. The most interesting fact was that the behaviour was independent of the value of the parameter α, unless α was very close to the endpoints $\alpha = 1$ or $\alpha = 0$. Precisely at the endpoints the avalanche distribution was exponential, rather than power-law. The crossover from power law to exponential when α approaches the endpoints was never clarified in simulations.

To treat this situation analytically, I devised a model which adapts the idea of self-organised branching process [86]. Branching processes are known to well describe the SOC models in high spatial dimensions, where the activity rarely returns back to the same site, for purely combinatorial reasons. The infinite-dimensional case is a kind of a "mean-field" approximation, so it seems strange to use it for a one-dimensional model, where the activity returns back always just in the next time step. The "loops" of activity must be somehow taken into account. I do it in the following way.

Before an avalanche starts, there are N_a sites with a grains, $a \in \{0, 1, 2\}$. The first assumption is that they are placed randomly, so a randomly chosen site has a grains with probability $p_a = N_a / \sum_b N_b$. Then, the probability of toppling when a grain arrives is $q_a p_a$. In the mapping to a branching process, each toppling is represented by one branching. Then, each branching corresponds to the transfer of two grains, one to the left and one to the right. Two new branches emerge from the site. The parent site gives birth to two daughter sites. If we supposed that the activity never returns to the same place, the branching probability at the two daughter sites would be equal and the same as at the parent site. But in one-dimensional case we know that the left daughter toppled just one step before, therefore the probabilities of finding a grains there are modified to $p'_a = q_{a+1} p_{a+1} / \sum_b q_{b+1} p_{a+1}$. Therefore, the branching probability of the left daughter is also modified. Using these definitions, the branching process is investigated by standard means of generating functions. It is found that the branching process is critical, with avalanche exponent $\tau = 3/2$, for $p_1 = \max(0, (2\alpha - 1)/\alpha)$, $p_2 = 1 - \alpha$. But how can we know if the values of

p_a are just these? Here comes in the idea of self-organised branching processes. In fact, it is not difficult to count the change in numbers N_a of sites occupied by a grains, after the avalanche, i.e. the branching process, ended. New Ns imply new ps, therefore each realisation of the branching process alters the parameters which enter the next realisation of the process. This way we obtain a sequence of branching processes, described by the evolution of their parameters p_a. It is relatively easy to find the fixed point and when we do it, we realise that it is just the set of ps which makes the branching process critical. Therefore, the self-organised criticality is proved by a calculation. Moreover, with little difficulty we can study also the crossover phenomena when α approaches the points 1 or 0, as well as effects of finite size of the lattice. I would like to stress just the result for the crossover. For α close to either 0 or 1 the avalanche size distribution behaves like

$$P(s) \simeq \frac{1}{s_o} F\Big(\frac{s}{s_0}\Big) \tag{1.5}$$

where $s_o = 1/(2\alpha(1-\alpha))$ and the scaling function is expressed using the modified Bessel function

$$F(x) = x^{-1}\mathrm{e}^{-x}\, I_1(x)\ . \tag{1.6}$$

But the most striking finding in this model is that the "mean-field" value of the avalanche exponent $\tau = 3/2$ is so close to the numerically observed value $\tau \simeq 1.55$. It remains a kind of mystery that the one-dimensional case can be so well approximated by the infinite-dimensional one. We shall see later another example of a similar paradox [SlaSznPrz08].

1.2.2 Complex networks

Where the complex networks come from

In the early days of the study of networks they were modelled by static random graphs. This is the case of Erdős-Rényi graph ensembles [36] as well as Molloy's and Reed's random graphs with prescribed degree sequence [87]. The former is defined as a set of all graphs $G = (\mathcal{V}, \mathcal{E})$ with fixed number of vertices $N = |\mathcal{V}|$, but variable number of edges $E = |\mathcal{E}|$ endowed with probability measure $P(G) = p^E(1-p)^{N(N-1)/2-E}$. The parameter $p \in [0,1]$ tunes the overall "density" of edges in the graph and the average degree $\langle d\rangle = Np$. The latter ensemble is defined just as the same set with the extra constraint that the degree sequence, i.e. the ordered list of the orders of all vertices, is equal to the prescribed sequence. The probability measure is supposed uniform on this set. (Of course, there may be sequences which are impossible, and the set is empty, but usually these pathological cases are neglected.)

It is evident that the degree distribution in the above described Erdős-Rényi ensemble is binomial, and for large number of vertices it approaches the Poisson distribution. (There are strong mathematical theorems concerning this fact that seems "evident" to a physicist.) However, empirical data for existing networks, like WWW, show great heterogeneity in degree distribution, which calls for another models of random graphs. To add more complexity, graph processes were introduced. Contrary to the static graph ensembles, in the graph process we construct a sequence of graphs by adding edges or vertices, or both. (In a more general framework, edges and vertices can be also removed. In fact, this will be the case of our model, too.) Each sequence is given a probability, and each sequence is a point in a probability space.

The best known among physicists is the Barabási-Albert (BA) graph process. It has also an advantage of being very educative. The countable infinite vertex set is numbered by non-negative integers. In each step, one edge is added. Suppose we are at step n and the degrees of the vertices 0 to $n-1$ are $d_0, \ldots, d_{n-1}$. The newly added edge joins the vertex n with the vertex $j \in \{0, \ldots, n-1\}$, with probability $p_j = (d_j + a)/\sum_{i=0}^{n-1}(d_i + a)$. The only parameter of the model is a and it determines the exponent of the resulting power-law tail in the degree distribution [88, 89]. Vertices with larger degree are preferred, hence the name "preferential attachment" for such a prescription.

It was established that the necessary condition for the emergence of the power-law tail is the linear dependence of the linking probability on the degree of the linked vertex. Such linear dependence can be implemented in various ways, the straightforward being just what is prescribed in the BA process: the probability is given by hand from outside. Of course, in reality the linking probability must arise from internal dynamics. The BA model does not account for that and this is its main weak point. One of the simplest internal mechanisms of the preferential attachment is node duplication [90, 91]. Now I come to my own work.

Ecosystems' evolution

As far as I know I was the first who used this principle in a model of evolving network, introducing a graph process which will be described below. To be fair, I should acknowledge the advice of Kim Sneppen, who suggested me to try it, when he visited Prague in 1997. Thus, he is the true inventor of the node duplication mechanism.

The work I speak about now is the paper [SlaKot00]. This is the result of a joint effort of myself and Miroslav Kotrla. To asses the fraction of my own contribution, I declare that I am the author of the formulation of the model, the computer code and all the numerical results. At the stage of the interpretation of the results both of us contributed equally. M. Kotrla suggested comparing the model with then-topical small-world networks, which implied another round of simulations, which I performed. I wrote the largest part of the text of the paper. The same share of authorship concerns also the preliminary letter [34] which preceded the full paper [SlaKot00]. The matter later evolved in a paper [35], where the majority of work was done by M. Kotrla.

In [SlaKot00] I modelled an ecosystem composed of species linked by interactions. The quantity and/or quality of the interactions is neglected, I consider only presence or absence of the interaction. Thus, the species are represented by vertices in a graph and the interactions are implemented as edges in the graph. The species are characterised by a unique number, called fitness, quantifying the survival abilities of the species. The dynamics of the ecosystem closely follows the Bak-Sneppen (BS) model of biological evolution [33] which accounts for the avalanche phenomena in extinction dynamics of the biosphere. The basic idea is that of the extremal dynamics, similar to the friction model discussed in [Slanina99]. In each step, the least fit species is replaced by a new one. Simultaneously, the fitness of the neighbours is also updated, reflecting the change in the interactions between species.

The BS model is self-organised critical and the statistics of extinction events follows a power-law. Unfortunately, the exponent in the model is about 1.1, while the empirical data from the fossil record show the value of about 2. Thus, the quantitative disagreement is discouraging.

I suggested to improve the model by allowing the network of interactions between species evolve. Indeed, the BS model supposes that an extinct species is immediately replaced by a new one, preserving all the interactions. To some extent this is true, but essentially an extinct species

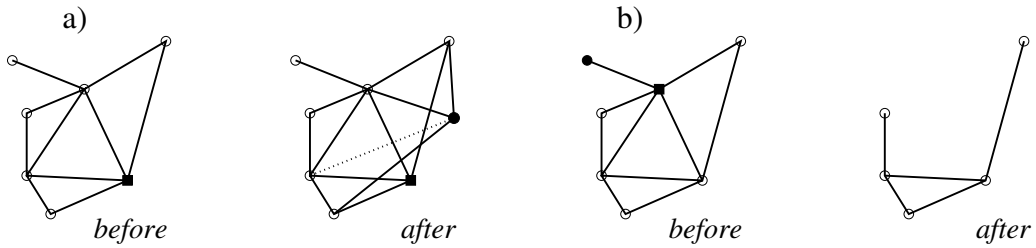

Figure 1.4: Illustration of the change in the network due to speciation (a) and extinction (b).

leaves an empty place which is only gradually filled by newly evolving species. Therefore, I introduced changes in the network according to the following rules (illustrated in Fig. 1.4). First, in the spirit of extremal dynamics, the species with lowest fitness is found and destined to mutation. This means that its fitness is replaced by a new random number. Also the fitnesses of all the neighbours are updated. Up to now, the rule is identical to the BS model. But in addition to that, the new fitness of the mutated species is compared to the fitnesses of all the neighbours. If it is the largest of all, the species is considered as very successful and gives rise to a completely new species. This means that a new vertex is added to the graph and the edges connecting the "mother" species are replicated (with the probability $p \in (0, 1]$) into the edges connecting the "daughter" species. This way, the idea of vertex duplication is implemented. If, instead, the fitness of the mutated species is lower than the fitnesses of all its neighbours, the species is deemed to extinction. This means that the vertex and all edges emanating from it are removed. In this way, the number of species fluctuates incessantly and the topology of the ecological network changes all the time.

The most important result is that the distribution of extinction events follows a power law with exponent $\simeq 2.3$, close to the empirical result. This is a substantial improvement in comparison with the original BS model. Next, we found a surprising result that the degree distribution in the graph is quite complicated. In short, we found that in the "equilibrium" regime, where the number of vertices stays close to the long-time average, the degree distribution has an exponential tail, while in the "transient" regime, where the number of vertices makes excursions much above the average, the degree distribution has a power-law tail. This is attributed to the fact that in such a regime the structure of the graph is dominated by its growth, much like the growing graph in the BA graph process. This was later confirmed by supplementary simulations (not included in the paper) in which I considered only speciation events and excluded all extinction events. The graph was therefore growing by definition. In this case I found that the degree distribution follows a clear power law. In fact, the empirical data on ecological networks are somewhat conflicting [92, 93]. There are reports of power-law distribution in some cases, while exponential distributions are found in other cases. In the light of my results, one can conjecture that the ecosystems with power-law distribution are in the state of expansion (not visible on the timescale of human life, but rapid on a scale on which biological evolution acts) while the exponentially-distributed ecosystems may perhaps be in an equilibrium for millions of years. But, as I stressed, these hypotheses are neither confirmed nor refused yet.

Spectral graph theory

Graphs are analysed by multitude of methods. One of them, which is particularly appealing to physics, is investigating eigenvalues and eigenvectors of matrices which encode the structure of the graph. This is the essence of a discipline called spectral graph theory [94]. In fact, at the beginning of this discipline we find E. Hückel [95], who revolutionised the quantum organic chemistry by the idea that many crucial properties of organic molecules follow just from the structural formula. Such formula can be viewed as a graph. The graph can be "coloured" attributing the vertices types of atoms and the edges types of bonds (single, double, etc.) and then proceed to solving the quantum-mechanical problem within the molecular-orbital method. The important point is that the structure of the molecule is encoded by a coloured graph, which is then encoded by a matrix (simplified Hamiltonian) whose spectrum and eigenvectors are to be found. While quantum chemistry diverged largely from this simplistic approach, spectral properties of matrices encoding the graph structure became of interest on their own. The specific question we are interested now in is the partitioning of a graph into modules. The notion of a module is somewhat vague, thus each problem requires a specific definition of what a module is. For example, if we want to cut the graph into two modules, spectral theory can help. We construct the adjacency matrix of a graph (ones represent an edge, zeros absence of an edge) and find the eigenvector corresponding to the second largest eigenvalue. Positive elements of the eigenvector denote vertices in one module, negative ones denote vertices in the other module. The method can be made more precise, but I shall not report it here, as the method I used is completely different, although it is based on spectral methods as well.

Small clusters within networks

Here I shall report my work [SlaKon10] which I performed in collaboration with the sociologist Z. Konopásek. His contribution consisted in putting the study in a sociological context, connecting it to previous literature and drawing consequences which the study of ours brings to the sociological community. My own contribution consists of collecting large amounts of empirical data from the WWW (using software written by myself), developing the numerical method of the spectral analysis and performing all the calculations.

In this study I looked at the network behind the e-commerce portal Amazon.com. There are products sold (still they are mainly books, but you can buy a bottle of California red wine as easy as fire resistant women's shirts there), there are customers and there are reviewers who comment on the quality of the products. I concentrated only on the products and reviewers, thus having a bipartite graph.

At first stage, I wrote a robot who downloaded automatically the information on all the reviewers and then I downloaded systematically all reviews written by these people. In the next stage, I analysed the network, finding power-law degree distributions on both the reviewers and products side. The main question was to find small densely connected clusters within the large network. The structure is encoded in the rectangular adjacency matrix M, rows corresponding to reviewers, columns to products. In order to apply the spectral method, I made a "collapse" to reviewers only, which is expressed in the matrix multiplication $A = MM^T$. Then, I diagonalised the matrix A. Contrary to previous approaches, the key quantity of my method was the inverse participation ratio (IPR). If $e_{i\lambda}$ is the ith element of the normalised eigenvector corresponding to the eigenvalue λ, IPR is $q^{-1} = \sum_i e_{i\lambda}^4$. Small IPR means delocalised state, hight IPR means localised state. The

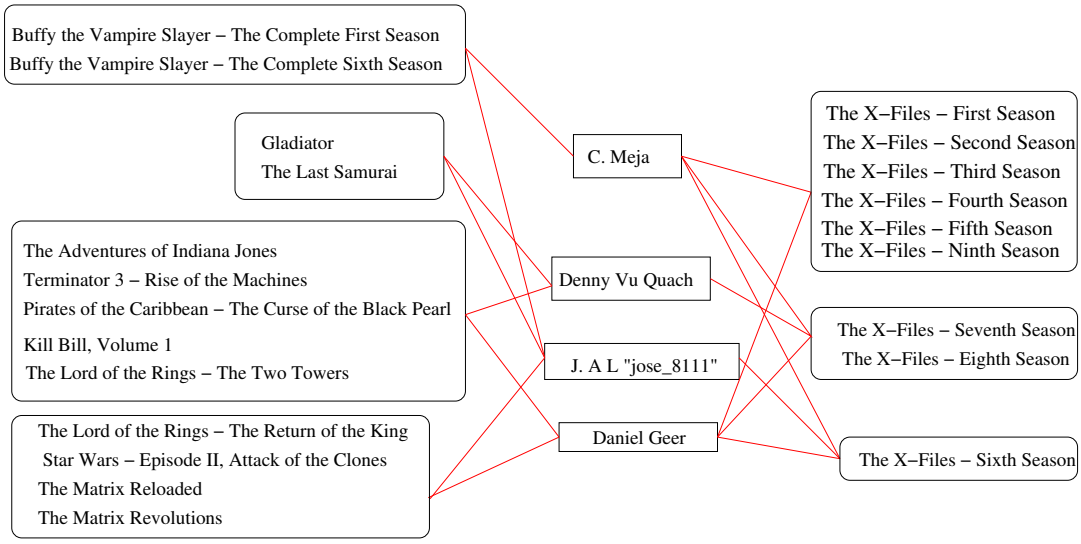

Figure 1.5: Example of a dense cluster in the Amazon.com reviewer network found by the spectral method.

idea consist just in finding the most localised states and identifying the clusters with the sets of sites where the localised eigenvectors have large enough value (above certain threshold). This way I was able to find groups of reviewers and products who share certain common characteristics. An example of such a cluster is in Fig. 1.5. The most important point is that I did not insert any preliminary semantic information. All the information was structural, encoded in the presence or absence of links connecting reviewers and products. Yet the clusters found bear obvious semantic information, interpreted a posteriori. For example the cluster shown in Fig. 1.5 connects sci-fi and fantasy movies. Another cluster found was centred around the songs of Beatles and Bob Dylan, with a small intrusion of the Led Zeppelin. Yet another cluster had as a common theme George W. Bush (there were fans as well as opposers, all united). And we could continue further. This shows that the method can indeed reveal hidden information starting just from the graph structure. For a sociological study, this may be an invaluable tool, as it does not spoil the research by personal prejudices of the scientist.

Zero hypothesis: a random graph spectrum ...

For studies like [SlaKon10] it is very useful to know the "background noise" or a zero hypothesis. i.e. the situation with no relevant information whatsoever. Without any idea of the zero hypothesis, we can find spurious clusters which are formed by pure chance. Therefore, it is natural to study the spectral properties of random graphs and compare the results with the findings on the empirical networks, like the Amazon one, studied in [SlaKon10].

In fact, there are many results available on the spectra of random graphs. The problem can be formulated as the analysis of sparse random matrices. Spectral properties of random matrices attract physicists since the pioneering works of Wigner [96] and Dyson [97]. For a review, we can recommend the book [98]. Sparsity of a matrix poses additional problems, investigated by Rodgers and Bray [99]. Using the replica method, they derived an equation, whose solution encodes all information on the density of states of a sparse random matrix corresponding to the Erddős-Rényi

random graph. Unfortunately, there are no exact solutions of the equation available. The best one can do is either to express the solution in terms of a series and find a few first terms, or to use instanton calculus (in principle equivalent to estimating the behaviour of large orders of the same series). Moreover, there are also numerical approaches, based on the cavity method [100].

In the work [Slanina11] I aimed at clarification of the mutual relation of the replica and cavity approaches. Replica method does not contain any explicit approximations, but relies on ill-justified mathematical procedures. Chiefly it is the analytic continuation from the set of positive integers to the entire complex plane, that raises concern. On the other hand, the cavity method is in principle only an approximation, but it is assumed exact in the limit of infinite system. Whether this assumption is correct or not, depends on the properties of the graph whose spectrum is to be computed. For example, if the graph is a tree, the cavity method is exact almost by definition. There is no general answer regarding to applicability of the cavity method on an arbitrary graph. Especially, we may ask if it works on the Erdős-Rényi graphs. This is what I investigated in [Slanina11].

The key quantity is the generating function of the (random) local Green function

$$\gamma(\omega) = \langle e^{-\omega\, g(z)} - 1 \rangle \ . \tag{1.7}$$

I found that it can be calculated by minimising a functional depending on $\gamma(\omega)$ and on an auxiliary function $\rho(\omega)$. The functional can be written explicitly as

$$\begin{aligned} \mathcal{F}[\gamma,\rho] = & -\int_0^\infty \frac{d\omega}{\omega}\,\gamma(\omega)\rho(\omega) + \frac{1}{\mu}\int_0^\infty \frac{d\omega}{\omega} e^{-\omega z+\mu\,\gamma(\omega)} \\ & + \frac{1}{2}\int_0^\infty \frac{d\omega}{\sqrt{\omega}}\int_0^\infty \frac{d\lambda}{\sqrt{\lambda}}\, I_1(2\sqrt{\omega\lambda})\rho(\omega)\rho(\lambda) \ . \end{aligned} \tag{1.8}$$

Using this variational formulation of the problem, I proved that cavity approach indeed coincides with replica in the limit of infinite system. Moreover, the variational approach has an advantage of being a starting point of consistent approximations, by limiting the set of allowed forms of the functions $\gamma(\omega)$ and $\rho(\omega)$. For example, assuming the form $\rho(\omega) = \mathrm{e}^{-\sigma\,\omega}$, where σ is independent of ω, we get an approximation called "effective medium approximation" by the random-matrix community, and "coherent-potential approximation" by the solid-state community (although the exact relation to CPA in its classic formulation [101] is not completely clear).

One of the improvements my method puts forward is the treatment of the tail of the spectrum. It is well known that the Lifschitz tail contains localised states which elude the CPA treatment. Beyond the CPA band edge, there is a continuum of levels which extends far away. There are general estimates of the form of the Lifschits tail, based on the instanton calculation [99], but any precise calculation of the tail is lacking. Starting with the variational approach, I was able to approximate the (continuous) tail by a sequence of bands, separated by (spurious) gaps. (I call it the single-shell approximation.) I also calculated the weights of the bands, confirming the general instanton result for the form of the tail. Therefore, my result is an improvement over the older ones, despite the presence of unphysical spurious gaps. Moreover, I was able to use the variational method for computing the spectra of correlation matrices (of the form $A = MM^T$, where M is a rectangular random matrix). In this case, I obtained significant improvement over the classical Marčenko-Pastur result [102].

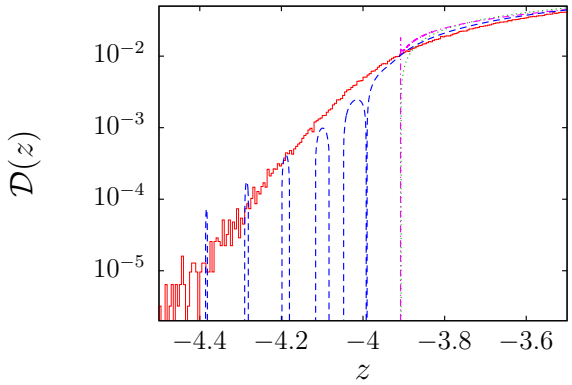

Figure 1.6: The detail of the left tail of the density of states of an Erdős-Rényi graph. The full line shows the result of numerical diagonalization, the dotted line is the result of effective medium approximation, and the dashed line is the single-shell approximation.

. . . and localisation

In the work [Slanina12] I continued this study, asking about the localisation properties of the eigenvectors. Localisation on random graphs is somewhat different from the usual localisation problem in solid-state physics. In a disordered conductor, the effect of localisation leads to inhibition of diffusion of the conducting electrons [47], therefore the conductance drops to zero. The very effect of eclectic current is related to the background presence of an Euclidean space in which the conducting or insulating sample is embedded. Indeed, the incoming and outgoing current very far from the sample is represented by plane waves, which are themselves related to the representations of the Euclidean symmetry group. The modification for purposes of spaces with discrete translational symmetry is straightforward. An electron state in the sample is considered non-conducting, i.e. localised, if it has negligible overlap with any plane- or Bloch-wave state.

On the other hand, random graphs of the Erdős-Rényi, Barabási-Albert, etc. types cannot be typically embedded into a finite-dimensional Euclidean space in any physically plausible way. Sometimes this fact is formulated saying that these graphs are effectively infinite-dimensional; but we consider the labels unimportant. The point is that there are no plane waves which carry the current into the sample and which are reflected or pass through. Localisation cannot be related to vanishing conduction. Instead, the quantity called inverse participation ratio (IPR) $q^{-1}(\lambda)$ is applied as a measure of localisation. It depends implicitly on the system size N and it is just the behaviour at $N \to \infty$ which determines the localisation. If λ belongs to the range of eigenvalues whose eigenvectors are extended, then $\lim_{N\to\infty} q^{-1}(\lambda) = 0$. If, on the contrary, λ falls into the localised regime, then the limit $\lim_{N\to\infty} q^{-1}(\lambda)$ stays non-zero.

In my article [Slanina12] I applied a similar approach as in [Slanina11], defining, in addition to the "one-particle" function $\gamma(\omega)$, its "two-particle" counterpart

$$\Gamma(\omega,\omega') = \langle (e^{-\omega\, g(z)} - 1)(e^{-\omega'\, g(z')} - 1) \rangle \; . \tag{1.9}$$

If the joint equations for $\gamma(\omega)$ and $\Gamma(\omega,\omega')$ were solved, IPR could be deduced. The exact solution is unknown, but I was able to solve it in the same single shell approximation as in [Slanina11], with the same unfortunate artifact of spurious gaps.

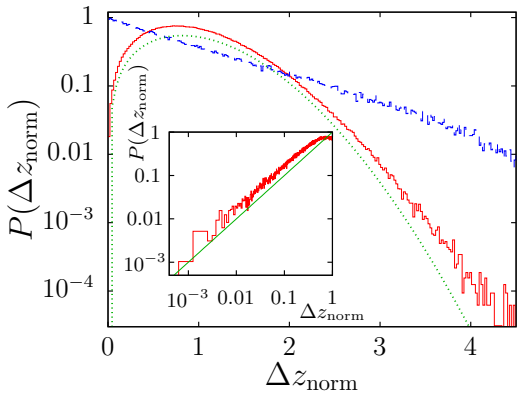

Figure 1.7: Distribution of normalised level spacings in the spectrum of random cubic graph with size $N = 1000$. The levels analysed are restricted to intervals $z \in [-0.1, 0.1]$ (solid line) and $z \in [-7, -6]$ (dashed line). The dotted line is the dependence $\propto \Delta z_{\rm norm} \exp\big(-a(\Delta z_{\rm norm})^2\big)$, with $a = 0.75$, which corresponds to the Gaussian orthogonal ensemble. In the inset we show the detail of the distribution at $z \in [-0.1, 0.1]$ for very small spacings. The straight line is the linear dependence $\propto \Delta z_{\rm norm}$.

For more reliable results I resorted to exact diagonalisation studies. I used random graphs of two types: first, the Erdős-Rényi graphs, second, the random cubic graphs, with a Gaussian random numbers added at the diagonals of the adjacency matrices. The size of graphs ranged from $N = 300$ to $N = 30000$ and the desired quantities, i.e. the density of states, IPR, and others, were averaged over as many as 10^5 realisations. (Less realisations for larger systems, of course.) From the analysis of the dependence of IPR on N I was able to determine the mobility edge, i.e. such a value of λ that separates the extended and localised states. The presence of localised states was established beyond any doubt. Interestingly, it was found that in the Erdős-Rényi graphs, the mobility edge is always quite close to the CPA band edge. (It is slightly beyond that, with the effect that there are still some extended states beyond the CPA edge, followed by localised states in the rest of the Lifschitz tail.) On the other hand, for the random cubic graphs with random diagonal the mobility edge is deep within the CPA band and the data suggest (although do not prove) that for a disorder strong enough there are only localised states present.

The result of [Slanina12] which I consider most important regards the level spacing statistics. It is a well-known fact that the eigenvalues of random matrices are spaced according to universal laws, which are independent of the form of the density of states, but reflect the symmetry properties of the ensemble of random matrices [98]. The classical example is the Gaussian Orthogonal Ensemble, where the level spacing statistics follows, with a very good accuracy, the Wigner formula

$$P_{\rm GOE}(x) \propto x\, {\rm e}^{-x^2} \ . \tag{1.10}$$

On the other hand, if the levels were scattered randomly, as in the case of a random matrix with all off-diagonal elements equal to zero, the statistics would be Poissonian

$$P_{\rm Poisson}(x) \propto {\rm e}^{-x} \ . \tag{1.11}$$

In the language of the quantum chaos theory, Wigner distribution corresponds to a chaotic system, while Poissonian to the non-chaotic, i.e. integrable one. Based on fairly general considerations

one can argue that the localised regime corresponds to Poissonian, while the extended regime to Wigner distribution of level spacings. This is just what I proved by exact diagonalisation, as seen in Fig. 1.7.

The reason why I consider the result important is the following. In the just explained sense we can interpret the metal-insulator transition due to crossing the mobility edge also a transition from chaotic to integrable phase. I consider this area very fruitful and open to new profound discoveries. One can, for example, speculate in the following direction: It is known that two-dimensional classical integrable systems solved by the Bethe ansatz have Poissonian distribution of energy levels. On the other hand, three-dimensional systems cannot be solved by Bethe ansatz and we can conjecture that they are chaotic. If there were a method which would be exact in 2 dimensions (reproducing Bethe ansatz) and at least approximate in 3 dimensions (not necessarily solving 3D Ising model exactly), the same method could be used to describe both localised and extended states in the localisation problem. Perhaps.

1.2.3 Sociophysics

Particles and games

In the quest of the unity of knowledge, people were always lead (and mislead) by the concepts and ideas that proved successful in a particular time and epoch. There were times when magnetism was called into service for explaining mysterious interactions between human souls. Newton's idea of an instant interaction at an arbitrary distance was perfectly in accord with the theory of the *unguentum armarium* tried as a means of planetary-wide synchronisation of clocks. In the early 19th century the unified theory of electricity was developed, based on purely chemical processes—chemistry was perhaps the most dynamic science at that time. And so on, and so forth. But laughing at such an old stuff is not very wise. In their proper times they were as serious theories as any other, as, for example the unified theory of elementary particles, based on the K-meson (thus avoiding the inaesthetic quarks) [103].

Nowadays, the scientific paradigm requires considering living beings, and especially humans, as inanimate entities. These views are sold to the general public under various sticky banners, like the selfish gene (although a specialist would explain to you that these are *not* genes, and *not* selfish, of course). Therefore, we cannot avoid the duty to try, how far we could go with the hypothesis that humans are just great molecules, with no soul at all. At the precise moment where this approach fails, the human soul rises. In a sense, this quest for a failure can be considered as experimental psychology.

It is physics whose job is explaining the properties of molecules, even if they are as big and as complex as human bodies. And physics can offer all the tools and skills accumulated in the studies of complex systems. As a brief introduction to the subject I would like to mention now just three models originating in physics, that are both very simple to formulate and very successful in elucidating social phenomena.

The society is viewed just as an ensemble of strongly interacting particles (i.e. human beings). Among the models physicists devised for strongly interacting entities, the Ising model is perhaps the best known. So, it seems quite natural that a situation in the society, where members should decide from two choices, was described in terms of the Ising model. We can imagine, for example, a big factory with angry workers who are about to go on strike. The two options are: strike "yes"

or "no". This is like spins choosing between "up" and "down". The social pressure due to the surrounding people is like the exchange interaction between spins; the combined pressure from the greedy employer and from the hungry children is like the external magnetic field. In this way the outburst of a strike is described by a phase transition [58].

The second is the voter model. In physics, it is used to describe catalysis [104, 105]. As a model of a society, it describes competition of two opinions. Again, the two options can be described by a two-state Ising variables S_i. The members of the society (we call them agents) are placed on the vertices of a lattice or a graph. To keep contact with physics, we can use a hypercubic lattice, or, to make the calculations easy, we put the agents on a complete graph. The system evolves as a Markov process in the following way. At each step, an agent i is chosen at random. Then, the agent looks at one of her neighbours (again chosen at random), say, the agent j. Then, the state is updated according to the neighbour

$$S_i(t+1) = S_j(t) \ . \tag{1.12}$$

Such a simple dynamics leads to surprisingly complex behaviour [106]. And most importantly, the model is exactly soluble on a hypercubic lattice in all dimensions. One step beyond the voter model is the Sznajd model, which is no longer exactly soluble. My own results in this line of research will be described later, when discussing the papers [SlaLav03] and [SlaSznPrz08].

The third is the so-called minority game. It is a scientific elaboration of a simple game called "zig-zag-zug", popular among children in Switzerland. It is played as follows. Three children stand face to each other, and stretch the right leg so that the tips of their shoes nearly touch each other. Then they say in unison "zig-zag-zug" and at the last "zug" they should either raise the foot or keep it down. If it happens that two players do the same move and the third remains alone, the third wins. The aim is to be in the minority. We can see something similar in an idealised description of the stock market. Imagine an ensemble of stockbrokers who decide either to sell or to buy a share in a company (e.g. in *Verenigde Oost-Indische Compagnie* if they lived in the early 17th century). When the majority of them buy, the price will probably rise and those who decided to sell can pocket a gain. And vice versa. We can see that if the *Beurs* worked as indicated, the minority option would be always profitable. The reality is always more complex, but the essence is grasped by the minority principle: who manages to be in the minority, wins. Clearly, the situation of agents is heavily frustrated, as by definition there is no universal strategy which would prescribe each agent to do the opposite than the majority does. The minority game model introduced by Challet and Zhang in 1997 [107] formulates this principle in a strict way. The most surprising feature of this model is the presence of a dynamical phase transition, which was studied in depth using the replica and generating functional methods [108, 109]. I contributed to this area by the paper [Slanina01] to be discussed in the next paragraph, as well as a few others [52, 110, 111].

Social imitation

In the paper [Slanina01] I took the minority game model as a starting point to study the consequences of imitation between agents.

In the minority game, each agent can choose between actions -1 or $+1$. The sum of actions of all agents is called attendance $A(t)$. Positive attendance means that the agents who chose -1 were in the minority and therefore are rewarded a point. Those in the majority are punished by taking off a point. The total number of points accumulated by an agent is her wealth (it can also

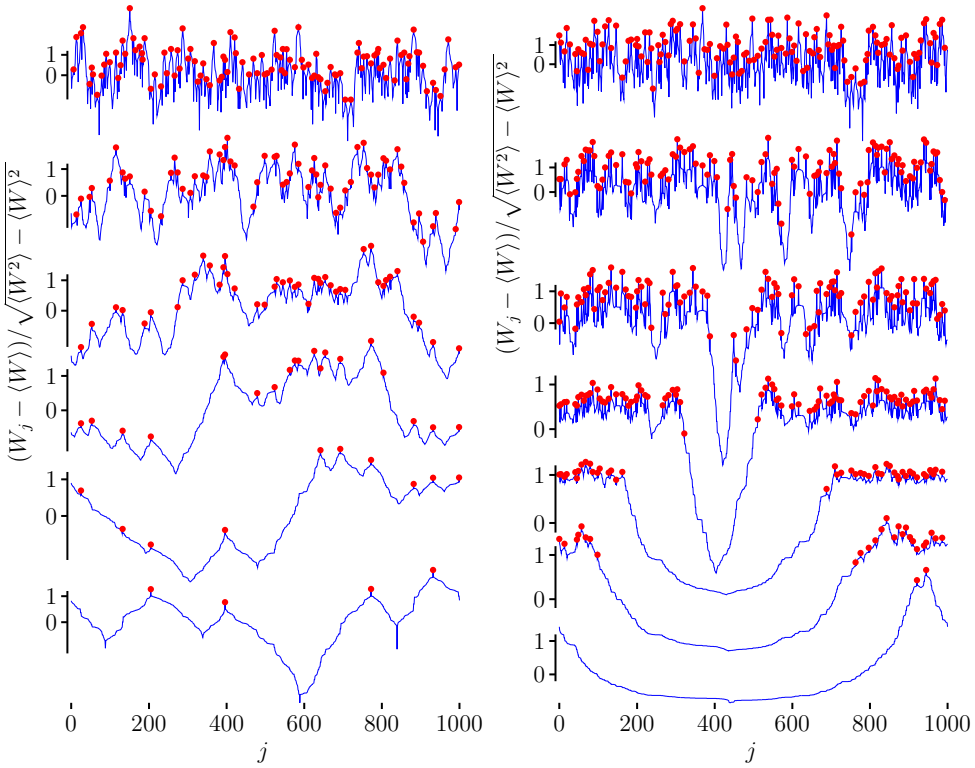

Figure 1.8: Two examples of time evolutions of the domains created by imitation. On the vertical scale, wealth of agents respective to average wealth, rescaled to average fluctuations. Time goes from the top to the bottom, which means that the top curve is the earliest, the bottommost is the last one. The heavy bullets indicate the leaders, i.e. agents who do not imitate anybody. These data of mine were actually published in the paper [52].

be negative). In order to predict the future, each agent owns two strategies which offer the agent actions according to the observed past outcomes. Besides the wealth of the agent, the "virtual" wealth, or score, is calculated for each strategy separately, which is the number of points which would be accumulated if the strategy was used all the time, with all other circumstances unchanged. The strategy which is actually used is the one with the highest score.

I modified the above scheme in the following way. I placed the agents on a social network, which in [Slanina01] was a simple linear chain, as well as in the preceding paper [110], while in the subsequent study [52] I used Erdős-Rényi and Barabási-Albert random graphs. When deciding her next action, the agent first compares her own wealth with that of the neighbours. If she is the richest of all, she uses the best of her own strategies. If she is not, she takes the same action as the richest neighbour. This way domains are formed within the social network, each of them acting in unison as a single big agent. Each domain has its leader, which is the richest agent of all within the domain. The other agents are imitators. During the evolution the fraction of imitators increases, as the domains grow in size, but eventually the fraction saturates. We can see the example of growing domains in Fig. 1.8. The model has two control parameters, the overall probability of imitation p and the price ε the imitators must pay to the imitated.

Besides the geometry of the imitation domains, we can observe the local and global measures of efficiency of the system. Globally, the efficiency of the minority game is measured by the

volatility, which in this context means the amplitude of fluctuations of the attendance around the most efficient state $A(t) = 0$. In the classical minority game, the volatility depends on the number of agents in a non-monotonous way. The minimum of volatility, i.e. the most efficient state is achieved at $N = N_c \equiv 2^M/\alpha_c$, where M is the length of the agents' memory and $\alpha_c = 0.3374...$ is a universal constant, defined as a root of a certain transcendental equation [108].

In my version I found that imitation increases the global efficiency (decreases the volatility) for $N > N_c$, which is quite natural, as the imitation effectively diminishes the number of agents and thus brings the system closer to the optimum. However, even for $N < N_c$ the imitation helps, if the tendency to imitation p is not too high: there is a minimum on the dependence of the volatility on p.

From the local perspective, the efficiency of the system was measured through the social tension, defined through the local differences in wealth between neighbours in the social network. It is quite interesting that the social tension depends strongly on the information cost ε. If the information is free, $\varepsilon = 0$, the imitation always lowers the tension. Indeed, the wealth inside domains more or less equalises and the tension is mostly due to the neighbourhood of the leader. But if the information is expensive, the leaders gain much more due to the fee paid by their followers, who are simply deemed to poverty. Imitation makes the social tension even stronger. In such a case, the remedy consists in lowering the number of leaders, i.e. increasing the incentive to imitation p. In plain words, if you already must be sucked by tycoons, let them be as few as possible.

Let me also add, as a note, that in the following paper [52] I worked in collaboration with my student H. Lavička on a generalisation to more complex social networks. We found, for example, that on the Erdős-Rényi graph the number of immediate followers is power-law distributed, despite the fact that the degree distribution of the underlying social network is Poissonian.

Sznajd and voter models on a full graph

The voter model shortly described earlier is very special as is allows for exact solution on a hypercubic lattice in every dimension. Without going into details, we can notice this fact when we write the equations of motion for the correlation functions. Usually, two-site correlation functions require three- or four-site correlation functions etc. so that the equations of motions never close. It is not the case for the voter model. The equation for single-site averages does not need any higher correlations, and the same holds for all other correlations.

There are more complex models in which this nice property is not satisfied any longer. One of them is the Sznajd model, named after the inventors Katarzyna Sznajd-Weron and Józef Sznajd (daughter and father) [112]. While in the voter model the opinion of a single agent is transmitted on her neighbour, in the Sznajd model it is necessary to have two neighbours of the same opinion in order that a neighbour of such a couple was converted to the same opinion. There are various cosmetic variants of the process, but all of them behave in essentially the same manner. For example, we can place the agents on a square lattice. If we find a pair of two neighbours of the same opinion, all the six nearest neighbours of the pair adopt the same opinion.

In the paper [SlaLav03] I calculated analytically the dynamics of the voter and Sznajd models in the case of agents placed on a full graph of N vertices. The co-author, the then-student of mine H. Lavička contributed by making numerical simulations which confirm my analytical results. In both voter and Sznajd model on a complete graph the state of the system is fully described by the magnetisation $m = (N_+ - N_-)/N$, where N is the total number of agents and $N_\pm$ are the numbers

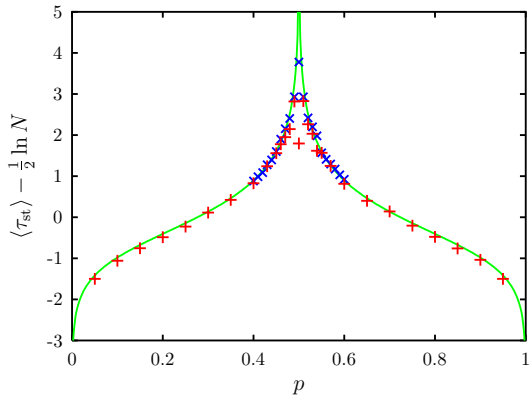

Figure 1.9: Average time of reaching the stationary state in the Sznajd model. The line is the exact analytic result, the points are the results of simulations by H. Lavička, for system size $N = 2000$ $(+)$ and $N = 4000$ $(\times)$.

of agents choosing the ± 1 options, respectively. We can write the master equations for the time dependence of the probability distribution of the magnetisation, which in the voter case is

$$\frac{\partial}{\partial \tau} P_m(m,\tau) = \frac{\partial^2}{\partial m^2} \left[(1-m^2)\, P_m(m,\tau) \right] \tag{1.13}$$

and in the Sznajd case is

$$\frac{\partial}{\partial \tau} P_m(m,\tau) = -\frac{\partial}{\partial m} \left[(1-m^2) m\, P_m(m,\tau) \right] \quad . \tag{1.14}$$

The solution of Eq. (1.13) consists of two δ-functions at the edges of the allowed interval, i.e. at $m = -1$ and $m = 1$, and of a regular part, which is a continuous function on the support $(-1, 1)$. The regular part is obtained by finding the (left as well as right) eigenfunctions of the (non-Hermitian) linear operator standing on the right-hand side of (1.13). As for the right eigenfunctions, they are proportional to the Gegenbauer polynomials. The eigenvalues determine the sequence of relaxation times. For a comparison, H. Lavička performed very careful simulations of the model, from which a few first relaxation times can be extracted. The agreement with the exact results is excellent.

Eq. (1.14) is a different case, as it contains only the first derivative. The diffusive term vanishes in the limit $N \to \infty$ leaving just a deterministic drift dynamics. We can be interested, e.g. in the average time to reach a stationary time in which all agents have the same opinion. It will depend on the fraction p of those who have had the opinion $+1$ at the beginning, and, of course, on the total number of agents N. The result is

$$\langle \tau_{\rm st} \rangle = -\ln \left(\frac{|2p-1|}{\sqrt{p(1-p)}} \frac{1}{\sqrt{N}} \right) \tag{1.15}$$

and as we can see in Fig. 1.9, the simulations agree very well with the exact theory. Note that the time to reach stationarity diverges at $p = 1/2$, signalling a dynamical phase transition. In contrast, in the voter model such a transition is absent.

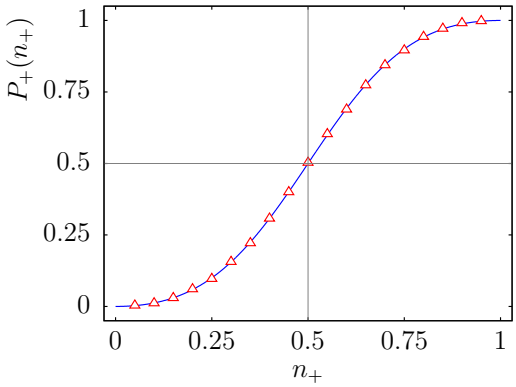

Figure 1.10: One-dimensional Sznajd model. Probability of reaching the final configuration of all sites in state $+1$, depending on the initial concentration n_+ of $+1$ sites. The points are numerical simulation data; the line is the analytical result obtained using the Kirkwood approximation.

One-dimensional Sznajd model

The complete graph corresponds to the limit of infinite dimension and in such a situation the mean-field theory is known to be reliable. On the other hand, one-dimensional systems are perhaps the farthest possible from what mean-field theories predict: there are no phase transitions, etc. However, in the paper [SlaSznPrz08] I showed how an approximation usually classified as mean-field-like, gives extraordinarily good results. The paper [SlaSznPrz08] is co-authored also by K. Sznajd-Weron and her student P. Przybyła. I did all the analytical calculations myself, the others performed all the computer simulations.

The point is that the equation of motion for the average $C_0(t) = \langle\sigma(y)\rangle$ contains higher correlations functions $C_1(n;t) = \langle\sigma(y)\sigma(y+n)\rangle$, $C_2(n,m;t) = \langle\sigma(y-n)\sigma(y)\sigma(y+m)\rangle$ etc. In particular, we obtain the equations

$$\begin{aligned} \frac{\mathrm{d}}{\mathrm{d}t}C_0(t) &= -C_2(1,1;t) + C_0(t) \\ \frac{\mathrm{d}}{\mathrm{d}t}C_1(1;t) &= -C_3(1,1,1;t) - C_1(1;t) + C_1(3;t) + 1\ . \end{aligned} \tag{1.16}$$

To close the chain, we use the Kirkwood approximation

$$\begin{aligned} C_2(1,1;t) &\simeq C_1(1;t)C_0(t) \\ C_3(1,1,1;t) &\simeq \big(C_1(1;t)\big)^2\ . \end{aligned} \tag{1.17}$$

This kind of approximation is usually called decoupling in the context of condensed matter physics. It is considered justified if the fluctuations are small, which is the same argument which also justifies the mean-field approximation. Therefore, decoupling and mean-field approximations are closely related, and indeed, in many cases (but not always) they are identical.

Making the Kirkwood approximation in (1.16), we can calculate the dynamics of the correlations and eventually find the probability P_+ that the final configuration will have all agents in state $+1$. It depends only on the initial concentration of $+1$ opinions, denoted n_+ and the result is

$$P_+(n_+) = \frac{n_+^2}{(1-n_+)^2 + n_+^2}\ . \tag{1.18}$$

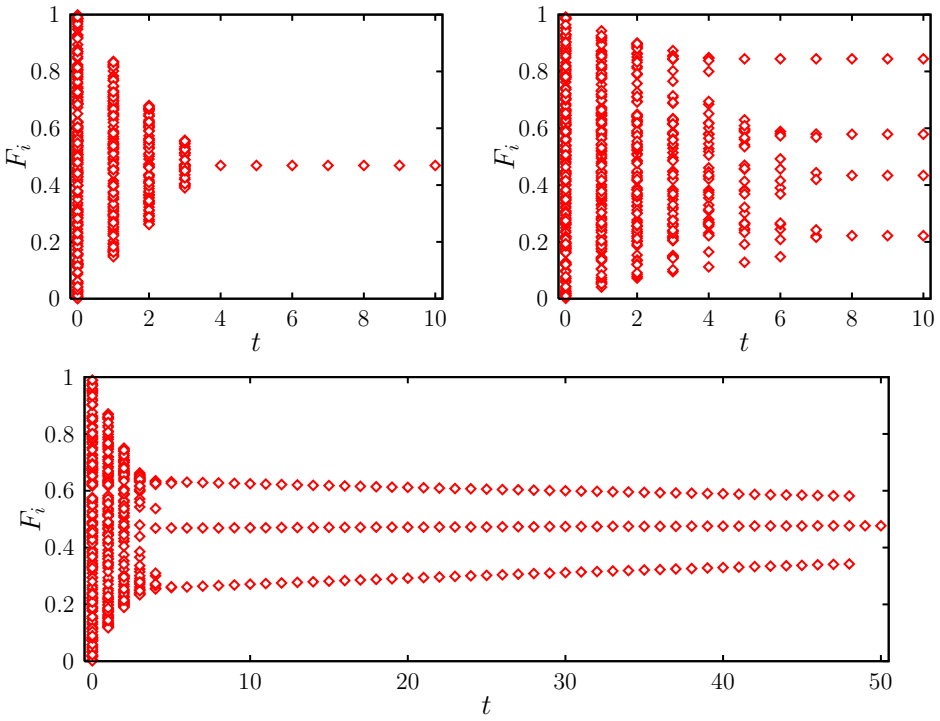

Figure 1.11: Evolution of the Hegselmann-Krause model. Each point represents one or more agents with a specified value of the opinion F_i. The total number of agents is $N = 200$. In the upper left panel, we show the case in which full consensus is reached. In the upper right panel, the population splits into several non-communicating stable groups. In the lower panel we show how the approach to consensus is slowed down when the confidence bound is close to its critical value.

We can see in Fig. 1.10 how the approximation (1.18) compares with the results of computer simulations (the simulation data for Fig. 1.10 were obtained by myself, rather than taken from [SlaSznPrz08]). In my personal view, the agreement is impressive. How is it possible that an approximation that should work well in high dimensions, is so good in one-dimensional case? I do not posses any satisfactory answer, neither I know any literature which would elucidate this phenomenon. Let us recall that similar thing was already observed in the one-dimensional ricepile [Slanina02]. Moreover, I came across such behaviour also in the analysis of the interacting gaps model of an order book [113] (more on order books and related issues will be found in the following).

Hegselmann-Krause model of consensus formation

In the voter, Sznajd and related models, agents have only very restricted choice of two opinions. In reality, people's views on many matters can vary in a wide range and multitude of intermediate positions are held. One step towards reality is the introduction of continuous options F, e.g. from the interval $[0, 1]$. When people meet, they adjust their opinions, thus moving within the allowed interval. The ultimate state may or may not be the full consensus, i.e. the state in which all agents occupy the same point within the interval. The first model of this kind was devised by DeGroot

[114] and if we simplify his findings a lot, one can say that sooner or later consensus is always reached, provided that there are no subgroups of agents who never communicate with the rest.

Such a conclusion is too trivial and contradicts all what we observe in society. Divisions and struggles are ubiquitous, consensus is very rare. To account for that, the idea of bounded confidence was implemented in such a sense that agents whose opinions within the interval $[0, 1]$ differ more than a certain level $\varepsilon > 0$, do not influence each other. If the agents are closer than ε, their opinions move towards each other, thus promoting the consensus.

One of the models of this type is the model of Hegselmann and Krause [115]. I investigated the model in the paper [Slanina11a]. The questions I asked are related to the fact that for ε large enough full consensus is reached, like in DeGroot's model, while for small ε the ensemble of agents eventually splits into groups which are more distant than ε, and therefore do not communicate with each other. Consensus is never reached. Examples of such evolution are shown in the two top panels in Fig. 1.11.

Moreover, close to the value of ε separating the consensus and no-consensus phase, the dynamics is slowed down, much like the dynamics in the vicinity of second-order equilibrium phase transitions (see the lower panel in Fig. 1.11). In the article [Slanina11a] I investigated this slowing down in a great detail. The essential finding was the role of mediators, i.e. individuals or tiny groups who are able to join and attract macroscopically large ensembles of agents. For example I found that the spectrum of relaxation times close to the transition not only contains long time values, but is composed of several distinct peaks. I deciphered these peaks as corresponding to mediator groups consisting of one, two, three, etc. agents.

The ultimate conclusion, although hypothetical, from this study seems rather paradoxical: the apparent dynamical phase transition from consensus to no-consensus phases seems to be a pure finite-size effect. In the thermodynamic limit, there will be always enough mediators who would guarantee the final consensus. When the number of agents increases, the transition become more and more pronounced and simultaneously shifts to lower values of ε. In an infinite system, the transition disappears.

In fact, such a situation is not uncommon in the models of social phenomena. Quite often the interesting phenomena are "just" finite-size effects. Rather than being discarded as marginal, these phenomena pose fundamental questions on how to deal with large but still finite systems. And this is one of the pivotal questions of the science of complexity.

1.2.4 Econophysics

A branch of sociophysics

Among the various aspect of social life economy is the one which touches virtually anybody. Therefore, in the ages of science it seems inevitable to describe and govern economy on a scientific basis. In the places like Prague such efforts are unfortunately often related to the bankrupt "scientific" theories of Marxism-Leninism. It is therefore quite understandable psychologically that the attempts to employ somewhat more exact intellectual habits *à la physique* in economics is not always welcome in the professional community. However, in my view it is vital to defend the scientific spirit even in the areas where it is considered suspicious. Therefore, I consider very useful to take all attempts to bring exactitude to the fields like economics. If physics proves really useful here, why not using it? This is the motivation for the field of econophysics. I will discuss

just two problems where physical approaches succeeded, at least partially. The first of them concerns the distribution of wealth in society, the second deals with the microscopic details of trading at the stock market.

Wealth distribution

The perspective for survival in a modern capitalist economy is often reduced to various measures of individual and corporate wealth. Disproportions in wealth distribution across society are also causes, either virtual or actual or both, of social tensions, resulting in incessant dynamics affecting the whole social structure. The distribution of wealth (expressed by diverse indicators) was therefore the first concern in quantitative analyses started in 19th century.

If there were a gallery of founding fathers of what is now econophysics, surely it would include Vilfredo Pareto. In his book *Cours d'économie politique* [65], published in 1897, he formulated the law for income distribution stating that the number N of individuals having an income greater than v is

$$N = \frac{A}{(v+b)^{\alpha}} \tag{1.19}$$

where b is a constant very close to zero and the value of the exponent α lies between 1 and 2.

A closer look reveals, unfortunately, small but systematic deviations from the power-law dependence, which are more pronounced at low incomes. Eventually, a consensus grew that the universal Pareto law is indeed applicable for a small fraction of society enjoying high incomes, while the rest of society is governed by non-universal laws, i.e. distribution of lower incomes is sensitive to the details of the actual social situation [116–118]. In fact, it is not so much the functional form of the Pareto law but its spatial and temporal stability that is intriguing. Indeed, while the value of the exponent α may slightly vary from one society to another, the very fact of the power-law tail in the distribution is valid almost everywhere. Some investigations suggest that the range of validity of the Pareto law may extend as far in the past as to ancient Egypt of the Pharaohs [119].

Non-conservative scattering model

In the early 1960s B. Mandelbrot came with the idea that wealth might be described according to the Lévy distribution [120] which possesses the nice property of having a power-law tail at $v \to \infty$ like Eq. (1.19). Interestingly, this line of thought led Mandelbrot further to the discovery of Lévy distribution in the price changes of cotton [66] and this was (according to his personal testimony) the turning point which eventually resulted in the introduction of fractals and their wonderful new world [121].

It was also Mandelbrot [120] who first suggested that the dynamics of wealth distribution in society might be modelled similarly as the energy distribution within a large ensemble of interacting particles. As particles (people) interact, energy (wealth) is redistributed among them. Unfortunately, as Mandelbrot noticed, energy is distributed exponentially, while wealth follows the Lévy distribution. Therefore, the analogy was not pursued further for a very long time.

Instead, wealth distributions were modelled by various stochastic processes of multiplicative-additive type. The main lesson from them was that in order to obtain a power-law tail the Pareto law requires, wealth must not be a strictly conserved quantity. And this is just the idea I used in my

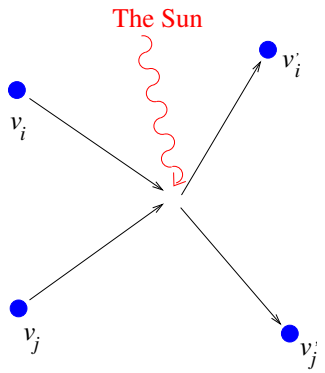

Figure 1.12: The ultimate source of the increase of total wealth of interacting agents is the energy coming from the Sun.

paper [Slanina04]. Partially I took inspiration from the earlier studies on the inelastic scattering processes in granular gases [122]. You can make a granular gas yourself in your garage if you shake an oil can partly filled with sand. The grains of sand keep moving as long as you keep shaking. The energy dissipation at collisions makes them come to rest quickly after you stop injecting energy from the outside.

I imagined an opposite situation. Instead of sand grains I considered individuals involved in an economic exchange. At each scattering event, the wealth is redistributed, but the total sum increases and, on average, interaction brings profit to all. Of course, the non-conservation of wealth is due to the fact that the whole economic system is open and the source of wealth increase can be traced up to the energy influx from the Sun (see Fig. 1.12). The wealths of the agents i and j affected by a scattering event change according to

$$\begin{pmatrix} v_i(t+1) \\ v_j(t+1) \end{pmatrix} = \begin{pmatrix} 1+\epsilon-\beta & \beta \\ \beta & 1+\epsilon-\beta \end{pmatrix} \begin{pmatrix} v_i(t) \\ v_j(t) \end{pmatrix} . \tag{1.20}$$

The parameter β measures the amount of the exchange, while ϵ is the non-conservation parameter. The situation $\epsilon < 0$ corresponds to the known case of granular gas with dissipation. Unfortunately, the solution cannot be analytically continued to positive ϵ, because there is a singularity just at $\epsilon = 0$. Therefore, the solution must be found anew. This is what I did in [Slanina04].

As the total wealth increases, there is no true stationary solution, but if the time-dependent distribution is rescaled by the average wealth, $w = v/\overline{v}$, the following distribution is finally found

$$\Phi(w) = \frac{(\alpha-1)^\alpha}{\Gamma(\alpha)}\, w^{-\alpha-1} \exp(-\frac{\alpha-1}{w}) . \tag{1.21}$$

Clearly, the distribution exhibits the desired power-law tail. The Pareto exponent α depends on the parameters β and ϵ. At very low incomes the probability is suppressed, in accordance with published empirical data [118]. Therefore, the result (1.21) can be considered as a fairly successful model for the wealth distribution seen in reality.

Price fluctuations and order books

It is not only the number on your account statement that matters to you. Equally important question is how much of this or that commodity you can buy, if you need it. That is, what are the prices

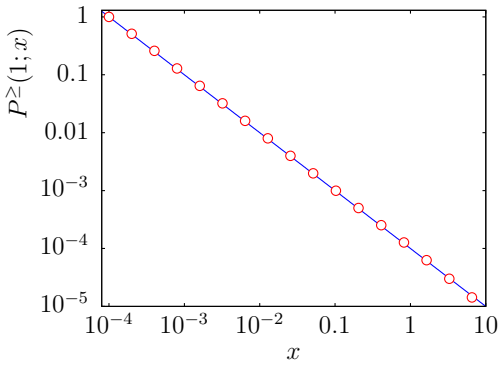

Figure 1.13: Cumulative distribution of one-step price changes in the matrix multiplicative process for order-book dynamics. The line is the power x^{-1}.

of things. The things which are traded most are the least useful by themselves: currencies, shares, bonds, and the like. These things are not sold in shops but at the stock market, more specifically at a stock exchange. The stock exchange is a highly complex organisation which, on one hand, provides a space for others to perform their trades, but on the other hand, pursues its own goals, or even more precisely, an organisation which is owned by somebody and serves to the goals of the owners.

In addition, the organisation is managed and structured so that these goals are achieved most efficiently. That is why the internal functioning of various stock exchanges (New York Stock Exchange, London Stock Exchange, Paris Bourse, NASDAQ, Deusche Börse, etc.) looks different. Now, the electronic trade becomes widespread and the instrument to match the offers to buy and sell is the order book.

Orders are requests of selling or buying a specified amount of shares or commodity. Limit orders specify the price at which the deal is to be executed. They wait until somebody is willing to accept such price. Market orders do not specify the price but are executed immediately at the best price available. The order book is the double list of waiting limit orders. New orders are inserted as they come and are wiped out when they meet a partner and are executed. Therefore, the order book is a dynamical system with a long memory. Physically, we can view the order book as a one-dimensional system, a price axis on which particles of two types are deposited. Particles of type A correspond to sell orders, particles of type B to buy orders. Clearly, particles of type A are always on the right of the particles of type B; otherwise a trade occurs and the orders are removed. The current price lies in the middle between the lowest A and the highest B.

There are many models of order books which differ in the ways the particles are deposited and the trades are performed. Two articles of mine [Slanina01a] and [Slanina08] will be discussed in the following. Moreover, I contributed to the field also by papers [113, 123] which deal with the interacting gaps model, introduced by Sorin Solomon. Interestingly, this model, as I and my student A. Svorenčík showed in [113], is yet another example of a one-dimensional system very well described by a mean-field-like approximation, as were the ricepile [Slanina02] and 1D Sznajd [SlaSznPrz08] models discussed above.

Random matrix multiplicative process

In the paper [Slanina01a] I investigated a very simple version of an order book. In reality, the density of orders on each side from the price is a very complicated and fluctuating function. A very drastic but useful approximation consists in taking only average densities $\rho_\pm$ above and below the price. Or, equivalently, we can work with the virtual price changes which are related to the densities as $x_\pm = 1/\rho_\pm$. It comes out that the dynamics of the vector $X = \binom{x_+}{x_-}$ due to arrival of orders and executing trades can be written as a matrix multiplication process $X(t+1) = M(t)X(t)$ where the matrix $M(t)$ is chosen randomly from the set $\{M_0, M_+, M_-\}$ with probabilities p_0, p_+, and p_-, respectively.

The distribution of price changes (the most studied quantity in empirical econophysics) is then given by the probability distribution of the elements of the vector X. It can be found very easily by numerical simulations (see Fig. 1.13) showing a power-law tail $\sim x^{-\alpha-1}$ with $\alpha = 1$. However, this is not a very appealing procedure, because numerical results can be already obtained using much more realistic models. Fortunately, and this is the central point of the paper [Slanina01a], there is a way how to calculate the exponent α analytically. I got the value $\alpha = 1$ exactly, in full accord with the numerics. The method can be further refined to include non-constant densities $\rho_\pm$. These results are not contained in [Slanina01a], but appear in my forthcoming book [71].

Deposition models

The model discussed in the previous paragraph is elegant but much too idealised to be directly comparable with reality. In [Slanina08] I performed detailed numerical study of several more realistic models of order books. The first of them was the model originally devised by Bak, Paczuski,and Shubik [124]. In this model, there are no market orders, but the limit orders may freely diffuse and particles of type A and B annihilate each other when they meet. In fact, it is an extreme case of a reaction-diffusion model. The immediate annihilation makes the analytical treatment more difficult, but here I concentrated on simulations anyway. Unfortunately, I found that the distribution of price changes totally contradicts the empirical data, so that this model is discarded from further considerations.

Much better does the generalisation of the old Stigler model [125], which is known under the name Genoa artificial market. I have shown that the distribution of price changes as well as long autocorrelations of absolute price changes are very well in accord with the empirics.

Still, the Genoa model does not reflect entirely the "microscopic" details of the deposition and execution of orders. The main ingredient lacking are the market orders. They are introduced in the models of Maslov [126] and Farmer et al [127], which I thoroughly investigate in the rest of the paper [Slanina08]. I found that the most promising scheme is the Maslov model with "evaporation" of orders (the person who issued the order is allowed to cancel it prematurely). In Fig. 1.14 we can see an example of the price-time diagram of the evolution of the order book in this model. (Note that the vertical axis shows the logarithm of price, not the price itself!) We can see that the price is pinned between the A and B particles, but time to time it performs big jumps when the density of orders on one side diminishes due to a random fluctuation. This way the simple fluctuations of density are translated into a very complex fluctuations of price, exhibiting power-law tails in distributions and very slow decay of autocorrelations, indicating a long memory. In

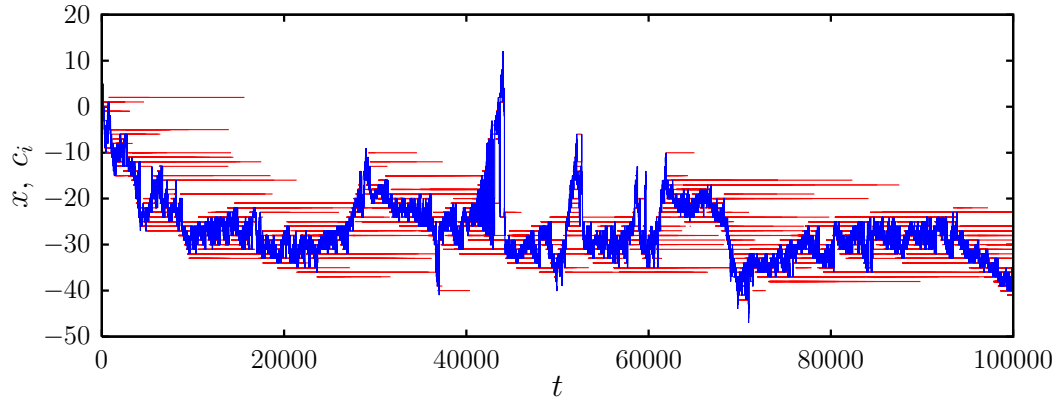

Figure 1.14: Example of the evolution of the Maslov model with cancellations. Each horizontal segment represents an order, placed where the segment starts and cancelled or executed where the segment ends. The rugged line is the time dependence of the logarithm of price.

short, the process is strongly non-Markovian. I consider this model a good candidate for realistic simulations of what happens on the stock market.

1.3 Summary

My works collected in this thesis pertain to a fluid area of inter-disciplinary physics. Despite the diversity of the problems solved, there are several common approaches which repeat themselves in most of them.

The first one is the use of stochastic processes. This is a simplification which is not obvious, as the models of non-equilibrium physical systems always tend to prefer many-particle systems with Hamilton dynamics, as testified by the emphasis on molecular dynamics simulations. Indeed, even the use of the Boltzmann equation may seem suspicious when we investigate the most fundamental questions like the fluctuation symmetries [128]. Similarly, the description of real granular media cannot stop at the level of stochastic sandpiles introduced by Bak [29] or dissipative scattering along the lines of the Maxwell model [122]. Therefore, the stochastic modelling may be insufficient when we require predictions comparable with reality.

On the other hand, the science of complexity considers irrelevant (very much like the renormalisation group theory) many of the features of the dynamics which are contained in the true Hamiltonian description. It is not too much exaggerated saying that in the complex dynamics the Hamiltonian is irrelevant and the system is described algorithmically. Indeed, most models described in this thesis are defined by a simulation algorithm, which is only afterwards translated into transition probabilities of a certain complicated Markov process. This is the case of all the self-organised critical models shown here, i.e. ricepile [Slanina02], cracking [Slanina99a], as well as friction [Slanina99] and evolution [SlaKot00] models; this is also the case of the order book models [Slanina08], minority game [Slanina01], and the opinion and consensus models [SlaLav03], [SlaSznPrz08], and [Slanina11a]. You can see that these methods permeat the whole thesis.

Besides the algorithmic character of the models described, the most frequent methodological approach was the use of the mean-field approximation, under several disguises. The most straight-

forward procedure is placing the interacting entities on a complete graph, or allowing everybody to interact with everybody else. This way we get rid of all problems due to the structure of the lattice or network on which the entities reside. This was done explicitly in the voter and Sznajd models on a complete graph [SlaLav03], and implicitly in the scattering model of wealth distribution [Slanina04].

Less transparent was the use of the mean-field schemes in one-dimensional systems, namely in the ricepile [Slanina02], the 1D Sznajd [SlaSznPrz08], and the (one-dimensional by definition) order-book model [Slanina01a]. Also the study of spectra and localisation in random graphs yielded closed analytical results only under mean-field-like assumptions on the solution [Slanina11]. In fact, virtually all the cases where the analytical calculations were successfully carried until the final result were also the cases where the mean-field ideology was the leading thread.

I think the small sample of interdisciplinary physics shown in this thesis suggests that physics can be useful to other disciplines: there is a method for analysing empirical networks; there are models of stock-market fluctuations; opinion-spreading models may help to understand election results. A complementary question is whether the interdisciplinary science can be also useful to physics. The results may seem ambiguous, but I still keep the optimistic attitude. For example, the physics of dry friction and cracking (as well as wear and fatigue) is to large extent open and little-understood. The ideas of self-organised criticality did bring progress, although they did not offer any miraculous answers. And this is the field to which i contributed by my piece of the puzzle [Slanina99], [Slanina99a].

To conclude, I do not want to exaggerate the importance of the physics of complex systems in the context of other rapidly developing fields. However, there are numerous difficult and challenging problems the physics of complexity offers and it is worth spending time in attempts to solve them. This is what I tried during the research which makes part of this thesis. The adventure was interesting; and I believe I brought home some fruits.

Bibliography

[1] G. Parisi, Physica A **263**, 557 (1999).

[2] P. W. Anderson, Science **177**, 393 (1972).

[3] K. G. Wilson, Phys. Rev. B **4**, 3174 (1971).

[4] K. G. Wilson, Phys. Rev. B **4**, 3184 (1971).

[5] F. Slanina and M. Kotrla, Physica A **256**, 1 (1998).

[6] P. Prusinkiewicz and A. Lindenmayer, *The Algorithmic Beauty of Plants* (Springer, New York, 1990).

[7] T. A. Witten Jr. and L. M. Sander, Phys. Rev. Lett. **47**, 1400 (1981).

[8] M. Kardar, G. Parisi, and Y.-C. Zhang, Phys. Rev. Lett. **56**, 889 (1986).

[9] Mehran Kardar, Nucl. Phys. **290**, 582 (1987).

[10] E. Medina, T. Hwa, M. Kardar, and Y.-C. Zhang, Phys. Rev. A **39**, 3053 (1989).

[11] L.-H. Gwa and H. Spohn, Phys. Rev. A **46**, 844 (1992).

[12] M. Mézard and G. Parisi, J. Phys. I France **1**, 809 (1991).

[13] M. Kotrla, M. Předota, and F. Slanina, Surf. Sci. **402-404**, 249 (1998).

[14] F. Slanina, J. Krug, and M. Kotrla, Phys. Rev. E **71**, 041605 (2005).

[15] S. F. Edwards and P. W. Anderson, J. Phys. F: Met. Phys. **5**, 965 (1975).

[16] D. Sherrington and S. Kirkpatrick, Phys. Rev. Lett. **35**, 1792 (1975).

[17] M. Mézard, G. Parisi, and M. A. Virasoro, *Spin Glass Theory and Beyond* (World Scientific, Singapore 1987).

[18] D. J. Amit, *Modeling Brain Function* (Cambridge University Press, Cambridge, 1989).

[19] M. Mézard, G. Parisi, and R. Zecchina, Science **297**, 812 (2002).

[20] S. Kirkpatrick, C. D. Gelatt Jr., and M. P. Vecchi, Science **220**, 671 (1983).

[21] N. Sourlas, in: From Statistical Physics to Statistical Inference and Back, ed. P. Grassberger, and J.-P. Nadal p. 195 (Kluwer Academic Publishers 1994).

[22] M. Mézard and G. Parisi, Phys. Rev. Lett. **82**, 747 (1999).

[23] M. Mézard and G. Parisi, J. Phys.: Condens. Matter **12**, 6655 (2000).

[24] G. Parisi, in: *Perspectives on Biological Complexity*, Eds. O. T. Solbrig and G. Nicolis (IUBS, Paris, 1994).

[25] G. Parisi and F. Slanina, Europhys. Lett. **17**, 497 (1992).

[26] G. Parisi, F. Ritort, and F. Slanina, J. Phys. A: Math. Gen. **26**, 247 (1993).

[27] G. Parisi, F. Ritort, and F. Slanina, J. Phys. A: Math. Gen. **26**, 3775 (1993).

[28] G. Parisi and F. Slanina, Eur. Phys. J. B **8**, 603 (1999).

[29] P. Bak, C. Tang, and K. Wiesenfeld, Phys. Rev. Lett. **59**, 381 (1987).

[30] P. Bak, *How nature works: The science of self-organized criticality* (Copernicus, New York, 1999).

[31] N. Eldredge and S. J. Gould, in: *Models in paleobiology*, ed. T. J. M. Schopf, p. 82 (Freeman, Cooper and Co., San Francisco, 1972).

[32] D. M. Raup and J. J. Sepkoski Jr., Science **215**, 1501 (1982).

[33] P. Bak and K. Sneppen, Phys. Rev. Lett. **71**, 4083 (1993).

[34] F. Slanina and M. Kotrla, Phys. Rev. Lett. **83**, 5587 (1999).

[35] M. Kotrla, F. Slanina, and J. Steiner, Europhys. Lett. **60**, 14 (2002).

[36] P. Erdős and A. Rényi, Pub. Math. Debrecen **5**, 290 (1959).

[37] M. E. J. Newman, A.-L. Barabási, and D. J. Watts (Eds.), *The Structure and Dynamics of Networks* (Princeton University Press, Princeton, 2006).

[38] S. Milgram, Psychology Today **1**, 61 (1967).

[39] D. J. Watts and S. H. Strogatz, Nature **393**, 440 (1998).

[40] A.-L. Barabási and R. Albert, Science **286**, 509 (1999).

[41] H. Kesten, Acta Mathematica **131**, 207 (1973).

[42] S. N. Dorogovtsev and J. F. F. Mendes, *Evolution of Networks* (Oxford University Press, Oxford, 2003).

[43] R. Pastor-Satorras and A. Vespignani, *Evolution and Structure of the Internet* (Cambridge University Press, Cambridge, 2004).

[44] G. Caldarelli, *Scale-Free Networks* (Oxford University Press, New York, 2007).

[45] M. E. J. Newman, *Networks* (Oxford University Press, New York, 2010).

[46] X. Jia, C. Caroli, and B. Velicky, Phys. Rev. Lett. **82**, 1863 (1999).

[47] P. W. Anderson, Phys. Rev. **109**, 1492 (1958).

[48] S. Fortunato, Phys. Rep. **486**, 75 (2010).

[49] M. Marsili, F. Vega-Redondo, and F. Slanina, Proc. Natl. Acad. Sci. U.S.A. **101**, 1439 (2004).

[50] F. Vega-Redondo, M. Marsili, and F. Slanina, Journal of the European Economic Association **3**, 628 (2005).

[51] F. Slanina and Y.-C. Zhang, Acta Phys. Pol. B **36**, 2797 (2005).

[52] H. Lavička and F. Slanina, Eur. Phys. J. B **56**, 53 (2007).

[53] F. Slanina, Adv. Compl. Syst. **15**, 1250053 (2012).

[54] P. A. M. Dirac, Proc. Roy. Soc. London A **123**, 714 (1929).

[55] F. Ritort, Poincaré Seminar **2**, 195 (2003).

[56] S. Galam, Physica A **336**, 49 (2004).

[57] N. A. Chigier and E. A. Stern (Eds.), *Collective Phenomena and the Applicatios of Physics to Other Fields of Science* (Brain Research Publications, Fayetteville, 1975).

[58] E. Callen and D. Shapero, Phys. Today **27**, 23 (July 1974).

[59] E. Majorana, Scientia **36**, 58 (1942).

[60] A. Comte, *Plan des travaux scientifiques nécessaires pour réorganiser la société* (1822).

[61] A. Comte, *Cours de philosophie positive*, tome IV, 46^{e} leçon (Bachelier, Paris, 1839).

[62] A. Quételet, *Du système social et des lois qui le régissent* (Guillaumin, Paris, 1848).

[63] D. Štys and M. Vlačihová, arXiv:1007.0472 (2010).

[64] G. von Buquoy, *Die Theorie der Nationalwirthschaft nach einem neuen Plane und nach mehrern eigenen Ansichten dargestellt*, (Breitkopf und Härtel, Leipzig, 1815).

[65] V. Pareto, *Cours d'économie politique* (Lausanne, F. Rouge, 1897).

[66] B. Mandelbrot, Journal of Business **36**, 394 (1963).

[67] R. N. Mantegna, Physica A **179**, 232 (1991).

[68] P. W. Anderson, K. J. Arrow, and D. Pines (Eds.), *The Economy as an Evolving Complex System* (Addison Wesley, Reading, 1988).

[69] R. N. Mantegna and H. E. Stanley, *Introduction to Econophysics: Correlations and Complexity in Finance* (Cambridge University Press, Cambridge, 2000).

[70] J.-P. Bouchaud and M. Potters, *Theory of Financial Risk and Derivative Pricing* (Cambridge University Press, Cambridge, 2003).

[71] F. Slanina, *Essentials of Econophysics Modelling* (Oxford University Press, Oxford, 2014).

[72] P. Bak, K. Chen, J. Scheinkman, and M. Woodford, Ricerche Economiche **47**, 3 (1993).

[73] A. Namatame, T. Kaizoji, and Y. Aruka (Eds.), *The Complex Networks of Economic Interaction* (Springer, Berlin, 2006).

[74] F. Slanina, in: *Encyclopedia of Complexity and Systems Science*, p. 8379 (Springer, New York, 2009).

[75] F. Slanina, in: *Oder, disorder, and criticality, vol. 3*, ed. Y. Holovatch, p. 201 (World Scientific, Singapore, 2012).

[76] B. N. J. Persson and E. Tosatti, eds., *Physics of Sliding Friction, NATO ASI Series, Applied Sciences, vol. 311* (Kluwer Academic Publishers, Dordrecht, 1996).

[77] Y. Frenkel and T. Kontorova, Zh. Eksp. Teor. Phys. **8**, 89 (1938).

[78] C. Caroli and B. Velicky, J. Phys. I France **7**, 1391 (1997).

[79] S. I. Zaitsev, Physica A **189**, 411 (1992).

[80] J. Šmíd and J. Novosad, Institution of Chemical Engineers Symposium Series **63**, D3/V/1 (1981).

[81] J. .P. Wittmer, P. Claudin, M. E. Cates, and J.-P. Bouchaud, Nature **382**, 336 (1996).

[82] C.-H. Liu, S. R. Nagel, D. A. Schecter, S. N. Coppersmith, S. Majumdar, O. Narayan, and T. A. Witten, Science **269**, 513 (1995).

[83] V. Frette, K. Christensen, A. Malte-Sørenssen, J. Feder, T. Jøssang, and P. Meakin, Nature **379**, 49 (1996).

[84] L. A. N. Amaral and K. B. Lauritsen, Phys. Rev. E **54**, R4512 (1996).

[85] M. Markošová, M. H. Jensen, K. B. Lauritsen, and K. Sneppen, Phys. Rev. E **55**, R2085 (1997).

[86] S. Zapperi, K. B. Lauritsen, and H. E. Stanley, Phys. Rev. Lett. **75**, 4071 (1995).

[87] M. Molloy and B. Reed, Random Structures and Algorithms **6**, 161 (1995).

[88] P. L. Krapivsky and D. Redner, Phys. Rev. E **63**, 066123 (2001).

[89] S. N. Dorogovtsev, J. F. F. Mendes, and A. N. Samukhin, Phys. Rev. Lett. **85**, 4633 (2000).

[90] S. N. Dorogovtsev, J. F. F. Mendes, and A. N. Samukhin, cond-mat/0011077.

[91] S. N. Dorogovtsev and J. F. F. Mendes, Proc. Roy. Soc. London B **268**, 2603 (2001).

[92] R. J. Williams and N. D. Martinez, Nature **404**, 180 (2000).

[93] S. Bornholdt and H. G. Schuster (Eds.), *Handbook of Graphs and Networks* (Wiley-VCH, Weinheim, 2003).

[94] F. R. K. Chung, *Spectral Graph Theory* (American Mathematical Society, 1997).

[95] E. Hückel, Z. Physik **70**, 204 (1931).

[96] E. P. Wigner, Ann. Math. **62**, 548 (1955).

[97] F. J. Dyson, J. Math. Phys. **3**, 140 (1962).

[98] M. L. Mehta, *Random Matrices* (Academic Press, San Diego, 1991).

[99] G. J. Rodgers and A. J. Bray, Phys. Rev. B **37**, 3557 (1988).

[100] R. Kühn, J. Phys. A: Math. Theor. **41**, 295002 (2008).

[101] B. Velický, S. Kirkpatrick, and H. Ehrenreich, Phys. Rev. **175**, 747 (1968).

[102] V. A. Marčenko and L. A. Pastur, Math. USSR–Sbornik **1**, 457 (1967).

[103] A. N. Kushnirenko, *Vvedenie v kvantovuyu teoriyu polya* (Vysshaya shkola, Moskva, 1971).

[104] P. L. Krapivsky, Phys. Rev. A **45**, 1067 (1992).

[105] L. Frachebourg and P. L. Krapivsky, Phys. Rev. E **53**, R3009 (1996).

[106] T. M. Liggett, *Interacting Particle Systems* (Springer, Berlin, 1985).

[107] D. Challet and Y.-C. Zhang, Physica A **246**, 407 (1997).

[108] D. Challet, M. Marsili, and Y.-C. Zhang, *Minority Games* (Oxford University Press, Oxford, 2005).

[109] A. C. C. Coolen, *The Mathematical Theory of Minority Games* (Oxford University Press, Oxford, 2005).

[110] F. Slanina, Physica A **286**, 367 (2000).

[111] M. Pištěk and F. Slanina, Physica A **390**, 2549 (2011).

[112] K. Sznajd-Weron and J. Sznajd, Int. J. Mod. Phys. C **11**, 1157 (2000).

[113] A. Svorenčík and F. Slanina, Eur. Phys. J. B **57**, 453 (2007).

[114] M. H. DeGroot, Journal of the American Statistical Association **69**, 118 (1974).

[115] R. Hegselmann and U. Krause, J. Artif. Soc. Soc. Simulation **5**, <http://jasss.soc.surrey.ac.uk/5/3/2.html> (2002).

[116] E. W. Montroll and M. F. Shlesinger, J. Stat. Phys. **32**, 209 (1983).

[117] M. Levy and S. Solomon, Physica A **242**, 90 (1997).

[118] W. J. Reed and B. D. Hughes, Phys. Rev. E **66**, 067103 (2002).

[119] A. Y. Abul-Magd, Phys. Rev. E **66**, 057104 (2002).

[120] B. Mandelbrot, International Economic Review **1**, 79 (1960).

[121] B. B. Mandelbrot, *The Fractal Geometry of Nature*, (W. H. Freeman, New York, 1983).

[122] E. Ben-Naim and P. L. Krapivsky, Phys. Rev. E **61**, R5 (2000).

[123] L. Muchnik, F. Slanina, and S. Solomon, Physica A **330**, 232 (2003).

[124] P. Bak, M. Paczuski, and M. Shubik, Physica A **246**, 430 (1997).

[125] G. J. Stigler, Journal of Business **37**, 117 (1964).

[126] S. Maslov, Physica A **278**, 571 (2000).

[127] M. G. Daniels, J. D. Farmer, L. Gillemot, G. Iori, and E. Smith, Phys. Rev. Lett. **90**, 108102 (2003).

[128] G. Gallavotti and E. G. D. Cohen, Phys. Rev. Lett. **74**, 2694 (1995).

Chapter 2

Collection of original papers

Section 1.2.1

[Slanina99] F. Slanina,
Collective behavior of asperities in dry friction at small velocities,
Phys. Rev. E 59, 3947-3953 (1999).

[Slanina99a] F. Slanina,
Cracking piles of brittle grains,
Phys. Rev. E 60, 1940-1945 (1999).

[Slanina02] F. Slanina,
Self-organized branching process for a one-dimensional rice-pile model,
Eur. Phys. J. B 25, 209-216 (2002).

Section 1.2.2

[SlaKot00] F. Slanina and M. Kotrla,
Random networks created by biological evolution,
Phys. Rev. E 62, 6170-6177 (2000).

[SlaKon10] F. Slanina and Z. Konopásek,
Eigenvector localization as a tool to study small communities in online social networks,
Adv. Compl. Syst. 13, 699-723 (2010).

[Slanina11] F. Slanina,
Equivalence of replica and cavity methods for computing spectra of sparse random matrices,
Phys. Rev. E 83, 011118 (2011).

[Slanina12] F. Slanina,
Localization of eigenvectors in random graphs,
Eur. Phys. J. B 85, 361 (2012).

Section 1.2.3

[Slanina01] F. Slanina,
Harms and benefits from social imitation,
Physica A 299, 334-343 (2001).

[SlaLav03] F. Slanina and H. Lavička,
Analytical results for the Sznajd model of opinion formation,
Eur. Phys.J. B 35, 279-288 (2003).

[SlaSznPrz08] F. Slanina, K. Sznajd-Weron, and P. Przybyła,
Some new results on one-dimensional outflow dynamics,
Europhys. Lett. 82, 18006 (2008).

[Slanina11a] F. Slanina,
Dynamical phase transitions in Hegselmann-Krause model of opinion dynamics and consensus,
Eur. Phys. J. B 79, 99-106 (2011).

Section 1.2.4

[Slanina04] F. Slanina,
Inelastically scattering particles and wealth distribution in an open economy,
Phys. Rev. E 69, 046102 (2004).

[Slanina01a] F. Slanina,
Mean-field approximation for a limit order driven market model,
Phys. Rev. E, 64 056136 (2001).

[Slanina08] F. Slanina,
Critical comparison of several order-book models for stock-market fluctuations,
Eur. Phys. J. B 61, 225-240 (2008).

[Slanina99]

PHYSICAL REVIEW E VOLUME 59, NUMBER 4 APRIL 1999

Collective behavior of asperities in dry friction at small velocities

František Slanina*
Institute of Physics, Academy of Sciences of the Czech Republic Na Slovance 2, CZ-18040 Praha, Czech Republic and Center for Theoretical Study Jilská 1, CZ-11000 Praha, Czech Republic
(Received 29 May 1998)

We investigate a simple model of dry friction based on extremal dynamics of asperities. At small velocities, correlations develop between the asperities, whose range becomes infinite in the limit of infinitely slow driving, where the system is self-organized critical. This collective phenomenon leads to effective aging of the asperities and results in velocity dependence of the friction force in the form $F \sim 1 - \exp(-1/v)$. [S1063-651X(99)06804-X]

PACS number(s): 05.65.+b, 46.55.+d

I. INTRODUCTION

Phenomena connected with mechanical properties of complex systems have been the subject of intensive study in the last decade. Generally speaking, the difficulty stems from the fact that both the macroscopic scale and mesoscopic scale are important. For example, the contact area of two grains of sand is a mesoscopic object, but its properties result in macroscopic behavior of a sand heap. Among the whole family of such problems, the dry friction emerged in recent years as a hot subject. Besides the intrinsic interest in the dynamics of contact interfaces sliding on top of each other, there are various systems studied recently, in which friction forces are dominant interactions determining the behavior. As examples, we may note two notoriously known phenomena: sand heaps and earthquakes. Equilibrium stress distribution in heaps of granular materials exhibits complicated localized structures [1,2]. The dynamics of tectonic plates gives rise to the power-law distribution of earthquakes, formulated in the Gutenberg-Richter law [3,4]. A one-dimensional counterpart of friction is, e.g., the dislocation movement, which is responsible for the plasticity of metals.

At least three regimes of friction may be distinguished. First, dry friction corresponds to tangential force acting on the contact of two macroscopic solid bodies. The slot between the bodies is empty. The friction emerges as a result of the rheological properties of the sliding bodies both at the macroscopic and mesoscopic scale. Second, the lubricated friction differs in the fact that the slot between bodies is filled with a liquid and the mechanical properties of the mesoscopic portions of the lubricant are responsible for friction. Third, friction of a single microscopic tip on a surface may be measured, which explores the microscopic properties of the surface [5]. Here we concentrate on the first possibility: dry friction.

Thorough experiments concerning sliding bodies were performed as early as the 18th century and led to the famous Amontons-Coulomb laws: the friction force is proportional to load and independent of the apparent contact area; for nonzero velocities, the friction force is independent of velocity (dynamical friction), while at zero velocity, the friction force is larger (static friction). These old results on the dry friction were reinvestigated experimentally relatively recently [6,7]. It was found that dynamical friction force is not constant, but increases continuously when the velocity is decreased.

From the theoretical point of view, the microscopic interpretation of the Amontons-Coulomb law was provided by Bowden and Tabor [8], and alternatively by Greenwood and Williamson [9]. In both approaches, the explanation is based on the picture of the set of mesoscopic contacts (asperities), scattered on the surface of the sliding bodies [10–14]. The typical size of the asperities is constant, while their number is proportional to normal load; hence the explanation of the Amontons-Coulomb law.

This picture is the basis of many current models of dry friction [7], especially the elastoplastic model developed by Caroli, Noziéres, and Velický [10,11]. The asperities are considered as multistable traps, which dissipate energy due to hysteresis. In the approximation of independent traps, even the dynamics of a single asperity is able to describe the friction process.

However, many features are not well understood, e.g., the velocity dependence of the friction force found in experiments [6,15]. It is explained either as a consequence of the plasticity of the asperities, which is considered as a thermally activated process [6] (this phenomenon is called aging of the asperities) or purely geometrically, based on the self-affine shape of the surfaces [12]. Within the approach based on the plasticity, the logarithmic dependence of the age of the asperity on time is supposed on the basis of experimental data, which suggest logarithmic velocity dependence of the friction force. On the other hand, the geometrical approach gives friction force proportional to v^{-1} for large velocities, while the behavior for small velocities depends on the fractal geometry of the surface.

In the description of the process of friction two levels may be distinguished. On the global level, the averaged effect of asperities can be successfully described using the elastoplastic model [10,11]. This approach is effectively a single-site one. Only one asperity is changing its state and the effect of all other asperities is described by the effective surrounding medium. The spatiotemporal correlations are considered to be of very short range, and the mutually sliding surfaces behave in a uniform way.

*Electronic address: slanina@fzu.cz

On the other hand, the local, short time level of description must take into account processes that happen at several (or many) asperities simultaneously, or within a very short period of time, so that they cannot be considered as uncorrelated. Several approaches in this direction were already proposed, based on geometrical considerations [12,13], on Frenkel-Kontorova [16], Burridge-Knopoff and train models [17,18], or on an extremal dynamics model with elastic interactions [14].

The extremal dynamics (ED) models are very appealing, because they may grasp the ''skeleton'' of the problem, despite their simplicity and rudimentary nature. Generally, ED is based on the assumption that only one site is evolving during one time step, namely the site which has the maximum (or minimum: it depends on the model in question) of the dynamical variable determining the state of the system. However, the price to pay is that the time scale fixed by the frequency of the updates of single sites is not directly related to the real time measured in an experiment.

Extremal dynamics models were successfully used in modeling various systems, such as invasion percolation, biological evolution [19], earthquakes [20], or dislocation movement [21,22]. The model we propose here is based on the ideas of ED models, adapted to the fact that in friction we are interested in macroscopic movement with nonzero velocity, while most ED models are appropriate to the case of infinitely slow movement.

Briefly, the evolution of our model proceeds at the most susceptible asperity, namely the asperity that bears maximum stress. A small mechanical perturbation, such as the release of stress at a single site, may result in a burst of activity of large spatiotemporal extent. Following the terminology used in the theories of self-organized criticality [19], we will call such spatiotemporal areas of activity avalanches. The correlations present in the model will be described through the statistical properties of the avalanches.

From time to time, the ED of asperities is interrupted by a macroscopic ''slip'' of the body as a whole, in which all asperities are completely renewed. By a combination of the ED evolution with such macroscopic slips, we introduce non-zero macroscopic sliding velocity into the model.

The rest of the article is organized as follows. In Sec. II the model is defined and the interpretation of the model parameters is given; in Sec. III the presence of self-organized criticality (SOC) is investigated in the case of zero macroscopic velocity, while the effect of nonzero velocity on the breakdown of SOC as well as the velocity dependence of the friction force are investigated in Sec. IV. Section V summarizes the results and draws conclusions from them.

II. MODEL

We propose the following model. There are N point contacts, asperities, each with stress b. The quantity b will be interpreted as the elastic energy stored in the asperity. The model is one dimensional (the generalization to the realistic two-dimensional case is straightforward) with periodic boundary conditions, so the points form a closed ring. In each step, the point with the highest stress $b_{\max}$ is found and released. The release of the stress means that the point is removed. However, in order to keep the number of points constant, a new point is introduced somewhere in the system.

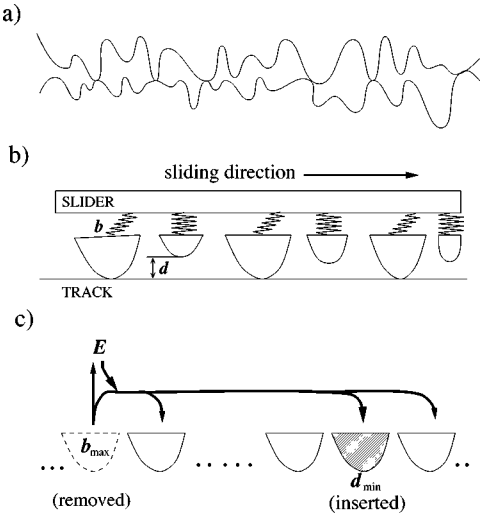

FIG. 1. Illustration of the model. A schematic drawing of two sliding interfaces in contact is given in (a); the idealization of the situation used in our model is depicted in (b). The elastic energy stored in the asperity is described by the quantity b; the slot between the potential asperity and the track is d. In (c), the redistribution in one step of extremal dynamics is shown schematically.

As a zeroth approximation, the location of the new point may be chosen at random. However, in reality the position of the new contact is determined by the detailed structure of the surfaces of the slider and track. The new contact is established at a place where the surfaces are closest one to another. So, another number d is attributed to each point representing the width of the slot between the surfaces, waiting in the vicinity of the asperity for further updates (the *actual* slot directly on the asperity is zero, of course). The situation is sketched in Figs. 1(a) and 1(b). In the update the location of minimum d is found. Here a new asperity is reintroduced. The values of b and d of the neighbors of the old and new sites are also updated. Generally, each site has $K-1$ neighbors that are affected. For simplicity, we assume $K=2$, and update only one neighbor (on the right-hand side).

Let us allow for very slow motion of the slider as a whole. The energy stored in the released asperity may be transferred entirely to other asperities, or a part of it may be converted into kinetic energy E. It may also happen that some of the kinetic energy is returned back to elastic energy of some asperities. The redistribution of energy in one update step is illustrated in Fig. 1(c).

It is natural to expect that, at higher velocities, the number of asperities affected by the transfer of the kinetic energy to the elastic one will be larger. We simplify this dependence by saying that for $E<E_{\rm thr}$ only the nearest neighbors are affected, while for $E\geqslant E_{\rm thr}$ the slider slips macroscopically over an average distance $x_{\rm slip}$. The average duration of the slip is $T_{\rm slip}$ and after that time all parameters b and d of all asperities are newly attributed at random and E is set to 0. Then, the dynamics starts again. In this process, the kinetic energy $\simeq E_{\rm thr}$ the system had before the slip is dissipated. This makes a difference with the theories of one asperity dynamics, where the energy is dissipated immediately after release of a single asperity. In our model we do not describe the processes that happen during the slip; e.g., we do not

[Slanina99]

examine the energy dissipated in the course of the slip. Similarly, we do not calculate the physical velocity corresponding to the kinetic energy E during the ED evolution. So, we isolate only those contributions to the friction force and the macroscopic slider velocity that originate in the ED process interrupted by instantaneous slips.

The average macroscopic velocity Δv stemming from the slips depends on the average time interval between two subsequent slips. We may determine this quantity $\overline{\Delta t}$ in the time units of the extremal dynamics process. Its relation to physical time is not straightforward, but we suppose that this ambiguity affects only units, in which we measure time and not the general dependence of the friction force on velocity. Thus, we write simply

$$\Delta v = 1/\overline{\Delta t}, \tag{1}$$

which corresponds to taking the average slip length x_{slip} as the length unit and average time needed to update single asperity as a time unit. The contribution Δv from the ED process is dominant if the time between slips is much larger than the duration of the slip, $\overline{\Delta t} \gg T_{\mathrm{slip}}$ (i.e., slips are instantaneous events) and the real length travelled between slips during the ED dynamics x_{ED} is much shorter than the slip length, $x_{\mathrm{ED}} \ll x_{\mathrm{slip}}$.

The contribution ΔF_{fric} to the friction force coming from this process is then proportional to the energy dissipated in one slip. Because we are using arbitrary units, we identify

$$\Delta F_{\mathrm{fric}} = E_{\mathrm{thr}}. \tag{2}$$

Let us now describe the extremal dynamics of the model more formally. The model consists of N sites connected in ring topology. Each site $i \in \{1,2,\ldots,N\}$ is connected to its right neighbor $r(i)$. The state of the model is described by the set $(E,b_1,b_2,\ldots,b_N,d_1,d_2,\ldots,d_N)$ and the function $r(i)$ which describe the connectivity of the sites. At the beginning, $E=0$ and both b_i and d_i are uniformly distributed in the interval (0,1). The updating steps are the following. (i) Find the maximum stress $b_{\max}=\max_i(b_i)$ located at site $i_{\max}$. Remember its old right neighbor $i_{\mathrm{old}}=r(i_{\max})$. (ii) Find the minimum slot $d_{\min}$ at site $i_{\min}$. (iii) Change of connectivity: The site $i_{\max}$ is removed by cutting its links to the left and right nearest neighbors and is reinserted between $i_{\min}$ and the site next to it on the ring. It will have a new right neighbor $i_{\mathrm{new}}=r(i_{\max})=r(i_{\min})$, and then set $r(i_{\min})=i_{\max}$. (iv) Kinetic effects: Set $E'=E+\delta b_{\max}$, $b'_{\max}=(1-\delta)b_{\max}$, $\Delta_1=(b_{\mathrm{M}}-b_{i_{\mathrm{old}}})\theta(b_{\mathrm{M}}-b_{i_{\mathrm{old}}})$, $\Delta_2=(b_{\mathrm{M}}-b_{i_{\mathrm{new}}})\theta(b_{\mathrm{M}}-b_{i_{\mathrm{new}}})$. If $E'>\Delta_1+\Delta_2$, we set $E=E'-\Delta_1-\Delta_2$, $b'_{i_{\mathrm{old}}}=b_{i_{\mathrm{old}}}+\Delta_1$, $b'_{i_{\mathrm{new}}}=b_{i_{\mathrm{new}}}+\Delta_2$. If not, we set $E=0$, $b'_{i_{\mathrm{old}}}=b_{i_{\mathrm{old}}}+E'/2$, $b'_{i_{\mathrm{new}}}=b_{i_{\mathrm{new}}}+E'/2$. (v) Stress redistribution: For r_1,r_2, random numbers distributed uniformly in the triangle $0<r_1<r_2<1$ we set $b_{i_{\max}}=r_1 b'_{\max}$, $b_{i_{\mathrm{old}}}=b'_{i_{\mathrm{old}}}+(r_2-r_1)b'_{\max}$, $b_{i_{\mathrm{new}}}=b'_{i_{\mathrm{new}}}+(1-r_2)b'_{\max}$. (vi) New values of slots d are attributed to old and new neighbors as well as to site $i_{\max}$, taking random numbers uniformly distributed in the interval (0,1). (vii) If $E \geqslant E_{\mathrm{thr}}$, slip occurs, which means that E is set to 0 and b_i and d_i distributed uniformly in the interval (0,1).

Rule (iv) concerning the kinetic effects means that elastic energy $\delta b_{\max}$ is transferred from the removed asperity to kinetic energy and the rest is left for the newly inserted asperity. The quantities Δ_1 and Δ_2 are absorbed by the neighbors, but only if they do not exceed the kinetic energy (which should be positive). If they do exceed it, each of the neighbors receives exactly half of the kinetic energy, which is thus totally absorbed.

The kinetic effects and the slip involve several parameters. First, the parameter δ describes how much of the elastic energy tends to be converted into the kinetic energy. If $\delta=0$, the kinetic effects are turned off.

The parameter b_{M} is the limit up to which an asperity can absorb a portion of kinetic energy and convert it back to elastic energy. It should be the property of the surface itself, without any resort to the load and velocity of the slider. If $\delta=0$, the parameter b_{M} does not enter the model.

The slip is determined by the parameter E_{thr}. In a more realistic description, it would be necessary to introduce the function $R(E)$, which would count the number of sites, including the extremal site $i_{\max}$, which are to be updated, provided the kinetic energy has the value E. Here we take the simplest form $R(E)=3+(N-3)\theta(E-E_{\mathrm{thr}})$. Even this parameter should be the property of the surface, irrespective of the load and velocity.

Finally, we comment on the interpretation of the quantity N, the average number of asperities. We suppose that it may serve as a measure of the external load. Consequently, N does not depend on the apparent contact area of the slider and the track. Larger N also means that update of single asperity has less impact on the whole system, namely, the transfer of elastic energy to kinetic energy is slower. The same effect has smaller δ, so it is the quantity δ/N that will appear in the velocity dependence of the friction force.

So, in order to conform with the Amontons-Coulomb law, we expect that the surface properties will enter the velocity dependence of the friction force through the parameter b_{M} and combinations E_{thr}/N and δ/N. We will see later that it is exactly the case.

III. INFINITELY SLOW MOVEMENT REGIME

Let us first investigate the case in which no slips are allowed, which can be expressed by the limit value $E_{\mathrm{thr}}=\infty$. In this case, the macroscopic movement is infinitely slow. If the elastic energy could not be transformed into kinetic energy E, i.e., if $\delta=0$, the model would be a slightly more complicated version of the Zaitsev model for dislocation movement [21], which is known to be self-organized critical. The criticality manifested by the power-law distribution of avalanche sizes is due to infinitely slow driving. It is natural to expect self-organized criticality also in our model for $\delta=0$. However, even for $\delta>0$ the condition of infinitely slow driving, which means technically that only one asperity is updated at a time, is also satisfied and SOC is expected as well.

We simulated systems of size $N=1000$. The first quantity we measured was the probability distribution of the stresses, $P(b)$ and maximum stresses $P_{\max}(b_{\max})$. The function $P(b)$ is continuous up to a critical value $b=b_{\mathrm{c}}$ and then suddenly drops to zero, which is behavior common in SOC extremal dynamics models. The value of b_c depends on δ. The typical

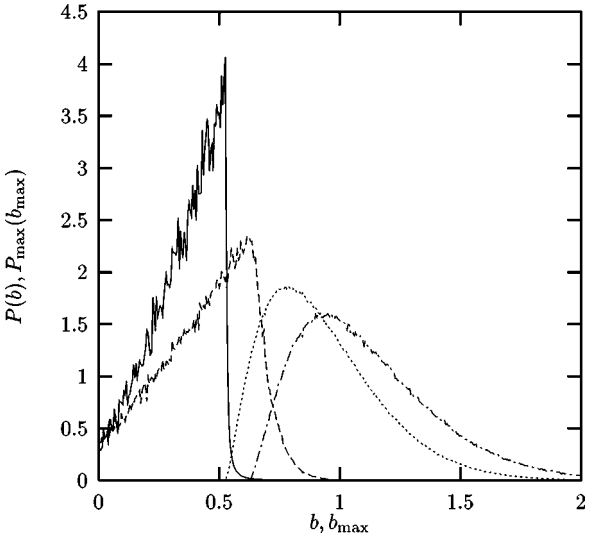

FIG. 2. Distribution of stresses $P(b)$ and maximum stresses $P_{\max}(b_{\max})$ for $N=1000$, $\delta=0.01$, and $b_M=0.9$. The energy threshold is infinite [full line for $P(b)$ and dotted for $P_{\max}(b_{\max})$] and $E_{\text{thr}}/N=0.08$ [dashed line for $P(b)$ and dash-dotted for $P_{\max}(b_{\max})$]. The number of steps is 10^6.

behavior is shown in Fig. 2 for $\delta=0.01$.

A fingerprint of self-organized criticality is, e.g., the scaling behavior of the forward λ-avalanche sizes

$$P_{\text{fwd}}(s)=s^{-\tau}g(s|\lambda-\lambda_c|^{1/\sigma}). \tag{3}$$

The λ avalanche starts when $b_{\max}$ exceeds the value λ and ends when $b_{\max}$ drops below the value λ again. The size s of the avalanche is the number of update steps from the start to the end of the avalanche. For numerical reasons it is simpler

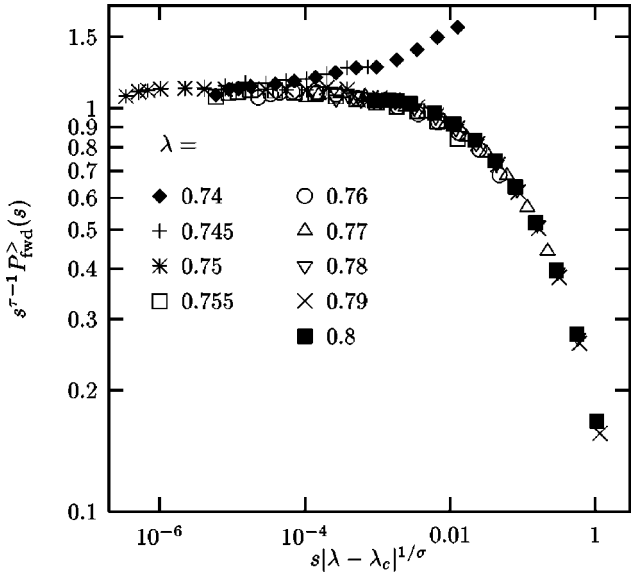

FIG. 3. Rescaled forward avalanche distribution for $N=1000$ and $\delta=0$. The critical threshold is $\lambda_c=0.7475$ and the scaling exponents are $\tau=1.28$ and $1/\sigma=2.6$. The number of steps is 10^8. The corresponding thresholds λ are indicated next to the symbols in the legend.

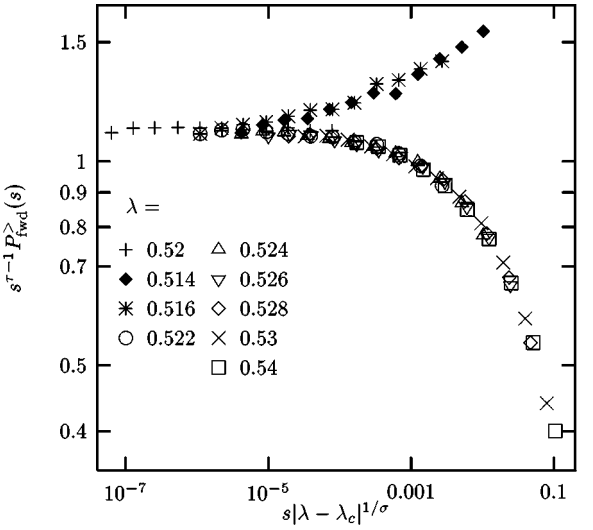

FIG. 4. Rescaled forward avalanche distribution for $N=1000$, $\delta=0.001$, and $b_M=0.9$. The critical threshold is $\lambda_c=0.519$ and the scaling exponents are $\tau=1.27$ and $1/\sigma=2.6$. The number of steps is 10^8. The corresponding thresholds λ are indicated next to the symbols in the legend.

to investigate scaling of integrated distribution, $P^{>}_{\text{fwd}}(s)=\int_s^\infty d\bar{s}\,P_{\text{fwd}}(\bar{s})$, from which the exponents τ and σ can be determined.

Figures 3 and 4 show the data collapse which confirms the scaling of the form (3). The best collapse was obtained for the following values of the parameters: (a) for $\delta=0$ we have $\lambda_c=0.7475$, $\tau=1.28$, and $1/\sigma=2.6$, and (b) for $\delta=0.001$ and $b_M=0.9$ we have $\lambda_c=0.519$, $\tau=1.27$, and $1/\sigma=2.6$.

There is a minor difference in the exponent τ giving the best fit for $\delta=0$ and $\delta=0.001$. However, we believe that this difference is within the numerical uncertainty of the results and the model belongs to the same universality class irrespective of parameter δ.

By qualitative inspection of the quality of the data collapse for different choices of the exponents, we estimate the error bars. Thus, we finish with the following critical exponents of our model:

$$\tau=1.27\pm0.02, \quad \sigma=0.38\pm0.02. \tag{4}$$

The forward avalanche exponent τ is greater than in the one-dimensional (1D) Zaitsev model [21,19], but close to the Sneppen interface growth model [23,19]. Another 1D model to be compared is the charge-density wave (CDW) model of Olami [24] and the anisotropic interface depinning model of Ref. [22], which have, however, significantly larger exponent τ. The closest universality class seems to be the one of the Sneppen model ($\tau=1.26$), but the value of $\sigma=0.35$ in this class is smaller than in our model.

Whether this difference is due to the finite-size effect or the two models being in a different universality class cannot be stated with certainty from our present data. Instead, we would like to stress a structural similarity of the two models, which may explain the similarity of exponents. Contrary to usual interface growth models [25], the Sneppen model is a nonlocal one. After a single growth event (deposition of a single particle), an unbounded sequence of further steps is

[Slanina99]

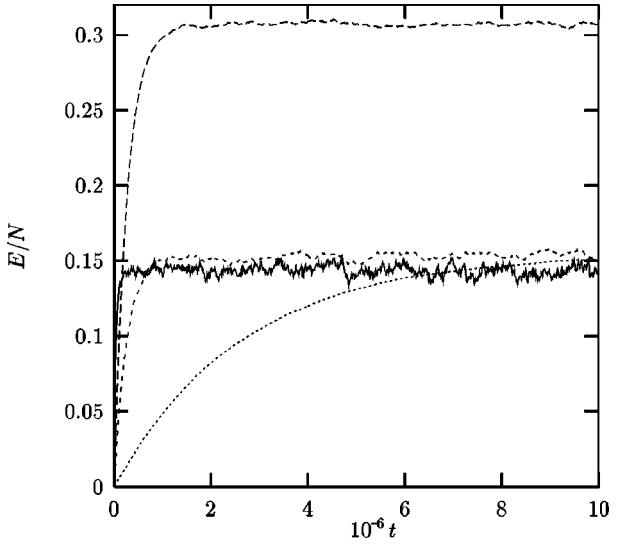

FIG. 5. Time evolution of the kinetic energy per asperity. The parameters are as follows: $N=1000$, $\delta=0.01$, and $b_M=0.9$ (full line), $N=10^4$, $\delta=0.001$, and $b_M=0.9$ (dotted line), $N=1000$, $\delta=0.001$, and $b_M=0.5$ (long dashed line), and $N=1000$, $\delta=0.001$, $b_M=0.9$ (short dashed line).

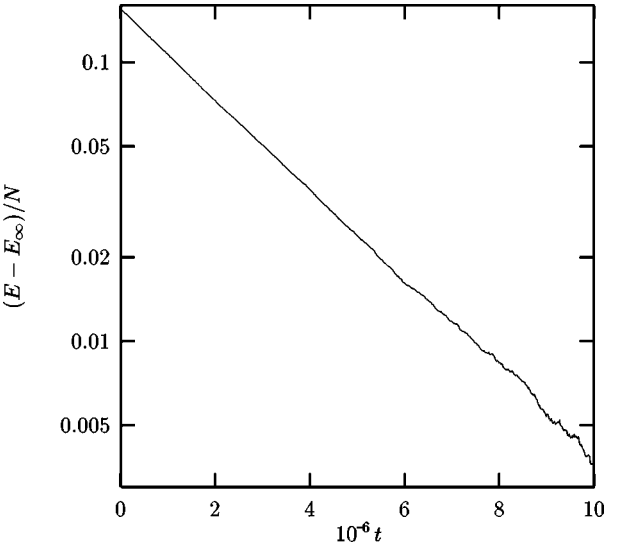

FIG. 6. Approach of the kinetic energy to its stationary value, for $N=10^4$, $\delta=0.001$, and $b_M=0.9$. The stationary value is taken as $E_\infty/N=0.155$.

performed in order to reestablish the single-step property of the interface. So, the range of interactions fluctuates during the evolution, according to the actual configuration of the interface. Similarly, the Zaitsev model, like most of other extremal dynamics models, is local in the sense that after finding an extremal site, its neighbors are also updated, while the range of neighborhood is fixed. In contrast, our model, like the Sneppen model, does not have a fixed range of interactions, but is established by the position of the minimum of the quantity d (the slot). We simulated also a version in which the site, where new asperity is inserted, is chosen at random, instead of using the slot d. In this case we observed mean-field behavior characterized by exponents $\tau=1.5$, $\sigma=0.5$.

IV. FRICTION AT NONZERO VELOCITY

In the preceding section we dealt with stationary properties of the model. In order to account for macroscopic movement, transient properties are of interest. First, we investigate the evolution of the kinetic energy E and its approach to the stationary value E_∞, if we forbid the slips, i.e., $E_{\rm thr}=\infty$. In Fig. 5 we show the time evolution of E/N for different values of the model parameters δ, b_M, and number of asperities N. The most important observation is that the stationary value E_∞/N depends on b_M, while the dependence on δ and N is within the noise level. (We observe that both large N and small δ suppress the relative fluctuations of the kinetic energy around the stationary value.) The physical significance is clear: the static friction force, which is according to Eq. (2) equal to E_∞, is proportional to N, which is in turn proportional to the normal load. Thus, we recover the Amontons-Coulomb law for static friction.

The approach of the kinetic energy to its stationary value is exponential, as is demonstrated in Fig. 6. This type of approach is directly reflected in the velocity dependence of the friction force, as we will see below.

If we set the threshold $E_{\rm thr}<E_\infty$, quasiperiodic behavior is observed: the kinetic energy grows, until it reaches the value of the threshold, and then the system is reinitialized. This regime is illustrated in Fig. 7. If the threshold is close to E_∞, the slips are less regular, due to fluctuations, but for smaller values of the threshold the slips occur with fixed frequency. The mean number of steps Δt between slips is determined by the way E approaches the stationary value. Because $E_{\rm thr}$ is related to the friction force by Eq. (2) and the mean period of slips to the velocity, according to Eq. (1), the velocity dependence of the friction force is measurable in our model. Figure 8 shows the results for various δ and $b_{\rm M}$. If we denote $F_0=E_\infty$ the static friction force, we observe by plotting the velocity dependence in semilogarithmic scale that the following law is well satisfied:

$$\Delta F_{\rm fric}=F_0\left[1-\exp\left(-A\frac{\delta}{\Delta v N}\right)\right] \tag{5}$$

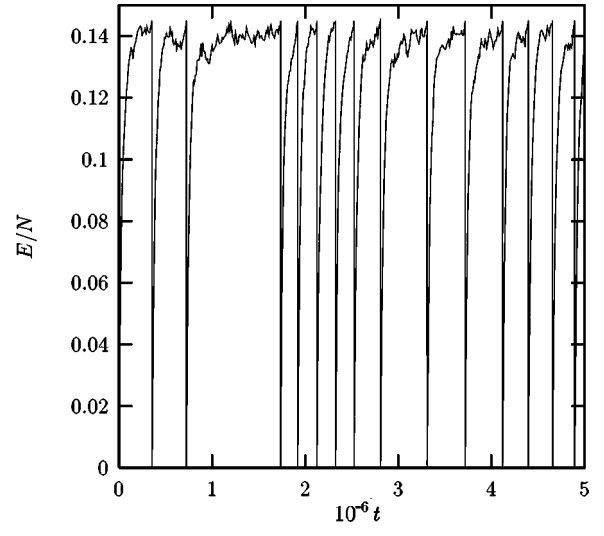

FIG. 7. Time dependence of the kinetic energy E, for $N=10^3$, $\delta=0.1$, and $b_M=0.9$. The slips occur in the moments when E drops to 0.

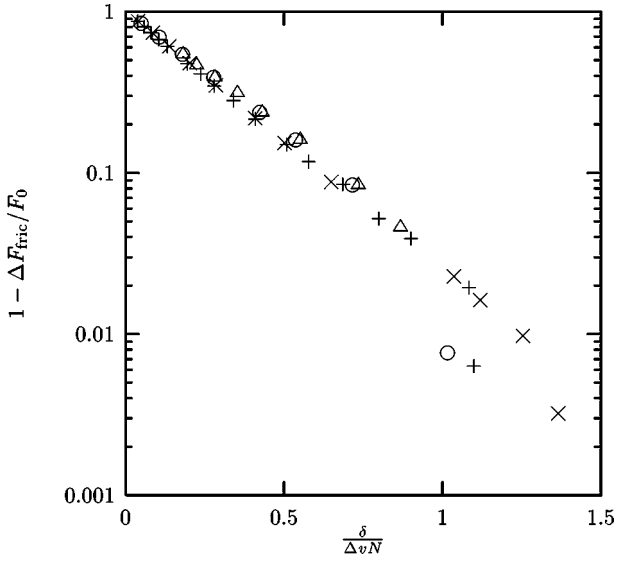

FIG. 8. Velocity dependence of the friction force, for $N=10^3$, $\delta=0.001$, $b_M=0.9(+)$, $N=10^3$, $\delta=0.001$, $b_M=0.5(\times)$, $N=10^3$, $\delta=0.01$, $b_M=0.9(\bigcirc)$, $N=500$, $\delta=0.01$, and $b_M=0.9(\triangle)$.

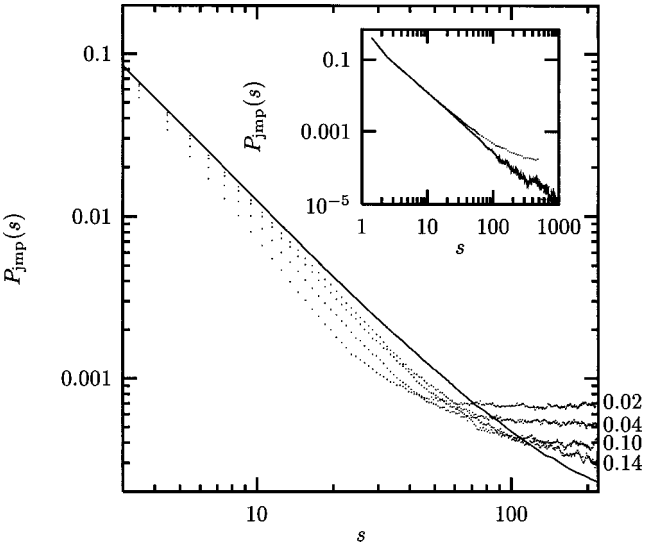

FIG. 9. Distribution of jump lengths for $N=10^3$, $\delta=0.001$, and $b_M=0.9$. The full line is the case without slips ($E_{\rm thr}=+\infty$). The dotted lines have slips allowed and the values of $E_{\rm thr}/N$ are indicated next to the position where the lines reach the right edge of the figure. In the inset, the distribution of jump lengths is given for $\delta=0$ and $N=10^4$ (full line), and $N=10^3$ (dotted line). Note that the inset makes it clear that the upward bend in the distribution for $E_{\rm thr}=+\infty$ is a mere finite-size effect.

with some constant A characteristic of the model. We have found $A=3.6\pm0.3$. The deviations from the above dependence for $\Delta v<\delta/N$ are due to time fluctuations of E, which lead to less regular slips. However, as we already mentioned, the relative fluctuations decrease with N, so we expect the dependence (5) to hold for all velocities in thermodynamic limit $N\to\infty$.

For large velocities the friction force decreases as $\Delta F_{\rm fric}\sim 1/\Delta v$. The same velocity dependence was found also using a different approach [12].

Because F_0 was found to be proportional to N, i.e., to the normal load, the form of Eq. (5) is in conformity with the Amontons-Coulomb law.

Now we turn to the influence of the macroscopic movement, connected to the slips on the self-organized critical behavior investigated in the last section. Each slip reinitializes the values of b and d and the evolution towards the critical attractor begins from scratch. This means that the long-range correlations characteristic of the critical state cannot fully develop. The difference can be seen already in the distribution of stresses, Fig. 2. The sharp edge in $P(b)$ observed in the infinitely slow driving is smeared out. The position of the edge determines the critical threshold λ_c for the forward avalanches, so we expect that no scaling of type (3) will hold, as soon as the macroscopic movement has nonzero velocity. However, the most direct way to investigate the breakdown of criticality due to the slips seems to us to be the calculation of the distribution of jump lengths. If in certain time step t the maximum stress was found at site i_t and in the next step at site i_{t+1}, we can compute spatial distance between these sites as follows. Let $r_t(i)$ be the function that determines the connectivity in time t, namely, $r_t(i)$ is the site connected to i on the right-hand side. The jump length s is defined as follows: starting from i_t and applying r_t we come to the right neighbor of the extremal site at time t, $r_t(i_t)$. Then, applying $s-l$ times the function r_{t+1} we must end at i_{t+1}. So, s is such that $i_{t+1}=r_{t+1}(r_{t+1}[\cdots r_{t+1}(r_t(i_t))\cdots])$, where r_{t+1} is applied $s-1$ times.

In the self-organized critical state the probability distribution of jump lengths is the power law $P_{\rm jmp}(s)=s^{-\pi}$. For $E_{\rm thr}=\infty$ it is actually observed in our model, as indicated in the inset in Fig. 9. The comparison of the distributions for $N=10^3$ and $N=10^4$ is shown in order to give an idea of the magnitude of the finite-size corrections to the power-law behavior.

The situation with nonzero macroscopic velocity, $E_{\rm thr}<E_\infty$, is shown in Fig. 9. When $E_{\rm thr}$ decreases, the velocity increases and the scale on which $P_{\rm jmp}(s)$ obeys a power law shrinks. The correlations do not have time enough to develop on the scale of the whole system, but only at shorter distances. So, we may connect the velocity dependence of the friction force to the level of correlations between the asperities, which are present in the system. In contrast to the theories where the velocity dependence stems from the aging of a single asperity, here the aging is a collective effect. The age corresponds to the range of correlations. For zero velocity the correlation length is infinite and the age is infinite as well.

V. CONCLUSIONS

We presented a model of dry friction based on the conception of slider and track interacting through a system of asperities. We proposed an extremal dynamics model in order to describe the processes during the movement of the slider. We found the decrease of the friction force with increasing velocity. For velocities approaching zero, the friction force has finite limit. The origin of the velocity dependence is not in a change of properties of a single asperity, but in collective effects, involving many asperities. At zero velocity, the system is in a highly correlated, self-organized

[Slanina99]

critical state. The values of the exponents are close to the Sneppen interface model; however, it is not clear from our data whether the universality class is the same.

Increasing the velocity gradually destroys the correlations. It is possible to view the buildup of the correlations as a collective asperity aging mechanism, as a counterpart to the single asperity aging due to plastic deformation. Such collective aging leads to a different velocity dependence of the friction force than in the models considering single asperity aging and may be thus tested experimentally. A two-dimensional variant of our 1D model would be necessary for a real comparison. However, generalization to an arbitrary dimension is straightforward.

This observation reveals also the limits of applicability of our model. It is appropriate to situations where the plastic deformation does not dominate. The model can be used in the regime of very small velocities, where the usual logarithmic velocity dependence is inappropriate. It may also be used to describe friction over highly elastic surfaces, like rubber or some plastics, where the slow aging of single asperities may not be dominant.

However, a simple modification of the model might also take into account the plastic aging: the stresses b may be allowed to depend explicitly on the time elapsed since the asperity was created. The specific form of this time dependence should be based on physical assumptions not contained in our model, like the thermally activated mechanism [6]. Thus, the interplay of collective and individual aging could be investigated. We expect that the nonuniversal form of the velocity dependence of the friction force arises from such interplay.

There can also be another source of velocity dependence different from the exponential one, which we found in our work. The function $R(E)$, which gives the number of changed asperities in one step, determines when the slips start and consequently what will be the average velocity for a given friction force. However, we expect that realistic forms of $R(E)$ have a more or less sudden increase at a certain value of E. We expect that all forms with a sufficiently sudden jump will give the same universal behavior as the stepwise form used by us.

As for the geometrical assumptions of the model, they are naturally very crude. The asperities in the model do not occupy places in a realistic one-dimensional Euclidean space, but rather on an abstract topological line. Taking into account the real geometry of the space would make more complicated the rules for finding the place where the new asperity is to be inserted. Also, the true elasticity of the medium should be taken into account. However, our results show that the velocity dependence of the friction force is governed by the way the self-organized critical state is approached. We believe that this behavior is universal and making the system more realistic would not alter the universality class, as long as the dimensionality and the extremal-dynamics character of the model is preserved.

ACKNOWLEDGMENTS

I wish to thank M. Kotrla and B. Velický for useful discussions.

[1] H. M. Jaeger, S. R. Nagel, and R. P. Behringer, Rev. Mod. Phys. **68**, 1259 (1996).
[2] F. Radjai, M. Jean, J.-J. Moreau, and S. Roux, Phys. Rev. Lett. **77**, 274 (1996).
[3] P. Bak and C. Tang, J. Geophys. Res. **94**, 15 635 (1989).
[4] Z. Olami, H. J. S. Feder, and K. Christensen, Phys. Rev. Lett. **68**, 1244 (1992).
[5] U. D. Schwarz, O. Zwörner, P. Köster, and R. Wiesendanger, Phys. Rev. B **56**, 6987 (1997).
[6] F. Heslot, T. Baumberger, B. Perrin, B. Caroli, and C. Caroli, Phys. Rev. E **49**, 4973 (1994).
[7] *Physics of Sliding Friction*, edited by B. N. J. Persson and E. Tosatti, Vol. 311 of *NATO Advanced Study Institute, Series E: Applied Sciences* (Kluwer Academic, Dordrecht 1996).
[8] *The Friction of Lubrication of Solids*, edited by F. P. Bowden and D. Tabor (Clarendon Press, Oxford, 1950).
[9] J. A. Greenwood and J. B. P. Williamson, Proc. R. Soc. London, Ser. A **295**, 300 (1966).
[10] C. Caroli and P. Nozières, in *Physics of Sliding Friction*, (Ref. [7]), p. 27.
[11] C. Caroli and B. Velicky, J. Phys. I **7**, 1391 (1997).
[12] A. Volmer and T. Nattermann, Z. Phys. B **104**, 363 (1997).
[13] A. Tanguy and S. Roux, Phys. Rev. E **55**, 2166 (1997).
[14] A. Tanguy, M. Gounelle, and S. Roux, Phys. Rev. E **58**, 1577 (1998).
[15] T. Baumberger, in *Physics of Sliding Friction*, (Ref. [7]), p. 1.
[16] M. Weiss and F.-J. Elmer, Z. Phys. B **104**, 55 (1997).
[17] F.-J. Elmer, in *Physics of Sliding Friction*, (Ref. [7]), p. 433.
[18] F.-J. Elmer, Phys. Rev. E **56**, R6225 (1997).
[19] M. Paczuski, S. Maslov, and P. Bak, Phys. Rev. **53**, 414 (1996).
[20] K. Ito, Phys. Rev. E **52**, 3232 (1995).
[21] S. I. Zaitsev, Physica A **189**, 411 (1992).
[22] S. Maslov and Y.-C. Zhang, Phys. Rev. Lett. **75**, 1550 (1995).
[23] K. Sneppen, Phys. Rev. Lett. **69**, 3539 (1992).
[24] Z. Olami (unpublished).
[25] T. Halpin-Healy and Y.-C. Zhang, Phys. Rep. **254**, 215 (1995).

[Slanina99a]

PHYSICAL REVIEW E VOLUME 60, NUMBER 2 AUGUST 1999

Cracking piles of brittle grains

František Slanina*
Institute of Physics, Academy of Sciences of the Czech Republic, Na Slovance 2, CZ-18221 Praha, Czech Republic and Center for Theoretical Study Jilská 1, CZ-11000 Praha, Czech Republic
(Received 6 October 1998)

A model which accounts for cracking avalanches in piles of grains subject to external load is introduced and numerically simulated. The stress is stochastically transferred from higher layers to lower ones. Cracked areas exhibit various morphologies, depending on the degree of randomness in the packing and on the ductility of the grains. The external force necessary to continue the cracking process is constant in a wide range of values of the fraction of already cracked grains. If the grains are very brittle, the force fluctuations become periodic in early stages of cracking. The distribution of cracking avalanches obeys a power law with exponent $\tau=2.4\pm0.1$. [S1063-651X(99)04108-2]

PACS number(s): 45.70.−n, 05.65.+b, 46.50.+a, 83.70.Fn

I. INTRODUCTION

There are many phenomena concerning granular matter which have attracted the attention of physicists [1]. The source of the complexity of sand and similar systems stems from a highly nonlinear mechanical response on the mesoscopic scale (i.e., on the scale of single grains) which brings about complicated behavior on many scales, up to the macroscopic one, even though there is usually no scale-free behavior [2]. This feature brings the physics of granular matter close to other complex mechanics phenomena, like friction [3] and wear [4], where the interplay of mesoscopic and macroscopic phenomena is the central point of attention.

The dynamics of sand may be studied from two points of view. Slow driving by adding single grains gives rise to avalanches [5,6] and stratification phenomena [7]. Intense driving by periodic or persistent external forces was observed to cause, for example, surface pattern formation (dunes, etc.) or grain-size separation [1]. The dynamics of the mixture of sand and air may lead to beautiful phenomena like the ticking of hourglasses [8].

On the other hand, the most frequently asked question about static properties was the stress distribution within sand heaps, either free or embedded in various kinds of containers [2,9–13]. The most famous phenomenon is perhaps the minimum of stress directly below the top of a conic sandpile, measured by Šmíd and Novosad [14] and later on explained theoretically by Bouchaud and co-workers [15–17]. The explanation is based on the fact that arches are created within the granular packing, which support most of the weight. A very important phenomenon connected with arching is the static avalanches due to large-scale reconstruction of arches, caused by very small external perturbation [18], and stick-slip motion of sand in a tube [19,20].

Both of the above phenomena are currently well described within the scalar arching model [19], which is a generalization of the scalar stress model developed for granular matter by Liu *et al.* [13,21,22].

A less studied phenomenon from the point of view of granular materials is the procedure in which the grains are produced, i.e., the fragmentation process [23,24]. The obvious practical importance of this process was stressed, e.g., in [25]. In statistical approaches to fragmentation [23], the grains which are cracked are considered either independently of each other or random two-particle collisions of the grains are taken into account. Such models are appropriate to the situation in mills. Different mechanisms should be at work when the bulk of the heap of granular particles is cracked by compression, like in manufacturing pills in the pharmaceutical industry. Similar problems were already addressed when studying the localization of deformation in two-dimensional heaps of plastic cylinders [26] and compaction of granular matter in silos under pressure [27].

In the present work, we introduce a model which considers the cracking of grains within a pile of other grains, some of them already cracked, others not. So we will not investigate the size distribution of fragments, like in Ref. [23], but the spatial configuration of clusters of cracked grains and also the external force fluctuations occurring during the process of cracking.

The article is organized as follows. In the next section the model is introduced. The Sec. III is a gallery of simulation results and the last section, Sec. IV, draws conclusions from the results obtained.

II. DESCRIPTION OF THE MODEL

Our model describes a two-dimensional pile of granular matter contained in a rectangular silo. A physical realization of this situation may be prepared by two parallel glass plates, the distance of which corresponds to the grain size. The lateral and bottom slots are closed, while the upper slot is open and a uniform external force is applied to the surface of the pile by a kind of piston. The grains are brittle (egg shells may serve as a popular example), which means that if the stress the grain supports exceeds a threshold value w_{thr}, the grain collapses. As a consequence of this, the stress pattern in the neighborhood of the collapsed grain changes, which may cause another grain collapse and finally leads to a kind of internal avalanche. During that process, the piston is kept immobile, so the total external force decreases, until the ava-

*Electronic address: slanina@fzu.cz

lanche stops. How much the force decreases as a consequence of cracking one grain is described by a material-dependent factor $\alpha<1$. We may expect that for more ductile grains the drop of the force will be smaller and the parameter α will be closer to 1. For this reason we will call α the ductility.

The stress within the pile is a tensor, but recent studies [17] showed that for many purposes only the diagonal element corresponding to the horizontal axis is important. This simplification leads to a scalar model of stress propagation in granular matter, which will be a basis of our model here.

We suppose the grains are placed regularly on a square lattice rotated by 45°, so that the columns and rows of grains correspond to the diagonals on the lattice. Each row is L grains wide; each column is H grains high. The grains are in contact with the nearest neighbors on the lattice. The randomness in the size, shape, and position of the grains is taken into account by a stochastic rule, which describes the propagation of stress.

Denote w_{ik} the stress on the grain in ith row (counted from above) and kth column. It transfers the fraction q_{ik} of the stress to its left bottom neighbor, the fraction $1-q_{ik}$ to its right bottom neighbor. We neglect the weight of the grains themselves, compared to the external force. So the rule of stress propagation is described by the equations

$$\begin{aligned} w_{i+1,k} &= q_{ik} w_{ik} + (1-q_{ik-1}) w_{ik-1} \quad \text{for odd } k, \\ w_{i+1,k} &= (1-q_{ik}) w_{ik} + q_{ik+1} w_{ik+1} \quad \text{for even } k. \end{aligned} \tag{1}$$

We impose cylindrical boundary conditions, $w_{i0}=w_{iL}$. The topmost row is subject to external forces $w_{1k}=f_k$. We will call the normalized sum $F=\Sigma_k f_k/L$ the total external force.

The simulation proceeds as follows. The numbers q_{ik} are taken randomly from the uniform distribution on the interval $((1-\beta)/2,(1+\beta)/2)$. Initially all f_k are set equal and the local stresses are computed according to rules (1). At time step t, the force is uniformly increased until stress on one noncracked grain, say, at position (i,k), reaches the threshold $w_{\mathrm{thr}}=1$. Then, the time is stopped and the cracking avalanche starts. The grain is cracked, which has two consequences.

First, the external force is lowered. We can introduce the response function $G(i,k;k')$ such that the reduction of the external force on column k' is $f_{k'}\to[1-G(i,k;k')]f_{k'}$. We suppose that the response is localized, $G\sim\exp(-|k-k'|/\xi)$, and the correlation length ξ is short, $\xi\ll L$. In this case we assume that the form $G(i,k;k')=(1-\alpha)\delta_{kk'}$ is a good approximation, which does not change the universality class of the model. This leads to a lowering of the force only on top of the column in which the cracked grain lies, $f_k\to\alpha f_k$.

Second, if grain in the same row to the left, i.e., $(i,k-1)$, is not cracked, the value of q corresponding to left top neighbor of (i,k) is set to 1. If $(i,k-1)$ is cracked, q is given a new random value from the uniform distribution on the interval $((1-\beta)/2,(1+\beta)/2)$. A similar rule applies on the right hand side: if $(i,k+1)$ is not cracked, the right top neighbor of (i,k) has a new $q=0$; if $(i,k+1)$ is cracked, the new q is a random number from the same distribution as above. These rules correspond to a very simple intuitive observation, that the cracked grain no longer bears the load, if it has neighbors, which can bear the load instead of it. However, if the neighbors are also already cracked grains, the stress propagation remains to be stochastic as it was before the cracking, but the realization of the randomness, i.e., the values of the numbers q, is changed.

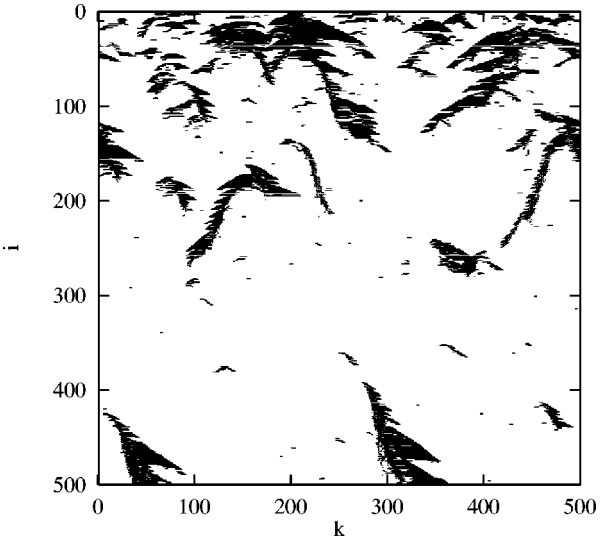

FIG. 1. Morphology of cracked areas for a sample with $L=500$ and $H=500$, after 5000 time steps. Every cracked grain is represented by a black dot. The parameters are $\alpha=0.9$ and $\beta=0.25$.

After each change of q's, the local stresses are recomputed, the grains which are not yet cracked and exceed the threshold are cracked, new q's are established, and this procedure is repeated until no noncracked grains exceeding the threshold are found and the avalanche stops. Then we proceed to the next time step $t+1$. The external force is increased up to the value when another grain is cracked again and a new cracking avalanche starts. We will call the avalanche size Δc the total number of grains cracked during the avalanche. This algorithm continues as long as there are any noncracked grains left.

Besides the size of the system, the model has two free parameters. The parameter α measures the ductility of the grains and β the degree of randomness in the stress propagation. The limit $\beta=0$ corresponds to the fully deterministic case.

III. SIMULATION RESULTS

When a grain is cracked, the load is mostly transferred to its neighbors, which have then increased their chances of being cracked. This leads to the creation of clusters of cracked grains, which grow and merge as the cracking proceeds. The typical morphology of the cracked clusters is shown in Fig. 1. We can observe the formation of ''arches'' with one dominant ''leg'' only. The shape of the ''legs'' resembles the letter S when they grow large. The dependence of the morphology on the ductility α and randomness β is shown in Figs. 2, 3, and 4. For larger β the typical size of the cracked clusters is smaller, while for small β the sample contains only few big ''arches,'' which are also more symmetric than those for larger randomness. The ductility has a different influence on the morphology: in the case of more

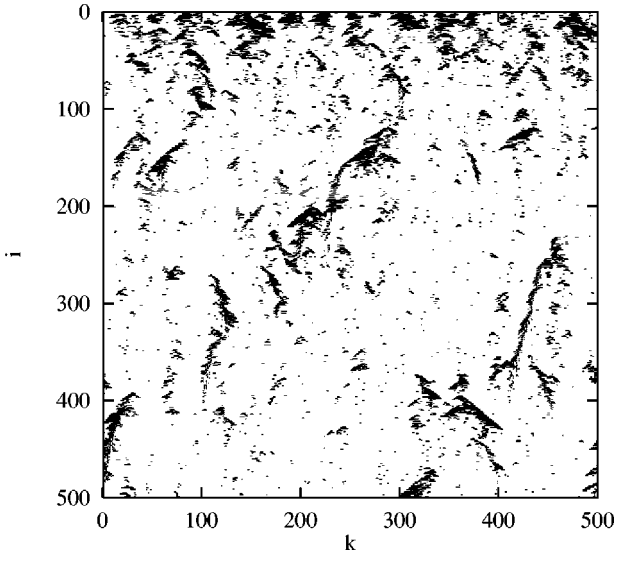

FIG. 2. Morphology of cracked areas for a sample with $L=500$ and $H=500$, after 5000 time steps. The parameters are $\alpha=0.9$ and $\beta=0.5$.

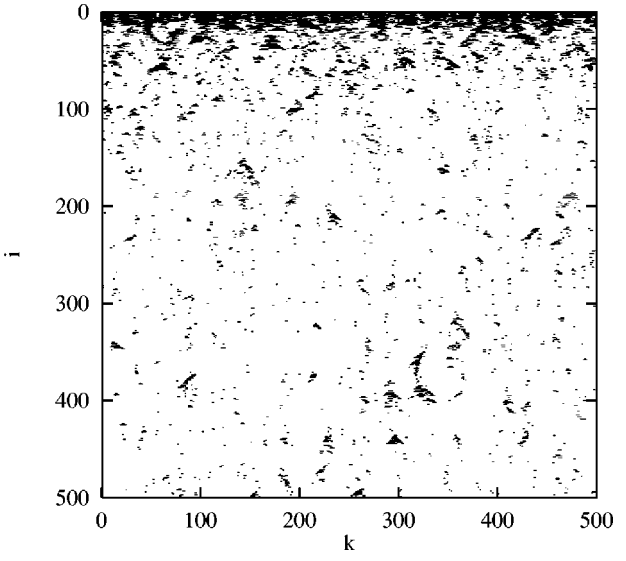

FIG. 4. Morphology of cracked areas for a sample with $L=500$ and $H=500$, after 10 000 time steps. The parameters are $\alpha=0.5$ and $\beta=0.5$.

brittle grains, i.e., with smaller α, the cracked areas are mostly concentrated in the top part of the sample, while more ductile grains lead to cracking equally probable in the whole bulk of the sample. (We performed simulations also for very ductile grains, α close to 1, and the trend was observed to shift the cracked regions to the bottom of the sample, when the ductility is increased.)

When the cracking proceeds, the force necessary to continue fluctuates. Each cracking avalanche means a drop of the force, which then rises again. Figure 5 shows the time dependence of the external force F and the fraction of cracked grains ν for a sample of 200×200 grains. We can see that the force fluctuates around a nearly time-independent value $F_{\mathrm{av}}\simeq0.55$ during the large part of the process, at least from time $t=1000$ to $t=5000$. This was even more clearly observed for larger samples (in our simulations 500×500). So the picture of the overall behavior of the force can be as follows. After a transient period, where the force suddenly drops and slowly rises again, a stationary cracking regime develops, characterized by constant average force F_{av}. This regime holds if the fraction of cracked grains is small; according to our observations $\nu<\nu_{\mathrm{max}}$ is a sufficient condition, where the value of ν_{max} depends slightly on α. For $\alpha=0.1$ we found $\nu_{\mathrm{max}}\simeq0.7$, while for $\alpha=0.9$ we observed $\nu_{\mathrm{max}}\simeq0.4$.

The value of the stationary force F_{av} decreases with β. We found the values in the range from $F_{\mathrm{av}}\simeq0.3$ for $\beta=1$ (maximum randomness) to $F_{\mathrm{av}}\simeq0.6$ for $\beta=0.1$ (minimum randomness studied).

Around the average force, there are fluctuations which reflect the unique realization of the disorder in our sample.

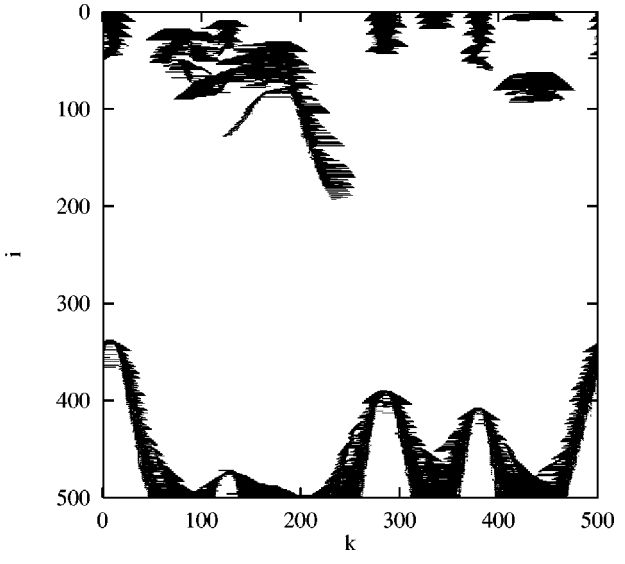

FIG. 3. Morphology of cracked areas for a sample with $L=500$ and $H=500$, after 5000 time steps. The parameters are $\alpha=0.9$ and $\beta=0.1$.

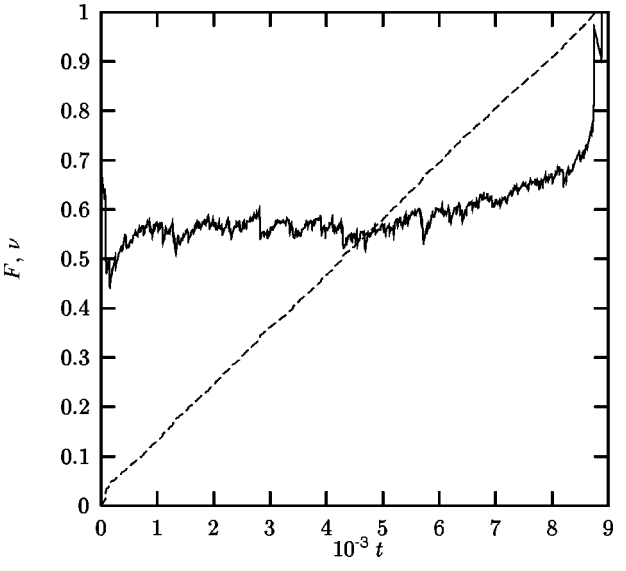

FIG. 5. Time evolution of external force F (solid line) and fraction of cracked grains ν (dashed line) for the sample with $L=200$, $H=200$, $\alpha=0.9$, and $\beta=0.25$.

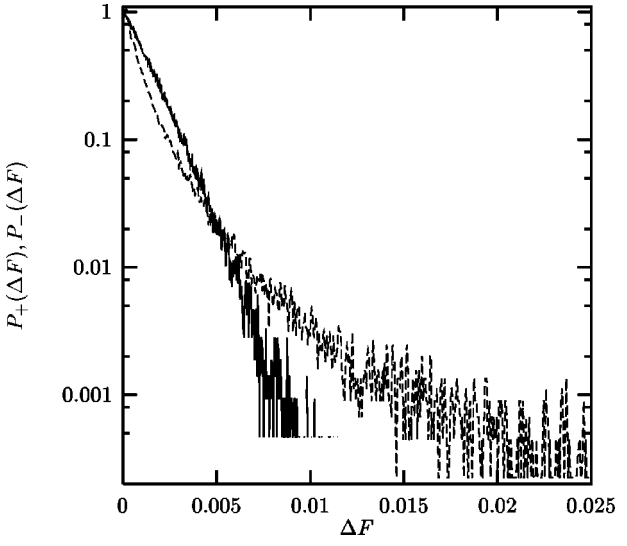

FIG. 6. Distribution of upward (solid line) and downward (dashed line) changes of the external force, for $L=200$, $H=200$, $\alpha=0.9$, and $\beta=0.25$. In order to avoid initial and final transient regimes, only the interval from time $t=1000$ to $t=8000$ was analyzed. The data are averaged over 20 independent runs.

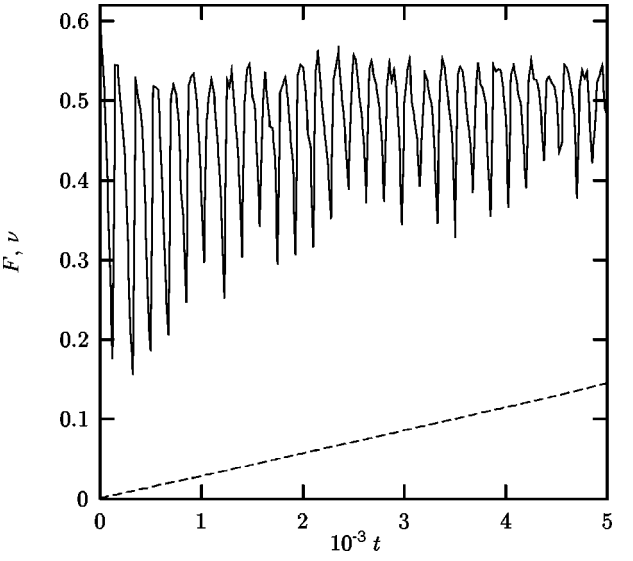

FIG. 7. Time evolution of external force F (solid line) and fraction of cracked grains ν (dashed line) for the sample with $L=200$, $H=200$, $\alpha=0.1$, and $\beta=0.25$.

We investigated statistical properties of the fluctuations. In Fig. 6 we show the distributions of upward changes $P_+(\Delta F)$ and downward changes $P_-(\Delta F)$ of the total external force from one step to the next one. The distribution of upward changes can be fitted well by an exponential, while the downward changes do not have any clear form of distribution: neither a Gaussian, exponential, stretched exponential, nor power-law fit was satisfactory. A distribution with a power-law tail seems to be a good candidate, but more data would be needed to settle this question.

For very small α (we observed the phenomenon for $\alpha=0.1$, but for $\alpha=0.3$ it was already absent) the fluctuations lose their purely random appearance and quasiregular force oscillations occur, which are especially pronounced in the early stages of the cracking process (i.e., for small ν). They can be clearly seen in Fig. 7. When the fraction of cracked grains increases, the oscillations gradually disappear. The oscillations perhaps correspond to the sudden drop of the force, observed for all α, followed by a gradual increase of the force again. While for small α many periods of the oscillation may be realized, for larger α the oscillations are ''overdamped'' and only a single period occurs.

A cracking avalanche starts from the stable state, in which the stress on all noncracked grains is below the threshold. The avalanche is initiated by an increase of external force up to a value which causes one grain to crack. This cracking may result in the cracking of other grains, and so on, until a new stable state is reached and the avalanche stops. We denote Δc the avalanche size, which is the number of grains cracked during the avalanche. We are interested in a statistical distribution of avalanche sizes. We expect that the distribution may be different in the initial transient period and in the stationary regime, in which the average force F_{av} is constant. So we investigated the distributions $P_l^>(\Delta c)$ defined as probabilities that the size of the avalanche, occurring in a time interval $(t_{l-1},t_l]$, with $t_0=0$, is larger than Δc.

Figure 8 shows the results for a 500×500 sample. The first two intervals, with final times $t_1=100$ and $t_2=300$, describe the situation in the transition regime. We can see that most of the avalanches have a typical size of about $\Delta c \simeq 400$. On the other hand, the next two intervals with end times $t_3=1000$ and $t_4=5000$ give distributions which can be fitted by a power law in the range of two decades. It can be also seen that the distribution is stable in time during the stationary cracking regime. We fitted the exponent of the power-law dependence $P^>(\Delta c)\sim(\Delta c)^{1-\tau}$ with the result

$$\tau=2.4\pm0.1. \tag{2}$$

We have found the same exponent (within error bars) for all values of the parameters studied. The only exception was

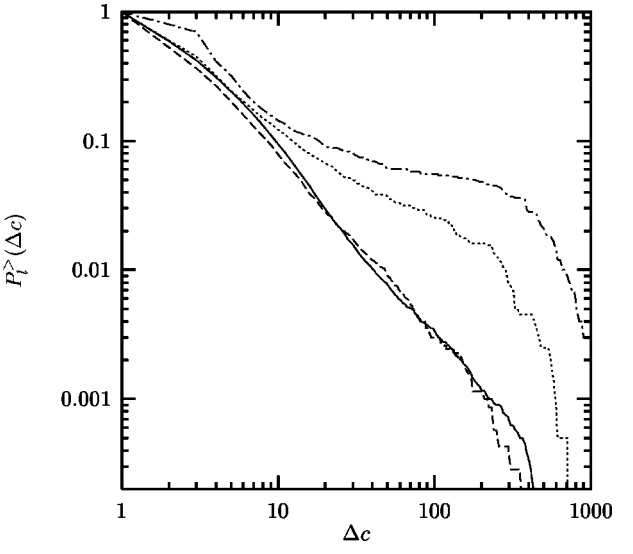

FIG. 8. Avalanche size distributions for $L=500$, $H=500$, $\alpha=0.9$, and $\beta=0.25$, in intervals determined by times $t_1=100$, $t_2=300$, $t_3=1000$, and $t_4=5000$. The lines denote the following distributions: dash-dotted line, $P_1^>$; dotted line, $P_2^>$; dashed line, $P_3^>$; solid line, $P_4^>$. $P_l^>$ corresponds to the interval $(t_{l-1},t_l]$.

[Slanina99a]

the case of $\beta=1$, where the distribution was close to exponential, instead of power law. The breakdown of the power law, when β approaches 1, remains to be studied.

IV. CONCLUSIONS

We have found that a two-dimensional pile of brittle grains packed in a rectangular container exhibits nontrivial behavior when an external force is applied from above and the grains are cracked. The cracked grains form clusters with different morphologies, depending on the ductility of the grains and on the degree of randomness in the packing. The degree of randomness seems only to determine the characteristic scale of the cracked clusters: lower randomness leads to larger clusters. This fact can be understood rather easily if we realize that a cluster occurs when the local stress exceeds the threshold necessary for a grain to be cracked. If the stress distribution is more uniform, fluctuations above the threshold are more distant one from the other.

A less expected feature is the influence of the ductility. Brittle grains have the tendency to crack in the top part of the container, while ductile grains are cracked mostly in the bottom part. This finding may play an important role in the separation of grains of different types.

During the cracking process the external force fluctuates around a general trend, which can be described as follows. If the grains are not too brittle ($\alpha \gtrsim 0.3$), the force drops suddenly and then rises slowly to a value which then remains constant for a great part of the whole cracking process. When the fraction of cracked grains approaches 1, the force increases again. So there exists a well-defined stationary cracking regime, preceded by a transient period and followed by a final stage. For very brittle grains, the force oscillates rather regularly even in the stationary regime.

Cracking one grain may result in an avalanche of further crackings. The distribution of avalanche sizes depends on time. While in the transient period the distribution is not scale invariant, in the stationary regime the distribution of avalanche sizes obeys a power law. This is an indication that a sort of criticality is present in the cracking process. The value of the exponent $\tau \simeq 2.4$ is larger than the avalanche exponents found in most self-organized critical (SOC) models known to us, where typically $\tau \leqslant 3/2$ [28–31]. On the other hand, the dynamics of our model resembles the Olami-Feder-Christensen (OFC) model of earthquakes [32], where the exponent varies in a wide range, comprising also the value found in our model. However, the mechanism leading to power-law scaling in the OFC model is not completely clear and the presence of SOC in that model is debated [33]. This may suggest that also in our model a new mechanism leading to criticality is at work, different from the usual SOC, represented by sandpile [28] or extremal dynamics [31] models.

This work does not compare the simulation results with experimental data, because we were not able to find any report of an experiment of this kind (loosely related are the experiments reported in [26]). It would be very welcome if a measurement in the direction suggested here was done in the future.

ACKNOWLEDGMENTS

I wish to thank E. Guyon for useful discussions and B. Velický for inspiring comments which motivated this work.

[1] H. M. Jaeger, S. R. Nagel, and R. P. Behringer, Rev. Mod. Phys. **68**, 1259 (1996).
[2] F. Radjai, M. Jean, J.-J. Moreau, and S. Roux, Phys. Rev. Lett. **77**, 274 (1996).
[3] *Physics of Sliding Friction*, edited by B. N. J. Persson and E. Tosatti, Vol. 311 of *NATO Advanced Study Institute, Series E: Applied Sciences* (Kluwer Academic, Dordrecht, 1996).
[4] Koji Kato, in *Materials Science and Technology*, edited by R. W. Cahn, P. Haasen, and E. J. Kramer (Weinheim, New York 1993), Vol. 6, p. 635.
[5] S. R. Nagel, Rev. Mod. Phys. **64**, 321 (1992).
[6] G. A. Held, D. H. Solina, D. T. Keane, W. J. Haag, P. M. Horn, and G. Grinstein, Phys. Rev. Lett. **65**, 1120 (1990).
[7] H. A. Makse, S. Havlin, P. R. King, and H. E. Stanley, Nature (London) **386**, 379 (1997).
[8] T. Le Pennec, K. J. Måløy, A. Hansen, M. Ammi, D. Bideau, and X.-L. Wu, Phys. Rev. E **53**, 2257 (1996).
[9] S. Ouaguenouni and J.-N. Roux, Europhys. Lett. **39**, 117 (1997).
[10] S. F. Edwards and C. C. Mounfield, Physica A **226**, 1 (1996).
[11] C. C. Mounfield and S. F. Edwards, Physica A **226**, 12 (1996).
[12] S. F. Edwards and C. C. Mounfield, Physica A **226**, 25 (1996).
[13] C.-H. Liu, S. R. Nagel, D. A. Schecter, S. N. Coppersmith, S. Majumdar, O. Narayan, and T. A. Witten, Science **269**, 513 (1995).
[14] J. Šmíd and J. Novosad, Inst. Chem. Eng. Symp. Ser. **63**, D3/V/1 (1981).
[15] J.-P. Bouchaud, M. E. Cates, and P. Claudin, J. Phys. I **5**, 639 (1995).
[16] J. P. Wittmer, P. Claudin, M. E. Cates, and J.-P. Bouchaud, Nature (London) **382**, 336 (1996).
[17] P. Claudin, J.-P. Bouchaud, M. E. Cates, and J. P. Wittmer, Phys. Rev. E **57**, 4441 (1998).
[18] P. Claudin and J.-P. Bouchaud, Phys. Rev. Lett. **78**, 231 (1997).
[19] P. Claudin and J.-P. Bouchaud, in *Physics of Dry Granular Media*, edited by H. J. Herrmann, J.-P. Hovi, and S. Luding (Kluwer Academic, Dordrecht, 1998), p. 129.
[20] P. Claudin and J.-P. Bouchaud, Granular Matter **1**, 71 (1998).
[21] S. N. Coppersmith, C.-h. Liu, S. Majumdar, O. Narayan, and T. A. Witten, Phys. Rev. E **53**, 4673 (1996).
[22] S. N. Coppersmith, Physica D **107**, 183 (1997).
[23] S. Redner, in *Disorder and Fracture*, edited by J. C. Charmet, S. Roux, and E. Guyon (Plenum Press, New York, 1990), p. 31.
[24] M. Marsili and Y.-C. Zhang, Phys. Rev. Lett. **77**, 3577 (1996).
[25] D. Bideau, E. Guyon, and L. Oger, in *Disorder and Fracture* (Ref. [23]), p. 255.
[26] C. Poirier, M. Ammi, D. Bideau, and J. P. Troadec, Phys. Rev. Lett. **68**, 216 (1992).

[27] P. Evesque, J. Phys. I **7**, 1501 (1997).
[28] Per Bak, Chao Tang, and Kurt Wiesenfeld, Phys. Rev. A **38**, 364 (1988).
[29] P. Grassberger and S. S. Manna, J. Phys. (France) **51**, 1077 (1990).
[30] S. Zapperi, K. B. Lauritsen, and H. E. Stanley, Phys. Rev. Lett. **75**, 4071 (1995).
[31] M. Paczuski, S. Maslov, and P. Bak, Phys. Rev. E **53**, 414 (1996).
[32] Z. Olami, H. J. S. Feder, and K. Christensen, Phys. Rev. Lett. **68**, 1244 (1992).
[33] H.-M. Bröker and P. Grassberger, Phys. Rev. E **56**, 3944 (1997).

[Slanina02]

Eur. Phys. J. B **25**, 209–216 (2002)
DOI: 10.1140/epjb/e20020023

THE EUROPEAN PHYSICAL JOURNAL B
EDP Sciences

Self-organized branching process for a one-dimensional rice-pile model

F. Slanina[a]

Institute of Physics, Academy of Sciences of the Czech Republic, Na Slovance 2, 18221 Praha, Czech Republic

Received 21 June 2001 and Received in final form 14 November 2001

Abstract. A self-organized branching process is introduced to describe one-dimensional rice-pile model with stochastic topplings. Although the branching processes are generally expected to describe well high-dimensional systems, our modification highlights some of the peculiarities present in one dimension. We find analytically that the crossover behavior from the trivial one-dimensional BTW behaviour to self-organized criticality is characterised by a power-law distribution of avalanches. The finite-size effects, which are crucial to the crossover, are calculated.

PACS. 05.65.+b Self-organized systems – 05.70.Jk Critical point phenomena – 45.70.-n Granular systems

1 Introduction

Since the pioneering work of Bak, Tang and Wiesenfeld (BTW) [1,2], the sand-pile model became one of prototype abstract models exhibiting self-organized criticality (SOC). The original BTW model and its variants (see *e.g.* [3–7]) consists of a cellular automaton slowly driven by stochastic perturbations. The state of each site is described by the number of grains on top of it. (Actually, this number represents the slope rather than the height, if we want to interpret the model as a real sand-pile. However, in the 1D model, investigated here, the description using slope and height variables are strictly equivalent.) If the number of grains exceeds a threshold, the site becomes active, a toppling occurs and grains are transferred to neighbouring sites, which then may become active and the process continues. The driving consists of adding grains at randomly chosen sites. The critical state is reached asymptotically in the limit of infinitely slow driving [8]. Fully deterministic versions were also studied, showing periodic [9,10] or self-similar but non-random behaviour [11].

Even though experiments on real sand-piles did not confirm SOC behaviour, due to inertia effects [12–18], in the experiments using rice [19,20] instead of sand it was found that large aspect ratio of the rice grains (in contrast to sand which consists at almost special grains) can lead to SOC behaviour [19], has grains much closer to spherical.

Another difference between a typical sand-pile and rice-pile experiments is that the rice-piles used in the experiments are quasi one-dimensional [19,20]. While the original BTW model in one dimension is trivial, there are several variants of the 1D BTW model which exhibit non-trivial behaviour [3,11,21–25]. Also the sand-piles on quasi one-dimensional stripes were investigated [26]. Several one-dimensional models devised especially for modelling the rice-piles were studied [27–37]. The models which take into account a possible long-range rolling of grains are able to describe the transition from SOC behaviour typical for rice-piles to the inertia-dominated behaviour of sand heaps [38,39].

Besides numerous exact results and renormalisation-group calculations (to cite only a few items of a vast bibliography, see [40–46]), the mean-field approximation [47–49] was very useful in clarifying the nature of the SOC state, even though it cannot give correct values of the exponents below the upper critical dimension.

It was soon realised that the mean-field approximation for sand-piles is related to the critical branching processes [50,51]. This idea lead to the introduction of a self-organized branching processes [52–57], which describe the approach to the critical state. Similar approaches consist of mapping the sand-pile to percolation on a Bethe lattice [58].

The approximation is based on the observation that in high dimensions, activity returns to the same site with a very small probability. So, we can suppose that in each step the toppling occurs at a site, which has never toppled before during the same avalanche. Each toppling is mapped to one branching. Statistical properties of avalanches are determined by the probability p of branching. This probability is itself determined self-consistently. If the avalanche is sub-critical, it does not fall off the system and the average number of grains, and thus p, increases. If, on the other hand, the avalanche is super-critical, it surely falls off the system, which leads to a decrease of the average number of grains and a decrease of p. It was shown [52], that this process sets the p exactly to the critical value, where the avalanche sizes s

[a] e-mail: slanina@fzu.cz

have power-law distribution $P(s) \sim s^{-\tau}$ with mean-field exponent $\tau = \frac{3}{2}$.

The purpose of this work is to modify the self-organized branching processes in order to describe one-dimensional rice-pile models. Our model will be designed to include the one-dimensional BTW model as a special case. Clearly we cannot obtain correct values of the exponents. Our main question will be, whether there is a sharp transition from trivial 1D BTW behaviour to SOC behaviour or what is the nature of the crossover from the former to the latter.

The paper is organised as follows. In the next section we define our version of the branching process, suitable for treating the one-dimensional rice-pile. We find the condition for the criticality and investigate the crossover from trivial one-dimensional BTW behaviour to the critical branching process. The self-organization toward the critical state is investigated in the Section 3. We first define the self-organized branching process, then find the fixed point of the dynamics and show that it exactly corresponds to a critical branching process. We finally investigate the influence of finite size effects and find the finite-size scaling form. Section 4 concludes and summarises the work.

2 Branching process for one-dimensional model

2.1 Ricepile model

The rice-pile models were already thoroughly investigated by numerical simulations. In fact, there are two variants of the one-dimensional rice-pile model. The so-called "Oslo model" [30–33] supposes that the critical slope depends on space and time, and assumes a new random value after each toppling event. Another approach [27–29] assumes that the toppling occurs with a certain probability, which depends on the actual slope. It is the second approach, which we will follow in this article. It may be also noted that a two-dimensional model which also implements stochastic topplings was studied before [59].

We recall shortly the definition of the model. We consider a chain of L sites. The state of site i, $i = 1, 2, ..., L$ is described by a slope $z_i = h_i - h_{i+1}$ where the height h_i is a non-negative integer, with boundary condition $h_{L+1} = 0$. If the pile is in a stable state and a grain is dropped on the site $i = 1$, the update then proceeds for all sites in parallel. We look for all sites which satisfy at least one of the two conditions (i) it just toppled, (ii) its right-hand or left-hand neighbour toppled [27]. If i is such a site, it topples with probability 1, if $z_i > 2$, with probability $\alpha \in [0, 1]$ if $z_i = 2$ and with probability 0 if $z_i < 2$. A toppling at the site i means that z_i is decreased by 2 and z_{i-1} and z_{i+1} are increased by 1.

For $\alpha = 0$ or $\alpha = 1$ we recover the standard one-dimensional BTW sand-pile model with critical slope $z_c = 1$ or $z_c = 2$, respectively. In the intermediate region, $0 < \alpha < 1$, self-organized criticality was found in numerical simulations, with avalanche exponent $\tau = 1.55 \pm 0.02$ [29]. However, it is not clear, what is the behaviour of the model for α close to either 1 or 0. It seems, that for a finite system the behaviour is SOC (modified by finite size effects) only if α is not too close to 1 or 0 [34,60]. The behaviour of the system when the system size diverges and α stays close 0 or 1 has not been clarified. We would like to study this question within the approximation provided by a self-organized branching process.

2.2 Characteristic functions

From the technical point of view we will use the method of a characteristic function (discrete Laplace transform), defined for a function $f(s)$ on integer numbers s as $\hat{f}(\zeta) = \sum_{s=0}^{\infty} \zeta^s f(s)$.

We will see that the distribution of avalanches have generic form

$$P(s) \sim s^{-\tau} \mathrm{e}^{-s/s_0} \tag{1}$$

for large s. In the mean-field approximation or in the branching process we have $\tau = 3/2$, while in the one-dimensional BTW sand-pile the exponent is $\tau = 0$. The process is critical, if the cutoff avalanche size s_0 diverges ($s_0 \to \infty$).

In the language of characteristic functions the behaviour (1) translates to the properties of the singularity in $\hat{P}(\zeta)$. Generally we have $\hat{P}(\zeta) \sim (\zeta - \zeta_0)^\eta +$ *nonsingular part*. For the one-dimensional BTW process we have $\eta = -1$, while a true branching process has $\eta = 1/2$. The cutoff is given by the distance of the singularity from the point $\zeta = 1$, namely $s_0 \simeq 1/|\zeta_0 - 1|$. The process is critical, if $\zeta_0 = 1$.

We will also see that the characteristic function for the branching process is typically the solution of a quadratic equation. The singular part of the characteristic function comes from the square root of the discriminant $D(\zeta)$ of the equation, *i.e.* $\hat{P}(\zeta) \sim \sqrt{D(\zeta)} +$ *nonsingular part*. Therefore, $\eta = 1/2$ and the cutoff is given by the solution of the equation $D(\zeta_0) = 0$. If $D(1) = 0$, we have $s_0 = \infty$ and the process is critical.

2.3 Branching process

Let us first recall how the branching process is used to describe the simplest case of the sand-pile model, for which in each toppling event two grains are transferred to two randomly chosen nearest neighbours (Manna model [6]). There are N_0 sites in state $z = 0$ and N_1 sites in state $z = 1$. The branching process starts by dropping a grain onto a randomly chosen site. The probability of becoming active (of toppling) is $p = \frac{N_1}{N_0+N_1}$. Two new branches arise from an active site. Each of them is active with probability p and a tree is created iteratively. The branching process stops, when no active sites are present at the endpoints of the tree. The number of active sites, or number of branchings, corresponds to the size of the avalanche. The

probability distribution of avalanche sizes can be easily obtained with the use of characteristic functions [52–56] and gives the mean-field value of the exponent $\tau = 3/2$

Approximating the sand- or rice-pice models by a branching process is well justified in high dimensions, where the activity returns to the same point with very small probability. It seems, therefore, that the use of a branching processes in the opposite limit, in one dimension, lacks sense, because the return of activity is very frequent. However, we can use a very simple property of the return of activity to make the approximation sensible. Indeed, the most frequent case when the activity returns to the same site is described by the following process.

If the site i is active (it topples), a grain is transferred to site $i+1$ which can become active. If that happens, another grain is transferred back to site i (and also to site $i+2$, but this is not important now) and thus the site i may become active again. This observation leads to the suitable modification of the branching process to describe the one-dimensional case. We should take into account explicitly the return of the activity just in the next step. We will do this by setting different branching probabilities for a site which was active at the previous step (*i.e.* the site to the left) and for the site which did not have to be (the site to the right).

Because the grains are added only on the site $i = 1$, we have $z_i \geq 0\ \forall i$. The condition that the site topples with probability 1 if $z > 2$ ensures that $z_i \leq 2\ \forall i$. We denote N_a as the number of sites with $z = a$. So, picking randomly a site, we have probability $p_a = N_0/(N_0 + N_1 + N_2)$ of having $z = a$, where $a = 0, 1, 2$.

Let us now describe the construction of the branching process corresponding to the one-dimensional rice-pile. There are three types of the points on the tree created by the branching process, according to the value of $z \in \{0, 1, 2\}$. We denote q_a the probability that a point with $z = a$ branches. The points with $z = 0$ do not branch, *i.e.* $q_0 = 0$, while the points with $z = 2$ always branch, so $q_2 = 1$. The points with $z = 1$ branch with probability α, *i.e.* $q_1 = \alpha$. The approximation consists in supposing that if a site did not topple in the previous step, it has probability p_a of having $z = a$, while if the site did topple in the last step, the probability of having $z = a$ is modified due to the previous toppling to the value

$$p'_a = \frac{q_{a+1}\, p_{a+1}}{\sum_{b=0}^{2} q_{b+1}\, p_{b+1}} \qquad (2)$$

where we used $p_3 = q_3 = 0$ for convenience.

If a branching occurs at a site, two new branches ("left" and "right") emanate from it. The probability that the right branch ends with a point with $z = a$ is p_a, while for the left branch the probability is p'_a. This way the tree corresponding to the branching process is created. The above described rules are illustrated in Figure 1.

The root of the tree should be treated separately. The reason is that in the ricepile model the avalanche starts by dropping a grain always on the left edge of the pile, *i.e.* on the site $i = 1$. If it topples, it transfers a grain only to the right, while the grain going to the left falls off the system. If we translated this feature to the description of our branching process, the root would consist either of a single non-branching point, or a point with a single branch (the right one) emerging from it. However, we are interested in the regime of long trees, where the different behaviour of the root from the rest of the tree is irrelevant. So, we assume that in the branching process the root also obeys the same rules as all other points. Thus, all points, including the root, have either zero or two branches emanating from then.

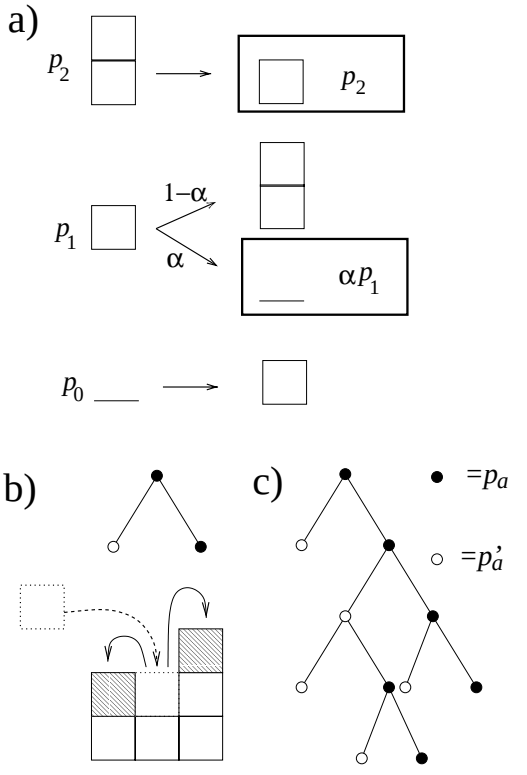

Fig. 1. Illustration of the branching process. In (a) the processes following a grain drop are depicted. The original configurations and their probabilities are in the left column, the final ones are in the right column. The possible final configurations resulting from a toppling are framed together with their non-normalized probabilities. In (b) the correspondence is shown between one branching event and the toppling, in which one new grain is added and two grains (shaded) are displaced to the left and to the right from the toppling site. In (c) a sample realization of the tree is sketched. The full circles placed on the right-hand branches correspond to probabilities p_a, while empty circles on the left-hand branches have modified probabilities p'_a.

The key quantity will be $P_n^a(s)$, the probability that a tree consisting of n levels starting with a point of type a contains s branchings. The probability of having s branchings (*i.e.* avalanche of size s) is then $P_n(s) = \sum_a p_a P_n^a(s)$. We can easily derive the recurrence relation for $P_n^a(s)$ which becomes particularly simple if we use the characteristic function. We obtain

$$\hat{P}_n^a(\zeta) = (1 - q_a) + q_a \zeta \sum_{b,c=0}^{2} p_b p'_c \hat{P}_{n-1}^b(\zeta) \hat{P}_{n-1}^c(\zeta) \ . \qquad (3)$$

A straightforward calculation leads to the following equations for the characteristic functions

$$\hat{P}_n^0(\zeta) = 1$$
$$\hat{P}_n^1(\zeta) = 1 - \alpha + \alpha \hat{P}_n^2(\zeta) \qquad (4)$$

and

$$P_n(s) = (\alpha p_1 + p_2) P_n^2(s) \ \text{ for } s > 0 \ . \qquad (5)$$

Therefore the basic quantity of interest will be the characteristic function $\hat{P}_n^2(\zeta)$. All properties of the branching process can be computed from it. The set of equations (3) thus represent a single recurrence equation for $\hat{P}_n^2(s)$, which in the limit $n \to \infty$ leads to quadratic equation for the stationary distribution $\hat{P}^2(\zeta) = \lim_{n\to\infty} \hat{P}_n^2(\zeta)$. We obtain explicitly

$$\frac{1}{\zeta}\hat{P}^2(\zeta) = \frac{(\alpha p_1 + (1-\alpha)p_2)(1 - \alpha p_1 - p_2)}{p_2 + \alpha p_1} + \frac{\alpha p_2 + 2\alpha(1-\alpha) p_1 p_2 + (1-2\alpha) {p_2}^2 + {p_1}^2 \alpha^2}{p_2 + \alpha p_1} \hat{P}^2(\zeta) + \alpha p_2 (\hat{P}^2(\zeta))^2 \quad . \qquad (6)$$

2.4 Criticality

The discriminant $D(\zeta)$ of equation (6) depends on the parameters p_1, p_2, and α. The branching process is critical if $D(1) = 0$. This implies the following relation

$$-\alpha p_1 - (1-\alpha) p_2 + 2\alpha p_1 p_2 + {p_1}^2 \alpha^2 + {p_2}^2 = 0 \qquad (7)$$

which determines a surface in the parametric space. On this surface the process is critical and the distribution of avalanche sizes has a power-law tail with exponent $\tau = 3/2$.

However, the latter statement is not strictly true in the sense that if the coefficient at the quadratic term in equation (6) is zero, the process is not a true branching process, because each parent can have at most one offspring. This corresponds to a process with an exponential distribution of avalanche sizes, which we will call, in this work, a "one-dimensional BTW process". The important feature which makes this different from a generic branching process is that there are no true branching points. Indeed, there may be a non-zero probability that the process stops at a given point, but there is zero probability of splitting into more than one branch. Therefore, the process does not generate tree-like structures, but linear chains of random length. Both the one-dimensional BTW and branching processes have the same general form (1) of the distribution of avalanches for large s, but the one-dimensional BTW process is characterised by the exponents $\tau = 0,\ \eta = -1$. Therefore, in addition to checking the criticality condition (7) we must also look at the behaviour close to the singularity.

We will prove in Section 3.2 that in the thermodynamic limit our rice-pile model self-organizes so that the parameters stabilise at values

$$p_1 = \max(0, \frac{2\alpha - 1}{\alpha})$$
$$p_2 = 1 - \alpha \ . \qquad (8)$$

If we insert these values into the criticality condition (7), we find that it is satisfied for an values of α, including the limit values of 0 and 1. At the same time we find that the singularity is always located at $\zeta_0 = 1$. (Indeed, as we discussed in section 2.2, the criticality of the process is equivalent to the condition $\zeta_0 = 1$.) However, we find that the type of the singularity corresponds to the exponents $\eta = 1/2$, $\tau = 3/2$ (critical branching process) only for α's within the open interval $(0, 1)$, while at the points 0 and 1 the model corresponds to one-dimensional BTW process. This can be easily interpreted in the language of sand- and rice-piles. Indeed, for $\alpha = 0$ and 1 the system recovers the behaviour of a one-dimensional BTW sand-pile, which does not exhibit critical behaviour in the usual sense. (In fact, the avalanche distribution *does* exhibit a power-law distribution: all avalanche sizes have the same probability, which corresponds to the power with exponent 0. But this situation is not usually described as critical behaviour).

2.5 Crossover behaviour

The question arises, how does the behaviour with exponent $\tau = 3/2$ inside the interval $[0, 1]$ cross over to the exponent $\tau = 0$ at the edges. As the critical behaviour is related to the singularities of the characteristic function, we will turn our attention to the investigation of the function $\hat{P}^2(\zeta)$ in more detail.

Indeed, we find that if we expand the solution of equation (6) for small values of the parameter ρ defined as

$$\rho(\zeta) = \frac{2\alpha(1-\alpha)}{\zeta^{-1} - 1 + 2\alpha(1-\alpha)} \qquad (9)$$

we can express the solution in terms of ρ and expand in the lowest order (for $\rho^2 \ll 1$)

$$\hat{P}^2(\zeta) = \frac{1}{\rho} - \sqrt{\frac{1}{\rho^2} - 1} \simeq \frac{\rho(\zeta)}{2} \quad . \qquad (10)$$

While, as noted earlier, the exact solution for $\hat{P}^2(\zeta)$ has always the singularity of the type $\eta = 1/2$ for $\zeta \to \zeta_0 = 1$, the approximate behaviour (10) has a singularity with $\eta = -1$ located at the point $\zeta_0' = (1 - 2\alpha(1-\alpha))^{-1} > 1$. When α goes to either 0 or 1, the value of ζ_0' approaches 1. This suggests the following scenario. For large avalanches, *i.e.* $1 - \zeta \ll \zeta_0' - 1$ the singularity at $\zeta_0 = 1$ is relevant and the avalanche size distribution has a power-law tail with exponent $\tau = 3/2$.

For shorter avalanches, *i.e.* $1 - \zeta$ larger or comparable to $\zeta_0' - 1$ the singularity at ζ_0' becomes dominant. Therefore, for short avalanches we have one-dimensional BTW

behaviour and $P(s) \sim \exp(-s/s_0)$ with a cutoff

$$s_0 = |1 - \zeta_0'|^{-1} = \frac{1 - 2\,\alpha\,(1-\alpha)}{2\,\alpha\,(1-\alpha)}\,. \tag{11}$$

The next step is to investigate the behaviour of s_0 when α approaches either 0 or 1. We find this by expanding the expression for ζ_0' as a function of α around the points 0 and 1, respectively. To make the notation more compact, let us introduce the variable $\mu \in \{0,1\}$, which distinguishes the two limit points $\alpha = 0$ and 1. We can see from (11) that the cutoff diverges as

$$s_0 \simeq \frac{1}{2\,|\alpha - \mu|} \tag{12}$$

for $\alpha \to \mu$.

On the other hand, sufficiently close to the singularity at $\zeta \to \zeta_0 = 1$ the exponent $\eta = 1/2$ is relevant. The question is, how close to $\zeta = 1$ does the behaviour cross over from one type to the other. We have one-dimensional BTW behaviour for $\rho^2 \ll 1$, and a critical branching process type of behaviour for $1 - \rho^2 \ll 1$. A typical crossover value $\zeta_{\rm cr}$ can be found by solving the equation

$$\rho(\zeta_{\rm cr}) = \frac{1}{2}\,. \tag{13}$$

The avalanche size distribution will exhibit the crossover around $s_{\rm cr} = 1/|1 - \zeta_{\rm cr}|$. For $s \ll s_{\rm cr}$ the one-dimensional BTW behaviour with exponential cutoff, diverging to infinity for $\alpha = 0$ and 1, will apply. While for $s \gg s_{\rm cr}$ the distribution will have a power-law tail with the usual mean-field exponent $-3/2$, and therefore exhibits self-organized criticality.

The point of the transition between SOC and one-dimensional BTW when α approaches 1 or 0 lies in the diverging crossover value for the avalanche size. Similarly as in the case of s_0, by solving equation (13) with definition (9) we find the following limiting behaviour

$$s_{\rm cr} \simeq \frac{1}{2\,|\alpha - \mu|} \simeq s_0 \tag{14}$$

for $\alpha \to \mu$.

We can see, comparing equations (12) and (14), that the cutoff for the one-dimensional BTW behaviour is asymptotically equal to the crossover at which the critical branching process behaviour sets on. This suggests the scaling form

$$P(s) \simeq \frac{1}{s_0(\alpha)}\,F(\frac{s}{s_0(\alpha)}) \tag{15}$$

valid for $s \gg 1$ and α close to 0 and 1. The scaling function has the form $F(x) \sim {\rm e}^{-x}$ for $x \ll 1$ and $F(x) \sim x^{-3/2}$ for $x \gg 1$. Indeed, we can find the Laplace transform of the scaling function as

$$\int_0^\infty {\rm e}^{-x(y-1)}\,F(x)\,{\rm d}x = y - \sqrt{y^2-1} \quad . \tag{16}$$

From here we obtain immediately the expression for the scaling function through the Bessel function of imaginary argument

$$F(x) = \frac{{\rm e}^{-x}}{x}\,I_1(x) \quad . \tag{17}$$

The expected behaviour for $x \ll 1$ and $x \gg 1$ can be verified directly by inspecting the asymptotic behaviour of the Bessel function.

3 Self-organization

3.1 Self-organized branching process

In the basic setup of our branching process, all three parameters α, p_1, p_2 are freely chosen. However, in the rice-pile model the only free parameter is α. The number of sites with given z can change during an avalanche, so that the probabilities p_1 and p_2 are also modified. This defines a flow in the space of parameters p_1, p_2. Our task now is to establish stable fixed points of the dynamics and check whether they satisfy the condition (7). If that happens, we can conclude that the system is self-organized critical.

There are four types of events, which can happen during an avalanche. Let us denote them as $T2$, $T1$, $E1$, and $E0$. In the event $T2$, a point with $z = 2$ receives a grain and topples. As a result, the number of sites with $z = 2$ is decreased by 1, $N_2 \to N_2 - 1$, and number of sites with $z = 1$ is increased by 1, $N_1 \to N_1 + 1$. Similarly, in the event $T1$ a point with $z = 1$ topples, $N_1 \to N_1 - 1$ and $N_0 \to N_0 + 1$. In event $E1$ a site with $z = 1$ receives a grain but does not topple, $N_1 \to N_1 - 1$ and $N_2 \to N_2 + 1$, and finally in event $E0$ a site with $z = 0$ receives a grain and does not topple, $N_0 \to N_0 - 1$ and $N_1 \to N_1 + 1$.

Using the variables $y \in \{T, E\}$ and $a, b \in \{0, 1, 2\}$, let us denote $s_{ayb,n}$ the number of events of the type yb occurring at the level n within the branching process, on condition that the very first site had $z = a$. There are $s_{ayb} = \sum_{n=0}^{\infty} s_{ayb,n}$ such events in the entire realisation of the branching process. On average, there are $\langle s_{yb}\rangle = \sum_a p_a \langle s_{ayb}\rangle$ events of the type yb. The averages $\langle s_{yb}\rangle$ are of central importance for the dynamics of the self-organization and can be easily obtained as follows.

For the characteristic function of the probability distribution of the number of events $s_{ayb,n}$ we obtain an equation analogous to (3). To study the self-organization, we will need only the average number of events, which is $\langle s_{ayb,n}\rangle$, calculated as the derivative of the characteristic function. Hence

$$\langle s_{ayb,n}\rangle = q_a \sum_c (p_c + p_c')\langle s_{cyb,n-1}\rangle. \tag{18}$$

This is a set of three recurrence relations, which may be reduced to one equation only, by considering the relations $\langle s_{0yb,n}\rangle = 0$ and $\langle s_{1yb,n}\rangle = \alpha\,\langle s_{2yb,n}\rangle$, valid for $n > 1$. If

we take as the basic quantity the average $\langle s_{2yb,n}\rangle$, we get a recurrence relation determining a geometric sequence

$$\langle s_{2yb,n+1}\rangle = \kappa\langle s_{2yb,n}\rangle \tag{19}$$

with quotient

$$\kappa = \frac{\alpha\, p_2 + (p_2 + \alpha\, p_1)^2}{p_2 + \alpha\, p_1}\,. \tag{20}$$

We recognise in the stationarity condition $\kappa = 1$ the equation (7), implying the criticality of the branching process.

Summation of the infinite geometric series immediately gives

$$\langle s_{yb}\rangle = \left(p_b + (p_b + p_b')\frac{\alpha\, p_1 + p_2}{1-\kappa}\right)\langle s_{byb,1}\rangle \tag{21}$$

where the initial conditions are given by $\langle s_{bTb,1}\rangle = q_b$ and $\langle s_{bEb,1}\rangle = 1 - q_b$.

The self-organization of the branching process is due to the changes in the numbers N_a, caused by the toppling (and non-toppling) events. These numbers determine the probabilities p_a. Therefore, for fixed α the self-organized branching process (SOBP) $\mathcal{S}(\alpha)$ consists of an (infinite) sequence of branching processes

$$\mathcal{S}(\alpha) = \tag{22}$$
$$[\mathcal{B}(\alpha, p_1^{(0)}, p_2^{(0)}), \mathcal{B}(\alpha, p_1^{(1)}, p_2^{(1)}), \mathcal{B}(\alpha, p_1^{(2)}, p_2^{(2)}), \dots]$$

where $\mathcal{B}(\alpha, p_1, p_2)$ is the branching process determined by fixed parameters α, p_1, p_2, defined above. The branching processes within the sequence differ only by the values of the parameters p_1, and p_2. Let us consider the tth branching process in the sequence. When realised, it changes the original values of the numbers N_a, or, equivalently, the values of the parameters p_a. The average change is uniquely determined by the average number of events $\langle s_{yb}\rangle$. So, the SOBP is entirely determined by the transition relations connecting the values of the parameters in the tth and $(t+1)$th step

$$p_i^{(t+1)} - p_i^{(t)} = T_i(p_1^{(t)}, p_2^{(t)}) \tag{23}$$

for $i \in \{1, 2\}$. We find explicitly

$$T_1(p_1, p_2) = \frac{\alpha p_1 + (1-\alpha)p_2 - \alpha(2-\alpha)p_1^2 - p_2^2 - 2(1-\alpha)p_1 p_2}{\alpha p_1 + (1-\alpha)p_2 + 2\alpha p_1 p_2 + p_2^2 + \alpha^2 p_1^2} \tag{24}$$
$$T_2(p_1, p_2) = \frac{\alpha(1-\alpha)p_1^2 + (1-2\alpha)p_1 p_2}{\alpha p_1 + (1-\alpha)p_2 + 2\alpha p_1 p_2 + p_2^2 + \alpha^2 p_1^2}.$$

3.2 Fixed point

The fixed point of the self-organization dynamics can be found immediately by equating the right-hand sides of equations (25) to zero. Direct solution of the two coupled equations gives three fixed points

$$p_1 = \quad 0, \quad p_2 = 0 \tag{25}$$
$$p_1 = \quad 0, \quad p_2 = 1-\alpha \tag{26}$$
$$p_1 = \tfrac{2\alpha-1}{\alpha}, \; p_2 = 1-\alpha \quad . \tag{27}$$

The correct solution is determined by stability considerations. The relations (25) are linearised around the fixed points and the eigenvalues of the resulting matrices of rank 2 are found. The result is that the fixed point (25) is always unstable, while (26) is stable for $\alpha \in [0, 1/2)$ and (27) is stable for $\alpha \in (1/2, 1]$. For $\alpha = 1/2$ the fixed points (26) and (27) coincide and both of them are marginally stable (*i.e.* the eigenvalues have zero real part).

Therefore, we find that the fixed point corresponds to the values of the probabilities

$$p_1 = \max\left(0, \frac{2\,\alpha - 1}{\alpha}\right)$$
$$p_2 = 1 - \alpha \tag{28}$$

which proves the already announced result of equation (8).

3.3 Finite-size effects

In the numerical simulations of the rice-pile model [33,34,36,60] attention is paid to the fact that the critical behaviour is observed only for large enough systems and with α not too close to neither 0 nor 1. We have already shown how the crossover length blows up when α approaches the edge values 0 or 1. It is obvious then, that for small systems the crossover value of the avalanche size may not be accessible and the critical regime in the tail of the distribution is not observed at all. In this subsection we will investigate the consequences of the finite length of the branching process. There are two phenomena where the finite size enters the problem. First, if the maximum number of generations in the branching process is L, instead of infinity, the distribution of the avalanche sizes will not extend to infinity either, but will be bounded by $s < s_{\max} = 2^L - 1$. Moreover, if we take for example $p_1 = 1$, $p_2 = 0$, $\alpha = 1$, then all avalanches will have size L, therefore a peak at $s = L$ will occur, and $P(s) = \delta(s - L)$. If we move slightly from this position by increasing p_2 and decreasing p_1 and α, a structure of multiple peaks located at $s = L,\ 2L-1,\ 3L-3, \ldots$ will appear. This makes the analysis very complicated.

The second consequence of finite size is the shift in the self-organized value of the parameters p_1 and p_2, which for finite L will deviate from the critical values. Therefore, the avalanche-size distribution will develop an exponential cutoff of the form $P(s) \propto s^{-3/2}\exp(-s/s_1)$.

As the first problem brings particular new difficulties, we will concentrate only on the second one. This makes the analysis less consistent, but feasible. Thus, we should stress that in the following we will suppose that the branching process in question has unbounded length, but the self-organization is made in such a way, that only the first L generations of the branching process are taken into account.

Instead of working with the finite-L version of equations (23) and (25), describing the approach to the fixed point, we can use the set of equations

$$\langle s_{E1}\rangle = \langle s_{T2}\rangle$$
$$\langle s_{E0}\rangle = \langle s_{T1}\rangle \tag{29}$$

which determine the position of the fixed point. The only information lost in equations (29) is the stability of the fixed points. However, we suppose the stability will not be affected by finite-size effects. Therefore, we will rely on the stability analysis performed for $L = \infty$ also in the case of finite L and calculate the finite-size corrections starting with equation (29).

The point is that equations (29) should also hold for finite L. In fact, the expression (21) for the averages $\langle s_{yb} \rangle$ assume the same form, only the factor $(\kappa - 1)$ arising in the $L = \infty$ version should be replaced by the factor $K = (\kappa - 1)/(\kappa^{L-1} - 1)$. Assuming K small for large L, we can find p_1 and p_2 in lowest order of K. Then, we return to the definition of K and find that $K \propto L^{-1}$, confirming that our approach is consistent.

Hence, for finite L we find, by solving equations (29) to lowest order of $1/L$, for $\alpha \in (0, 1/2)$

$$p_1 = -\frac{1-\alpha}{(2\alpha-1)^2}\,\frac{\ln(1-\gamma)}{L} + O(\frac{1}{L^2})$$
$$p_2 = 1 - \alpha - \frac{1-\alpha}{2\alpha-1}\,\frac{\ln(1-\gamma)}{L} + O(\frac{1}{L^2}) \qquad (30)$$

and for $\alpha \in (1/2, 1)$

$$p_1 = \frac{2\alpha-1}{\alpha} + \frac{5\alpha^2 - 5\alpha + 1}{(2\alpha-1)^2\,\alpha}\,\frac{\ln(1-\gamma)}{L} + O(\frac{1}{L^2})$$
$$p_2 = 1 - \alpha + \frac{1-\alpha}{2\alpha-1}\,\frac{\ln(1-\gamma)}{L} + O(\frac{1}{L^2}) \qquad (31)$$

where we denoted

$$\gamma = \frac{1}{2}\frac{1-2\alpha}{1-\alpha} \quad \text{for} \quad \alpha \in (0, 1/2)$$
$$\gamma = \frac{1}{2}\frac{2\alpha-1}{\alpha} \quad \text{for} \quad \alpha \in (1/2, 1) \quad . \qquad (32)$$

The above formulae confirm that the explicit limit $L \to \infty$ gives the same result as obtained previously when working directly with $L = \infty$.

Using these results we can find the position of the square-root singularity in the characteristic function for the avalanche size distribution, solving equation $D(\zeta_0) = 0$. The distance from 1 then determines the exponential cutoff of the distribution. We find

$$1/s_1 = |\zeta_0 - 1| = \frac{\sigma(\alpha)}{L^2} + O(\frac{1}{L^3}) \qquad (33)$$

where

$$\sigma(\alpha) = \frac{\ln^2(1-\gamma)}{4\,\alpha\,(1-\alpha)} \quad \text{for} \quad \alpha \in (0, 1) \qquad (34)$$

and asymptotically for $L \to \infty$ and α fixed the avalanche distribution becomes the function of $s\,L^{-2}$ only,

$$P(s; \alpha, L) \propto L^{-3}\,G(sL^{-2}\,\sigma(\alpha)) \qquad (35)$$

and the scaling function has the form

$$G(x) = x^{-3/2}\mathrm{e}^{-x} \quad . \qquad (36)$$

This scaling holds well for all α with the exception of the point $\alpha = 1/2$, where we have $\gamma = 0$ and hence $\sigma(\alpha) = 0$. Then, the next order in $1/L$ takes over and the scaling changes.

Let us use again the variable $\mu \in \{0, 1\}$, which distinguishes the two limiting points $\alpha = 0$ and 1. The factor $\sigma(\alpha)$ diverges as $\sigma(\alpha) \simeq \sigma_0\,|\alpha - \mu|^{-1}$ for $\alpha \to \mu$, where $\sigma_0 = (\ln 2)^2/4$. Therefore, we can write the following scaling form for the avalanche size distribution

$$P(s; \alpha, L) \propto L^{-3}|\alpha - \mu|^{-\frac{3}{2}}\,G(s\,L^{-2}|\alpha - \mu|^{-1}\,\sigma_0) \qquad (37)$$

for $\alpha \to \mu$.

We can see that the power-law distribution holds only for avalanches shorter than $L^2\,|\alpha - \mu|$. In other words, if the parameter α is close to the end-points of the interval $[0, 1]$, we need to have systems of the size $L \gg 1/\sqrt{|\alpha - \mu|}$ in order to be able to observe any sign of self-organized criticality.

In the above calculations we tacitly assumed that we are beyond the regime we have called "one-dimensional BTW" in Section 2.5. This means $s \gg s_{\mathrm{cr}}$. In fact, we can always reach this regime by choosing L large enough. Therefore the presence of the one-dimensional regime does not influence the scaling behaviour for large L. More precisely, we should have $L^2\,|\alpha - \mu| \gg s_{\mathrm{cr}}$. But because s_{cr} itself diverge for $\alpha \to \mu$ as $|\alpha - \mu|^{-1}$, we obtain a stronger condition for the scaling (37) to be valid, namely

$$L \gg |\alpha - \mu|^{-1} \qquad (38)$$

if $\alpha \to \mu$.

4 Conclusions

We investigated analytically the self-organized critical rice-pile model. We defined a self-organized branching process, suitable for one-dimensional problems. The model is characterised by the parameter $\alpha \in [0, 1]$, the probability of toppling at a sub-threshold site. For both limiting values $\alpha = 0$ and $\alpha = 1$ the model is equivalent to the one-dimensional BTW model with trivial (uniform) distribution of avalanches.

We found that in the thermodynamic limit the system is self-organized critical for all values of α within the open interval $(0, 1)$, with power-law tail in the distribution of avalanche sizes with mean-field value of the exponent, $\tau = \frac{2}{3}$. However, the power-law behaviour holds only for avalanches longer than a certain crossover value of the avalanche size. The crossover diverges when α approaches either of the limiting points of the interval $[0, 1]$. We also found the scaling as well as the exact form of the scaling function for avalanche distribution close to these limit points. This describes how the one-dimensional BTW behaviour develops when approaching the limiting points.

The finite-size effects play important role in determining whether the model is self-organized critical or not. In our model the SOC behaviour starts to occur at larger sizes and the closer we are to the limiting points $\alpha = 0$

or 1. We found the form of the finite size and scaling in our self-organized branching process and determined the necessary condition for the the power-law regime in the avalanche distribution to be observable, when we approach the limiting points.

I wish to thank Mária Markošová for numerous useful discussions which motivated me in this work. I am indebted to Petr Chvosta for clarifying comments regarding stochastic processes. This work was supported by the Grant Agency of the Czech Republic, project No. 202/00/1187.

References

1. P. Bak, C. Tang, K. Wiesenfeld, Phys. Rev. Lett. **59**, 381 (1987).
2. P. Bak, C. Tang, K. Wiesenfeld, Phys. Rev. A **38**, 364 (1988).
3. L.P. Kadanoff, S. R. Nagel, L. Wu, S.-M. Zhou, Phys. Rev. A **39**, 6524 (1989).
4. P. Grassberger, S.S. Manna, J. Phys. France **51**, 1077 (1990).
5. S.S. Manna, Physica A **179**, 249 (1991).
6. S.S. Manna, J. Phys. A **24**, L363 (1991).
7. A. Chessa, H.E. Stanley, A. Vespignani, S. Zapperi, Phys. Rev. E **59**, R12 (1999).
8. D. Sornette, A. Johansen, I. Dornic, J. Phys. I France **5**, 325 (1995).
9. K. Wiesenfeld, J. Theiler, B. McNamara, Phys. Rev. Lett. **65**, 949 (1990).
10. M. Markošová, P. Markoš, Phys. Rev. A **46**, 3531 (1992).
11. P. Helander, S.C. Chapman, R.O. Dendy, G. Rowlands, N.W. Watkins, Phys. Rev. E **59**, 6356 (1999).
12. H.M. Jaeger, C.-H. Liu, S.R. Nagel, Phys. Rev. Lett. **62**, 40 (1989).
13. J. Rajchenbach, Phys. Rev. Lett. **65**, 2221 (1990).
14. G.A. Held, D.H. Solina, D.T. Keane, W.J. Haag, P.M. Horn, G. Grinstein, Phys. Rev. Lett. **65**, 1120 (1990).
15. S.R. Nagel, Rev. Mod. Phys. **64**, 321 (1992).
16. C.P.C. Prado, Z. Olami, Phys. Rev. A **45**, 665 (1992).
17. G.C. Baker, A. Mehta, Phys. Rev. E **53**, 5704 (1996).
18. G. Baumann, D.E. Wolf, Phys. Rev. E **54**, R4504 (1996).
19. V. Frette, K. Christensen, A. Malte-Sørenssen, J. Feder, T. Jøssang, P. Meakin, Nature **379**, 49 (1996).
20. A. Malthe-Sørenssen, J. Feder, K. Christensen, V. Frette, T. Jøssang, Phys. Rev. Lett. **83**, 764 (1999).
21. A. Mehta, G.C. Barker, Europhys. Lett. **27**, 501 (1994).
22. A. Malthe-Sørenssen, Phys. Rev. E **54**, 2261 (1996).
23. S. Lübeck, K.D. Usadel, Fractals **1**, 1030 (1993) (`cond-mat/9807021`).
24. R. Dickman, M. Alava, M.A. Muñoz, J. Peltola, A. Vespignani, S. Zapperi, Phys. Rev. E **64**, 056104 (2001), `cond-mat/0101381`.
25. V.B. Priezzhev, E.V. Ivashkevich, A.M. Povolotsky, C.-K. Hu, Phys. Rev. Lett. **87**, 084301 (2001).
26. S. Maslov, C. Tang, Y.-C. Zhang, Phys. Rev. Lett. **83**, 2449 (1999).
27. L.A.N. Amaral, K.B. Lauritsen, Phys. Rev. E **54**, R4512 (1996).
28. L.A.N. Amaral, K.B. Lauritsen, Physica A **231**, 608 (1996).
29. L.A.N. Amaral, K.B. Lauritsen, Phys. Rev. E **56**, 231 (1997).
30. K. Christensen, A. Corral, V. Frette, J. Feder, T. Jøssang, Phys. Rev. Lett. **77**, 107 (1996).
31. M. Paczuski, S. Boettcher, Phys. Rev. Lett. **77**, 111 (1996).
32. S.-D. Zhang, Phys. Lett. A **233**, 317 (1997).
33. M. Bengrine, A. Benyoussef, F. Mhirech, S.D. Zhang, Physica A **272**, 1 (1999).
34. M. Bengrine, A. Benyoussef, A. El Kenz, M. Loulidi, F. Mhirech, Eur. Phys. J. B **12**, 129 (1999).
35. M. Markošová, M.H. Jensen, K.B. Lauritsen, K. Sneppen, Phys. Rev. E **55**, R2085 (1997).
36. M. Markošová, Phys. Rev. E **61**, 253 (2000).
37. S.-D. Zhang, Phys. Rev. E **61**, 5983 (2000).
38. P.M. Gleiser, S.A. Cannas, F.A. Tamarit, B. Zheng, Phys. Rev. E **63**, 042301 (2001).
39. P.M. Gleiser, Physica A **295**, 311 (2001).
40. D. Dhar, R. Ramaswamy, Phys. Rev. Lett. **63**, 1659 (1989).
41. D. Dhar, S.N. Majumdar, J. Phys. A. **23**, 4333 (1990).
42. M. Markošová, J. Phys. A **28**, 6903 (1995).
43. M. Kloster, S. Maslov, C. Tang, Phys. Rev. E **63**, 026111 (2001).
44. L. Pietronero, A. Vespignani, S. Zapperi, Phys. Rev. Lett. **72**, 1690 (1994).
45. E.V. Ivashkevich, Phys. Rev. Lett. **76**, 3368 (1996).
46. Y.-C. Zhang, Phys. Rev. Lett. **63**, 470 (1989).
47. C. Tang, P. Bak, J. Stat. Phys. **51**, 797 (1988).
48. K. Kawasaki, T. Koga, Physica A **224**, 1 (1996).
49. A. Vespignani, S. Zapperi, Phys. Rev. E **57**, 6345 (1998).
50. P. Alstrøm, Phys. Rev. A **38**, 4905 (1988).
51. R. García-Pelayo, Phys. Rev. E **49**, 4903 (1994).
52. S. Zapperi, K.B. Lauritsen, H.E. Stanley, Phys. Rev. Lett. **75**, 4071 (1995).
53. K.B. Lauritsen, S. Zapperi, H.E. Stanley, Phys. Rev. E **54**, 2483 (1996).
54. G. Caldarelli, C. Tebaldi, A.L. Stella, Phys. Rev. Lett. **76**, 4983 (1996).
55. M. Vergeles, A. Maritan, J.R. Banavar, Phys. Rev. E **55**, 1998 (1997).
56. J. Chu, C. Adami, `cond-mat/9903085`.
57. J. Chu, C. Adami, Proc. Nat. Acad. Sci. **96**, 15017 (1999).
58. O. Sotolongo-Costa, A. Vazquez, J.C. Antoranz, Phys. Rev. E **59**, 6956 (1999).
59. H.F. Ouyang, Y.N. Lu, E.J. Ding, Phys. Rev. E **48**, 2413 (1993).
60. M. Markošová (unpublished).

[SlaKot00]

PHYSICAL REVIEW E VOLUME 62, NUMBER 5 NOVEMBER 2000

Random networks created by biological evolution

František Slanina* and Miroslav Kotrla†
Institute of Physics, Academy of Sciences of the Czech Republic, Na Slovance 2, CZ-182 21 Praha 8, Czech Republic
(Received 21 April 2000; revised manuscript received 14 July 2000)

We investigate a model of an evolving random network, introduced by us previously [Phys. Rev. Lett. **83**, 5587 (1999)]. The model is a generalization of the Bak-Sneppen model of biological evolution, with the modification that the underlying network can evolve by adding and removing sites. The behavior and the averaged properties of the network depend on the parameter p, the probability to establish a link to the newly introduced site. For $p=1$ the system is self-organized critical, with two distinct power-law regimes with forward-avalanche exponents $\tau=1.98\pm0.04$ and $\tau'=1.65\pm0.05$. The average size of the network diverges as a powerlaw when $p\to1$. We study various geometrical properties of the network: the probability distribution of sizes and connectivities, size and number of disconnected clusters, and the dependence of the mean distance between two sites on the cluster size. The connection with models of growing networks with a preferential attachment is discussed.

PACS number(s): 05.40.−a, 87.10.+e, 87.23.Kg

I. INTRODUCTION

Irregular networks or random graphs [1] composed of units of various kinds are very frequent both in nature and society (which is, however, nothing but a special segment of nature). Examples range from vulcanized polymers, silica glasses, force chains in granular materials [2], and mesoscopic quantum wires [3] to food webs [4], herding effects in economics [5], worldwide-web links [6], ''small-world'' networks of personal contacts between humans [7,8], and scientific collaboration networks [9].

The modeling of such networks is not quite easy and analytical results are relatively rare (examples, without any pretence of completeness, can be found in [1,5,10,11]). Numerical simulations are still one of the principal tools. However, even in the case when the properties of a given class of random networks are relatively well established, either analytically or numerically, as is the case of small-world networks, the serious question remains as to why these networks occur in nature. In other words, what are the dynamical processes which generate these networks.

Indeed, one can study, for example, various networks of the mutual dependence of species in a model of coevolution [12–14], but it is difficult to infer from these studies only which networks are closer to reality than the others. In the context of biological evolution models, there were recently a few attempts to let the networks evolve freely, in order to check which types of topologies might correspond to ''attractors'' of the process of natural evolution [15–20].

The model introduced by us in a preceding Letter [17] is based on extremal dynamics and basically follows the Bak-Sneppen model of biological evolution [13]. Extremal dynamics (ED) models [21] are used in a wide area of problems, ranging from growth in a disordered medium [22], dislocation movement [23], and friction [24] to biological evolution [13]. Among them, the Bak-Sneppen (BS) model plays the role of a testing ground for various analytical as well as numerical approaches (see, for example, [21,25–30]).

The idea of ED is the following. The dynamical system in question is composed of a large number of simple units, connected in a network. Each site of the network hosts one unit. The state of each unit is described by a single dynamical variable b, called the barrier. In each step, the unit with minimum b is mutated by updating the barrier. The effect of the mutation on the environment is taken into account by changing b also at all sites connected to the minimum site by a network link. Because a perturbation can propagate through the links, we should expect that the topology of the network can affect substantially the ED evolution.

The general feature of ED models is the avalanche dynamics. The forward λ avalanches are defined as follows [21]. For a fixed λ we define active sites as those having barrier $b<\lambda$. The appearance of one active site can lead to an avalanchelike proliferation of active sites in successive time steps. The avalanche stops when all active sites disappear again. Generically, there is a value of λ for which the probability distribution of avalanche sizes obeys a power law without any parameter tuning, so that the ED models are classified as a subgroup of self-organized critical models [31]. (This, of course, can hold only for networks of unlimited size.) The set of exponents describing the critical behavior determines the dynamical universality class the model belongs to.

It was found that the universality class depends on the topology of the network. Usually, regular hypercubic networks [21] or Cayley trees [30] are investigated. For random neighbor networks, the mean-field solution was found to be exact [32,26]. Also the tree models [30] were found to belong to the mean-field universality class. A one-dimensional model in which the links were wired randomly with the probability decaying as a power μ of the distance was introduced [33,34]. It was found that the values of critical exponents depend continuously on μ. The BS model of a small-world network was also studied [35].

Recently, the BS model on random networks, produced by bond percolation on a fully connected lattice, was studied

*Email address: slanina@fzu.cz
†Email address: kotrla@fzu.cz

[15]. Two universality classes were found. Above the percolation threshold, the system belongs to the mean-field universality class, while exactly at the percolation threshold, the avalanche exponent is different. A dynamics changing the topology in order to drive the network to critical connectivity was suggested.

There are also several recent results for random networks produced by different kinds of dynamics than ED, especially for the threshold networks [18] and Boolean networks [19,20].

The geometry of the worldwide web was intensively studied very recently. It was found experimentally that the network exhibits scale-free characteristics, measured by the power-law distribution of the connectivities of the sites [6,36]. Similar power-law behavior was observed also in the actor collaboration graph and in power grids [6]. A model was suggested [6] to explain this behavior, whose two main ingredients are continual growth and preferential attachment of new links, with sites with higher connectivity having a higher probability to receive additional links. The latter feature resembles the behavior of additive-multiplicative random processes, which are well known to produce power-law distributions [37,38].

The model introduced in [6] is exactly soluble [39]. Variants including aging of sites [40,41] and decaying and rewiring links [42,43] were also studied. The preferential attachment rule, which apparently requires unrealistic knowledge of the connectivities of the whole network before a single new link is established, was justified in a very recent work [44], where a higher probability of attachment at highly connected sites results from a local search by walking on the network.

In the preceding Letter [17] we concentrated on the self-organized critical behavior and extinction dynamics of a model in which the network changes dynamically by adding and removing sites. It was shown that the extinction exponent is larger than the upper bound for the BS model (given by the mean-field value) and is closer to the experimentally found value than any previous version of the BS model. In the present work we introduce in Sec. II a generalized version of the model defined in [17] and further investigate the self-organized critical behavior in Sec. III. However, our main concern will be with the geometric properties of the network, produced during the dynamics. These results are presented in Sec. IV. Section V gives conclusions from the results obtained.

II. EVOLUTION MODEL ON EVOLVING NETWORK

We consider a system composed of varying number n_u of units connected in a network, subject to extremal dynamics. Each unit bears a dynamical variable b. In the context of biological evolution these units are species and b represent the barrier against mutations. For the main novelty of our model consisting in adding (speciation) and removing (extiction) units, let us first define the rules for extinction and speciation. The rules determining which of the existing units will undergo speciation or extinction will be specified afterwards.

(i) If a unit is chosen for extinction, it is completely removed from the network without any substitution and all links it has are broken.

(ii) If a unit is chosen for speciation, it acts as a ''mother'' giving birth to a new, ''daughter'' unit. A new unit is added to the system and links are established between the new unit and the neighbors of the ''mother'' unit: each link of the ''mother'' unit is inherited with probability p by the ''daughter'' unit. This rule reflects the fact that the new unit is to a certain extent a copy of the original, so the relations to the environment will be initially similar to the ones the old unit has. Moreover, if a unit which speciates has only one neighbor, a link between ''mother'' and ''daughter'' is also established.

The extremal dynamics rule for our model is the following.

(iii) In each step, the unit with minimum b is found and mutated. The barrier of the mutated unit is replaced by a new random value b' taken from the uniform distribution on the interval $(0,1)$. Also the barriers of all its neighbors are replaced by new random numbers from the same distribution.

The rules determining whether a unit is chosen for extiction or speciation are the following.

(iv) If the newly assigned barrier of the mutated unit b' is larger than the new barriers of all its neighbors, the unit is chosen for speciation. If b' is lower than the barriers of all neighbors, the unit is chosen for extinction. In other cases neither extinction nor speciation occcurs. As a boundary condition, we use the following exception: if the network consists of a single isolated unit only, it is always chosen for speciation.

(v) If a unit is chosen for extinction, all its neighbors which are not connected to any other unit are also chosen for extinction. We call this kind of extinction singular extinction.

Rule (iv) is motivated by the following considerations. We assume that well-adapted units proliferate more rapidly and the chance for speciation is bigger. However, if the local biodiversity, measured by the connectivity of the unit, is bigger, there are fewer empty ecological niches and the probability of speciation is lower. On the other hand, poorly adapted units are more vulnerable to extinction, but at the same time larger biodiversity (larger connectivity) may favor survival. Our rule corresponds well to these assumptions: speciation occurs preferably at units with a high barrier and surrounded by fewer neighbors; extinction is more frequent at units with lower barriers and lower connectivity. Moreover, we suppose that a unit completely isolated from the rest of the ecosystem has a very low chance to survive. This leads to rule (v).

From rule (iv) alone follows the equal probability of adding and removing a unit, because the new random barriers b are taken from the uniform distribution. At the same time rule (v) enhances the probability of the removal. Thus, the probability of speciation is slightly lower than the probability of extinction. The degree of disequilibrium between the two depends on the topology of the network at the moment and can be quantified by the frequency of singular extinctions. The number of units, n_u, perform a biased random walk with reflecting boundary at $n_u=1$. The bias towards small values is not constant, though, but fluctuates as well.

The above rules are illustrated by the examples shown in Fig. 1. The networks in (a) show the effect of speciation: a new site is created and some to the links to the mother's

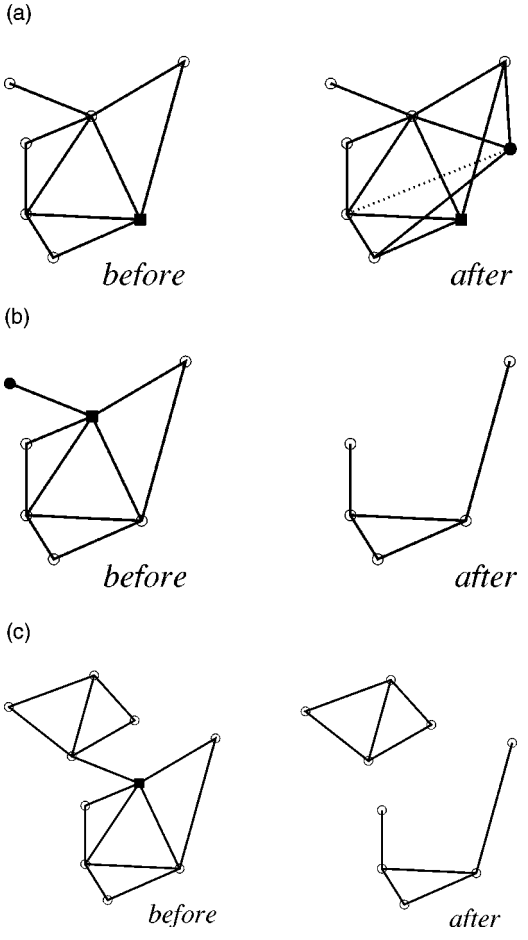

FIG. 1. Schematic illustration of the dynamical rules of the model. Speciation is shown in (a), where the solid square represents the extremal unit, which speciates, solid circle the new, daughter unit, and open circles other units, not affected by the speciation event. The dotted link illustrates that for $p<1$ some of the mother's links may not be inherited by the daughter. Extinction is shown in (b), where the extremal unit, which is removed, is indicated by the solid square. The unit denoted by the solid circle is the neighbor removed by the singular extinction. In (c) an example of an extinction event is shown, which leads to the splitting of the network into disconnected clusters.

neighbors are established. In (b) extinction is shown. One of the units is removed also due to a singular extinction [rule (v)]. In (c) we illustrate the possibility that in the extinction event the network can be split into several disconnected clusters.

III. SELF-ORGANIZED CRITICAL BEHAVIOR

A. Crossover scaling

The model investigated in the preceding Letter [17] corresponds to the value $p=1$. We found that in this case the model is self-organized critical. We defined newly the mass extinctions as the number of units removed during an avalanche. The distribution of mass extinctions obeys a power law with the exponent $\tau_{\rm ext}=2.32\pm0.05$. In this section we present an improved analysis of the data for the self-organized critical behavior.

We measured the distribution of forward λ avalanches [21] and we observed, contrary to the BS model, that two

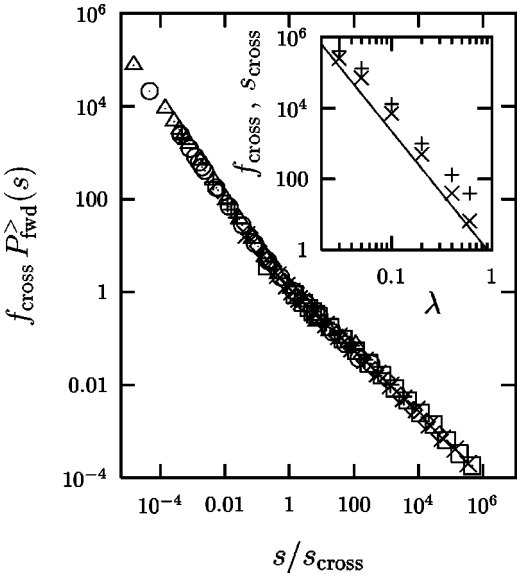

FIG. 2. Rescaled distribution of forward avalanches in the case $p=1$, for the values $\lambda=0.03(\triangle)$, $\lambda=0.05(\bigcirc)$, $\lambda=0.1(+)$, $\lambda=0.2(\diamond)$, $\lambda=0.4(\times)$, and $\lambda=0.6(\square)$, The superscript $>$ in $P^{>}_{\rm fwd}(s)$ is to indicate that we count all avalanches larger than s. In the inset we plot the dependence of the scaling parameters $s_{\rm cross}$ $(+)$ and $f_{\rm cross}(\times)$ on λ. The solid line is the power law $\lambda^{-\sigma'}$ with exponent $\sigma'=3.5$. The number of time steps was 3×10^8 and the data are averaged over 12 independent runs.

power-law regimes with two different exponents occur. The crossover value $s_{\rm cross}$ which separates the two regimes depends on λ. We observed that the distributions for different λ collapse onto a single curve if plotted against the rescaled avalanche size $s/s_{\rm cross}$, i.e.,

$$P^{>}_{\rm fwd}(s)f_{\rm cross}=g(s/s_{\rm cross}), \tag{1}$$

where $g(x)\sim x^{-\tau+1}$ for $x\ll1$ and $g(x)\sim x^{-\tau'+1}$ for $x\gg1$. The data are plotted in Fig. 2. For the values of the exponents, we found $\tau=1.98\pm0.04$ and $\tau'=1.65\pm0.05$.

We investigated the dependence of the scaling parameters $s_{\rm cross}$ and $f_{\rm cross}$ on λ and we found that both of them behave as a power law with approximately equal exponent, $s_{\rm cross}\sim f_{\rm cross}\sim\lambda^{-\sigma'}$ with $\sigma'\simeq3.5$ (see inset in Fig. 2). The role of critical λ at which the distribution of forward avalanches follows a power law is assumed by the value $\lambda=0$. This result is easy to understand. In fact, in models with fixed (or at least bounded) connectivity c, the critical λ is roughly $1/c$. As will be shown in the next section, in our case the size of the system and average connectivity grow without limits, and thus the critical λ tends to zero. Note that it is difficult to see this result without resort to the data collapse (1). Indeed, for any finite time of the simulation, the connectivity and the system size reach only a limited value and the critical λ seen in the distribution of forward avalanches has apparently a nonzero value.

B. Comparison with the Bak-Sneppen model

If we compare the above findings with the BS model, we can deduce that in our model, with $p=1$, the exponent τ corresponds to the usual forward-avalanche exponent, while

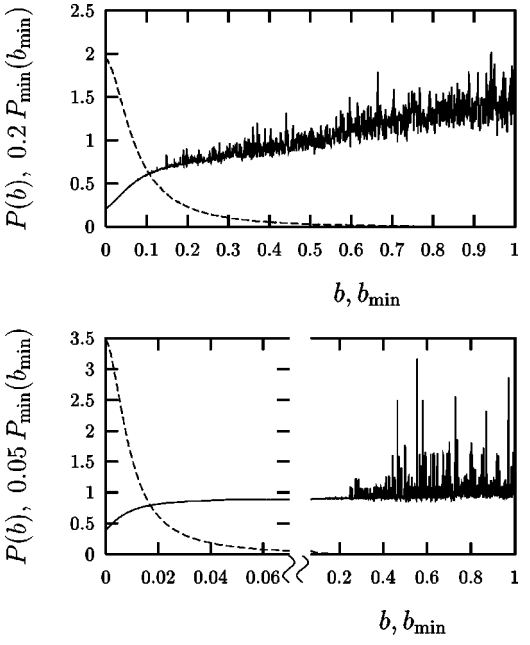

FIG. 3. Distribution of barriers b (solid line) and minimum barriers $b_{\min}$ (dashed line) for $p=0.95$ (upper plot) and $p=1$ (lower plot). In both cases the number of time steps was 10^7.

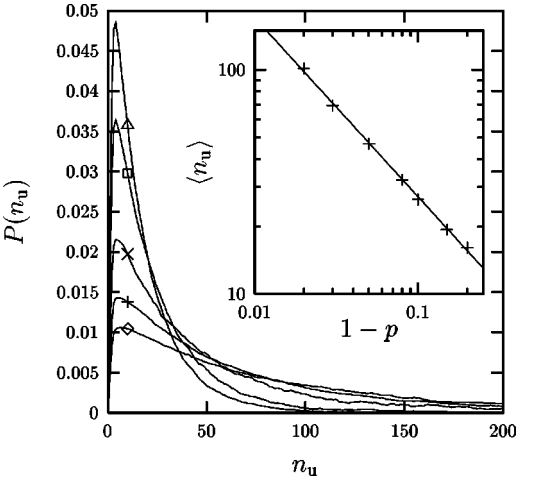

FIG. 4. Distribution of the number of units for different values of p[(△)0.85,(□)0.9,(×)0.95,(+)0.97,(◇)0.98]. Data are averaged over 10^8 time steps. Inset: dependence of the averaged number of units on p. The solid line corresponds to the power law $\langle n_u \rangle \propto (1-p)^{-0.8}$.

the exponent τ' is new. The above described scaling (1) breaks down for $p<1$ because the connectivity and the system size are limited (cf. the next section).

The main difference from the usual BS model is the existence of the second power-law regime for $s \gg s_{\text{cross}}$. It can be particularly well observed for values of λ close to 1, where the crossover avalanche size s_{cross} is small. We have seen that such avalanches start and end mostly when the number of units is close to its minimum value equal to 1. Between these events the evolution of the number of units is essentially a random walk, because singular extinctions are rare [17]. This fact can explain why the exponent τ' is not too far from the value 3/2 corresponding to the distribution of the first returns to the origin for the random walk. The difference is probably due to the presence of singular extinctions.

We measured also the distribution of barriers $P(b)$ and the distribution of barriers on the extremal site $P_{\min}(b_{\min})$. In Fig. 3 we can compare the results for $p=1$ and $p=0.95$. The sharp step observed in the BS model is absent here, because the connectivity is not uniform. (For comparison, we measured also the barrier distribution in the model of Ref. [15], where the network is static, but the connectivity is not uniform. Also in that case the step was absent and the distribution was qualitatively very similar to the one shown in Fig. 3.) The large noise level for b close to 1 is due to the fact that units with larger b undergo mutations rarely.

IV. NETWORK GEOMETRY

In this section we analyze the geometrical properties of the network and their dependence on the parameter p.

A. Size of the network

The first important feature of the networks created by the dynamics of the model is their size or the number of units within the network. This is a strongly fluctuating quantity, but on average it grows initially and after some time it saturates and keeps fluctuating around some average value, which depend on p. Figure 4 shows the probability distribution of number of units n_u for several values of p. The average number of units $\langle n_u \rangle$ was computed from these distributions and its dependence on p is shown in the inset of Fig. 4. We can see that the average network size diverges for $p \to 1$ as a power law, $\langle n_u \rangle \propto (1-p)^{-\alpha_n}$ with the exponent $\alpha_n \simeq 0.8$.

We can see from Fig. 5 that the distribution of the number of units has an exponential tail. This corresponds to the fact that the time evolution of the network size is a random walk with reflecting boundary at $n_u=1$, with a bias to lower values, caused by the singular extinctions (for an analysis of biased random walks repelled from zero see, e.g., [37]). From the decrease of average size with decreasing p we deduce that the bias due to singular extinctions has a larger effect for smaller p, i.e., if the new unit created in a speciation event has fewer links to the neighbors.

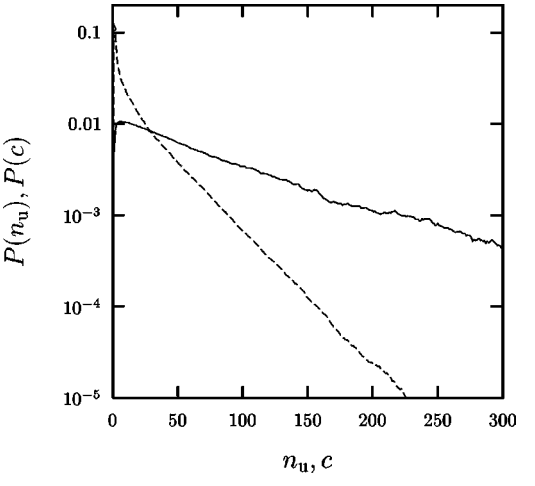

FIG. 5. Distribution of the number of units (solid line) and connectivity (dashed line), for $p=0.98$, averaged over 10^8 time steps.

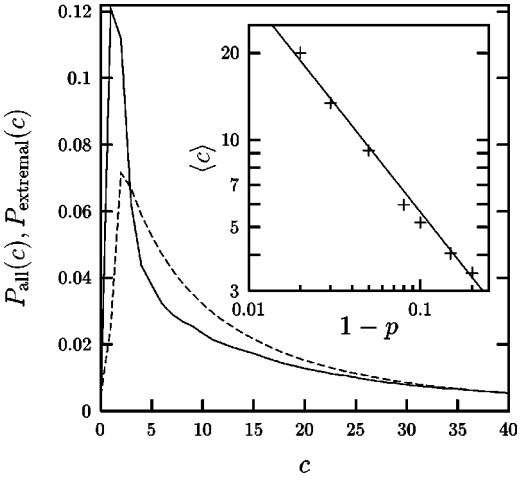

FIG. 6. Distribution of the connectivity for all sites (solid line) and for extremal sites only (dashed line), in the stationary regime for $p=0.98$, averaged over 10^8 time steps. Inset: dependence of the averaged connectivity on p. The solid line corresponds to the power law $\langle c \rangle \propto (1-p)^{-0.75}$.

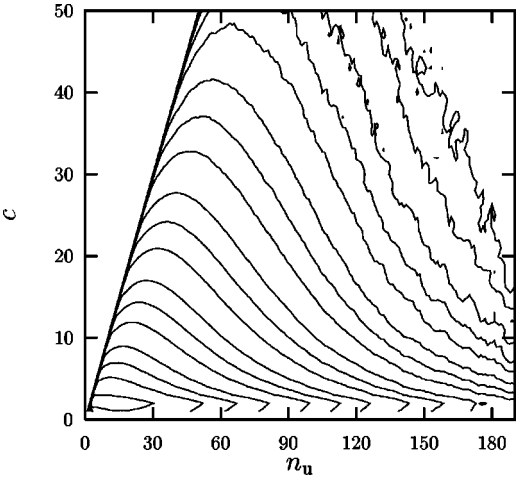

FIG. 7. Contour plot of the joint probability density $P(n_{\rm u},c)$ for the number of units and connectivity, for $p=0.8$, averaged over 3×10^9 time steps. The contours correspond to the following values of the probability density (from inside to outside): 5×10^{-R}, 2×10^{-R}, and 10^{-R}, with orders $R=3,4,5,6,7,8$.

B. Connectivity

In Fig. 6 we show the probability distribution of the connectivity of network sites $P_{\rm all}(c)$ and the distribution of the connectivity of the extremal unit $P_{\rm extremal}(c)$. We can observe the tendency that the extremal unit has a larger connectivity than average. This is in accordance with the findings of Ref. [15] obtained on static networks. It can be also easily understood intuitively. Indeed, in a mutation event the barriers of neighbors of the mutated unit are changed. So the neighbors have an enhanced probability to be extremal in the next time step. Therefore, sites with a higher number of neighbors have a larger probability that a mutation occurs in their neighborhood and that they are then mutated in the subsequent step.

The average connectivity $\langle c \rangle$ computed from the distributions $P_{\rm all}(c)$ is shown in the inset of Fig. 6. We can observe that analogically to the system size also the average connectivity diverges for $p\to1$ as a power law, but the value of the exponent is slightly different. We find $\langle c \rangle \propto (1-p)^{-\alpha_c}$ with the exponent $\alpha_c \simeq 0.75$. From the data available we were not able do decide whether the exponents α_n and α_c are equal within the statistical noise.

In Fig. 5 we can see that also the distribution of the connectivity has an exponential tail, similarly to the distribution of the network size. We measured also the joint probability density $P(n_{\rm u},c)$ for the number of units and the connectivity. The result is shown as a contour plot in Fig. 7. We can see that also for large networks (large $n_{\rm u}$) the most probable connectivity is small and nearly independent of $n_{\rm u}$. This means that the overall look of the network created by the dynamics of our model is that there are a few sites with large connectivity, surrounded by many sites with low connectivity.

An interesting observation can be drawn from the results shown in Fig. 8. It depicts the joint probability density as a function of the connectivity at fixed system sizes. We can see that for smaller system sizes, closer to the average number of units, the distribution is exponential, while if we increase the system size a power-law dependence develops. For example for the system size fixed at $n_{\rm u}=170$ we observe a power-law behavior $P(n_{\rm u},c)\sim c^{-\eta}$ nearly up to the geometric cutoff $c<n_{\rm u}$. The value of the exponent was about $\eta\simeq2.3$.

This finding may be in accordance with the power-law distribution in growing networks [6,39]. Indeed, in our model the power-law behavior applies only for networks significantly larger than the average size. Such networks are created during time-to-time fluctuations leading to a temporary expansion of the network. So the power law is the trace of expansion periods in the network evolution, corresponding to continuous growth in the model of [6]. The preferential attachment, which is the second key ingredient in [6], has also an analog in our model; highly connected units are more likely to be mutated, as was already mentioned in the discussion of Fig. 6. However, here the preference of highly connected sites is a dynamical phenomenon, resulting from the extremal dynamics rules of our model.

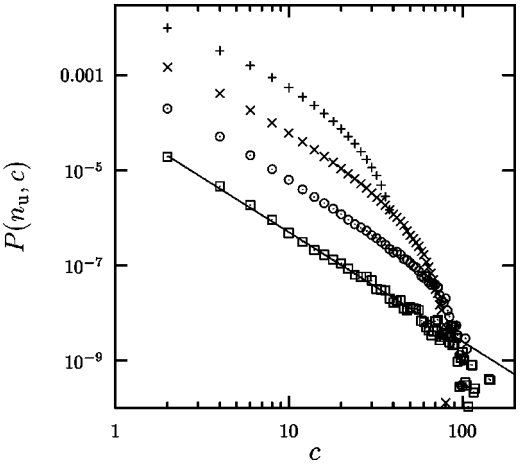

FIG. 8. Distribution of the connectivity for a fixed number of units, for $p=0.8$ and sizes $n_{\rm u}=40$ (+), 80 (×),120 (⊙), and 170 (□). The straight line is a power law with exponent −2.3. The data are the same as those used in Fig. 7.

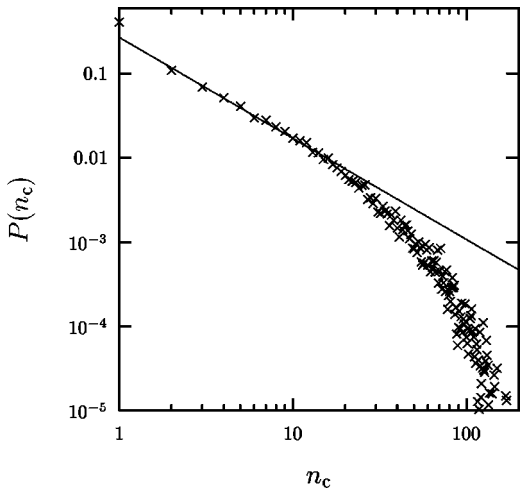

FIG. 9. Distribution of the number of clusters, for $p=0.98$. The straight line is a power law with exponent -1.2. The data were averaged over three independent runs 5×10^8,5×10^8, and 10^8 time steps long.

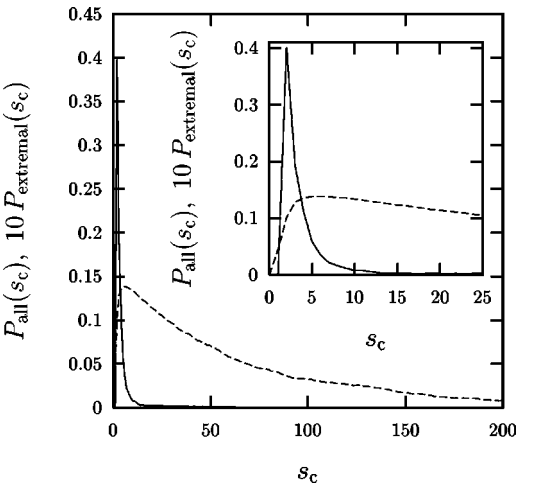

FIG. 10. Distribution of the cluster sizes s_c for $p=0.98$, averaged over 10^8 time steps. Solid line, all clusters; dashed line, clusters containing the extremal site. Inset: detail of the same distribution.

C. Clusters

As noted already in the Sec. II, the network can be split into several disconnected clusters. The clusters cannot merge, but they may vanish due to extinctions. We observed qualitatively that after initial growth the number of clusters exhibits stationary fluctuations around an average value, which increases when p approaches 1. We measured both the distribution of the number of clusters and the distribution of their sizes. In Fig. 9 we show the distribution of the number of clusters. The most probable situation is that there is only a single cluster. However, there is a broad tail, which means that even a large number of clusters can be sometimes created. The tail has a power-law part with an exponential cutoff. The value of the exponent in the power-law regime $P(n_c)\sim n_c^{-\rho}$ was about $\rho\simeq1.2$. We have observed that the width of the power-law regime is larger for larger p. This leads us to the conjecture that in the limit $p\to1$ the number of clusters is power-law distributed.

On the other hand, the distribution of cluster sizes shown in Fig. 10 has a maximum at very small values. This is due to two effects. First, already the distribution of network size has a maximum at small sizes, and second, if the network is split into many clusters, they have a small size and remain unchanged for a long time. The reason why small clusters change very rarely (and therefore can neither grow nor disappear) can be also seen from Fig. 10, where the distribution of the sizes of the clusters containing the extremal site is shown. The latter distribution is significantly different from the size distribution for all clusters and shows that the extremal site belongs mostly to large clusters. In fact, we measured also the fraction indicating how often the extremal unit is in the largest cluster if there is more than one cluster. For the same run from which the data shown in Fig. 10 were collected, we found that this fraction is 0.97, i.e., very close to 1. A similar ''screening effect'' was reported also in the Cayley tree models [30]: the small isolated portions of the network are very stable and nearly untouched by the evolution.

D. Mean distance

An important feature of a random network is also the mean distance $\bar{d}$ between two sites, measured as the minimum number of links which should be passed in order to get from one site to the other. In D-dimensional lattices, the mean distance depends on the number of sites N as $\bar{d}\sim N^{1/D}$, while in completely random networks the dependence is $\bar{d}\sim\ln N$. In small-world networks, the crossover from the former to the latter behavior is observed [7,8].

The dependence of the average distance within a cluster on the size of the cluster in our model is shown in Fig. 11. We can observe a global tendency to decrease $\bar{d}$ when increasing p. This result is natural, because a larger p means more links from a randomly chosen site and thus a shorter distance to other sites. The functional form of the size dependence is not completely clear. However, for larger cluster sizes, greater than about 25, the dependence seems to be faster than logarithmic, as can be seen from the inset in Fig.

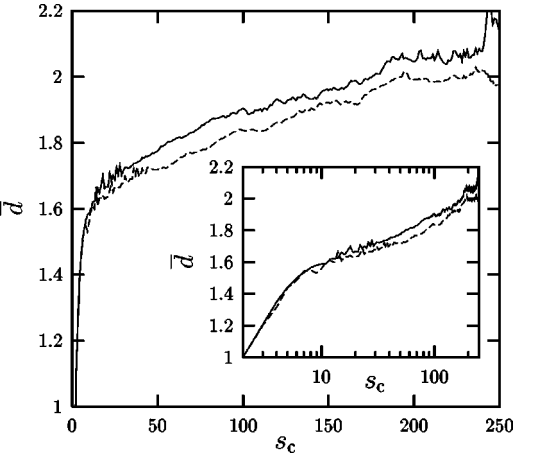

FIG. 11. Dependence of the average distance of two sites within the same cluster on the cluster size, for $p=0.95$ (solid line) and $p=0.97$ (dashed line), averaged over for 10^7 time steps. In the inset we show the same data in the log-linear scale.

11. So the networks created in our model seem to be qualitatively different from the random networks studied previously, as far as we know.

V. CONCLUSIONS

We studied an extremal dynamics model motivated by biological evolution on a dynamically evolving random network. The properties of the model can be tuned by the parameter p, the probability that a link is inherited in the process of speciation. For $p=1$ the model is self-organized critical and the average system size and connectivity grow without limits. Contrary to the usual BS model, we find two power-law regimes with different exponents in the statistics of forward λ avalanches. The crossover avalanche size depends on λ and diverges for $\lambda \to 0$ as a power law. The reason why the critical λ is zero in this model is connected with the fact that time-averaged connectivity diverges for $p=1$.

We investigated the geometrical properties of the random networks for different values of p. The average network size and average connectivity diverge as a power of $1-p$. The probability distribution of system sizes has an exponential tail, which suggests that the dynamics of the system size is essentially a biased random walk with a reflecting boundary, The value of the bias grows with decreasing p. The joint distribution of size and connectivity shows that even for large network sizes the most probable connectivity is low. Hence, there are few highly connected sites linked to the majority of sites with small connectivity. Moreover, situations where the system size is far above its mean value are characterized by a power-law distribution of the connectivity, like in models of growing networks with preferential attachment.

The network can consist of several mutually disconnected clusters. Even though the most probable situation contains only a single cluster, the distribution of cluster numbers has a broad tail, which shows a power-law regime with exponential cutoff. We observed the ''screening effect,'' characterized by a very small probability that the extremal site is found in any other cluster than the largest one. So there is a central large cluster, where nearly everything happens, surrounded by some small peripheral clusters, frozen for the major part of the evolution time.

We measured also the mean distance measured along the links within one cluster. The distance grows very slowly with the cluster size; however, the increase seems to be faster than logarithmic.

Summarizing, we demonstrated that the extremal dynamics, widely used in previous studies on macroevolution in fixed-size systems, is useful in creating random networks of variable size. It would be of interest to compare the properties of the networks created in our model with food webs and other networks found in nature. For example studies of food webs in isolated ecologies [4] give for network sizes about 30 average connectivities in the range from 2.2 to 9, which is not in contradiction with the findings of our model. However, more precise comparisons are necessary for any reliable conclusions about real ecosystems.

ACKNOWLEDGMENTS

We wish to thank K. Sneppen, A. Markoš, and A. Pękalski for useful discussions.

[1] B. Bollobás, *Random Graphs* (Academic Press, London, 1985).
[2] F. Radjai, M. Jean, J.-J. Moreau, and S. Roux, Phys. Rev. Lett. **77**, 274 (1996).
[3] T. Kottos and U. Smilansky, Ann. Phys. (N.Y.) **274**, 76 (1999).
[4] R.J. Williams and N.D. Martinez, Nature (London) **404**, 180 (2000).
[5] R. Cont and J.-P. Bouchaud, Macroeconomic Dynamics **4**, 170 (2000).
[6] A.-L. Barabási and R. Albert, Science **286**, 509 (1999).
[7] D.J. Watts and S.H. Strogatz, Nature (London) **393**, 440 (1998).
[8] M.E.J. Newman, e-print cond-mat/0001118.
[9] M.E.J. Newman, e-print cond-mat/0007214.
[10] M.E.J. Newman, C. Moore, and D.J. Watts, Phys. Rev. Lett. **84**, 3201 (2000).
[11] R.V. Kulkarni, E. Almaas, and D. Stroud, Phys. Rev. E **61**, 4268 (2000).
[12] S. A. Kauffman, *The Origins of Order: Self-organization and Selection in Evolution* (Oxford University Press, Oxford, 1993).
[13] P. Bak and K. Sneppen, Phys. Rev. Lett. **71**, 4083 (1993).
[14] R.V. Solé and S.C. Manrubia, Phys. Rev. E **54**, R42 (1996).
[15] K. Christensen, R. Donangelo, B. Koiller, and K. Sneppen, Phys. Rev. Lett. **81**, 2380 (1998).
[16] S. Jain and S. Krishna, Phys. Rev. Lett. **81**, 5684 (1998).
[17] F. Slanina and M. Kotrla, Phys. Rev. Lett. **83**, 5587 (1999).
[18] S. Bornholdt and T. Rohlf, Phys. Rev. Lett. **84**, 6114 (2000).
[19] S. Bornholdt and K. Sneppen, Phys. Rev. Lett. **81**, 236 (1998).
[20] S. Bornholdt and K. Sneppen, e-print cond-mat/0003333.
[21] M. Paczuski, S. Maslov, and P. Bak, Phys. Rev. E **53**, 414 (1996).
[22] K. Sneppen, Phys. Rev. Lett. **69**, 3539 (1992).
[23] S.I. Zaitsev, Physica A **189**, 411 (1992).
[24] F. Slanina, Phys. Rev. E **59**, 3947 (1998).
[25] P. Grassberger, Phys. Lett. A **200**, 277 (1995).
[26] J. de Boer, A.D. Jackson, and T. Wettig, Phys. Rev. E **51**, 1059 (1955).
[27] Yu.M. Pis'mak, J. Phys. A **28**, 3109 (1995).
[28] M. Marsili, P. De Los Rios, and S. Maslov, Phys. Rev. Lett. **80**, 1457 (1998).
[29] P. De Los Rios, A. Valleriani, and J.L. Vega, Phys. Rev. E **56**, 4876 (1997).
[30] N. Vandewalle and M. Ausloos, J. Phys. I **5**, 1011 (1995).
[31] P. Bak, C. Tang, and K. Wiesenfeld, Phys. Rev. Lett. **59**, 381 (1987).
[32] J. de Boer, B. Derrida, H. Flyvbjerg, A.D. Jackson, and T. Wettig, Phys. Rev. Lett. **73**, 906 (1994).
[33] R. Cafiero, P. De Los Rios, A. Valleriani, and J.L. Vega, Phys. Rev. E **60**, R1111 (1999).

[34] P.M. Gleiser, F.A. Tamarit, and S.A. Cannas, e-print cond-mat/9907084.
[35] R.V. Kulkarni, E. Almaas, and D. Stroud, e-print cond-mat/9905066.
[36] A.-L. Barabási, R. Albert, and H. Jeong, Physica A **281**, 69 (2000).
[37] D. Sornette and R. Cont, J. Phys. I **7**, 431 (1997).
[38] D. Sornette, Phys. Rev. E **57**, 4811 (1998).
[39] S.N. Dorogovtsev, J.F.F. Mendes, and A.N. Samukhin, e-print cond-mat/0004434.
[40] S.N. Dorogovtsev and J.F.F. Mendes, e-print cond-mat/0001419.
[41] P.L. Krapivsky, S. Redner, and F. Leyvraz, e-print cond-mat/0005139.
[42] R. Albert and A.-L. Barábasi, e-print cond-mat/0005085.
[43] S.N. Dorogovtsev and J.F.F. Mendes, e-print cond-mat/0005050.
[44] A. Vázquez, e-print cond-mat/0006132.

[SlaKon10]

Advances in Complex Systems, Vol. 13, No. 6 (2010) 699–723

DOI: 10.1142/S0219525910002840

EIGENVECTOR LOCALIZATION AS A TOOL TO STUDY SMALL COMMUNITIES IN ONLINE SOCIAL NETWORKS

FRANTIŠEK SLANINA*,‡ and ZDENĚK KONOPÁSEK†,§

*Institute of Physics, Academy of Sciences of the Czech Republic,
Na Slovance 2, CZ-18221 Praha, Czech Republic

†Center for Theoretical Study,
Charles University in Prague, Academy of Sciences of the Czech Republic,
Jilská 1, Praha, Czech Republic
‡slanina@fzu.cz
§zdenek@konopasek.net

Received 16 June 2010
Revised 31 August 2010

We present and discuss a mathematical procedure for identification of small "communities" or segments within large bipartite networks. The procedure is based on spectral analysis of the matrix encoding network structure. The principal tool here is localization of eigenvectors of the matrix, by means of which the relevant network segments become visible. We exemplified our approach by analyzing the data related to product reviewing on Amazon.com. We found several segments, a kind of hybrid communities of densely interlinked reviewers and products, which we were able to meaningfully interpret in terms of the type and thematic categorization of reviewed items. The method provides a complementary approach to other ways of community detection, typically aiming at identification of large network modules.

Keywords: Social network; random matrix; internet.

1. Introduction

The complexity of our societies is studied by social analysts in various ways. Qualitative inquiries and case studies usually put little emphasis on formalized description, partly to avoid oversimplification, or even trivialization of the phenomena under study. On the other hand, sophisticated mathematical procedures are increasingly used in order to grasp complexity in a specific way, as a formalized property of larger systems. One of the branches of the latter stream is represented by the analysis of social networks using mathematical theory of graphs. Our approach adheres precisely to this field of research and yet, it follows a slightly different direction than most efforts in contemporary network analysis.

The purpose of this paper is twofold. First, we want to present a specific solution to a rather standard problem of social network analysis, which is identification of communities within complex networks. Second, we want to discuss some alternative perspectives on the concept of "social network". We suggest that our method might

[SlaKon10]

provide a suitable tool for empirical research in respective directions, enabling the analyst to determine those "hot spots" within the network that usually escape attention.

To make the wider methodological context of our paper clearer, let us start with some notes on networks and network analysis in contemporary sociology. The use of the term "network" in contemporary sociology vary from loose metaphors [17] to rather specific and technical meanings [23, 83], compatible with the network science as understood in mathematics or physics.

Social network analysis has a complex history, with roots involving the sociometric analysis of Moreno in the beginning of 20th century, the Harvard researchers of the 1930s and 1940s who studied interpersonal configurations and cliques and, finally, the group of anthropologists based in Manchester who, roughly at the same time, instead of emphasizing integration and cohesion as their predecessors, focused on conflict and change, see [83, pp. 7–37]. In the 1960s, a key turn to mathematization occurred, which gave this field a new impulse and high ambitions. Today, encouraged by the rise of interest in networks in other scientific disciplines, social network analysis is sometimes seen as an approach that may entirely redefine the social sciences, while integrating them into a broader interdisciplinary research program [19]. Formalized analytical procedures hugely contributed to the fact that social network analysis has become a firm basis for social science discussions [90]. However, integration of mathematical analytic thinking with sociological imagination is an intricate task. As noted by [31], the application of formalized methods of social network analysis is often marked by neglecting substantive and theoretical sociological consequences. Also, despite the growing popularity of mathematical modeling, qualitative, or ethnographic studies of "network sociality" [92] keep their relevance, hand in hand with quantitative approaches.

Given this complicated background, our aim, in this paper, is rather modest. We want to introduce and illustrate a new mathematical method for identification of small parts of complex networks with higher level of commonalities and for studying their basic formal properties. As an example and possible field of application we have chosen networks of product reviewing on the Amazon.com portal. Here, the simplest possible ties structuring the network are the connections established by two reviews written on the same product. In other words, what reviewers may have in common is the product reviewed by them. The configurations when one product, e.g. a book or a CD, is reviewed by two or more reviewers are frequent, of course, and not much special. But if the same reviewers are similarly connected via some other items too, the situation gets more exciting. We can assume that network segments with higher density of such links represent small communities of reviewers with similar interests. Our first and main objective is to find these small communities.

Identification of such small-size groupings has always been one of the key tasks in social network analysis. Identification of these network segments is an

[SlaKon10]

interesting empirical finding in itself. Other times, however, the need to focus on smaller network segments is rather methodological than substantial or theoretical: for instance, when David and Pinch [22] analyzed the phenomenon of review plagiarism on Amazon.com, they had to "localize" the phenomena in order to make it more understandable in detail. Thus, they had to reduce their sample while focusing on those segments of the vast amount of data available in which reviewed products were "somewhat similar to one another" and thus vulnerable to "recycling" practices they were interested in. This is a characteristic situation: complex networks, including the social ones, are quite often huge, only hardly analyzable in details, with respect to local deviations or little extremities. This is especially true for on-line networks. When studying internet-related network structures, analysts can quickly become overloaded with data and it is difficult to tell what exactly to look at. The urgent question becomes: how to locate tiny islands of relevance in the ocean of data archived on the Internet? We offer a possible mathematical method for precisely such a task — a more flexible and background-sensitive one (a "softer" one, in a way) than those already described and used in the field.

We should also stress at this point that our task differs from the well-studied problem of splitting the network into several modules, which may perhaps overlap, but as an ensemble, they cover the network entirely. This is the case in metabolic networks, to mention just one example [72, 46]. In our case, we want to focus on a few "hot spots", small communities of interest within the network, leaving all the rest behind.

2. Reviewing Networks on Amazon.com as a Sociological Problem

Before demonstrating the mathematical procedures, let us also briefly mention some sociological contexts of the chosen example. Sociologists have pointed out the increasing importance of the symbolic content of contemporary economics, which is often associated, among others, with users' or consumers' active involvement in the complex processes of product evaluation, qualification, and formation [2, 59]. The role of consumers is particularly enhanced by the Internet and by the ways computer technologies shape social networks [15].

A specific and significant part of these processes has been recognized as "peer-production of relevance/accreditation" [8, p. 75], or simply as "reputational economy" [22]. By reviewing or commenting items in online shops, classifying and rating them, individual consumers become co-producers of coordinates for others' economic decision making. They engage in a complex action that cannot be simply grasped in purely economic terms. As noted by [62, p. 322], spaces of E-commerce are characteristic by countless devices creating diversity of forms of encounter between products and consumers [93].

User reviews and comments, for instance, not only serve the purposes of the seller, but also the consumer community, while simultaneously being the means for

[SlaKon10]

identity building of reviewers themselves [37]. In-depth study of all these complex phenomena seems crucial for better understanding of contemporary "technological economies" [6].

What kind of groupings are we interested in when we try to locate segments of reviewers connected by shared reviewed products? We might be tempted to talk about virtual communities. But these would not be "virtual communities" in the usual sense [78, 91]; and they would not be "online social networks" as typically imagined by social scientists. Both these concepts characteristically refer to groups of people who directly communicate to each other with the help of computer networks — i.e. who know (about) each other and interact by means of online forums, instant messaging, or facebook. Our groups of Amazon.com reviewers represent a slightly different kind of entities, though. These people usually do not communicate by addressing each other and quite often they even do not know each other. They do not belong to the group by virtue of intentional interaction with the others, but "merely" by doing similar things in a relatively uncoordinated way: writing reviews on specific products. If [45, 44] drew our attention to the importance of "weak ties" in social networks, i.e. to the significance of ordinary informal acquaintances (in comparison to family ties and formal hierarchies), we could speak here of a kind of "ultra-weak ties". These ties are "virtual" in the sense that they are not "real enough" in the usual sociological meaning; yet, they are materialized and articulated — although not by the reviewers themselves only. We can clearly see the connections on the Amazon.com web pages: the reviews of these people are listed together, accompanying the respective item in the catalog. Moreover, the reviewers do not become members of this community completely unintentionally, but by means of quite intentional and personal act of assessing the product and writing the review. They create the community by highly mediated interactions, as if "by the way", together and via the technology of online shopping.

In the following section, we present mathematical tools for identification, representation and elementary description of precisely such communities. The proposed procedures may have a value especially in relation to subsequent sociological analysis of these local anomalies, as its precondition.

3. Finding Small Communities in Networks

3.1. *Motivation*

The problem of identification parts of the network bearing some relevant structural information, can be relatively easily formulated in mathematical terms. The methodological problem is to know which one of the variety of possible mathematical formulations of community detection is suitable for the given purpose. Let us stress that we neither aim at improving the existing schemes nor present an algorithm which should compete with the established ones. Instead, we are bringing an alternative scheme which reveals structures not covered by other schemes of community detection. That is why we not only present a description of the method

[SlaKon10]

and its application to one real-world example, but also spend time putting it into a wider context of sociological thinking.

3.2. *Background*

For a long time, the standard way of mathematical modeling of social networks [90, 23] was the "classical" theory of random graphs [11, 24] initiated by the work by Erdős and Rényi [32]. However, in the last decade a new class of networks became studied and the name "complex networks" became common denomination for them [4, 1, 88, 27, 12, 28, 70]. Compared with the "classical" models of random networks, they grasp much better the networks found in reality and at the same time their models are much more involved than bare random dropping of edges as in the Erdős–Rényi model. The most immediate characteristics common to the complex networks is their degree distributions with power-law tails [4].

The strong inhomogeneity of complex networks, implicit in their degree distribution, changes many aspects of their behavior. In the context of our work, new approaches for finding the communities become relevant. While the methods for determining cliques, k-cliques and motifs [90, 23] work well if the zero-hypothesis on the network structure is the Erdős–Rényi random graph, methods better suited for complex networks were developed [54, 33, 68, 69, 77, 76, 72, 40, 16, 46, 39, 5, 57, 38, 82, 61, 58, 5, 56]. The central quantity for majority of them is the modularity measure Q, which is to be made maximal. This is achieved by various optimization algorithms.

Here we will rely on the method of describing the global properties of networks using the spectral theory of graphs [20]. It deals with eigenvalues and eigenvectors of various matrices representing the graph structure, which are the adjacency matrix, Laplacian and more. It was already used for finding clusters or communities in networks through the properties of eigenvectors corresponding to the second largest eigenvalue [67, 16, 21, 25]. In one step, it gives the best partitioning of the network into two modules and repeating the algorithm recursively, the communities are found. Our approach is different, though. It is similar in spirit to the analysis of covariance matrices in finance [73, 75], where economic sectors are attributed to eigenvectors corresponding to the second, the third, etc. largest eigenvalue.

The first level of understanding spectral properties of a random matrix comprises the knowledge of the density of eigenvalues. The second involves the localization properties of the eigenvectors. It is the latter that is central for our approach.

Let us say first a few words on the eigenvalue density. Spectra of "classical" random graphs, like the Erdős–Rényi model, are closely related to "classical" models of random matrices [64]. The typical shape of the eigenvalue density is the Wigner semi-circle with sharp edges, with the largest eigenvalue split far off from the bulk of all other eigenvalues. The first complication arising in the spectrum of a random graph is the sparseness of the adjacency matrix, which leads to the emergence of Lifschitz tails. This appears already in the Erdős–Rényi model. Despite considerable

[SlaKon10]

effort [79], the Lifschitz tail in ER graph is still not known in all detail. Asymptotic formula was obtained by several approaches, showing that the density of states is nonzero at arbitrarily large eigenvalues and it decays faster than any power law [79, 84].

It was soon realized that complex networks, characterized by power-law degree distributions, have also non-standard spectral properties [34, 42, 29, 30, 33, 71, 53, 35, 51, 36, 85, 21, 14, 94, 26, 86]. First, there is a cusp in the middle part of the density of eigenvalues, and second, perhaps more importantly, the tail of the eigenvalue density seems to be described by a power law [34, 42]. Numerical diagonalization on toy models [29, 30] as well as some analytical estimates confirmed power-law tails in the density of states. The replica trick [80, 65], as well as the cavity method [30, 81] were later adapted for scale free networks. It was found that the spectrum has a power-law tail characterized by the exponent $2\gamma - 1$ related to the degree exponent γ of the network. Further improvements of the method were introduced recently [50, 10].

As we shall see, our method is similar to those used in the study of covariance matrices of stock-market fluctuations [41, 55, 73, 74, 75, 89, 3, 48, 13]. They are modeled as random matrices of the form $M\,M^T$, where M is a random rectangular matrix. The density of states has the Marčenko–Pastur form [63] with sharp edges, which are smeared out into Lifschitz tails if the matrix is sparse [66].

Most attention was paid to the states in the tail, i.e. located beyond the edge of the Marčenko–Pastur density and below the maximum eigenvalue, which is always split off. These states are supposed to carry the non-trivial information about the stock market and, indeed, the shape of the corresponding eigenvectors was used to identify business sectors. It was supposed that the eigenvectors were localized on items within specific sector [43, 75, 52]. More sophisticated approaches were also developed [89].

Our method owes largely to the spectral analysis of covariance matrices. However, we improve these approaches by systematic use of the quantitative measure of localization of the eigenvectors, which is the inverse participation ratio. In an intuitive manner, a similar approach was already used in the analysis of gene coexpression data [49]. Within this approach, we do not aim at factoring the entire network into some number of modules, or communities, which may or may not be overlapping, but in any case covering, as an ensemble, the whole network. Instead, we want to find small parts of the network which differ structurally from the rest. We may also describe our approach as "contrast coloring" of the network, which makes certain relevant parts visible against the irrelevant background.

3.3. *Spectral analysis of matrices encoding the structure*

Our analysis will be devoted to bipartite graphs. There are two types of nodes, making up sets $\mathcal{R}$ and $\mathcal{I}$. Anticipating our application to the Amazon.com network, we think of members of $\mathcal{R}$ as reviewers and members of $\mathcal{I}$ as items to be reviewed.

[SlaKon10]

All information on the network structure is contained in the adjacency matrix M with elements $M_{ri} \in \{0, 1\}$. The out-degree of node $r \in \mathcal{R}$ is $k_r = \sum_i M_{ri}$, and the in-degree of the node $i \in \mathcal{I}$ is $k_i = \sum_r M_{ri}$.

In the bipartite graph, the spectral properties are deduced from the contracted matrices $B = M \cdot M^T$ and $C = M^T \cdot M$. The interpretation of these matrices is obvious; e.g. B_{rs} tells us how many neighbors the nodes r and s have in common. Similar construction is used frequently in bipartite networks. As an example, let us cite the network of tag co-occurrence in the analysis of collaborative tagging systems [18] or recommendation algorithms investigated in [95].

In order to partially separate the effects of the network structure from the influence of degree distribution, we rescale the matrix elements by the product of square roots of the out-degrees. This way, we get the matrix

$$A_{rs} = \frac{B_{rs}}{\sqrt{k_r k_s}} \tag{1}$$

with all diagonal elements equal to 1. We can also be more explicit and write $A_{rs} = (\sum_i M_{ri} M_{si})/\sqrt{(\sum_i M_{ri})(\sum_i M_{si})}$. Obviously, the matrix A is symmetric.

The matrix A is then diagonalized. Let us see what information can be extracted from the eigenvalues and eigenvectors. First, for any square $N \times N$ matrix D encoding the structure of a graph we can interpret the traces $\frac{1}{N}\mathrm{Tr}D^k$ as density of circles of length k. This number is equal to the kth moment of the density of eigenvalues of D. In our case, the role of D is assumed by the contracted matrix B and the kth moment of B expresses the density of cycles of length $2k$ on the bipartite graph. If we use the matrix A instead, the moments of the spectrum are related to the density of weighted cycles. Each time the cycle goes through the vertex $r \in \mathcal{R}$, it assumes the weight $1/k_r$. Therefore, cycles connecting vertexes with large degree are counted with lower weight. This is just what we want here: to put accent on peripheral, less-connected areas of the network, rather than on the hubs. If we did not rescale the matrix as in Eq. (1), the weight of the hubs, or strongly-connected nodes in general, would overshadow the major part of the network, where the small communities may lie hidden.

We expect that the spectrum has a power-law tail. Indeed, it will be confirmed in the specific example of Amazon.com, which we shall show later. The power-law tail implies that the density of cycles beyond certain length diverges. In terms of the limit $N \to \infty$, it means that the number of such cycles increases faster than linearly with N. The exponent of the power-law tail tells us what is the threshold for the cycle length, beyond which the cycles are anomalously frequent compared to the Erdős–Rényi graph.

What does all this mean for the problem of finding small compact communities? If we for example use the method of cliques or k-cliques, we tacitly assume that the "background" network does not contain many of these cliques by pure chance. But if, for example, the tail of the spectrum of D has exponent 4, the third moment diverges, which means that there are extremely many triangles. No triangle, or

[SlaKon10]

community of size 3, can therefore be considered as informationally relevant. That is why we consider the information on the spectrum of the network an important auxiliary information.

The new algorithm we propose for finding small compact communities relies on the properties of the eigenvectors. Let us denote $e_{\lambda r}$ the rth element of the eigenvector of the matrix A, corresponding to the eigenvalue λ. To study the localization, we need to calculate the inverse participation ratio (IPR) defined as

$$q^{-1}(\lambda) = \sum_{r=1}^{N} (e_{\lambda r})^4, \tag{2}$$

where normalization $\sum_{r=1}^{N} (e_{\lambda r})^2 = 1$ is assumed.

While IPR says quantitatively to which extent an eigenvector is localized, this information alone is not sufficient, if we want to draw the distinction between localized and extended states. First, it makes no sense to ask, if a particular vector is localized, as opposed to extended, or not. What does make sense, however, is the question whether the states around certain eigenvalue are localized. The way to establish that fact is by finite-size analysis. Indeed, if N is the dimension of the vector space we work with, then

$$q^{-1}(\lambda) \sim \begin{cases} O(1), & N \to \infty \quad \text{localized state,} \\ O(N^{-1}), & N \to \infty \quad \text{extended state.} \end{cases} \tag{3}$$

Second, also the shape of the density of eigenvalues changes with the system size. When we increase N, the spectrum broadens. In the textbook example of the Erdős–Rényi graph, the spectrum has sharp band edges. The edge of ER spectrum moves as $N^{1/2}$ when N grows and if we compare the IPR at different system sizes, we must measure the eigenvalues relative to the band edge. Therefore, to compare the behavior at different sizes, we take a random subset of the network, containing N_{sub} nodes. Typically, we choose $N_{\mathrm{sub}} = N/2$. Then, we plot the density $D(\lambda)$ of eigenvalues for both original network and the density $D_{\mathrm{sub}}(\lambda)$ for the random subset. The densities are rescaled by the factor s, the value of which is found empirically so that the data for $D(\lambda)$ and $D_{\mathrm{sub}}(1 + (\lambda - 1)s)$ overlap as much as possible. The form of this rescaling involves the shift of the eigenvalues by 1, because the matrix A has spectrum centered around the value $\lambda = A_{rr} = 1$. With s found, we plot the IPR for the network and the subset, with the same rescaling as used for the eigenvalues density. The regions, where we observe that $q^{-1}(\lambda)$ remains roughly the same for the network and its subset, are the candidate areas where the localized states are to be found.

We continue the procedure by determining the eigenvectors with largest q^{-1} within the areas of localized states. The elements of these vectors tell us what nodes of the network belong to the small community. To this end, we fix a threshold T and retain only those nodes $r \in \mathcal{R}$ for which the elements exceed the threshold in absolute value, $|e_{\lambda r}| > T$. We do not propose any exact method for fixing T. For the sake

[SlaKon10]

of consistency, T must be chosen so that the number of nodes retained is roughly $1/q^{-1}$. In practical applications, we observed the number of retained nodes when T was gradually decreased from $T = 1$. At a certain crossover value of T, we saw that the number of nodes suddenly started increasing substantially to much larger values than $1/q^{-1}$. Hence, we fixed T somewhat below this crossover. We believe that this procedure could be made automatic by a software implementation, but we did not do that.

Let us make an important remark at this point. Clearly, we can find some localized states also in a randomized version of the network. These states are results of pure chance and do not bear significant information. Therefore, we cannot exclude that also in the true empirical network, some of the localized states occur just accidentally and thus some of the clusters found are spurious. The choice of the threshold T only cannot discriminate between the true and the spurious clusters. However, looking at the dependence of IPR on eigenvalue for the true and the randomized network (as will be seen later in Fig. 4) we can see the regions where IPR is large and differs markedly between true and randomized networks. The localized states found in these regions (in Fig. 4, it is near the lower edge of the density of states) correspond to clusters that are non-random and do bear relevant information.

This way, we find those vertexes $r \in \mathcal{R}$, which form the community $\mathcal{C}_{\mathcal{R}} = \{r \in \mathcal{R} : |e_{\lambda\, r}| > T\}$. Next, we proceed by finding those $i \in \mathcal{I}$ which are connected to them. Here we can distinguish two levels. First, a vertex $i \in \mathcal{I}$ can be connected to at least two different vertexes from $\mathcal{C}_{\mathcal{R}}$. Then, we say that it belongs to the connectors of the community, $\mathcal{C}_{\mathcal{I}}^{\mathrm{con}} = \{i \in \mathcal{I} : \exists r, s \in \mathcal{C}_{\mathcal{R}} : r \neq s \wedge M_{si} = M_{ri} = 1\}$. Furthermore, those $i \in \mathcal{I}$ which are connected to just one vertex of $\mathcal{C}_{\mathcal{R}}$ form a more weakly bound part of the community, which we call cloud, $\mathcal{C}_{\mathcal{I}}^{\mathrm{cloud}} = \{i \in \mathcal{I} : \exists r \in \mathcal{C}_{\mathcal{R}} \setminus \mathcal{C}_{\mathcal{I}}^{\mathrm{con}} : \wedge M_{ri} = 1\}$. We can explicitly see the asymmetry in constructing the community. This is due to the fact that we focused on the diagonalization of the contraction matrix acting in the space $\mathcal{R}$. The procedure can be, of course, performed also in the opposite direction, diagonalizing the contraction on $\mathcal{I}$. Both ways are equally justified on the formal level. The choice should be dictated by practical reasons and by the interpretation we want to draw from the data in any specific application.

To sum up, our procedure for finding small communities in bipartite networks consists of the following steps.

(1) Diagonalize the matrix A, $A_{rs} = (\sum_i M_{ri}\, M_{si})/\sqrt{(\sum_i M_{ri})(\sum_i M_{si})}$. The output is the density of states $D(\lambda)$ and the inverse participation ratio $q^{-1}(\lambda)$.
(2) Do the same for random subset of the network, containing half of the nodes, and find the proper rescaling factor s, so that rescaled density of states for the network and the subset coincide. By rescaling the IPR using the same factor s, determine the regions, in which localized states are to be found.
(3) Within the localized region, find the eigenvectors with highest IPR.

[SlaKon10]

(4) For each of the eigenvectors found, determine the threshold T and establish the set $\mathcal{C}_\mathcal{R}$ of nodes r, for which $|e_{\lambda r}| > T$. This set is the projection of the community to the set $\mathcal{R}$.
(5) Find the connector and cloud components of the community on the side of the set $\mathcal{I}$.

4. An Example: Reviewing Networks on Amazon.com

4.1. *Basic structural features*

The e-commerce site Amazon.com is one of the oldest and best known on the WWW. It has a very rich internal structure, but the user usually sees only a small part relevant to the service requested in a particular moment. As already announced, we shall investigate one aspect of the Amazon.com trading, namely the network made up of connections between the items to be sold and the reviewers who have written reports on these items.

This network is a bipartite graph, with items $i = 1, 2, \ldots, N_{\mathrm{itm}}$ on one side and reviewers $r = 1, 2, \ldots, N_{\mathrm{rev}}$ on the other side. The sets of vertexes $\mathcal{R}$ and $\mathcal{I}$ introduced in the methodical section above, correspond to the sets of reviewers and items, respectively.

The reviews written are edges connecting these two sets. The structure of the network can be uniquely described by the matrix M, where the element M_{ri} equals 1 if the reviewer r wrote a review on item i, and 0 otherwise.

The data were downloaded using a very simple crawler in the period from 28 July 2005 to 27 September 2005. First, a list of total $N_{\mathrm{all}} = 1{,}714{,}512$ reviewers was downloaded; at that time the list containing all Amazon reviewers was accessible through the web. (It is no more so.) The list was naturally ordered by the rank Amazon assigns to each reviewer. On average, reviewers with higher rank have written more reviews, but there are exceptions. For example, at the time of data collection, the No. 1 reviewer, Harriet Klausner, had written 9581 reviews, while the No. 2, Lawrance M. Bernabo, 10,603 reviews. This suggests that it is not only quantity but also quality which counts when Amazon ranks their reviewers. We do not touch here the obvious question how the most prolific reviewers do manage reading and reviewing several books per day, throughout many years. As we investigate only structural features here, these problems are left aside.

In the next step, we went through the reviewers' list, from the top rank downwards. We looked only at about 10^5 first reviewers and stopped there, as we considered the sample sufficiently representative. The remaining reviewers are only occasional writers, contributing by one or at most a few reviews. For each reviewer we found all reviews written by her or him and registered the name of the item reviewed (mostly books and CDs, of course, but in general all kinds of goods do appear) as well as some other details about the review. In total, we examined 99,622 reviewers who wrote 2,036,091 reviews on 645,056 items.

[SlaKon10]

4.2. *Degree distributions*

The simplest and most accessible local property of the network is the degree distribution. In the list of reviewers, we put down also the reported number of reviews written by the particular person. We neglected the possible error in this number due to various inconsistencies. We believe that the random discrepancies between the number of reviews reported and number of reviews which can actually be found in the system do not influence the statistics in any significant measure. We show the distribution as out-degree distribution in Fig. 1. We can observe clear power-law dependence except for the few highest degrees. The exponent fitted is $\gamma_{\text{out}} \simeq 2.2$.

Similarly we can extract the in-degree distribution from the list of reviews. The statistics of the number of reviews per item is also shown in Fig. 1 and a power-law dependence is found again. The corresponding exponent is now $\gamma_{\text{in}} \simeq 2.35$.

The power distribution is by no means surprising, in view of the vast literature on complex networks. The data provide a clear check that Amazon.com also belongs to the class of networks with power-law degree distribution.

4.3. *Distribution of eigenvalues*

Now we are in a position to calculate the contraction matrix A acting on the set of reviewers, and diagonalize it. As an additional study, we compare the results with randomized version of the reviewer-item network. This way we discriminate between the influence of the network structure and genuinely random factors.

To this end, we reshuffle the edges in the reviewer-item graph, while keeping the degrees of all vertexes unchanged. The matrix M is replaced by M^R and, correspondingly, the matrix A is replaced by A^R. Again, we can write $A^R_{rs} =$

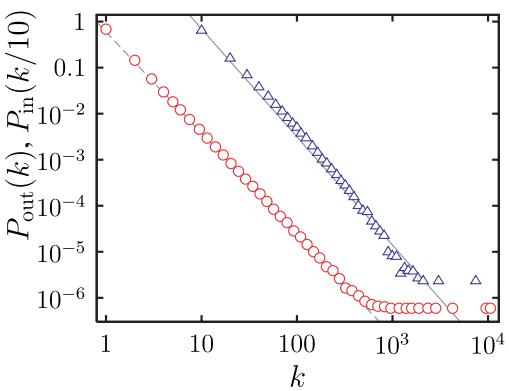

Fig. 1. Degree distribution of the bipartite reviewer-product network on Amazon.com. Circles indicate the data for out-degree (reviews per reviewer), triangles for in-degree (reviews per item). The latter data are shifted rightwards by one decade for better visibility. The lines are the power laws $\propto k^{-2.2}$ (dashed line) and $\propto k^{-2.35}$ (solid line).

[SlaKon10]

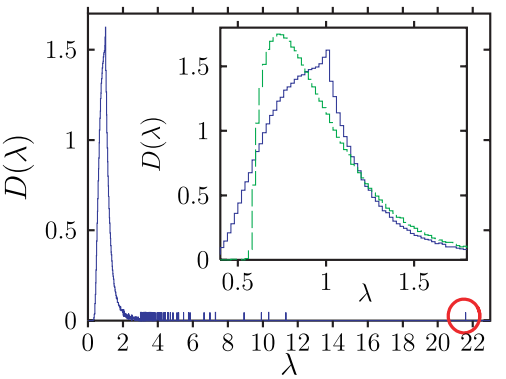

Fig. 2. (Color online) Distribution of eigenvalues of the reviewer-reviewer matrix. The size of the segment is $N = 10{,}000$. For $\lambda < 3$, the distribution is plotted as a histogram, while the larger eigenvalues, $\lambda > 3$ are shown as individual vertical ticks. The largest eigenvalue is indicated by the circle. In the inset, we show the detail of the central part of the same plot. Also in the inset, the dashed (green) line is the distribution of eigenvalues of the matrix obtained by reshuffling the reviewer-item graph.

$(\sum_i M^R_{ri} M^R_{si})/\sqrt{k_r k_s}$. The only information on the network structure retained here is the order sequence. As we showed in the last section, it obeys a power law, so the features found in analyzing A^R are entirely due to power-law degree distribution, but without further structural details.

We diagonalize the matrices A and A^R. Their eigenvalues $\lambda_1 \geq \lambda_2 \geq \cdots \geq \lambda_N$ are accumulated around the value $\lambda = 1$, which corresponds to the uniform diagonal value of both the true and the randomized matrices. The distributions are plotted in Figs. 2 and 3. Let us describe now what we can see here.

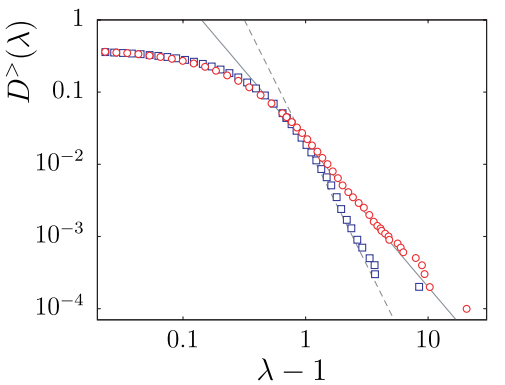

Fig. 3. Detail of the upper part of the distribution of eigenvalues. The behavior is observed using the integrated density of eigenvalues. Circles correspond to the original reviewer–reviewer matrix with $N = 10{,}000$, and the triangles correspond to the same graph subject to permutation of all its edges. The full line is the power $\propto (\lambda - 1)^{-2}$, with the dashed line is the power $\propto (\lambda - 1)^{-3.4}$.

[SlaKon10]

In Fig. 2, we plot the histogram of the eigenvalues of the matrix A. Most of them fall within the interval $\lambda \in [0, 3]$, with sharp maximum in the eigenvalue density at $\lambda = 1$. The eigenvalues density is much smaller for $\lambda > 3$ and we show their positions as separate ticks. Although the notions "bulk" and "tail" are not very precise here, we shall use them pragmatically, calling bulk the part with $\lambda \lesssim 3$ and tail the part with $\lambda \gtrsim 3$.

In Fig. 2, we can also see the spectrum of the randomized matrix A^R. The power-law distribution of degrees is preserved. In the spectrum, we can observe certain remarkable changes. In the bulk of the density of states, as shown in the inset of Fig. 2, the spectrum of the reshuffled network lacks the characteristic tip at the value $\lambda = 1$ and its shape at the lower end of the spectrum is quite different. Most importantly, a sharp band edge develops. On the other hand, at the upper tail of the density of states, the changes are of minor importance.

In Fig. 3, we can compare the behavior of integrated density of states, $D^>(\lambda) = \sum_{i,\lambda_i>\lambda} \frac{1}{N}$ in the region of large eigenvalues. For the original matrix A, we observe a power-law decay in the tail $D^>(\lambda) \sim (\lambda-1)^{-\tau}$ with $\tau \simeq 2$. For the matrix A^R, the tail is again quite reasonably fitted on a power law, but with larger exponent. Let us recall that the divergence of the moments of the eigenvalue density is related to the statistics of cycles on the network. For the reshuffled network, the divergence occurs at higher moments, therefore at cycle lengths longer than in the original network. This effect seems to be a tiny one, but this is just a subtle structural difference which goes beyond the bare degree distribution. In short, the Amazon network has many more short loops than how many could be expected knowing only its degree sequence. This suggests the presence of small self-reinforcing communities. Although we do not see them yet at this stage, we can perceive their existence through the density of states of the matrix A.

Interestingly, similar conclusions about small communities were reached in the study of collaborative tagging systems [18], where two-node correlations were calculated in order to estimate the quantity of non-randomness, or semantic information content.

4.4. *Localization*

Having investigated the eigenvalues, let us now turn to the properties of the eigenvectors. We show in Fig. 4 how the IPR depends on the eigenvalue. For the matrix A we can see larger localization around the center of the spectrum at $\lambda = 1$. Farther from the center the localization is weaker, but it increases again at the tails, more strongly at the lower tail, while more gradually at the upper tail. Note also some isolated highly localized states in the bulk of the eigenvalue distribution.

Now we compare the results with the random subset of $N_{\rm sub} = 5000$. We found that the density of eigenvalues coincides very well if we choose the scaling factor $s = \sqrt[3]{2} = \sqrt[3]{N/N_{\rm sub}}$. With the same scaling we plot the IPR in Fig. 5. We can see that the absence of a clearcut band edge is complemented by the absence of any

[SlaKon10]

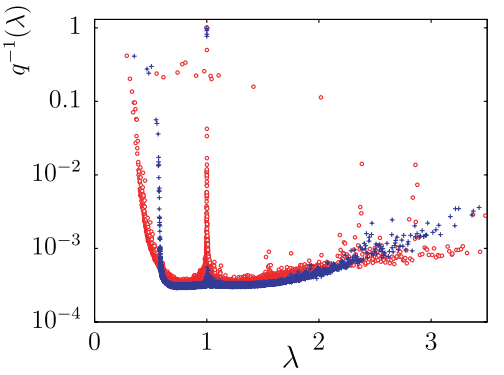

Fig. 4. Inverse participation ratio for the reviewer–reviewer matrix with $N = 10{,}000$ (○), and the same for matrix obtained by reshuffling the reviewer-item graph (+). Each point denotes the IPR for the eigenvector corresponding to the indicated eigenvalue λ.

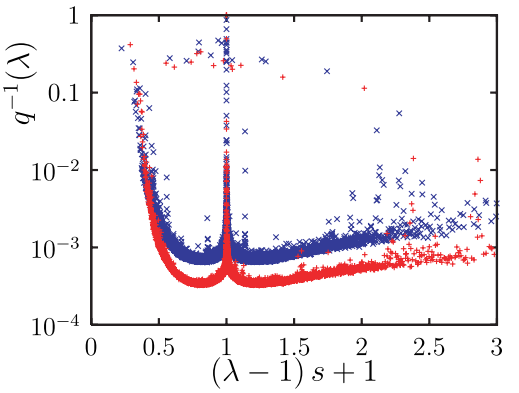

Fig. 5. Inverse participation ratio for the reviewer–reviewer matrix. The horizontal axis is rescaled by the factor s explained in the text. We show the data for the matrix with $N = 10{,}000$ (+, $s = 1$), and for the random subset with $N_{\mathrm{sub}} = 5000$ of the same matrix (×, $s = \sqrt[3]{2}$). Each point denotes the IPR for the eigenvector corresponding to the indicated eigenvalue λ.

region of localized states at the upper end of the spectrum. The lower end does show localized states, though. Therefore, the candidates for compact communities are to be found close to the lower end of the spectrum. In the next section, we describe what we have found there.

5. Finding and Interpreting the Communities

As we have said, the most localized states are the candidates for small and densely interlinked communities of reviewers. We counted as members of the community only those reviewers, whose element in the eigenvector was larger than a threshold, $|e_{\lambda r}| > T$. The value of the threshold T was found by trial-and-error, so that all relevant nodes, on which localization appears, were kept, while the remaining ones,

[SlaKon10]

interpreted as a noisy neighborhood, were left out. This adjustment of thresholds also indicates that the borders of the communities found in this way are not sharp. In our set of 10^4 reviewers, the number of communities which can be considered as well-localized is about $\simeq 10$. We were able to explicitly draw and interpret 7 communities. With the average size of the communities around 6 people, the fraction of reviewers in small compact communities can be estimated to about 0.5%. In other words, we have been able to find relatively rare cases when fractional segments of the network display anomalously high density of mutual links. However, we expect that this fraction would rapidly grow if more reviewers are included from the top of the Amazon list downwards. From this point of view the small percentage of the reviewers in small communities is partly an artifact due to the choice of the reviewers starting from the top of the list of the most productive Amazon.com reviewers.

Now, let us look at several specific examples of the communities found. The first example of such a small grouping is shown in Fig. 6. (In this case, we took the 5th most localized vector, $q^{-1} = 0.095675$, corresponding eigenvalue $\lambda = 0.359$, and the threshold was taken as $T = 0.2$.) The items reviewed by the reviewers within the community found in this way are of two types. First, there are those reviewed by at least two reviewers from the community. These items keep the community together and we call them "connectors". We show them in Fig. 6 linked to their corresponding reviewers. However, one should note that the reviewers themselves play the role of "connectors" for the items, to the same extent as the items are "connectors" for the reviewers. Second, there are items reviewed by only one reviewer of the community. These items form a kind of "cloud" around the core of the network segments. We do not show the "cloud" in our figures, but we shall discuss its meaning later.

What are the product-connectors in the given community (Fig. 6)? We can see that the maximum number of reviewers for one item is 4 and it holds for two audio recordings: "The Beatles (The White Album)" and "Abbey Road" also by Beatles. Thus, the core of the community is kept together by one of the most popular music bands ever. The remaining items are thematically close. They refer to other records by Beatles and also by Beatles ex-members, or to the music of Bob Dylan. Ex-Beatles and Dylan cover about a half of the items each. The only exception is a small set of five recordings of other pop-classics, namely four of Led Zeppelin and one of Rolling Stones. In short, all items fall into the range of notoriously known pop-music stars. It is interesting that this characteristic does not concern the connecting items only, but majority of all other reviews by the members of the community (not included in the graph). Thus, not only the connectors, but also the "cloud" bears the same characteristics.

Therefore, the interest of these reviewers lies, in general, within a rather narrow scope determined by the pair Dylan–Beatles, with some small excursions farther into mainstream pop-music, similar to the small "Led Zeppelin" set in Fig. 6. For example, the reviewer gdb has also written on CDs by U2 and David Bowie, while the "cloud" reviews by Cristian Domarchi (not listed in Fig. 6) pertain only to other

[SlaKon10]

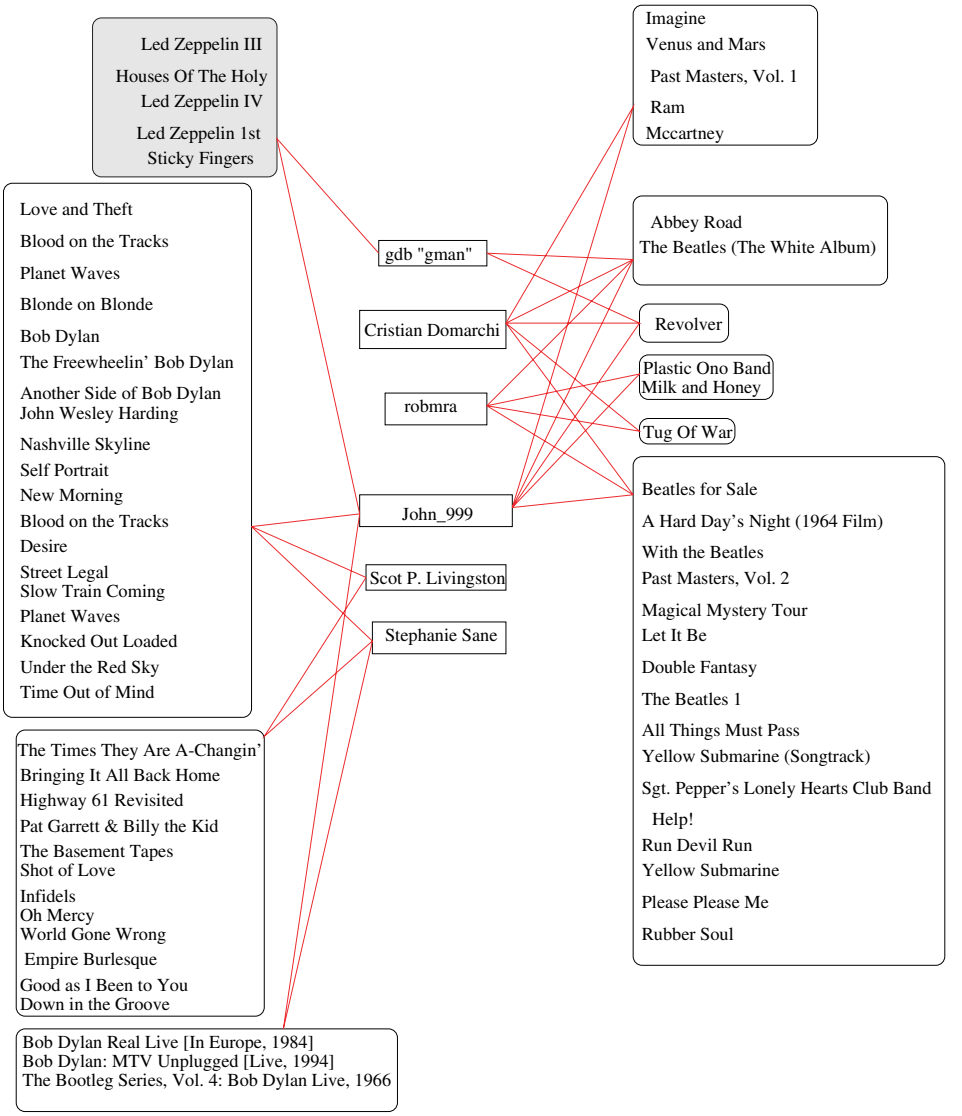

Fig. 6. The "pop-music" community in the network producing a very localized eigenvector of the matrix A. In the middle, code-names of the reviewers, on the right, recordings by The Beatles (mostly as a band, some other by individual members), on the left, recordings by Bob Dylan, with exception of the shaded box which contains four times music by Led Zeppelin and once Rolling Stones.

recordings by ex-Beatles plus one book; among all the 6 reviewers, only Stephanie Sane shows interests which go clearly beyond the Dylan–Beatles repertoire, reviewing a good deal of books, mostly mystery and detective fiction.

A similar picture is provided by the analysis of other communities. Let us very briefly describe two more of them.

[SlaKon10]

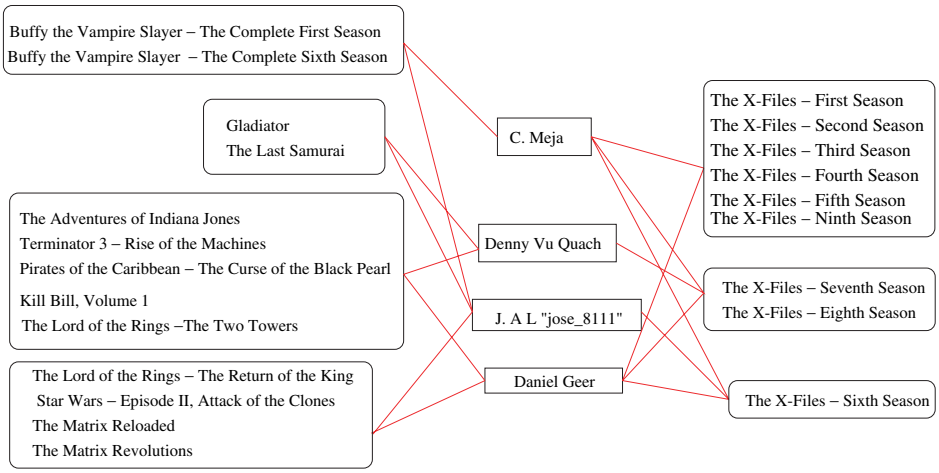

Fig. 7. The "pop-movie" community in the network producing a very localized eigenvector of the matrix A. In the middle, code-names of the reviewers, on the right, the X-Files series, on the left, other popular movies.

The first one (Fig. 7) belongs to another pop-cultural domain, this time concentrating on DVD movies with a sci-fi and fantasy flavor. Again, we found that the reviewers are active within rather narrow bounds. They focus on widely popular titles, overlapping very little with any other possible themes or genres. Only a small part of the reviews by the members of the community are related to something else, e.g. to books by M. Proust and T. Mann.

The third and last example we want to mention is shown in Fig. 8. In analogy with the former examples, the "pop-music" and "pop-movie" communities, we may call this one a "pop-politics" community. The reviewers here concentrate on books

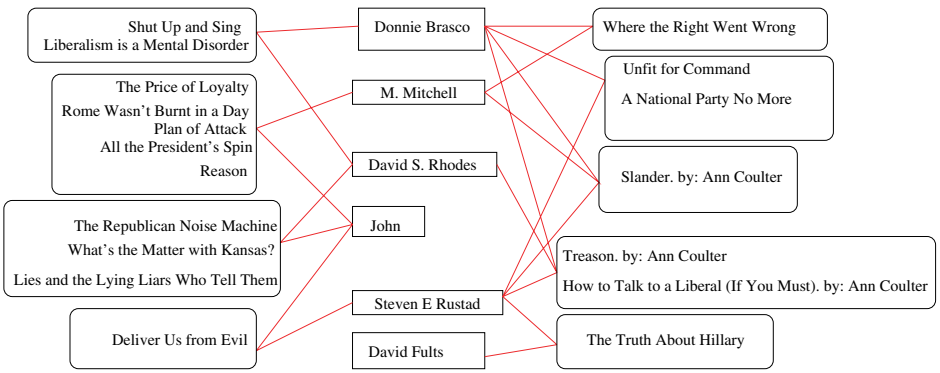

Fig. 8. The "pop-politics" community in the network producing a very localized eigenvector of the matrix A. In the middle, code-names of the reviewers, on the left and right, books treating mainly the clash of (neo-) conservatives versus liberals in the USA. Note that Ann Coulter is the most prominent book author in this community.

[SlaKon10]

discussing the presidency of G. Bush, the evils of liberal ideology, as compared with neo-conservatism, and so on. The core of the community is kept together by the books of Ann Coulter, who is known as a militant anti-liberal writer. Majority of the books in this group is targeted at the widest public, as is the music by The Beatles and movies of the "X-Files" type. Their themes are not esoteric, these products are not aiming at specialized audiences; yet, the zeal of the reviewers makes a "cult" of them. Again, this community is narrowly defined by the interest in these popular issues and not much else. In the "cloud" of other items reviewed by the members of this community we find some other books by Ann Coulter, accompanied by books such as (the titles are self-explaining, we believe) *Worse Than Watergate: The Secret Presidency of George W. Bush*; *Blinded by the Right: The Conscience of an Ex-Conservative*; *A Matter of Character: Inside the White House of George W. Bush*; *The Family: The Real Story of the Bush Dynasty*; *Chain of Command The Road from* 9/11 *to Abu Ghraib*, and similar. Out of the six reviewers, only Donnie Brasco shows some additional field of interest, having written about various pop-music CDs as well.

Let us sum up these observations (supported also by analyses of other small communities we were able to find in the sample). Our expectations that strongly localized eigenvectors would reveal some specific small communities was fulfilled in the sense that we have indeed found groups of zealots, concentrated on relatively narrow segments of commodities sold on Amazon.com. Individual interests of these reviewers only scarcely reach beyond the theme common to the community.

On the other hand, however, it would be misleading to imagine these people as eccentrics focused on highly specialized, marginal or even extreme cultural artifacts. The subjects of their reviews are quite ordinary, clearly part of the cultural mainstream. And, by their tastes, the reviewers themselves seem belonging to wide audiences, often focused on classics or well-established pop-cultural products. In other words, anomalous tiny fragments of this huge network, characteristic by various authors repeatedly writing reviews on the same items, refer typically not to some marginal cultural forms with specialized contents, but rather to widely shared cultural tastes and mainstream enthusiasts.

A more detailed analysis of these findings is beyond the scope of this methodological paper and its analytical illustration. Very probably, several possible explanations could turn valid in parallel, including the nature of the Amazon.com portal (primarily designed for general audiences and as wide consumer population as possible), possibly higher probability that reviews on widely favored artifacts get "localized" etc. What should perhaps be stressed here, however, is the peculiar character of the communities or network segments under discussion. It is clear that the tiny network fragments counting 5 or 10 reviewers and dozens of reviews cannot represent "big" consumer populations and "widespread" artifacts in some straightforward way. Rather, they may provide a rather specific ("small-scale") way of looking at a mass-scale phenomenon. Let us tell something more about this specificity.

[SlaKon10]

We have already noted that the network and its segments we are studying is not a "social network" as traditionally envisaged. The interaction constituting the network is so massively mediated and by-produced (while remaining observable, "real" enough and grounded in intentional social action) that we leave the territory of what is usually counted by social scientists as a "group" or "community". But even more is at stake in this direction. A closer view of our findings reveals that one cannot unambiguously say whether the "connecting" reviewed products provide interpretive framework for statements about the reviewers, or whether — on the contrary — it is the reviewers and their actions that provide clues for interpreting communities of products. In other words, we are unable to determine whether we study groupings of people (connected by products) or of commodities (connected by people). In fact, we should better try to understand both within a single hybrid network, meaningfully connected. While studying phenomena of product reviewing, products and reviewers cannot be separated. The sets of products represented in our figures (Figs. 6–8) do not simply make sense (and do not hold together) without the reviews written about them by the represented reviewers. Indeed, the products grouped by, e.g. purchases carried out by Amazon.com users would look different. On the other hand, the groups of reviewers would not make sense without the particular reviewed products (their amount and nature). Thus, we believe the segments identified in our example can directly represent neither populations of consumers nor entire sections in the Amazon.com commodities catalog. Rather, they represent, in a complex way and as if under a specific lens, a phenomenon of online user reviewing, better understanding of which may contribute to our knowledge of contemporary popular culture and technologically mediated economic processes.

6. Conclusion

Thanks to numerous sociological efforts in the field of social network analysis as well as the work on networks done in other scientific disciplines such as theoretical physics, various mathematical tools have been developed. They aim either at determining large-scale structures in complex networks or at identification of smaller network segments such as cliques or acquaintances. In this work, we introduced a new mathematical procedure relatively close to the latter type of task. We believe the method is very suitable for finding the most relevant small segments of complex networks, when "relevance" cannot or need not be equaled to some absolute level of mutual connectivity between the nodes. We argue that this is often the case, because important social forces or processes are often related to highly mediated and heterogeneous groupings, typically constituted as by-products of various, differently oriented actions, and where people characteristically and usually do not intentionally address each other and even do not know each other (here, we could speak of "ultra-weak" ties). The proposed method based on well-localized eigenvectors is well-capable to find these small communities with anomalously high density of mutual links and therefore reveal a kind of semantic information hidden in the

[SlaKon10]

network, otherwise often neglected. As such, our method may be a good starting point for more fine-grained further analysis of given phenomena.

As an empirical example, we have chosen the data available from the Amazon.com online shopping portal. We studied the network constituted by users writing reviews of the same products offered for purchase on the website during the summer 2005, when the data were gathered. Reviewers become connected if they have written a review on an identical item. When such connections locally proliferate, we get a grouping of relevance.

These groupings are not directly related to the top-lists of popularity, but reveal the most focused points in the network. They are constituted by socially rather distant ties, i.e. by a kind of ultra-weak ties, namely highly mediated links by-produced during processes primarily aimed at something else than addressing each other to establish acquaintance or become closer.

The first important result of our analysis is the power-law tail in the density of eigenvalues. This feature is partially, but not entirely, due to the power-law degree distribution. Comparing the spectrum arising from the network with the spectrum of a random network with the same degree sequence, we find a power-law tail in both cases, but the exponent is significantly smaller in the original network. Generally, such a tail implies that the density of cycles beyond certain length diverges when the size of the network tends to infinity. The difference in the exponent means that some shorter cycles keep finite density in the randomized network, while in the original one they are much more abundant. This means that the Amazon network contains much more compact groupings than what would be expected knowing only its degree sequence.

To see at least some of these small groupings, we looked at well-localized eigenvectors. These localized states represent small communities or network segments and bear semantic information hidden in the network. We call them "hot spots", as they represent local structures which differ from the surrounding background. We were able to explicitly find some of these communities and attribute meaning to them. The three of them briefly discussed in this paper can be labeled as pop-music, pop-movie, and pop-politics communities. The reviewers of these communities are very strongly focused on one narrow segment. This segment itself belongs usually to mass or popular culture, so it cannot be considered as marginal or esoteric. It is the enthusiasm of the reviewers which singles the segment out of the sea of millions products traded on Amazon.com.

Our analysis shows that only about half per cent of the reviewers belong to these network segments in the small sample of 10^4 reviewers. However, we expect that this fraction would rapidly grow if more reviewers are included from the top of the Amazon list downwards. If carefully treated and interpreted, the identified network segments may be useful for enhancing our knowledge of mass or popular culture and complex economic processes related to e-consumerism. Especially, it would be interesting to make systematic classification of the small communities.

[SlaKon10]

Besides these specific findings, we would like to highlight another, more general feature. When analyzing the chosen example, it turned out that conventional talking about "networks of reviewers" might be sociologically misleading. Our groupings, in fact, were constituted not only by people writing reviews on the same products, but also (simultaneously) by products reviewed by the same reviewers. That is why we decided to switch to a more appropriate term "networks of reviewing". This term indicates the hybrid nature of networks we have been dealing with and it allows better talking about processes of online economy rather than about bare structures composed of its human agents. In this respect, our approach is well-compatible with the currently increasing emphasis on heterogeneity as an essential quality of collectivities studied by social scientists [60].

The method can be applied in a straightforward way to any kind of network, wherever the data can be collected easily. However, technical limitations of the method may arise in networks larger that several tens of thousands of vertices, due to computer memory limitations. As shown also by the example of Amazon.com, online networks are often larger than that. Then, we must decide which subset of the whole network can be considered representative. In our case, we chose the subset of the most productive reviewers, but other networks might require other criteria.

Acknowledgments

František Slanina wishes to thank Y.-C. Zhang for encouragement and inspiring comments and to Fribourg University for support and hospitality during the stay when this study was started. This work was carried our within the project AV0Z10100520 of the Academy of Sciences of the Czech republic and was supported by the MŠMT of the Czech Republic, Grant no. OC09078 and by the Research Program CTS MSM 0021620845.

References

[1] Albert, R. and Barabási, A.-L., Statistical mechanics of complex networks, *Rev. Mod. Phys.* **74** (2002) 47–97.

[2] Allen, J., Symbolic economies: The "culturalization" of economic knowledge, in *Cultural Economy: Cultural Analysis and Commercial Life*, Gay, P. D. and Pryke, M. (eds.) (Sage, London, Thousand Oaks and New Delhi, 2002), pp. 39–58.

[3] Ausloos, M. and Lambiotte, R., Clusters or networks of economies? A macroeconomy study through Gross Domestic Product, *Physica A* **382** (2007) 16–21.

[4] Barabási, A.-L. and Albert, R., Emergence of Scaling in Random Networks, *Science* **286** (1999) 509–512.

[5] Barber, M. J., Modularity and community detection in bipartite networks, *Phys. Rev. E* **76** (2007) 066102.

[6] Barry, A. and Slater, D. (eds.), *The Technological Economy* (Routledge, London and New York, 2005).

[7] Beer, D., Making friends with Jarvis Cocker: Music culture in the context of Web 2.0, *Cult. Sociol.* **2** (2008) 222–241.

[SlaKon10]

[8] Benkler, Y., *The Wealth of Networks: How Social Production Transforms Markets and Freedom* (Yale University Press, New Haven and London, 2006).

[9] Berger, P. L. and Luckmann, T., *The Social Construction of Reality: A Treatise in the Sociology of Knowledge* (Penguine Books, Harmondsworth, 1967).

[10] Bianconi, G., Spectral properties of complex networks, arXiv:0804.1744 (2008).

[11] Bollobás, B., *Random Graphs* (Academic Press, London, 1985).

[12] Bornholdt, S. and Schuster, H. G., *Handbook of Graphs and Networks* (Wiley-VCH, Weinheim, 2003).

[13] Bouchaud, J.-P. and Potters, M., Financial applications of random matrix theory: a short review, arXiv:0910.1205, to appear in *Handbook of Random Matrix Theory*.

[14] Burioni, R. and Cassi, D., Random walks on graphs: Ideas, techniques and results, *J. Phys. A* **38** (2005) R45.

[15] Callon, M., Méadel, C. and Rabeharisoa, V., The economy of qualities, in *The Technological Economy*, Barry, A. and Slater, D. (eds.) (Routledge, London and New York, 2005), pp. 28–50.

[16] Capocci, A., Servedio, V. D. P., Caldarelli, G. and Colaiori, F., Detecting communities in large networks, *Physica A* **352** (2005) 669–676.

[17] Castells, M., Toward a sociology of the network society, *Contemp. Sociol.* **29** (2000) 693–699.

[18] Cattuto, C., Schmitz, C., Baldassarri, A., Servedio, V. D. P., Loreto, V., Hotho, A., Grahl, M. and Stumme, G., Network Properties of Folksonomies, *AI Communications* **20** (2007) 245–262.

[19] Christakis, N. A. and Fowler, J. H., *Connected: The Surprising Power of our Social Networks and How They Shape Our Lives* (Hachette Book Group, New York, 2009).

[20] Chung, F. R. K., *Spectral Graph Theory* (American Mathematical Society, 1997).

[21] Danon, L., Duch, J., Arenas, A. and Diaz-Guilera, A., Comparing community structure identification, *J. Stat. Mech.* (2005) 09008.

[22] David, S. and Pinch, T., Six degrees of reputation: The use and abuse of online review and recommendation systems, in *Living in a Material World: Economic Sociology Meets Science and Technology Studies*, Pinch, T. and Swedberg, R. (eds.) (The MIT Press, Cambridge, MA and London, 2008), pp. 341–374.

[23] Degenne, A. and Forse, M., *Introducing Social Networks* (Sage, London, Thousand Oaks and New Delhi, 1994).

[24] Diestel, R., *Graph Theory* (Springer, New York, 2000).

[25] Donetti, L. and Muñoz, M. A., Detecting network communities: a new systematic and efficient algorithm, *J. Stat. Mech.* (2004) P10012.

[26] Donetti, L. and Muñoz, M. A., Improved spectral algorithm for the detection of network communities, Physics/0504059 (2005).

[27] Dorogovtsev, S. N. and Mendes, J. F. F., Evolution of random networks, *Adv. Phys.* **51** (2002) 1079–1187.

[28] Dorogovtsev, S. N. and Mendes, J. F. F., *Evolution of Networks* (Oxford University Press, Oxford, 2003).

[29] Dorogovtsev, S. N., Goltsev, A. V. and Mendes, J. F. F., Pseudofractal Scale-free Web, *Phys. Rev. E* **65** (2002) 066122.

[30] Dorogovtsev, S. N., Goltsev, A. V., Mendes, J. F. F. and Samukhin, A. N., Spectra of complex networks, *Phys. Rev. E* **68** (2003) 046109.

[31] Emirbayer, M. and Goodwin, J., Network analysis, culture, and the problem of agency, *Am. J. Sociol.* **99** (1994) 1411–1453.

[32] Erdős, P. and Rényi, A., On random graphs I, *Pub. Math. Debrecen* **5** (1959) 290–297.

[SlaKon10]

[33] Eriksen, K. A., Simonsen, I., Maslov, S. and Sneppen, K., Modularity and Extreme Edges of the Internet, *Phys. Rev. Lett.* **90** (2003) 148701.

[34] Farkas, I. J., Derényi, I., Barabási, A.-L. and Vicsek, T., Spectra of "Real-World" graphs: Beyond the semi-circle law, *Phys. Rev. E* **64** (2001) 026704.

[35] Farkas, I., Derényi, I., Jeong, H., Néda, Z., Oltvai, Z. N., Ravasz, E., Schubert, A., Barabási, A.-L. and Vicsek, T., Networks in life: Scaling properties and eigenvalue spectra, *Physica A* **314** (2002) 25–34.

[36] Ferrer i Cancho, R., Capocci, A. and Caldarelli, G., Spectral methods cluster words of the same class in a syntactic dependency network, cond-mat/0504165 (2005).

[37] Foot, K., Internet use and meaning, materiality, and sociality through activity theory. Presentation at the 4S Annual Conference, Washington D.C., Oct. 31, 2009 (2009).

[38] Fortunato, S., Community detection in graphs, *Phys. Rep.* **486** (2010) 75–174.

[39] Fortunato, S. and Castellano, C., Community structure in graphs, in *Encyclopedia of Complexity and System Science* (Springer, New York, 2009).

[40] Fortunato, S., Latora, V. and Marchiori, M., Method to find community structures based on information centrality, *Phys. Rev. E* **70** (2004) 056104.

[41] Galluccio, S., Bouchaud, J.-P. and Potters, M., Rational decisions, random matrices and spin glasses, *Physica A* **259** (1998) 449–456.

[42] Goh, K.-I., Kahng, B. and Kim, D., Spectra and eigenvectors of scale-free networks, *Phys. Rev. E* **64** (2001) 051903.

[43] Gopikrishnan, P., Rosenow, B., Plerou, V. and Stanley, H. E., Quantifying and interpreting collective behavior in financial markets, *Phys. Rev. E* **64** (2001) 035106.

[44] Granovetter, M., The strength of weak ties: A network theory revisited, *Sociol. Theor.* **1** (1983) 201–233.

[45] Granovetter, M., The Strength of Weak Ties, *Am. J. Sociol.* **78** (1973) 1360–1380.

[46] Guimerà R. and Amaral, L. A. N., Functional cartography of complex metabolic networks, *Nature* **433** (2005) 895–900.

[47] Hacking, I., *The Social Construction of What?* (Harvard University Press, Cambridge, 1999).

[48] Heimo, T., Tibély, G., Saramäki, J., Kaski, K. and Kertész, J., Spectral methods and cluster structure in correlation-based networks, *Physica A* **387** (2008) 5930–5945.

[49] Jalan, S., Solymosi, N., Vattay, G. and Li, B., Random matrix analysis of localization properties of gene coexpression network, *Phys. Rev. E* **81** (2010) 046118.

[50] Kühn, R., Spectra of Sparse Random Matrices, *J. Phys. A: Math. Theor.* **41** (2008) 295002.

[51] Kamp, C. and Christensen, K., Spectral analysis of protein–protein interactions in Drosophila melanogaster, *Phys. Rev. E* **71** (2005) 041911.

[52] Kim, D.-H. and Jeong, H., Systematic analysis of group identification in stock markets, *Phys. Rev. E* **72** (2005) 046133.

[53] Kim, B. J., Hong, H. and Choi, M. Y., Netons: Vibrations of complex networks, *J. Phys. A: Math. Gen.* **36** (2003) 6329.

[54] Kullmann, L., Kertész, J. and Mantegna, R. N., Identification of clusters of companies in stock indices via Potts super-paramagnetic transitions, *Physica A* **287** (2000) 412–419.

[55] Laloux, L., Cizeau, P., Bouchaud, J.-P. and Potters, M., Noise dressing of financial Correlation Matrices, *Phys. Rev. Lett.* **83** (1999) 1467–1470.

[56] Lambiotte, R. and Ausloos, M., Uncovering collective listening habits and music genres in bipartite networks, *Phys. Rev. E* **72** (2005) 066107.

[57] Lancichinetti, A., Fortunato, S. and Kertész, J., Detecting the overlapping and hierarchical community structure of complex networks, *New J. Phys.* **11** (2009) 033015.

[SlaKon10]

[58] Lancichinetti, A., Kivela, M., Saramäki, J. and Fortunato, S., Characterizing the community structure of complex networks, *PLoS ONE* **5** (2010) e11976.

[59] Lash, S. and Urry, J., *Economies of Signs and Space* (Sage, London, 1994).

[60] Latour, B., *Reassembling the Social: An Introduction to Actor–Network Theory* (Oxford University Press, Oxford, 2005).

[61] Leskovec, J., Lang, K. J. and Mahoney, M. W., Empirical Comparison of Algorithms for Network Community Detection, in *WWW '10: Proceedings of the 19th International Conference on World Wide Web* (2010), pp. 631–640.

[62] Licoppe, C., Understanding and reframing the electronic consumption experience: The interactional ambiguities of mediated coordination, in *Living in a Material world: Economic Sociology Meets Science and Technology Studies*, Pinch, T. and Swedberg, R. (eds.) (The MIT Press Cambridge, MA and London, 2008), pp. 317–340.

[63] Marčenko, V. A. and Pastur, L. A., Distribution of eigenvalues for some sets of random matrices, *Math. USSR–Sbornik* **1** (1967) 457–483.

[64] Mehta, M. L., *Random Matrices* (Academic Press, San Diego, 1991).

[65] Nagao, T. and Rodgers, G. J., Spectral density of complex networks with a finite mean degree, *J. Phys. A: Math. Theor.* **41** (2008) 265002.

[66] Nagao, T. and Tanaka, T., Spectral density of sparse sample covariance matrices, *J. Phys. A: Math. Theor.* **40** (2007) 4973–4987.

[67] Newman, M. E. J., Finding community structure in networks using the eigenvectors of matrices, *Phys. Rev. E* **74** (2006) 036104.

[68] Newman, M. E. J. and Girvan, M., Mixing patterns and community structure in networks, in *Statistical Mechanics of Complex Networks*, Pastor-Satorras, R., Rubí, J. and Diaz-Guilera, A. (eds.) (Springer, Berlin, 2003), pp. 66–87.

[69] Newman, M. E. J. and Girvan, M., Finding and evaluating community structure in networks, *Phys. Rev. E* **69** (2004) 026113.

[70] Newman, M., Barabási, A.-L. and Watts, D. J., *The Structure and Dynamics of Networks* (Princeton University Press, Princeton, 2006).

[71] Noh, J. C. and Rieger, H., Random walks on complex networks, *Phys. Rev. Lett.* **92** (2004) 118701.

[72] Palla, G., Derényi, I., Farkas, I. and Vicsek, T., Uncovering the overlapping community structure of complex networks in nature and society, *Nature* **435** (2005) 814–818.

[73] Plerou, V., Gopikrishnan, P., Rosenow, B., Amaral, L. A. N. and Stanley, H. E., Universal and nomuniversal properties of cross correlations in financial time series, *Phys. Rev. Lett.* **83** (1999) 1471–1474.

[74] Plerou, V., Gopikrishnan, P., Rosenow, B., Amaral, L. A. N. and Stanley, H. E., Random matrix approach to cross correlations in financial data, *Physica A* **287** (2000) 374–382.

[75] Plerou, V., Gopikrishnan, P., Rosenow, B., Amaral, L. A. N., Guhr, T. and Stanley, H. E., Random matrix approach to cross correlations in financial data, *Phys. Rev. E* **65** (2002) 066126.

[76] Radicchi, F., Castellano, C., Cecconi, F., Loreto, V. and Parisi, D., Defining and identifying communities in networks, *Proc. Natl. Acad. Sci. USA* **101** (2004) 2658–2663.

[77] Reichardt, J. and Bornholdt, S., Detecting Fuzzy Community Structures in Complex Networks with a Potts Model, *Phys. Rev. Lett.* **93** (2004) 218701.

[78] Rheingold, H., *The Virtual Community: Homesteading on the Electronic Frontier* (Addison-Wesley, Reading, MA, 1993).

[79] Rodgers, G. J. and Bray, A. J., Density of states of a sparse random matrix, *Phys. Rev. B* **37** (1988) 3557–3562.

[SlaKon10]

[80] Rodgers, G. J., Austin, K., Kahng, B. and Kim, D., Eigenvalue spectra of complex networks, *J. Phys. A: Math. Gen.* **38** (2005) 9431–9437.

[81] Rogers, T., Castillo, I. P., Kühn, R. and Takeda, K., Cavity approach to the spectral density of sparse symmetric random matrices, *Phys. Rev. E* **78** (2008) 031116.

[82] Sawardecker, E. N., Amundsen, C. A., Sales-Pardo, M. and Amaral, L. A. N., Comparison of methods for the detection of node group membership in bipartite networks, *Eur. Phys. J.* **72** (2009) 671–677.

[83] Scott, J., *Social Network Analysis: A Handbook* (Sage, London, Thousand Oaks and New Delhi, 2000).

[84] Semerjian, G. and Cugliandolo, L. F., Sparse random matrices: the eigenvalue spectrum revisited, *J. Phys. A: Math. Gen.* **35** (2002) 4837–4851.

[85] Simonsen, I., Eriksen, K. A., Maslov, S. and Sneppen, K., Diffusion on complex networks: a way to probe their large-scale topological structures, *Physica A* **336** (2004) 163–173.

[86] Slanina, F. and Zhang, Y.-C., Referee networks and their spectral properties, *Acta Phys. Pol. B* **36** (2005) 2797–2804.

[87] Star, S. L. and Griesemer, J. R., Institutional ecology, "translations" and boundary objects: Amateurs and professionals in Berkeley's museum of vertebrate zoology, 1907–39, *Soc. Stud. Sci.* **19** (1989) 387–420.

[88] Strogatz, S. H., Exploring complex networks, *Nature* **410** (2001) 268–276.

[89] Tibély, G., Onnela, J.-P., Saramäki, J., Kaski, K. and Kertész, J., Spectrum, intensity and coherence in weighted networks of a financial market, *Physica A* **370** (2006) 145–150.

[90] Wasserman, S. and Faust, K., *Social Network Analysis: Methods and Application* (Cambridge University Press, Cambridge, 1994).

[91] Wellman, B., Salaff, J., Dimitrova, D., Garton, L. and Al, E., Computer networks as social networks: Collaborative work, telework, and virtual community, *Ann. Rev. Sociol.* **22** (1996) 213–238.

[92] Wittel, A., Toward a network sociality, *Theory, Culture and Society* **18** (2001) 51–76.

[93] Woolgar, S., Reflexive Internet? The British experience of new electronic technologies, in *The Network Society: A Cross-cultural Perspective*, Castells, M. (ed.) (Edward Elgar, Cheltenham and Northampton, MA, 2004), pp. 125–143.

[94] Zhao, F., Yang, H. and Wang, B., scaling invariance in spectra of complex networks: A diffusion factorial moment approach, *Phys. Rev. E* **72** (2005) 046119.

[95] Zhou, T., Ren, J., Medo, M. and Zhang, Y.-C., Bipartite network projection and personal recommendation, *Phys. Rev. E* **76** (2007) 046115.

[Slanina11]

PHYSICAL REVIEW E **83**, 011118 (2011)

Equivalence of replica and cavity methods for computing spectra of sparse random matrices

František Slanina*

Institute of Physics, Academy of Sciences of the Czech Republic, Na Slovance 2, CZ-18221 Prague, Czech Republic

(Received 4 October 2010; revised manuscript received 1 December 2010; published 21 January 2011)

We show by direct calculation that the replica and cavity methods are exactly equivalent for the spectrum of an Erdős-Rényi random graph. We introduce a variational formulation based on the cavity method and use it to find approximate solutions for the density of eigenvalues. We also use this variational method for calculating spectra of sparse covariance matrices.

DOI: 10.1103/PhysRevE.83.011118 PACS number(s): 05.40.−a, 89.75.−k, 63.50.Lm

I. INTRODUCTION

Random matrix theory is a discipline with a wide range of physical applications and many beautiful mathematical results [1]. One of the aspects that makes the problem extremely complex is the fact that real physical systems are embedded in three-dimensional Euclidean space. Their Hamiltonian is often a random matrix, but the randomness is constrained in a highly nontrivial way.

The constraints are relatively less severe in the atomic nucleus, where the three dimensionality of physical space is of secondary importance. Hence the spectacular success of the early works in random matrix theory, due to Wigner [2,3] and Dyson [4]. On the other hand, the fundamental constraint arising from the two-body character of the interaction within the (model of an) atomic nucleus induces several drastic changes [5–9]. Most importantly, the density of states is not a semicircle, as suggested by Wigner, but rather it follows a Gaussian shape. Therefore, sharp band edges are missing, and Lifschitz tails develop. For the current state of the problem, see, e.g., the review [10].

An even more complicated situation arises in all random extended systems, such as disordered or amorphous semiconductors, where we must take into account the Euclidean constraints. Perhaps the easiest of these constraints is the sparsity of the Hamiltonian matrix, which is due to the finite range of interactions. If we forget the even more severe complications due to the precise number of spatial dimensions (in reality one, two, or three), we are left with the problem of determining the spectrum of a random sparse matrix.

An important breakthrough was achieved using the replica method, which was introduced in the context of random matrices in Ref. [11]. Rodgers and Bray, in their classic work [12], solved the problem in the sense that they found an integral equation for a quantity from which the density of states is readily obtained. Unfortunately, that equation still resists all attempts for an exact analytic solution. In Ref. [12], two approximative solutions were found: first, in the form of a series expansion, whose leading term coincides with the Wigner semicircle law; and, second, using a nonperturbative argument, introduced earlier in Ref. [13], the shape of the Lifschitz tails in the density of states was found.

The replica method for treating spectra of sparse matrices was further developed [14–28]. In particular, the variational formulation of the replica equations [19,20,27] enabled generating self-consistent approximations, namely, the effective medium approximation (EMA), which is analogous to the coherent potential approximation used for electrons in random potential. In these approximations, Lifschitz tails in the spectrum are absent. Further sophistication of the method consists of the single defect approximation (SDA), which obtains the Lifschitz tail in the form of an infinite sequence of delta peaks.

The complexity of the problem becomes evident when we compare these results with the density of states obtained by numerical diagonalization of large sample matrices [27,29–33]. The Lifschitz tail is smooth, while the bulk of the density of states is the combination of a continuous component with a set of delta peaks. The most marked of these peaks is at the origin, others at eigenvalues $z = \pm 1, \pm\sqrt{2}$, etc. All these structures should emerge from the solution of the Rodgers-Bray integral equation, but EMA, as well as SDA, misses all of them. The set of delta peaks was studied separately in Refs. [20,32], but a theory that would combine naturally both these peaks and the continuous component is still unavailable.

More recently, spectra of sparse matrices encoding the structure of random graphs were studied successfully using the cavity approach (see, e.g., Ref. [34]). It is based on the fact that large random graphs are locally isomorphic to trees. This was used, e.g., in Refs. [35–37] to calculate spectra of adjacency matrix and Laplacians on complex networks. In Refs. [35,36], a "self-consistent" version of SDA was used to obtain the asymptotic shape of the Lifschitz tails, which decay as a power law in the case of scale-free networks. In Ref. [37] a more sophisticated calculation led to an integral equation similar to Rodgers and Bray's [12], from which the asymptotics of Lifschitz tails is found. The cavity method provides an easy way [33] to obtain the Wigner semicircle law, as well as the Marčenko-Pastur law for a spectrum of covariance matrices. It can be also used as an efficient numerical procedure [33], reproducing all peculiarities of the density of states, including Lifschitz tails and delta peaks. The mathematical justification for the use of the cavity approach can be found in Ref. [38].

A very powerful method for computing spectral properties of random matrices is based on supersymmetry and was developed in Refs. [39,40] (see also the review [41] and a recent development in Ref. [42]). Initially, the results of replica and supersymmetric methods were found to be in conflict,

*slanina@fzu.cz

which resulted in serious criticism of the replica trick in general [43]. The density of states of sparse random matrices was calculated using supersymmetry [44], leading to an equation that was later [45] shown equivalent to the replica result of Ref. [12]. However, the correlation of eigenvalues, which was investigated in Ref. [46] using supersymmetry for the case of sparse matrices, was not reproduced correctly in the replica method, until the integral over all saddle points was properly taken in Ref. [47]. Since then, the replica method regained its reputation as an equivalent alternative to supersymmetric methods. This was further supported by a series of papers [48–50]. Finally, let us mention the works that approach the density of states by computing the moments exactly [31,51].

In this paper, we show an alternative method to obtain the Rodgers-Bray integral equation using the cavity approach. Therefore, we prove exact equivalence of the replica and cavity methods in this case, which was previously assumed only on the basis of topological considerations for random Erdős-Rényi graphs. Moreover, as an important by-product of this proof, we present a variational formulation of the problem, which serves as a useful generator of self-consistent approximations.

II. PROJECTOR METHOD

We shall investigate the spectrum of the adjacency matrix L of an Erdős-Rényi random graph with N vertices. Therefore, the probability distribution of the matrix elements factorizes

$$\pi(L) = \prod_{i<j} [\pi_1(L_{ij})\delta(L_{ij} - L_{ji})] \prod_i \delta(L_{ii}), \tag{1}$$

where the probability density for a single off-diagonal element is

$$\pi_1(x) = \left(1 - \frac{\mu}{N}\right)\delta(x) + \frac{\mu}{N}\delta(x-1). \tag{2}$$

The key ingredient of all subsequent analysis is the resolvent:

$$R(z) = (z - L)^{-1} \tag{3}$$

and its average $\langle R(z)\rangle$ over disorder, taken with the distribution (1). It contains information on the average density of states (here we assume z on the real axis):

$$\mathcal{D}(z) = \lim_{\epsilon\to 0^+} \frac{1}{N\pi} \mathrm{Tr}\,\langle R(z - i\epsilon)\rangle. \tag{4}$$

In the spirit of the cavity method, we focus on a single vertex, surrounded by the rest of the graph. To calculate the diagonal element of the resolvent on this vertex, we use the projector method, formulated generally in Ref. [52]. For a different route that also leads to equivalent results, see Ref. [34]. Let us have an arbitrary projector P and its complement $P^C \equiv 1 - P$. Then the projected resolvent is [52]

$$PRP = \frac{P}{P(z-L)P - PLP^C \frac{P^C}{z-L} P^C L P}. \tag{5}$$

We denote the singled-out vertex as $i = 0$. Let P_0 be the projector to this vertex. Furthermore, denote $i = 1,2,\ldots,k$ neighbors of the vertex 0 on the graph represented by the matrix L and denote also a P_i projector to the neighbor i. Let us use composite indices for other vertices. If k_i is the number of neighbors of i, denote $[i,1],[i,2],\ldots,[i,k_i-1]$ as the neighbors of vertex i, except the vertex 0. The projectors to the second neighbors of 0 will be denoted using these indices, so $P_{i,i'}$ is projector on the vertex $[i,i']$. By analogy, we define the projectors to third, fourth, etc., neighbors of 0. Note that on a general graph, some of the projectors may coincide due to the presence of cycles.

The cavity approach consists of replacing the graph by a tree, which is locally isomorphic to it, i.e., neglecting all cycles on the graph. Algebraically, it is equivalent to the assumption that the complementary projectors can be written as direct sums of projectors corresponding to separate branches of the tree:

$$\begin{aligned} P_0^C &= P_{(1)} \oplus P_{(2)} \oplus \cdots \oplus P_{(k)}, \\ P_{(i)} P_i^C &= P_{(i,1)} \oplus P_{(i,2)} \oplus \cdots \oplus P_{(i,k_i-1)}, \\ P_{(i,i')} P_{i,i'}^C &= P_{(i,i',1)} \oplus P_{(i,i',2)} \oplus \cdots \oplus P_{(i,i',k_{i,i'}-1)}, \\ &\vdots \end{aligned} \tag{6}$$

where $P_{(i)}P_i = P_i$, $P_{(i,i')}P_{i,i'} = P_{i,i'}$, and so forth.

Using the projectors we define the series of scalar functions related to the resolvent:

$$\begin{aligned} g(z) &= P_0 R(z) P_0, \\ g_i(z) &= P_i \frac{{P_0}^C}{z-L} P_i, \\ g_{i,i'}(z) &= P_{i,i'} \frac{P_{(i)}\,{P_i}^C}{z-L} P_{i,i'}, \\ g_{i,i',i''}(z) &= P_{i,i',i''} \frac{P_{(i,i')}\,{P_{i,i'}}^C}{z-L} P_{i,i',i''}, \\ &\vdots \quad . \end{aligned} \tag{7}$$

From (5) and the assumptions (6) we have the chain of equations for these functions:

$$\begin{aligned} g(z) &= \frac{1}{z - \sum_{i=1}^{k} g_i(z)}, \\ g_i(z) &= \frac{1}{z - \sum_{i'=1}^{k_i-1} g_{i,i'}(z)}, \\ g_{i,i'}(z) &= \frac{1}{z - \sum_{i''=1}^{k_{i,i'}-1} g_{i,i',i''}(z)}, \\ &\vdots \quad . \end{aligned} \tag{8}$$

On a random tree, the degrees k, k_i, $k_{i,i'}$ are random variables, and therefore $g(z)$, $g_i(z)$, $g_{i,i'}(z)$, etc., are also random functions of z. To describe their properties, we define their generating functions (dependence on z becomes implicit):

$$\begin{aligned} G(\omega) &= \langle e^{-\omega\, g(z)}\rangle, \\ G_1(\omega) &= \langle e^{-\omega\, g_i(z)}\rangle, \\ G_2(\omega) &= \langle e^{-\omega\, g_{i,i'}(z)}\rangle, \\ G_3(\omega) &= \langle e^{-\omega\, g_{i,i',i''}(z)}\rangle, \\ &\vdots \quad . \end{aligned} \tag{9}$$

If the graph in question is the Erdős-Rényi random graph, all the degrees in the corresponding random tree are independent and distributed according to the Poisson distribution $P(k) = e^{-\mu}\,\mu^k/k!$. The average degree μ is the only free parameter of this model.

Calculation of the generating functions (9) is facilitated by the integral representation

$$g(z) = \frac{1}{z - \sum_{i=1}^{k} g_i(z)} = \int_0^\infty e^{-\lambda[z-\sum_{i=1}^{k} g_i(z)]}\, d\lambda \tag{10}$$

and similarly for the other g's. Assuming for the moment that k is fixed, we get, after some algebra, the following relation between $G(\omega)$ and $G_1(\omega)$:

$$G(\omega) = 1 + \sqrt{\omega} \int_0^\infty \frac{d\lambda}{\sqrt{\lambda}}\, I_1(2\sqrt{\omega\lambda})\, e^{-\lambda z}\, [G_1(\lambda)]^k. \tag{11}$$

Now we take into account the Poisson distribution of degrees, which gives

$$G(\omega) = 1 + \sqrt{\omega} \int_0^\infty \frac{d\lambda}{\sqrt{\lambda}}\, I_1(2\sqrt{\omega\lambda})\, e^{-\lambda z + \mu[G_1(\lambda)-1]}. \tag{12}$$

Repeating the same steps for further generating functions we get

$$G_1(\omega) = 1 + \sqrt{\omega} \int_0^\infty \frac{d\lambda}{\sqrt{\lambda}}\, I_1(2\sqrt{\omega\lambda})\, e^{-\lambda z + \mu[G_2(\lambda)-1]}. \tag{13}$$

Note that the form of the relation between G and G_1 is the same as between G_1 and G_2 and generally between G_m and G_{m+1} for any $m > 0$. This is due to the special property of the Poisson distribution, $kP(k)/\mu = P(k-1)$. For any other distribution this does not hold.

For an infinitely large tree we suppose that the generating functions $G_m, m = 1,2,3,\ldots$ converge to a common limit, and we can impose the condition of stationarity $G_1(\omega) = G_2(\omega)$. Therefore, we define a single function $\gamma(\omega) = G(\omega) - 1$, for which we have a closed equation:

$$\gamma(\omega) = \sqrt{\omega} \int_0^\infty \frac{d\lambda}{\sqrt{\lambda}}\, I_1(2\sqrt{\omega\lambda})\, e^{-\lambda z + \mu\gamma(\lambda)}. \tag{14}$$

It is strictly equivalent to Eq. (18) in Ref. [12] (the Rodgers-Bray equation), which was obtained using the replica method. Hence we conclude that the explicit calculation showed the equivalence of the replica and cavity approaches in the case of the Erdős-Rényi graph, which is just the situation in which the Rodgers-Bray equation holds. Note, however, that the direct computation we used here would fail if the degree distribution was not Poissonian.

III. VARIATIONAL PROBLEM

The key result (14) can be reformulated in a different way more appropriate for approximate solution. As a first step, we define an auxiliary function $\rho(\omega) = e^{-\omega z + \mu\gamma(\omega)}$. Instead of the single equation (14), we can solve the pair:

$$\begin{aligned} \gamma(\omega) &= \sqrt{\omega} \int_0^\infty \frac{d\lambda}{\sqrt{\lambda}}\, I_1(2\sqrt{\omega\lambda})\, \rho(\lambda), \\ \rho(\omega) &= e^{-\omega z + \mu\gamma(\omega)}. \end{aligned} \tag{15}$$

Direct solution of (15) is as difficult as solving (14). However, we can find a functional, whose stationary point is just defined by Eqs. (15). We can check explicitly that such a functional is

$$\begin{aligned} \mathcal{F}[\gamma,\rho] = &-\int_0^\infty \frac{d\omega}{\omega}\, \gamma(\omega)\rho(\omega) \\ &+ \frac{1}{2}\int_0^\infty \frac{d\omega}{\sqrt{\omega}} \int_0^\infty \frac{d\lambda}{\sqrt{\lambda}}\, I_1(2\sqrt{\omega\lambda})\rho(\omega)\rho(\lambda) \\ &+ \frac{1}{\mu}\int_0^\infty \frac{d\omega}{\omega} e^{-\omega z + \mu\gamma(\omega)}. \end{aligned} \tag{16}$$

Note that we derived, within the cavity approach, a result that is analogous to the functional obtained in Ref. [27] using the replica trick.

The variational formulation of the problem is useful as a generator of approximations. In Ref. [20] a variational ansatz was used to derive the density of states in the EMA. Let us see now how it is obtained in our cavity procedure. If we take the exponential ansatz for the auxiliary function $\rho(\omega)$, namely,

$$\rho(\omega) = e^{-\sigma\,\omega}, \tag{17}$$

all integrals in (16) can be performed explicitly, and we can extremalize the functional with respect to σ and $\gamma(\omega)$. In this way we find the cubic equation:

$$\sigma^3 - z\,\sigma^2 + (\mu - 1)\,\sigma + z = 0. \tag{18}$$

It is identical to Eq. (23) in Ref. [20] obtained by the replica method. The solution can be obtained analytically, and the density of states is extracted using the formula

$$\mathcal{D}(z) = \lim_{\epsilon\to 0^+} \mathrm{Im}\frac{1}{\pi\,\sigma(z - i\epsilon)}. \tag{19}$$

We can further improve the calculation by the following trick, which we shall refer to as the "single-shell approximation" within this paper. We may formally write the pair of Eqs. (15) as a set of four equations:

$$\begin{aligned} \gamma(\omega) &= \sqrt{\omega} \int_0^\infty \frac{d\lambda}{\sqrt{\lambda}}\, I_1(2\sqrt{\omega\lambda})\, \rho(\lambda), \\ \rho(\omega) &= e^{-\omega z + \mu\,\overline{\gamma}(\omega)}, \\ \overline{\gamma}(\omega) &= \sqrt{\omega} \int_0^\infty \frac{d\lambda}{\sqrt{\lambda}}\, I_1(2\sqrt{\omega\lambda})\, \overline{\rho}(\lambda), \\ \overline{\rho}(\omega) &= e^{-\omega z + \mu\,\gamma(\omega)}. \end{aligned} \tag{20}$$

These equations can be obtained as a condition of stationarity for the functional:

$$\begin{aligned} \mathcal{F}_1[\gamma,\rho,\overline{\gamma},\overline{\rho}] = &-\int_0^\infty \frac{d\omega}{\omega}[\gamma(\omega)\overline{\rho}(\omega) + \overline{\gamma}(\omega)\rho(\omega)] \\ &+ \int_0^\infty \frac{d\omega}{\sqrt{\omega}} \int_0^\infty \frac{d\lambda}{\sqrt{\lambda}}\, I_1(2\sqrt{\omega\lambda})\rho(\omega)\overline{\rho}(\lambda) \\ &+ \frac{1}{\mu}\int_0^\infty \frac{d\omega}{\omega} e^{-\omega z}(e^{\mu\,\gamma(\omega)} + e^{\mu\,\overline{\gamma}(\omega)}). \end{aligned} \tag{21}$$

If Eqs. (20) were solved exactly, we would have $\gamma(\omega) = \overline{\gamma}(\omega)$ and $\rho(\omega) = \overline{\rho}(\omega)$. The same also would hold in the case of the effective medium approximation, which amounts to taking the ansatz $\rho(\omega) = \overline{\rho}(\omega) = e^{-\sigma\,\omega}$, so apparently the set (20) does not bring any advantage over (15). However, relaxing

the condition $\rho(\omega) = \overline{\rho}(\omega)$ we can get an improvement in an approximate solution. Indeed, we can take the ansatz

$$\rho(\omega) = e^{-\sigma\,\omega} \tag{22}$$

as in EMA but allow $\overline{\rho}(\omega)$ to adjust itself freely so that $\mathcal{F}_1$ is stationary. In this way we introduce an error, because $\rho(\omega) \neq \overline{\rho}(\omega)$ and $\gamma(\omega) \neq \overline{\gamma}(\omega)$, but we gain a better approximation for the density of states.

After some algebra, we get the following equation for the quantity $\tau = z\,\sigma$:

$$z^2 = \mu + \tau + e^{-\mu} \sum_{l=1}^{\infty} \frac{\mu^l}{(l-1)!}\,\frac{l}{\tau - l}. \tag{23}$$

The fact that the equation depends on z^2 means that the spectrum is symmetric with respect to the point $z = 0$. For a general z on the real axis, Eq. (23) can be easily solved numerically. We find that there are at most two roots with nonzero imaginary parts (complex conjugate to each other). Those values of z for which all solutions are real correspond to gaps in the spectrum. The general picture is that there is a very narrow gap around $z = 0$, separating two halves of a wide band, containing most of the eigenvalues. We can call this band (not quite precisely) the "bulk" of the density of states.

In the middle of the bulk, there is a δ-function contribution just at $z = 0$, whose weight can be found exactly and is equal to $e^{-\mu}$. On both sides of the bulk, there are a series of small side bands separated by gaps. The density of states therefore has the form

$$\mathcal{D}(z) = e^{-\mu}\delta(z) + \mathcal{D}_c(z), \tag{24}$$

where $\mathcal{D}_c(z)$ is a continuous function. The interpretation of the δ-function is straightforward. It corresponds to single isolated vertices, whose fraction is just equal to $e^{-\mu}$, and they all contribute with the same eigenvalue 0.

Some analytical information on the continuous part $\mathcal{D}_c(z)$ can be found from an approximate solution of Eq. (23). For $e^{-\mu} \ll 1$ we can find approximately the edge of the gap around $z = 0$. We get

$$\mathcal{D}_c(z) \simeq \frac{1}{2\pi\,z}\sqrt{4\psi(\mu)\,z^2 - e^{-2\mu}}, \tag{25}$$

where we denote

$$\psi(\mu) = e^{-\mu} \sum_{l=1}^{\infty} \frac{\mu^l}{l!\,l} = \mu\,e^{-\mu}\,{}_2F_2(1,1;2,2;\mu). \tag{26}$$

We can see that the gap edge is at $z_0 = \frac{1}{2}e^{-\mu}/\sqrt{\psi(\mu)}$.

For the tails, we can calculate analytically the side bands in an approximation that becomes exact for $|z| \to \infty$. The computation goes as follows. Each of the side bands can be identified with one term in the infinite sum over l in (23). The tails of the spectrum corresponding to large $|z|$ are identified with large l. In the crudest approximation, the solution is $\tau \simeq l$. Therefore, we introduce a new variable η by $\tau = l + \eta$. So (23) assumes the form

$$z^2 = \mu + l + \eta + e^{-\mu}\,\frac{\mu^l}{(l-1)!}\,\frac{l}{\eta} + e^{-\mu} \sum_{l'=1(l'\neq l)}^{\infty} \frac{\mu^{l'}}{(l'-1)!}\,\frac{l'}{l - l' - \eta}. \tag{27}$$

For large l we can expand the infinite series in powers of η and keep only the lowest terms, so

$$z^2 = \mu + \Delta_l(\mu) + l + [1 - \Gamma_l(\mu)]\,\eta + e^{-\mu}\,\frac{\mu^l}{(l-1)!}\,\frac{l}{\eta} + O(\eta^2), \tag{28}$$

where

$$\Delta_l(\mu) = e^{-\mu} \sum_{l'=1(l'\neq l)}^{\infty} \frac{\mu^{l'}}{(l'-1)!}\,\frac{l'}{l - l'}, \qquad \Gamma_l(\mu) = e^{-\mu} \sum_{l'=1(l'\neq l)}^{\infty} \frac{\mu^{l'}}{(l'-1)!}\,\frac{l'}{(l - l')^2}. \tag{29}$$

So, for each l large enough, we have two "bubbles" of a nonzero density of states. The two bubbles are symmetric to each other with respect to the origin. The "bubbles" are separated by gaps, so each "bubble" has well-defined lower and upper edges, z_{l-} and z_{l+}, respectively. For large l the approximate form of the "bubble" is given by the solution of a quadratic equation in η, so

$$\mathcal{D}_l(z) \simeq \frac{|z|}{\pi}\left\{[1 - \Gamma_l(\mu)]\frac{e^{-\mu}\,l\,\mu^l}{(l-1)!} - \left[\frac{z^2 - \mu - l - \Delta_l(\mu)}{2}\right]^2\right\}^{1/2} \times \left\{\frac{e^{-\mu}\,l\,\mu^l}{(l-1)!} + (z^2 - \mu - l)l + [1 - \Gamma_l(\mu)](l)^2\right\}^{-1}. \tag{30}$$

The width of the bubble $z_{l+} - z_{l-}$ approaches zero for $l \to \infty$. This justifies considering η as a small parameter in the expansion (28). For large l the "bubbles" have a semicircle shape, and their weight is

$$W_l = \int_{z_{l-}}^{z_{l+}} \mathcal{D}_l(z)\,dz \simeq \frac{1}{2}\,e^{-\mu}\,\frac{\mu^l}{l!}. \tag{31}$$

We recognize the Poisson distribution with mean μ. This reflects the Poisson distribution of degrees of the random graph. The factor $1/2$ stems from the fact that we have two bubbles for each l. The center of the bubble corresponding to l is at $z_l = \sqrt{l + \mu + \Delta_l(\mu)}$; thus the distance between two successive bubbles is $\Delta z_l \simeq (4z_l)^{-1/2}$. Hence we deduce the approximate density of states in the tails, for $|z| \to \infty$:

$$\mathcal{D}_{\text{tail}}(z) \simeq \frac{e^{-\mu}\,|z|\,\mu^{z^2}}{\Gamma(z^2 - 1)} \simeq \frac{e^{-\mu}}{\sqrt{2\pi}}\left(\frac{e\mu}{z^2}\right)^{z^2}. \tag{32}$$

This is the shape of the Lifschitz tail, which was already obtained by Refs. [12] and [20].

To assess the quality of the approximations used, we compare the results arising from EMA [Eq. (18)], from the single-defect [20,33], and single-shell [Eq. (23)] approximations with an average density of states obtained by numerical diagonalization of sample matrices. In Fig. 1 we can see the

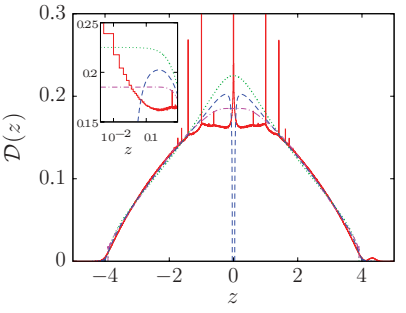

FIG. 1. (Color online) Density of states for the adjacency matrix of an Erdős-Rényi graph, with average degree $\mu = 3$. The solid line shows the result of the numerical diagonalization of a matrix of size $N = 1000$, averaged over 75 000 random realizations. The dotted line is the result of an effective medium approximation, the dot-dashed line is the single-defect approximation, and the dashed line is the single-shell approximation. In the inset, a detail of the density of states around the center of the band is plotted in semilogarithmic scale.

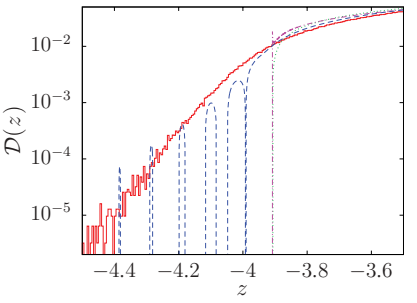

FIG. 2. (Color online) The detail of the left tail of the density of states shown in Fig. 1. The solid line shows the result of numerical diagonalization, the dotted line is the result of effective medium approximation, the dot-dashed line is the single-defect approximation, and the dashed line is the single-shell approximation.

spectrum for $\mu = 3$ and matrices of size $N = 1000$ averaged over 75 000 realizations. We can clearly identify the delta peaks, as well as the complicated shape of the continuous part of the spectrum near the center of the bulk. Interestingly, both EMA and the single-shell approximations are very good if we are neither close to the center nor at the tails of the spectrum. Close to the center, the shape of the density of states is rather complex, as shown in the inset in Fig. 1. There is a shallow depression, followed by a divergence at $z = 0$. The form of the singularity at $z = 0$ seems to be close to a logarithmic divergence, although the data do not provide decisive evidence. None of the three approximations reproduce this singularity. EMA and SDA are constant around $z = 0$, while the single-shell approximation exaggerates the depression around $z = 0$ to such an extent that a spurious gap is created. This is an artifact of the approximation. However, the delta peak at the origin is, correctly, present in the single-shell approximation.

A similar comparison also was done at the tail of the density of states. We can see in Fig. 2 a detail of the same data as shown in Fig. 1. Note that, for any finite N, the density of states is not mirror symmetric with respect to the line $z = 0$, because the average value of the off-diagonal elements of the matrix L is strictly positive. Only in the limit $N \to \infty$ does the spectrum become symmetric. The single largest eigenvalue is split off the rest of the spectrum [53], and the small bump in the positive tail corresponds to this effect. In the limit $N \to \infty$ this bump would vanish, as the weight of the single largest eigenvalue becomes negligible compared to the rest of the spectrum.

As shown in Fig. 2, we can see that the single-shell approximation is superior to both EMA and SDA in the tail region, from two aspects. First, the spurious band edge of EMA and SDA is shifted toward larger $|z|$, so that the interval in which $\mathcal{D}(z)$ is well reproduced is wider. Second, the single-shell approximation also displays nonzero density of states in some regions of the Lifschitz tails, although, instead of exhibiting a smooth behavior everywhere, the density of states is concentrated in "bubbles." The gaps separating the "bubbles" are again artifacts of the approximation, to the same extent as the sharp band edge is an artifact of EMA and SDA. On the other hand, it is an important improvement over SDA [20]. The delta peaks of SDA are widened into continuous bands in our approach. In fact, this is to be expected, because the single-shell approximation can be rightly interpreted as a self-consistent version of SDA. Therefore, it should be better than SDA in principle, although this *a priori* judgment may turn out to be incorrect in practice, as the single-shell approximation is better than SDA sometimes (in the tail) but worse elsewhere (around $z = 0$).

Finally, let us note that similar "bubbles" at the tails were also seen in approximations derived using the replica method by Ref. [21] for the Laplacian of a random graph and by Ref. [25] for sparse covariance matrices.

IV. COVARIANCE MATRICES

Another application of the method presented here is investigation of sparse covariance matrices. They can be considered as arising from a bipartite graph where edges connect vertices from the set A with vertices from the set B. We denote the size of the sets N_A and N_B, respectively. In the thermodynamic limit, $N_A \to \infty$, $N_B \to \infty$, we fix the ratio $\alpha = N_A/N_B$ constant. In the bipartite analog of an Erdős-Rényi random graph, the degrees of vertices in A and B follow Poisson distributions with average degree μ_A and μ_B, respectively, where $\mu_B/\mu_A = \alpha$. The problem has a long history, starting with the work of Marčenko and Pastur [54], and was investigated recently by the replica method in Ref. [25].

The adjacency matrix of the bipartite graph has the form

$$L = \begin{pmatrix} 0 & M^T \\ M & 0 \end{pmatrix}, \tag{33}$$

where the first block of indices corresponds to set A, and the second block to set B. We define the contraction, or covariance, matrix $C_A = M^T M$, which acts solely in the set A (and similarly $C_B = M M^T$, which acts solely in the set B). The spectra of the matrices L, C_A, and C_B are closely related. We define $\mathcal{D}_A(z) = \lim_{\epsilon \to 0^+} \mathrm{Im} \sum_{i \in A} [(z - i\epsilon - L)^{-1}]_{ii}/(N_A \pi)$ as the partial density of states of L

restricted to the set A and $\mathcal{D}_{CA}(z) = \lim_{\epsilon\to 0^+} \mathrm{Im} \sum_{i\in A}[(z - i\epsilon - C_A)^{-1}]_{ii}/(N_A\pi)$ as the density of states of the correlation matrix C_A. It can be easily shown that

$$\mathcal{D}_{CA}(z) = \frac{1}{\sqrt{z}}\mathcal{D}_A(\sqrt{z}). \tag{34}$$

This relation remains in force also after averaging over the randomness in the matrix M. Therefore, to calculate the average density of states of the covariance matrix C_A it is enough to investigate the matrix element $\langle[(z - L)^{-1}]_{ii}\rangle$ for any $i \in A$. To this end, we define the generating functions

$$\begin{aligned} \gamma_A &= \langle e^{-\omega[(z-L)^{-1}]_{ii}}\rangle - 1 \text{ for } i \in A, \\ \gamma_B &= \langle e^{-\omega[(z-L)^{-1}]_{jj}}\rangle - 1 \text{ for } j \in B. \end{aligned} \tag{35}$$

The further procedure follows closely that of the previous section. Finally, we get a set of four coupled equations, very similar to the set we encountered in the single-shell approximation:

$$\begin{aligned} \gamma_A(\omega) &= \sqrt{\omega}\int_0^\infty \frac{d\lambda}{\sqrt{\lambda}} I_1(2\sqrt{\omega\lambda})\,\rho_B(\lambda), \\ \rho_B(\omega) &= e^{-\omega z + \mu_A \gamma_B(\omega)}, \\ \gamma_B(\omega) &= \sqrt{\omega}\int_0^\infty \frac{d\lambda}{\sqrt{\lambda}} I_1(2\sqrt{\omega\lambda})\,\rho_A(\lambda), \\ \rho_A(\omega) &= e^{-\omega z + \mu_B \gamma_A(\omega)}. \end{aligned} \tag{36}$$

We can easily check that the solution of these equations makes the following functional stationary:

$$\begin{aligned} &\mathcal{F}_{AB}[\gamma_A,\rho_A,\gamma_B,\rho_B] \\ &= -\int_0^\infty \frac{d\omega}{\omega}\,[\gamma_A(\omega)\rho_A(\omega) + \gamma_B(\omega)\rho_B(\omega)] \\ &\quad + \int_0^\infty \frac{d\omega}{\sqrt{\omega}}\int_0^\infty \frac{d\lambda}{\sqrt{\lambda}}\, I_1(2\sqrt{\omega\lambda})\rho_A(\omega)\rho_B(\lambda) \\ &\quad + \int_0^\infty \frac{d\omega}{\omega} e^{-\omega z}\left(\frac{1}{\mu_A}\, e^{\mu_A \gamma_B(\omega)} + \frac{1}{\mu_B}\, e^{\mu_B \gamma_A(\omega)}\right). \end{aligned} \tag{37}$$

For an approximate solution of Eqs. (36) we use again a variational ansatz. In analogy with EMA, we assume the following form:

$$\begin{aligned} \rho_A(\omega) &= e^{-\sigma_A \omega}, \\ \rho_B(\omega) &= e^{-\sigma_B \omega}. \end{aligned} \tag{38}$$

The insertion of (38) in (37) produces finally two uncoupled cubic equations for σ_A and σ_B. The equation relevant for us is

$$\begin{aligned} &z\,\sigma_B^3 + [(1-\alpha)\mu_A + \alpha - 1 - z^2]\,\sigma_B^2 \\ &\quad + (\mu_A\,\alpha + 1 - 2\alpha)\,z\,\sigma_B + z^2\,\alpha = 0, \end{aligned} \tag{39}$$

where we used $\alpha = \mu_B/\mu_A$. The average density of states for the covariance matrix C_A is found considering the first equation of (36) and the relation (34); thus

$$\mathcal{D}_{CA}(z) = \frac{1}{\pi\sqrt{z}} \lim_{\epsilon\to 0+} \mathrm{Im}\frac{1}{\sigma_B(\sqrt{z} - i\epsilon)}. \tag{40}$$

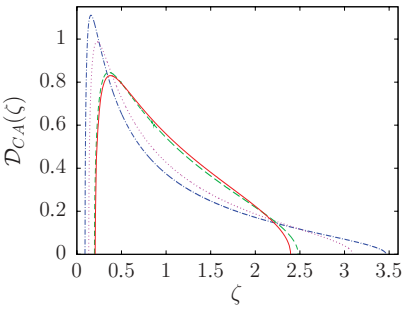

FIG. 3. (Color online) Density of states for the correlation matrix based on a sparse adjacency matrix, for $\alpha = 0.3$. The average degree is $\mu_A = 3$ (dash-dotted line), 5 (dotted line), and 50 (dashed line). The full line is the Marčenko-Pastur density (41), i.e., the limit $\mu_A \to \infty$.

The solution can be obtained analytically, but we shall not show the formula here. However, we can check that in the limit $\mu_A \to \infty$ with α and $\zeta = z/\mu_A$ fixed we get

$$\mathcal{D}_{CA}(\zeta) = \frac{1}{2\pi\alpha\,\zeta}\sqrt{[(1+\sqrt{\alpha})^2 - \zeta][\zeta - (1-\sqrt{\alpha})^2]}, \tag{41}$$

which is the Marčenko-Pastur (MP) density of states [54].

In Fig. 3 we show the density of states as function of $\zeta = z/\mu_A$ for several values of μ_A, as found by the solution of (39). We can see that the approach to MP density is rather slow. We found that the difference can be considered small only at about $\mu_A \simeq 50$.

V. CONCLUSIONS

We considered a random graph of large size $N \to \infty$ of two types: first, a "classical" Erdős-Rényi graph, and, second, a random bipartite graph. We calculated the density of eigenvalues for adjacency matrices of these graphs. In the case of the bipartite graph, the final result was the density of states of the covariance matrix, defined by a contraction of the adjacency matrix.

Our contribution to the problem of spectra of sparse random matrices consists of showing that the cavity approach, i.e., approximation of the random graph by a random tree, is exactly equivalent to the calculation by the replica method in the thermodynamic limit. Furthermore, we demonstrated how the cavity calculation can be formulated as a variational problem, similar to but substantially simpler than the variational formulation arising from the replica method. At minimum, we do not need to consider the possibility of replica-breaking solutions, which are known to exist and contribute to the finite-size corrections [47]. We can interpret it also in the following manner. Since we are working directly with an infinite-size system, $N = \infty$, the physics behind the replica-breaking states has no effect.

The variational formulation introduced here is a very practical starting point for approximations. The exponential ansatz leads to results identical to the effective-medium approximation studied earlier [20]. However, using our variational scheme, the approximation can be easily improved by what we call a "single-shell approximation." It produces the Lifschitz tail in the density of states in the form of a series of "bubbles." We are able to calculate the weight and distance of

the bubbles. Hence we arrive at average density of states in the tail, which is identical to the result of Rodgers and Bray [12]. Furthermore, we applied the method also to the spectra of sparse covariance matrices, where we easily derived a formula generalizing the Marčenko-Pastur density of states.

The variational formulation introduced here can be used not only as a generator of approximations, but also as a basis of numerical methods. Indeed, there is no principal obstacle for numerical extremalization of the functional of two variables. This contrasts with the variational methods based on the replica trick, where the replica limit $n \to 0$, involving analytic continuation, must be done after extremalization, which makes the method numerically unfeasible.

We believe that the method can also be applied for other types of random graphs. We must, however, admit a serious limitation of our method, which is the Poisson distribution of degrees of the graph. Therefore, it is, for example, not applicable directly for graphs with a power-law degree distribution. We believe that the roots of this limitation lie quite deep. For example, to the best of our knowledge, there is no replica calculation available for random graphs defined by their degree sequence only. On the other hand, there are no results from the cavity method for those random graphs with a power-law degree distribution, for which replica calculations do exist, like those of Ref. [23]. The point is, that for a Erdős-Rényi graph, it is well established that the local topology is isomorphic to a random tree. For a graph with a general degree sequence, not obeying Poisson statistics, this may or may not be true. The question of equivalence or not of the replica and cavity methods is intimately related to the question of local isomorphism to a tree, which is rather complex and not solved in general. Hence, a successful treatment of such cases by both the replica and cavity methods in parallel would require, very probably, completely novel ideas.

ACKNOWLEDGMENTS

I gladly acknowledge inspiring discussions with J. Mašek. This work was carried out within the project AV0Z10100520 of the Academy of Sciences of the Czech Republic and was supported by the MSMT of the Czech Republic, Grant No. OC09078.

[1] M. L. Mehta, *Random Matrices* (Academic Press, San Diego, 1991).
[2] E. P. Wigner, Ann. Math. **62**, 548 (1955).
[3] E. P. Wigner, Ann. Math. **65**, 203 (1957).
[4] F. J. Dyson, J. Math. Phys. **3**, 140 (1962).
[5] J. B. French and S. S. M. Wong, Phys. Lett. B **33**, 449 (1970).
[6] O. Boghias and J. Flores, Phys. Lett. B **34**, 261 (1971).
[7] O. Boghias and J. Flores, Phys. Lett. B **35**, 383 (1971).
[8] S. S. M. Wong and J. B. French, Nucl. Phys. A **198**, 188 (1972).
[9] O. Bohigas, J. Flores, J. B. French, M. J. Giannoni, P. A. Mello, and S. S. M. Wong, Phys. Rev. C **10**, 1551 (1974).
[10] H. A. Weidenmüller and G. E. Mitchell, Rev. Mod. Phys. **81**, 539 (2009).
[11] S. F. Edwards and R. C. Jones, J. Phys. A: Math. Gen. **9**, 1595 (1976).
[12] G. J. Rodgers and A. J. Bray, Phys. Rev. B **37**, 3557 (1988).
[13] Y. Kim and A. B. Harris, Phys. Rev. B **31**, 7393 (1985).
[14] A. J. Bray and G. J. Rodgers, Phys. Rev. B **38**, 11461 (1988).
[15] M. Mezard, G. Parisi, and A. Zee, Nucl. Phys. B **559**, 689 (1999).
[16] A. Cavagna, I. Giardina, and G. Parisi, Phys. Rev. Lett. **83**, 108 (1999).
[17] A. Cavagna, I. Giardina, and G. Parisi, J. Phys. Condens. Matter **12**, 6295 (2000).
[18] R. Monasson, Eur. Phys. J. B **12**, 555 (1999).
[19] G. Biroli and R. Monasson, J. Phys. A: Math. Gen. **32**, L255 (1999).
[20] G. Semerjian and L. F. Cugliandolo, J. Phys. A: Math. Gen. **35**, 4837 (2002).
[21] D. S. Dean, J. Phys. A: Math. Gen. **35**, L153 (2002).
[22] Jean-Yves Fortin, J. Phys. A: Math. Gen. **38**, L57 (2005).
[23] G. J. Rodgers, K. Austin, B. Kahng, and D. Kim, J. Phys. A: Math. Gen. **38**, 9431 (2005).
[24] G. M. Cicuta and H. Orland, Phys. Rev. E **74**, 051120 (2006).
[25] T. Nagao and T. Tanaka, J. Phys. A: Math. Theor. **40**, 4973 (2007).
[26] T. Nagao and G. J. Rodgers, J. Phys. A: Math. Theor. **41**, 265002 (2008).
[27] R. Kühn, J. Phys. A: Math. Theor. **41**, 295002 (2008).
[28] G. Bianconi, e-print arXiv:0804.1744.
[29] S. N. Evangelou, J. Stat. Phys. **69**, 361 (1992).
[30] S. N. Evangelou and E. N. Economou, Phys. Rev. Lett. **68**, 361 (1992).
[31] M. Bauer and O. Golinelli, J. Stat. Phys. **103**, 301 (2001).
[32] O. Golinelli, e-print arXiv:cond-mat/0301437.
[33] T. Rogers, I. P. Castillo, R. Kühn, and K. Takeda, Phys. Rev. E **78**, 031116 (2008).
[34] P. Cizeau and J. P. Bouchaud, Phys. Rev. E **50**, 1810 (1994).
[35] S. N. Dorogovtsev, A. V. Goltsev, J. F. F. Mendes, and A. N. Samukhin, Phys. Rev. E **68**, 046109 (2003).
[36] S. N. Dorogovtsev, A. V. Goltsev, J. F. F. Mendes, and A. N. Samukhin, Physica A **338**, 76 (2004).
[37] A. N. Samukhin, S. N. Dorogovtsev, and J. F. F. Mendes, Phys. Rev. E **77**, 036115 (2008).
[38] C. Bordenave and M. Lelarge, e-print arXiv:0801.0155.
[39] K. B. Efetov, Adv. Phys. **32**, 53 (1983).
[40] J. J. M. Verbaarschot, H. A. Weidenmuller, and M. R. Zirnbauer, Phys. Rep. **129**, 367 (1985).
[41] T. Guhr, A. Müller-Groeling, and H. A. Weidenmüller, Phys. Rep. **299**, 189 (1998).
[42] J. E. Bunder, K. B. Efetov, V. E. Kravtsov, O. M. Yevtushenko, and M. R. Zirnbauer, J. Stat. Phys. **129**, 809 (2007).
[43] J. J. M. Verbaarschot and M. R. Zirnbauer, J. Phys. A: Math. Gen. **18**, 1093 (1985).
[44] G. J. Rodgers and C. De Dominicis, J. Phys. A: Math. Gen. **23**, 1567 (1990).
[45] Y. V. Fyodorov and A. D. Mirlin, J. Phys. A: Math. Gen. **24**, 2219 (1991).
[46] A. D. Mirlin and Y. V. Fyodorov, J. Phys. A: Math. Gen. **24**, 2273 (1991).
[47] A. Kamenev and M. Mézard, J. Phys. A: Math. Gen. **32**, 4373 (1999).

[48] E. Kanzieper, Nucl. Phys. B **596**, 548 (2001).
[49] E. Kanzieper, e-print arXiv:0909.3198 (to appear in The Oxford Handbook of Random Matrix Theory).
[50] V. A. Osipov and E. Kanzieper, Phys. Rev. Lett. **99**, 050602 (2007).
[51] A. Khorunzhy and G. J. Rodgers, J. Math. Phys. **38**, 3300 (1997).
[52] P.-O. Löwdin, J. Appl. Phys. **33**, 251 (1962).
[53] Z. Füredi and J. Komlós, Combinatorica **1**, 233 (1981).
[54] V. A. Marčenko and L. A. Pastur, Math. USSR–Sbornik **1**, 457 (1967).

[Slanina12]

Eur. Phys. J. B (2012) 85: 361
DOI: 10.1140/epjb/e2012-30338-1

THE EUROPEAN PHYSICAL JOURNAL B

Regular Article

Localization of eigenvectors in random graphs

F. Slanina[a]

Institute of Physics, Academy of Sciences of the Czech Republic, Na Slovance 2, 18221 Praha, Czech Republic

Received 23 April 2012 / Received in final form 24 July 2012
Published online 29 October 2012 –

Abstract. Using exact numerical diagonalization, we investigate localization in two classes of random matrices corresponding to random graphs. The first class comprises the adjacency matrices of Erdős-Rényi (ER) random graphs. The second one corresponds to random cubic graphs, with Gaussian random variables on the diagonal. We establish the position of the mobility edge, applying the finite-size analysis of the inverse participation ratio. The fraction of localized states is rather small on the ER graphs and decreases when the average degree increases. On the contrary, on cubic graphs the fraction of localized states is large and tends to 1 when the strength of the disorder increases, implying that for sufficiently strong disorder all states are localized. The distribution of the inverse participation ratio in localized phase has finite width when the system size tends to infinity and exhibits complicated multi-peak structure. We also confirm that the statistics of level spacings is Poissonian in the localized regime, while for extended states it corresponds to the Gaussian orthogonal ensemble.

1 Introduction

After more than 50 years, Anderson localization [1] remains one of the most puzzling problems of theoretical physics [2]. Although many results have been accumulated [3–5], open questions remain even in the very basic issue of the definition of the proper criterion of localization (as a single example, see e.g. [6]). From our viewpoint, however subjective it might be, we can classify the approaches to the phenomenon of localization into three big groups. In this introductory sketch we shall emphasize the results concerning Bethe lattices, as they are directly related to our work.

First, "physical" theories aim at grasping the essence without necessarily reaching the mathematical rigor. A typical examples are the scaling theory [7], the self-consistent theory [8–10], the approach based on parquet diagrams [11] and the approaches based on replica [12] and supersymmetry [13] methods. For our work, the relevant sources are the results concerning localization on Bethe lattice [14–20], where the exact self-consistent equation was formulated and the localization threshold was computed. The phase diagram exhibits extended states in the regime of weak disorder and energies sufficiently close to the band center. Otherwise the states are localized. There is a well defined mobility edge, separating extended states on one side from the localized states on the other side. Although in principle we cannot exclude mixed regimes [21], in which localized and extended states would coexist arbitrarily close to each other within a finite interval, such a mixed regime was not yet observed.

Second, "mathematical" theories prove rigorously the localization properties, but are limited to a few models where the known methods of proof work. Still, there is a good deal of results available now, see e.g. [22]. The result relevant for us is the proof of localization in the Bethe lattice [21,23]. However, the rigorous approaches work directly with infinite systems, thus avoiding the difficulties in taking the thermodynamic limit. On the other hand, it is the behavior of the system with increasing size that is physically most interesting. Hence, the physical interpretation of the rigorous results remains the matter of debate.

Third, one may resort to purely numerical computations, see e.g. [24] for electron localization or [25] for localization of acoustic waves. More sophisticated approaches rely on the cavity approximation (which becomes exact on trees) and numerical solution of thus obtained equation [26–32].

The results on the localization in Bethe lattices bring the problem close to the field of spectral theory [33] of random graphs [34], as many models of random graphs are locally tree-like. Therefore, all local properties of such random graphs should tend to Bethe lattice in thermodynamic limit. Mathematically, spectra of random graphs are the same thing as spectra of random sparse matrices. The latter were studied in depth using various methods [29,35–43]. Localization of eigenvectors was found both by exact numerical diagonalization [26,31,40,44–46] and using the cavity method [27–30]. Here the study of random matrices touches again the problem of localization on a Bethe lattice, as we mentioned above.

Besides the academic interest in the localization phenomenon, numerous examples of practical application of

[a] e-mail: slanina@fzu.cz

the ideas of localization can be denonstrated, mainly in the area of complex networks [47–50] or in the field of the analysis of biological [51] and social networks [52,53].

We quoted several times the results showing the presence of localization threshold for disordered Hamiltonians on Bethe lattices. The fact is now confirmed by rigorous mathematic methods, as well as physical arguments and numerical work on finite samples. However, several problems remain. First, it is not quite clear how the rigorous mathematic results should be translated to the reality of physical experiments. Second, the Bethe lattice is pathological from many points of view. Indeed, strictly speaking, in numerical studies we work with a Cayley tree, rather than Bethe lattice. The difference resides in the boundary conditions. In the Cayley tree the volume of "surface" sites is comparable to "bulk" sites, while the negligibility of the former is the basis for the existence of basic physical quantities, like the free-energy density. In the present work we shall try to avoid the problem of surface by working with random graphs. Our approach is based on the belief that in thermodynamic limit the Bethe lattice and random graph results coincide. For a mathematical justification, see [54].

In our previous work [55] we showed that the cavity approach, which may be considered as an approximation, coincides with the replica approach, which is assumed to be exact, in thermodynamic limit. The variational formalism introduced in [55] enables us to consistently formulate approximations.

The present work is a continuation of that of reference [55]. First, we show how the formalism of [55] can be extended to study localization. The equations found are in principle exact, but as soon as we resort to approximations developed and used in reference [55], we find that these approximations are insufficient to capture localization. Therefore, in the rest of the study we resort to exact numerical diagonalization followed by finite-size scaling analysis.

2 Cavity equations for localization

Among the diverse criteria of localization, the most suitable for our purposes is the behavior of the inverse participation ratio (IPR). Let L be a $N \times N$ real symmetric matrix with eigenvalues λ_i, $i = 1, \ldots, N$ and corresponding normalized eigenvectors $e_{j\lambda_i}$. We shall assume implicitly, that the matrix elements of L are random variables with properties described later. The resolvent will be denoted $R(\zeta) = (\zeta - L)^{-1}$ and its diagonal element $g_i(\zeta) = R_{ii}(\zeta)$ for $\zeta \in \mathbb{C}\backslash\{\lambda_i; i = 1, \ldots, N\}$. The IPR at $\lambda = \lambda_i$ for some i is

$$q^{-1}(\lambda) = \sum_j e_{j\lambda}^4 = \lim_{\varepsilon \to 0^+} \frac{\varepsilon \sum_i g_i(\lambda + \mathrm{i}\varepsilon)\, g_i(\lambda - \mathrm{i}\varepsilon)}{\mathrm{Im} \sum_i g_i(\lambda + \mathrm{i}\varepsilon)} \,. \quad (1)$$

For the proof of the latter equality, see [30,56]. The definition (1) applies for fixed system size N. On the other hand, the question we ask in the analysis of localization is, whether the states within a certain interval, $\lambda \in I$, remain localized when $N \to \infty$ for all typical realizations of the disorder. Therefore, we should define more properly the average IPR in the interval I as

$$\langle q_I^{-1} \rangle = \left\langle \frac{1}{N_I} \sum_{i:\lambda_i \in I} \sum_j e_{j\lambda_i}^4 \right\rangle , \quad (2)$$

where $\langle \ldots \rangle$ means averaging over the realizations of L and $N_I = \sum_{i:\lambda_i \in I} 1$ is the number of eigenvalues within the interval I. Then, if we find that $\langle q_I^{-1} \rangle \to 0$ as $N \to \infty$, the states in I will be considered extended, while non-zero limit would imply localization of at least some of the states in the interval I. We shall assume that the extended states, if they exist, are found around the center of the spectrum, while localized states, if any, should be expected at the upper and lower tails. More complicated cases will not be treated here. The mobility edges are then defined as numbers $z_{\mathrm{mob}}^- < z_{\mathrm{mob}}^+$ such that

$$\lim_{N\to\infty} \langle q_I^{-1} \rangle \begin{cases} = 0 & \text{for any } I \subset [z_{\mathrm{mob}}^-, z_{\mathrm{mob}}^+], \\ > 0 & \text{for any } I \subset (-\infty, z_{\mathrm{mob}}^-) \\ & \quad \text{or } I \subset (z_{\mathrm{mob}}^+, \infty) \,. \end{cases} \quad (3)$$

Let us now sketch the formalism using the cavity method. It consists in neglecting loops, so that it becomes exact on Bethe lattice, or on any tree in general. We denote $g(\zeta)$ the diagonal element of the resolvent at the root of the tree. Following [55] we introduce the generating functions

$$\begin{aligned} \gamma(\omega) &= \left\langle e^{-\omega\, g(\zeta)} - 1 \right\rangle , \\ \Gamma(\omega, \omega') &= \left\langle \left(e^{-\omega\, g(\zeta)} - 1 \right) \left(e^{-\omega'\, g(\zeta')} - 1 \right) \right\rangle . \end{aligned} \quad (4)$$

The dependence on ζ and ζ' is assumed implicitly. We can extract the linear and bilinear terms from the generating functions as $\gamma(\omega) = \omega \left(s_1(\zeta) + O(\omega) \right)$ and $\Gamma(\omega, \omega') = \omega\omega' \left(s_2(\zeta, \zeta') + O(\omega, \omega') \right)$. Hence we deduce the expression for the average IPR in the limit $N \to \infty$

$$q^{-1}(z)|_{N\to\infty} = \lim_{\varepsilon \to 0^+} \frac{\varepsilon\, s_2(z + \mathrm{i}\varepsilon, z - \mathrm{i}\varepsilon)}{\mathrm{Im}\, s_1(z + \mathrm{i}\varepsilon)} . \quad (5)$$

Strictly speaking, the expression (5) is incorrect for two reasons. First, the order of the limits $\varepsilon \to 0^+$ and $N \to \infty$ is reversed, because the cavity approach works effectively with infinite N from the very beginning. Second, in (5) the average over disorder is performed separately in the numerator and in the denominator, while if done properly, the averaging must involve the fraction as a whole. Without entering into deep discussions, we assume that neither of the two "mistakes" induce a fundamental fault into the results. To support this assumption we can note, first, that also references [30,57] rely on the harmless exchange of the order of limits. Second, as for the independent averaging of the numerator and denominator, it is justified if we suppose that $g_i(\lambda + \mathrm{i}\varepsilon)$ is a self-averaging quantity, because in that case the disorder-average of the denominator is safely replaced by the sum $1/N \sum_i \bullet$.

Eur. Phys. J. B (2012) 85: 361

If the degrees of the random graph are Poisson distributed, as is the case for the Erdős-Rényi random graph, with average μ, we obtain, for the one-particle generating function $\gamma(\omega)$ a self-consistent equation in the form

$$\gamma(\omega) = \sqrt{\omega}\int_0^\infty \frac{d\lambda}{\sqrt{\lambda}} I_1(2\sqrt{\omega\lambda})\,\rho(\lambda),$$
$$\rho(\omega) = e^{-\omega z+\mu\,\gamma(\omega)}\,. \qquad (6)$$

At this level, introduction of the auxiliary function $\rho(\omega)$ seems arbitrary, but it acquires clear sense in the variational approach developed in [55].

For calculating IPR, the two-particle quantities are needed. Without repeating the steps which lead to equation (6), we can write the equation for $\Gamma(\omega,\omega')$ as

$$\Gamma(\omega,\omega') = \sqrt{\omega\omega'}\int_0^\infty \frac{d\lambda}{\sqrt{\lambda}}\int_0^\infty \frac{d\lambda'}{\sqrt{\lambda'}} I_1(2\sqrt{\omega\lambda}) \times I_1(2\sqrt{\omega'\lambda'})\,\rho(\lambda)\,\rho(\lambda')e^{\mu\,\Gamma(\lambda,\lambda')}. \qquad (7)$$

Solving equations (6) and (7) should in principle give full description of the localization phenomenon. Note that the formalism used in [14,28] should be a special case of ours. Indeed, references [14,28] work with the joint probability density for real and imaginary part of $g(z+\mathrm{i}\varepsilon)$, which is equivalent to the joint generating function for $g(z+\mathrm{i}\varepsilon)$ and $g(z-\mathrm{i}\varepsilon)$.

Full solution of equations (6) and (7) is not yet known. Approximative schemes for solving equation (6) were shown in [55], partially repeating the older results of [40,42]. The simpler one of the approximations used in [55] is the effective-medium approximation (EMA), which can be formulated as an ansatz $\rho(\omega) = e^{\omega\,\sigma(\zeta)}$. For $\sigma(\zeta)$ we find the cubic equation

$$\sigma^3 - \zeta\,\sigma^2 + (\mu-1)\,\sigma + \zeta = 0\,. \qquad (8)$$

The density of states is non-zero only within the interval $[z_-, z_+]$ where $\mathrm{Im}\,\sigma(z+\mathrm{i}\varepsilon)$ is non-zero in the limit $\varepsilon\to 0^+$. Therefore, EMA exhibits sharp band edges, which is wrong, because the true spectrum contains Lifschitz tails extending arbitrarily far. Nevertheless, it is instructive to try to use EMA as a starting point for approximative solution of equation (7). We insert in equation (7) the functions $\rho(\lambda)$, $\rho(\lambda')$, containing $\sigma(\zeta)$ obtained by solving equation (8). Still, the resulting integral equation for Γ is not readily soluble, so we apply further approximation, leaving only the lowest (bilinear) term in the expansion of $\Gamma(\omega,\omega')$ and expanding $e^{\mu\Gamma}$ on the right-hand side into series. This way we obtain an equation for s_2 and the solution is then supplied into equation (5). The IPR is then expressed through the function $\sigma(z)$ for $z\in\mathbb{R}$. Finally we get

$$q^{-1}(z) = \frac{\big(3\sigma^2(z) - 2z\sigma(z) + \mu - 1\big)\sigma^4(z)}{\big(\sigma^2(z)-1\big)\big(\sigma^4(z)-\mu\big)} \qquad (9)$$

for $z\in\mathbb{R}\backslash[z_-,z_+]$ and $q^{-1}(z)=0$ for $z\in[z_-,z_+]$. The result is shown in Figure 1 for $\mu=3$. We shall see later

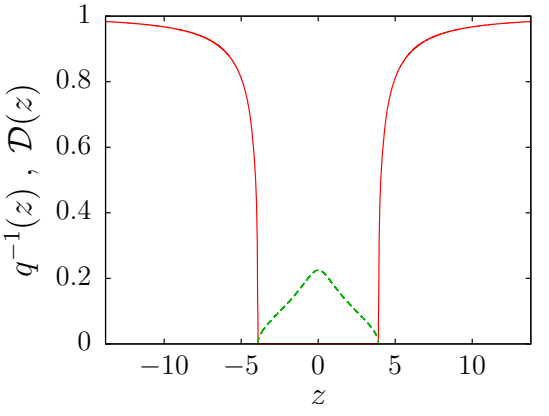

Fig. 1. (Color online) Inverse participation ratio (solid line) and density of states (dashed line) calculated using the effective medium approximation, for Erdős-Rényi graph with average degree $\mu = 3$.

that this expression reflects qualitatively well the behavior of IPR at the tails of the spectrum. However, the result (9) is rather illusory, because localization indicated by non-zero IPR occurs only in the areas where density of states is strictly zero. The mobility edge coincides with the band edge. Therefore, the fraction of localized states is zero within such an approximation. We can try to improve the result applying the single-shell approximation (SSA) introduced in [55]. Within this approximation, we obtain for σ the equation

$$z^2 = \mu + z\sigma + e^{-\mu}\sum_{l=1}^{\infty}\frac{\mu^l}{(l-1)!}\,\frac{l}{z\sigma - l}. \qquad (10)$$

As for the density of states in the Lifschitz tail, SSA does give some improvement, although severe artifacts of the approximation remain, namely the spurious band gaps inside the Lifschitz tail (see Fig. 5 and [55] for details). In the same way as in EMA, we can take the function $\sigma(\zeta)$ obtained in SSA, insert it into equation (7) and expand $\Gamma(\omega,\omega')$ into series. Thus, we obtain

$$q^{-1}(z) = \left(\frac{2}{1-e^{-\mu}\sum_{l=1}^{\infty}\frac{\mu^l}{(l-1)!}\,\frac{l}{(z\sigma-l)^2}} - \frac{\sigma}{z}\right)^{-1} \times \frac{\sigma^4(z)}{\sigma^4(z)-\mu}. \qquad (11)$$

The result is shown in Figure 2. Contrary to EMA, the dependence of the inverse participation ratio on eigenvalue is not monotonous, and the "interruptions", where $q^{-1}(z)=0$ occur exactly at the intervals where the density of states is non-zero. Therefore, SSA suffers from the same flaw as EMA, that is the IPR is non-zero only if density of states is zero. The conclusion of this section is that analytical solution of equation (7) would require more sophisticated methods than those at our disposal.

In the rest of this work, we will rely on exact numerical diagonalization results. However, the position of the band edge, as found in EMA, will serve as a benchmark for the

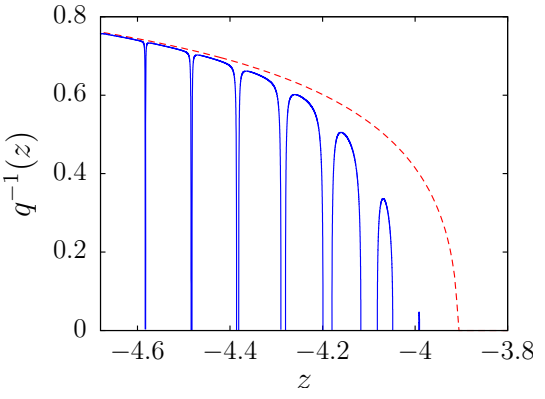

Fig. 2. (Color online) Inverse participation ratio, for Erdős-Rényi graph with average degree $\mu = 3$ calculated using the effective medium approximation (dashed line) and single-shell approximation (solid line).

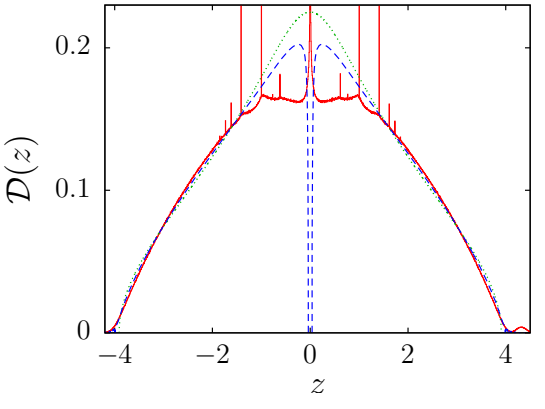

Fig. 3. (Color online) The density of states for the adjacency matrix of the ER graph with $\mu = 3$, $N = 1000$, averaged over 115 000 realizations (full line). For comparison, approximate results using EMA (dotted) and single-shell approximation of [55] (dashed) are shown.

position of the mobility edge and will be compared with numerical results.

3 Localization in Erdős-Rényi graphs

The first model we shall investigate is the adjacency matrix L of the Erdős-Rényi random graph. Apart from the fact that L is symmetric matrix with zero on the diagonal, the matrix elements are independent and equally distributed. The probability density for a single off-diagonal element is

$$\pi_1(x) = \left(1 - \frac{\mu}{N}\right)\delta(x) + \frac{\mu}{N}\delta(x-1). \qquad (12)$$

We investigated in depth the spectrum of L in [55]. In Figure 3 we reproduce one of the results. The density of states has a very complicated structure, with many singularities and δ-function components. For example, an acute, perhaps logarithmic, singularity resides at the center of the spectrum, at $z = 0$, as shown in Figure 4. The theory

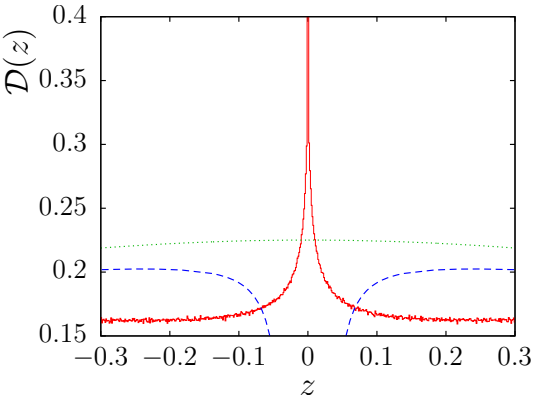

Fig. 4. (Color online) Detail of the data of Figure 3, showing the singularity at $z = 0$.

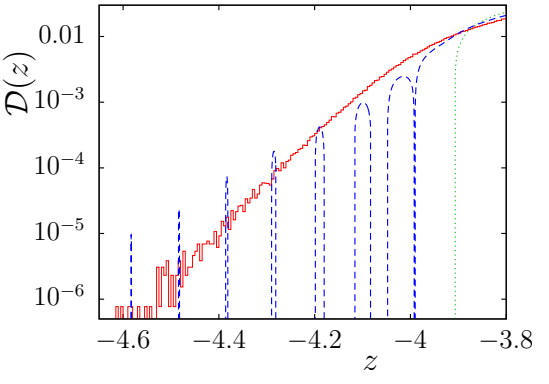

Fig. 5. (Color online) Lower tail of the data of Figure 3. Note that the single-shell approximation is superior to EMA in the Lifschitz-tail region, but still it is far from satisfactory.

exposed in reference [41] could in principle bring an explanation of that singularity, bud we did not perform the calculations in this direction.

It is interesting to compare such suppression of localization in ER graphs with the localization which occurs in weakly diluted systems, where the localization is enhanced instead, by the mechanism of maximum entropy walk [58]. Indeed, on irregular graphs, for example the common ER graph or a regular graph with a few edges removed, the standard random walk does not possess maximum entropy. The requirement of entropy maximization introduces a non-local constraint, which, rather unexpectedly, favors localization.

At the tails of the spectrum, there is no sharp band edge, but a Lifschitz tail develops. The asymptotic form of the Lifschitz tail is now well established [35,42,55] and our numerical results can be seen in Figure 5.

It is just the Lifschitz tail where the localization is expected. To have a first glance on that, we plot the IPR averaged over several tens of thousand realizations. In Figures 6 and 7 we show the results for $N = 1000$ and for $\mu = 3$ and $\mu = 5$, respectively. Comparing the behavior of IPR with the density of states, as shown in Figure 3, we observe the same complicated structure of singularities. Generally, IPR is large at the tails, as well as close to the singularities in the density of states. One would

Eur. Phys. J. B (2012) 85: 361

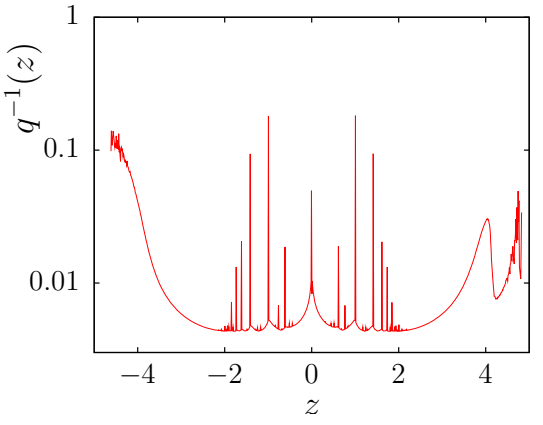

Fig. 6. (Color online) Inverse participation ratio averaged over 115 000 realizations, for ER graph with $\mu = 3$ and $N = 1000$.

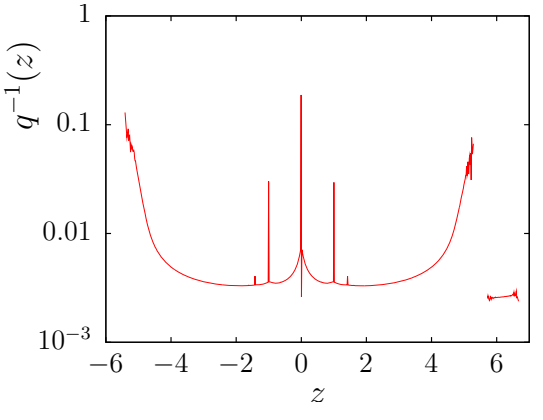

Fig. 7. (Color online) Inverse participation ratio averaged over 65 000 realizations, for ER graph with $\mu = 5$ and $N = 1000$.

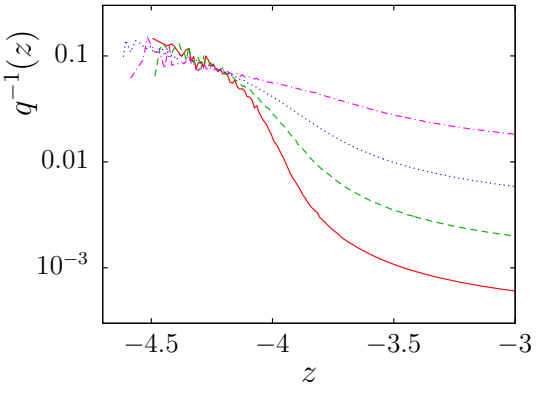

Fig. 8. (Color online) Inverse participation ratio at the lower tail of the spectrum for ER graph with $\mu = 3$. The system size is $N = 10^4$ (solid line), 3000 (dashed line), 1000 (dotted line), and 300 (dash-dotted line). The data are averaged over 900, 10 000, 65 000 and 130 000 realizations, respectively.

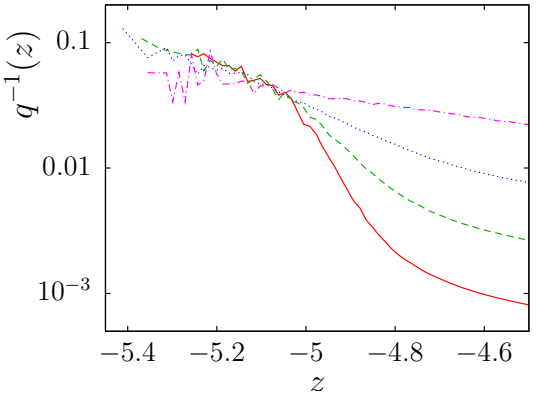

Fig. 9. (Color online) Inverse participation ratio at the lower tail of the spectrum for ER graph with $\mu = 5$. The system size is $N = 10^4$ (solid line), 3000 (dashed line), 1000 (dotted line), and 300 (dash-dotted line). The data are averaged over 800, 5000, 65 000 and 50 000 realizations, respectively.

naively expect that localization would occur in all regions where IPR is large, but it is true only in the tails. As we stressed earlier, we must check the behavior of IPR when N grows. Close to the singularities, we found IPR large, but consistently decreasing with increasing system size. On the contrary, localization in Lifschitz tails is clearly visible, as indicated in Figures 8 and 9. In the following, we decided to work with the lower tail, because the upper tail is somewhat obscured by the single maximum eigenvalue which behaves differently than all the rest of the spectrum. We can see that below certain value of z, the IPR is independent of N, within the range of statistical errors, while above this value, IPR decreases with N. We identify this value with the mobility edge. We shall describe the method of extracting the mobility edge from the data in the next section. Here we make only a few observations.

First, this definition of mobility edge is practical but it is not the only possible. Moreover, there might be even some doubts of it. Indeed, above the mobility edge the IPR should not only decrease with N, but decrease in a specific manner, namely as $1/N$, otherwise the states cannot be considered properly extended. Therefore, the alternative definition of the mobility edge would be as follows. We declare the states in the interval I extended, if $\langle q_I^{-1} \rangle \sim N^{-1}$ for $N \to \infty$, otherwise the states are considered localized. The data from Figures 8 and 9 indicate that the mobility edge defined in the latter way would lie somewhat higher than in the former. The difference may well be just a finite-size effect, but we cannot exclude also the possibility that it reflects a real phenomenon, namely presence of states which are neither properly extended, nor exponentially localized. For example, the eigenvectors can be characterized by tails decreasing slower than any exponential, but on the level of knowledge provided by our numerical data this is a mere speculation. However, note that eigenvectors with power-law tails do occur in certain models [59,60] and an interval of coexistence of extended and localized states was also hypothesized in [21]. In all the rest we shall stick to the former definition of the mobility edge for purely practical reasons.

Second, comparing the IPR calculated using EMA and SSA, shown in Figure 2 with numerical findings in Figures 8 and 9, we observe a qualitative agreement. On the other hand, quantitatively, EMA and SSA give much too high values of IPR. So, however defective EMA and

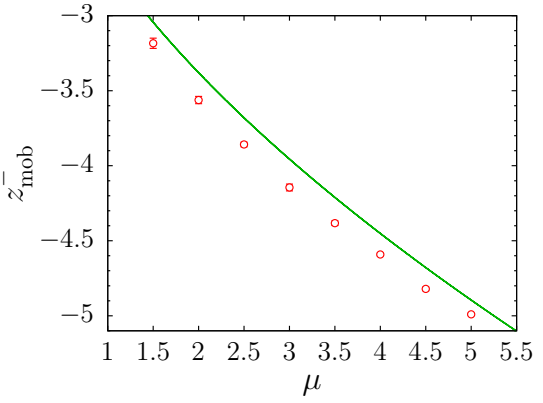

Fig. 10. (Color online) Position of the mobility edge at the lower tail of the spectrum, for ER graph. Where not shown, error bars are smaller than the symbol size. The solid line is the band edge calculated in EMA.

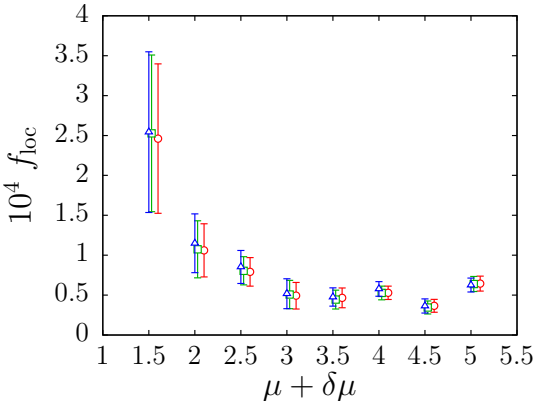

Fig. 11. (Color online) Fraction of states below the lower mobility edge, for ER graph. We compare the results for $N = 10\,000$ (triangles), 3000 (squares), and 1000 (circles). For better visibility, the points are slightly shifted rightwards by $\delta\mu = 0$, 0.03, and 0.1 for $N = 10\,000$, 3000, and 1000, respectively.

SSA are with respect to localization, they do provide a hint of how IPR should behave.

Third, the data suggest that IPR for infinite system approaches a non-zero limit when we approach the mobility edge from the localized side. Because in extended regime IPR is strictly zero for infinite system, IPR should exhibit a discontinuity at the mobility edge. This confirms results obtained earlier in [61] using a supersymmetric method.

Let us continue with the analysis of our results. Having established the mobility edge, we want to know how it depends on the average degree of the ER graph. This dependence is shown in Figure 10. For comparison, we show also the position of the band edge, as found in EMA. We can see that the mobility edge is slightly below the EMA band edge, but the two quantities share a common trend. Therefore, the EMA band edge can serve as a useful zeroth approximation for the line of separation between localized and extended states. This criterion was used, without further justification, in the context of diffusion models for biological evolution [62].

In order to see quantitatively, how much globally relevant the localization phenomenon is, we measure the fraction of eigenvalues below the mobility edge

$$f_{\rm loc} = \left\langle \frac{1}{N} \sum_{i:\lambda_i < z^-_{\rm mob}} 1 \right\rangle . \tag{13}$$

Supposing that the spectrum is mirror-symmetric, as it should be in the limit $N \to \infty$, the total fraction of localized states is $2f_{\rm loc}$. We can see the results in Figure 11. The first thing to note is that the results are practically independent of system size, so we can safely claim that they represent the fraction of localized eigenvalues for infinite system. The fraction decays with average degree μ, until it saturates around $\mu \simeq 3$ at a value close to $f_{\rm loc} \simeq 0.5 \times 10^{-4}$. It is suposed that this fraction should drop to zero in the limit $N \to \infty$, because it is known that all states are extended in an ER graph, on condition that $\mu \to \infty$ simultaneously with $N \to \infty$ (Ref. [63]). The numerical procedure does not enable us to work with large enough N to see that explicitly. Therefore, we consider the saturation a finite-size effect.

4 Localization in random cubic graphs

4.1 Diagonal disorder

The second family of graphs investigated here are the random cubic graphs, i.e. random graphs satisfying the only constraint that the degree of all vertices is equal to 3. We decided to study this family as a kind of direct opposite of the ER graph. In ER graph, the properties are mostly due to inhomogeneity in the degrees. In cubic graph all degrees are equal. In ER graph, there is no diagonal disorder. In cubic graph, the relevant disorder is only on the diagonal. Of course, one can study also models which interpolate the two extremes, but we shall not do that in the present work. We shall rather compare the differences between the extremes.

The off-diagonal elements of the matrix L to study are identical to the adjacency matrix of the graph, while diagonal elements of L are independent Gaussian random variables, with probability density

$$\pi_{\rm diag}(L_{ii}) = \frac{1}{\sqrt{2\pi}\,\eta} \exp\left(-\frac{L_{ii}^2}{2\eta^2}\right). \tag{14}$$

In thermodynamic limit the local topology of the graph is identical to the Bethe lattice with coordination number 3 and the randomness of the structure, i.e. the off-diagonal disorder, must be irrelevant, as long as we investigate local properties of the graph and its size goes to infinity. For example, the density of states for the random graph with $\eta = 0$ must approach a non-random function identical to the well-known density of states of the Bethe lattice

$$\mathcal{D}_{\rm Bethe}(z) = \frac{3}{2\pi} \frac{\sqrt{8 - z^2}}{9 - z^2}. \tag{15}$$

Eur. Phys. J. B (2012) 85: 361

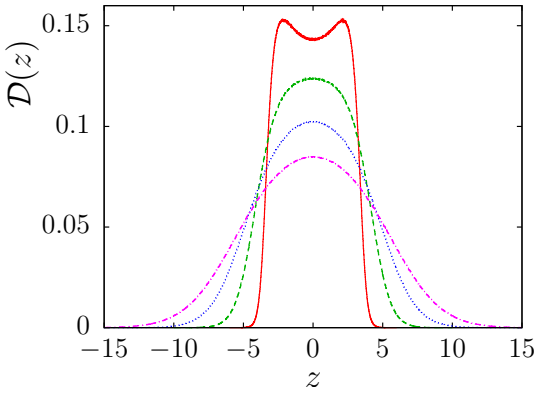

Fig. 12. (Color online) Density of states for random cubic graph with diagonal disorder, for $N = 1000$. The disorder strength is $\eta = 1$ (solid line), 2 (dashed line), 3 (dotted line), and 4 (dash-dotted line). The data are averaged over 40 000 realizations.

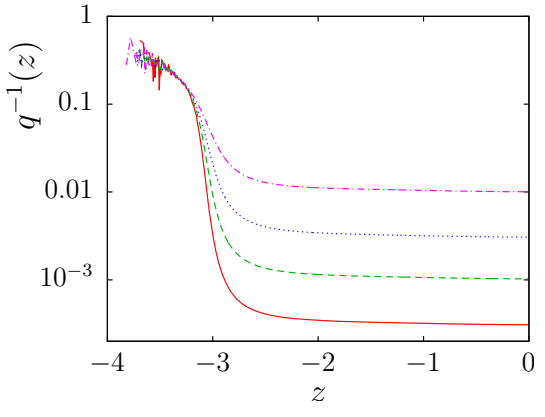

Fig. 13. (Color online) Inverse participation ratio at the lower tail of the spectrum for random cubic graph with disorder strength $\eta = 0.5$. The system size is $N = 10^4$ (solid line), 3000 (dashed line), 1000 (dotted line), and 300 (dash-dotted line). The data are averaged over 550, 11 000, 65 000, and 160 000 realizations, respectively.

The non-trivial ingredient is the randomness in diagonal elements of the matrix L and this is the feature which leads to localization here. The situation is somewhat complementary to the ER case investigated in the last section. In ER graphs, localization is due to off-diagonal disorder, while here the diagonal disorder is responsible.

4.2 Mobility edge

We show in Figure 12 the density of states for several disorder strengths. The density of states is smooth and free of singularities, which are typical of the spectrum of ER graphs. The localized states occur in the Lifschitz tails, as we can clearly see in Figures 13–15. Qualitatively, we observe that localization is much stronger than in ER graphs and the IPR reaches values very close to 1. On the other hand, establishing the mobility edge is more difficult, because the deviations of the curves for different N are much smaller and obscured by statistical noise.

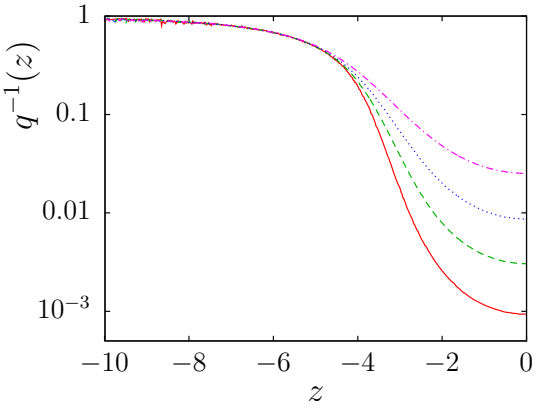

Fig. 14. (Color online) Inverse participation ratio at the lower tail of the spectrum for random cubic graph with disorder strength $\eta = 2$. The system size is $N = 10^4$ (solid line), 3000 (dashed line), 1000 (dotted line), and 300 (dash-dotted line). The data are averaged over 610, 10 000, 65 000, and 160 000 realizations, respectively.

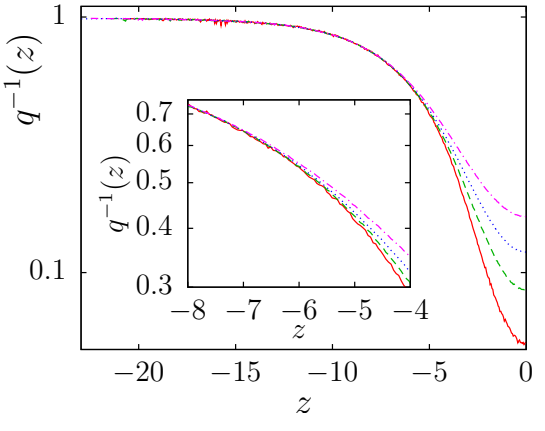

Fig. 15. (Color online) Inverse participation ratio at the lower tail of the spectrum for random cubic graph with disorder strength $\eta = 4$. The system size is $N = 10^4$ (solid line), 3000 (dashed line), 1000 (dotted line), and 300 (dash-dotted line). The data are averaged over 550, 10 000, 65 000, and 160 000 realizations, respectively. In the inset, detail of the data illustrating the difficulty to establish the mobility edge precisely.

We illustrate it in the inset of Figure 15. In such a situation it is necessary to develop a method for extracting the mobility edge as reliably as possible. The method is illustrated in Figure 16. The procedure we used consists in comparing the difference of average IPR for two system sizes, $\Delta q^{-1} = q^{-1}(N) - q^{-1}(N')$ with the level of statistical noise δq^{-1}. The estimate for the mobility edge $z^{-}_{\mathrm{mob}}(N, N')$ is found where the difference Δq^{-1} as a function of z crosses the noise level δq^{-1}. The error produced in this method is estimated in a similar manner, as difference of points where $\Delta q^{-1}(N, N')$ crosses δq^{-1} and where it crosses twice as large noise $2\delta q^{-1}$. The error bars shown if Figures 10 and 17 are obtained in this way. We found that the estimate $z^{-}_{\mathrm{mob}}(N, N')$ depends quite strongly on the sizes N, N'. Therefore, we further extrapolate the values found to infinite system, as shown in the inset of Figure 16.

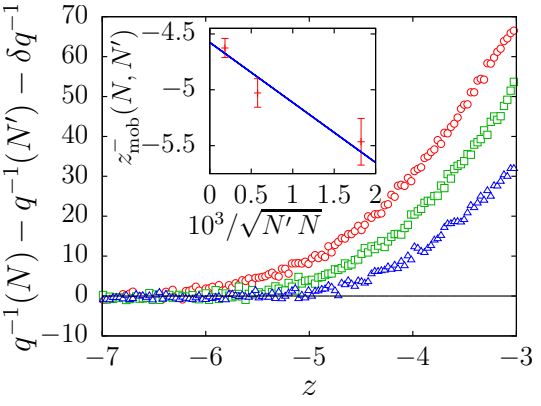

Fig. 16. (Color online) An example of the procedure for establishing the mobility edge. The symbols correspond to the pairs of sizes $N = 300$, $N' = 1000$ (circles); $N = 1000$, $N' = 3000$ (squares); $N = 3000$, $N' = 10\,000$ (triangles). The estimated mobility edge for this pair is located where the data fall below zero. In the inset, extrapolation of the estimated mobility edge to infinite system size.

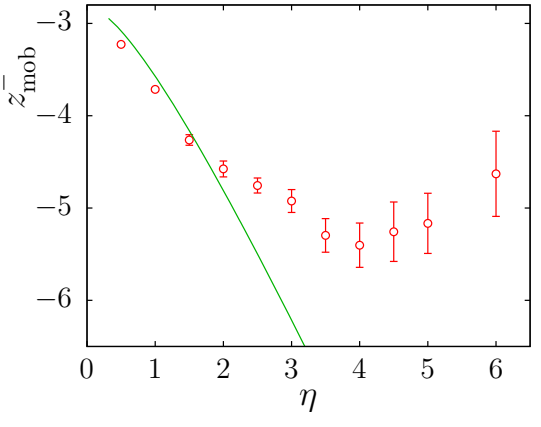

Fig. 17. (Color online) Position of the mobility edge at the lower tail of the spectrum, for random cubic graph. The solid line is the band edge calculated in EMA.

The dependence of the mobility edge on disorder strength is shown in Figure 17. As in the case of ER graphs, we compare the dependence of the mobility edge on disorder strength with the position of the band edge calculated using the effective medium approximation. While in ER graph the EMA band edge and the mobility edge go in parallel, in random cubic graph they behave differently. While the EMA band edge grows in absolute value, thus reflecting the overall broadening of the density of states for increasing disorder, the mobility edge remains deep within the range of the EMA band. For disorder stronger than about $\eta \simeq 4$ the interval of extended states starts narrowing. This agrees qualitatively with earlier results on Anderson localization on Bethe lattice [15,23] which state that for strong enough disorder, $\eta > \eta_c$, all states are localized. Note that the same qualitative behavior was also found by diagrammatic methods for lattices in large Euclidean dimensions [11].

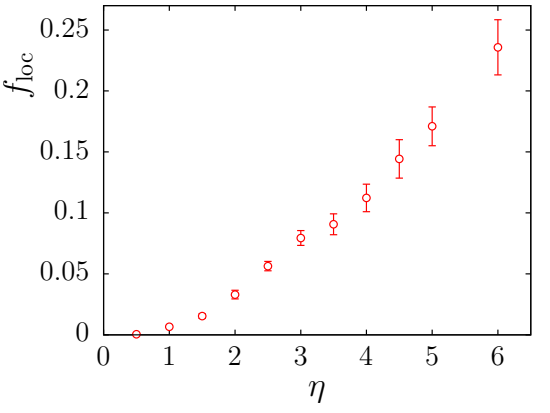

Fig. 18. (Color online) Dependence of the fraction of states below the lower mobility edge on the strength of the disorder, for random cubic graph. The size is $N = 10^4$.

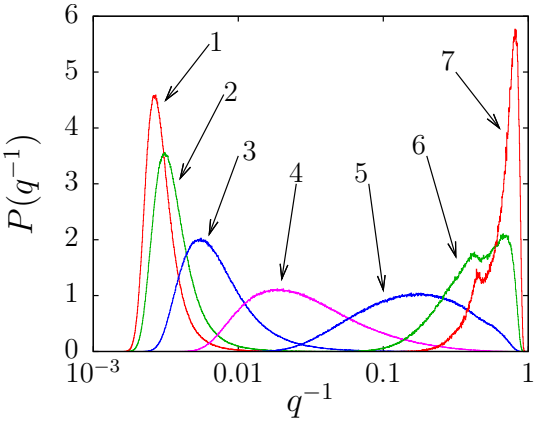

Fig. 19. (Color online) Histogram of IPR, for states with eigenvalues within a fixed interval, for $\eta = 2$ and $N = 3000$. The arrows point to curves corresponding to intervals $z \in [-0.5, 0.5]$ (line 1), $[-1.5, -0.5]$ (line 2), $[-2.5, -1.5]$ (line 3), $[-3.5, -2.5]$ (line 4), $[-4.5, -3.5]$ (line 5), $[-5.5, -4.5]$ (line 6), and $[-6.5, -5.5]$ (line 7). The data are accumulated from 17 000 independent realizations.

The fraction of states below the lower mobility edge is shown in Figure 18. Again, the behavior is completely different from the situation in ER graph. The fraction of localized states is large and grows with the strength of the disorder. We are unable to reach higher disorder strengths η, because establishing the precise value of the mobility edge is increasingly difficult. However, our data are consistent with the claim that beyond a critical strength of disorder the fraction reaches its maximum, i.e. $f_{\rm loc} = 1/2$ for $\eta > \eta_c$.

4.3 IPR distribution

In addition to the dependence of the average IPR on z, we are interested also in the fluctuations of IPR, if we restrict the eigenvalue to a fixed interval $z \in [z_1, z_2]$. Indeed, we found that the fluctuations may be very large, extending up to several orders of magnitude. We show in Figure 19

Eur. Phys. J. B (2012) 85: 361

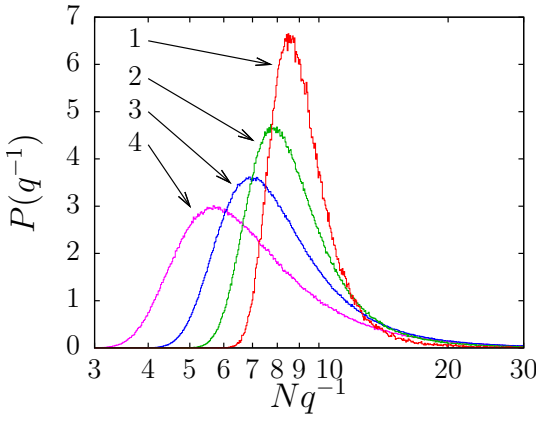

Fig. 20. (Color online) Histogram of IPR in the range of extended states, $z \in [-0.1, 0.1]$, for $\eta = 2$ and different sizes of the system, $N = 10^4$ (line 1), $N = 3000$ (line 2), $N = 1000$ (line 3), and $N = 300$ (line 4). The data are accumulated from 610, 17 000, 130 000, and 270 000 independent realizations, respectively.

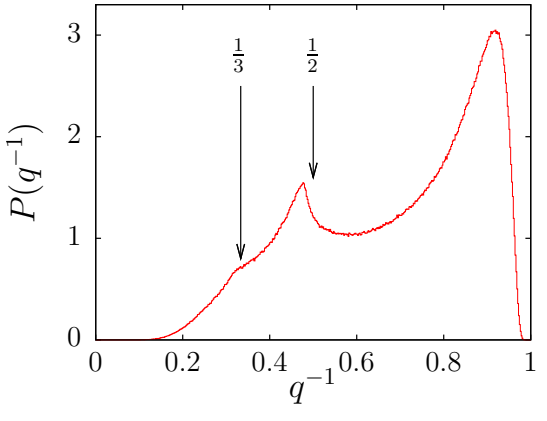

Fig. 21. (Color online) Histogram of IPR in the range of localized states, $z \in [-8.5, -7.5]$, for $\eta = 5$ and $N = 1000$. The arrows indicate special values if IPR, $q^{-1} = 1/2$ and $q^{-1} = 1/3$. The data are accumulated from 280 000 independent realizations.

a series of histograms for the window $[z_1, z_2]$ sliding from extended states through the transition region, to localized states. As expected, the width of the distribution is largest around the transition, but even in the localized regime it spans about one decade.

Let us first look at the extended states. The average IPR is expected to scale as $1/N$. Therefore, we plot the histogram against the rescaled value Nq^{-1}, in order to see the convergence for increasing N. Indeed, we can observe in Figure 20 that the position of the peak approaches to a limit and simultaneously, the width of the peak shrinks. This suggests that in the extended phase, IPR is a self-averaging quantity.

On the contrary, we found that in the localized phase the distribution of IPR is independent of size. Moreover, as the example in Figure 21 shows, there are non-trivial structures in the distribution. In Figure 21 we clearly see two distinct peaks and a cusp. Interestingly, the positions

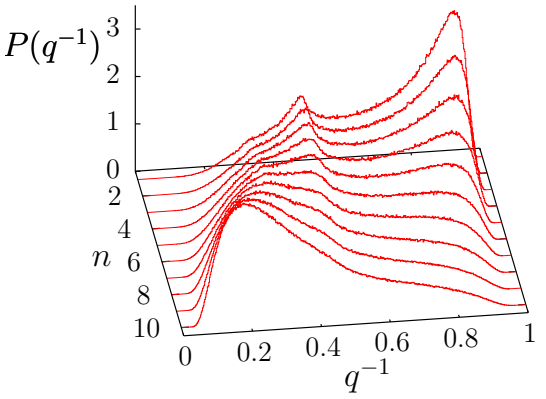

Fig. 22. (Color online) Series of histograms of IPR in the range of localized states, for $\eta = 5$ and $N = 1000$. The index of the curve n corresponds to the interval of eigenvalues according to the formula $z \in [-8.6 + 0.5n, -8.4 + 0.5n]$. The data are accumulated from 280 000 independent realizations.

of these three structures are slightly below some special values of IPR, namely $q^{-1} = 1$, $q^{-1} = 1/2$, and $q^{-1} = 1/3$. With our data available, we are unable to see further structures at $q^{-1} = 1/4$ etc., but we may speculate that they are also present.

Further on, we want to see how these structures evolve when we sweep through the regime of localized states, changing the value of z. We plot in Figure 22 the series of histograms for $z \in [-8.6 + 0.5n, -8.4 + 0.5n]$, $n = 1, 2, \ldots, 10$. For large $|z|$, i.e. deep in the localized phase, the peak at $q^{-1} \simeq 1$ dominates, but when we decrease $|z|$, i.e. when we approach the transition, the peak $q^{-1} \simeq 1/2$ takes over, and further on the peak at $q^{-1} \simeq 1/3$ becomes most visible. Simultaneously the peaks broaden and shift to lower values of IPR, so that the structure of distinct peaks is less and less clear.

We can interpret the special positions of the peaks at $q^{-1} = 1$, $q^{-1} = 1/2$, etc. as coming from eigenvectors localized mostly at one, two, etc. sites. In order to support this interpretation, we measured also the weighted average distance between sites. To this end, we first find the shortest paths between each pair of vertices in the current realization of the random cubic graph. Denote $d(i, j)$ the length of this path for vertices i and j. Of course, $d(i, i) = 0$ for every i. Then, for each normalized eigenvector $e_{i\lambda}$ we calculate the weighted average

$$\overline{d}(\lambda) = \frac{\sum_{i,j=1}^{N} d(i,j) e_{i\lambda}^2 e_{j\lambda}^2}{\sum_{i,j=1}^{N} e_{i\lambda}^2 e_{j\lambda}^2} \,. \tag{16}$$

For a vector strictly localized at one single site we get the average distance $\overline{d} = 0$, for a vector localized on a pair of neighbors it is $\overline{d} = 1/2$ and for a vector localized on a pair of sites at distance 2 we have $\overline{d} = 1$. The two latter cases give the same IPR, $q^{-1} = 1/2$, so the average distance brings further information on the eigenvector. We plot in Figure 21 the joint distribution of IPR and average distance, in the form of two-dimensional histogram. The value of $P(q^{-1}, \overline{d})$ is discriminated by the color, higher

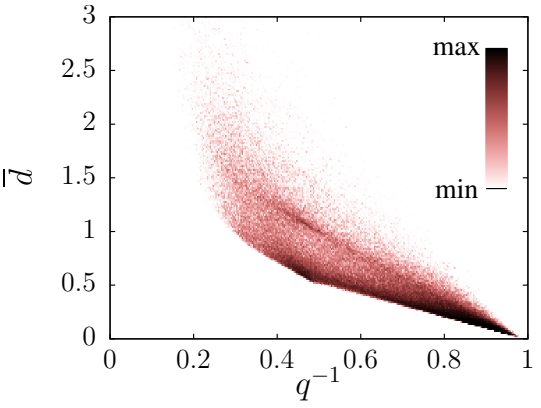

Fig. 23. (Color online) Two-dimensional histogram of IPR and average distance of sites, in the range of localized states, $z \in [-7.1, -6.9]$, for $\eta = 5$ and $N = 1000$. Darker color indicates higher value of the histogram. The data are accumulated from 30 000 independent realizations.

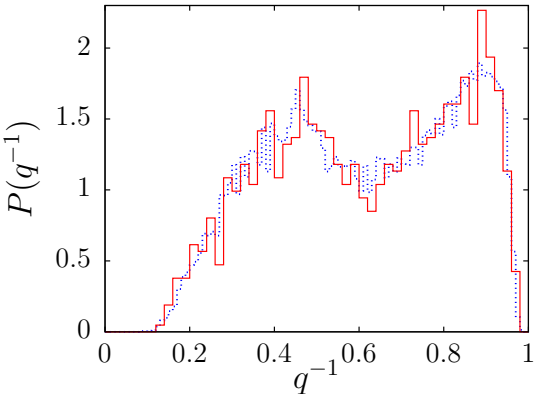

Fig. 24. (Color online) Histogram of IPR in the range of localized states, $z \in [-7.5, 6.5]$, for $\eta = 6$ and $N = 30\,000$. The solid line is the histogram for a single realization, while the dotted line is the cumulative histogram for 20 independent realizations.

values being darker. We clearly observe two black spots corresponding to peaks of the distribution. The first one is located about $q^{-1} \simeq 0.85$ and $\overline{d} \simeq 0.2$, implying states localized around one single site. The shift from the point $q^{-1} = 1$, $\overline{d} = 0$ is due to decaying tails of the eigenvector. The second peak is slightly shifted from the ideal position $q^{-1} = 1/2$, $\overline{d} = 1/2$. Clearly, it corresponds to states localized on a pair of neighbors, again with decaying tails. We can also see a darker spot around the position $q^{-1} = 1/2$, $\overline{d} = 1$. This small peak indicates states localized around a pair of sites at distance 2, i.e. on second neighbors.

One might rise a serious suspicion, that each of the peaks in the histogram of IPR corresponds to different realization. If that were true, the multi-peak structure would be the artifact of accumulating data from many independent realizations into one histogram. To check it, we calculated the same histogram for a large system, $N = 30\,000$. In the localized phase, we found two distinct peaks also in the histogram for one single realization. Moreover, comparing the histograms for a single realization and for 20 independent realizations, we see the same shape of the distribution, within statistical errors, as seen in Figure 24. Therefore, the observed peculiarities in the IPR distribution are characteristic of single realizations.

4.4 Level spacings

An important feature of the localization transition, stressed already in the early works [14,15], is the qualitative change in fluctuations of the imaginary part of the resolvent close to the real axis. It was used for establishing the mobility edge e.g. in reference [28]. In fact, this feature is due to the change in level-spacing statistics [46]. Extended states are supposed to obey the level-spacing distribution common to Gaussian orthogonal ensemble (GOE) of random matrices [64], i.e. in a very good approximation

$$P_{\mathrm{GOE}}(x) \propto x e^{-x^2}. \tag{17}$$

(in this expression x is the distance of eigenvalues normalized to the average level spacing). On the other hand, localized states should obey the Poisson statistics

$$P_{\mathrm{Poisson}}(x) \propto e^{-x}. \tag{18}$$

Intuitively, the change in statistics can be understood in terms of level repulsion, which is substantial for extended, but very small for localized states. Therefore, localized states behave as if they were nearly independent and their energies scattered randomly, which gives rise to the Poisson statistics. Because Poisson statistics is characteristic for integrable systems, while statistics like (17) is the fingerprint of a chaotic system, the localization transition can be viewed also as a chaotic-integrable transition.

We analyzed the random cubic graph of size $N = 1000$ and disorder strength $\eta = 2$ and we extracted the level spacing statistics for the spacings between eigenvalues, normalized to the average spacing within certain interval. We used the interval $z \in [-0.1, 0.1]$ as a typical representative of extended states and $z \in [-7, -6]$ as a representative of localized states. The results are shown in Figure 25. The difference in statistics is clearly visible. The detail in the inset of Figure 25 shows also that the behavior for small level spacings is close to linear in the extended phase, in accord with equation (17). We checked also that the distribution for localized states decays exponentially, as in equation (18). Thus, it is clearly demonstrated that the level spacing statistics gets transformed from Poisson to GOE when we go from localized to extended regime in the spectrum.

To make this argument quantitative, we calculate the moments of the distribution of level spacings $\langle(\Delta z)^k\rangle = \int (\Delta z)^k P(\Delta z) \mathrm{d}\Delta z$ within the interval $z \in [z_-, z_+]$. Then, we plot in Figure 26 the relative variance of the distribution $\langle(\Delta z)^2\rangle / \langle \Delta z\rangle^2 - 1$. We can clearly see the peak around the transition between localized and delocalized states, marking a qualitative change in the level spacing distribution.

Eur. Phys. J. B (2012) 85: 361

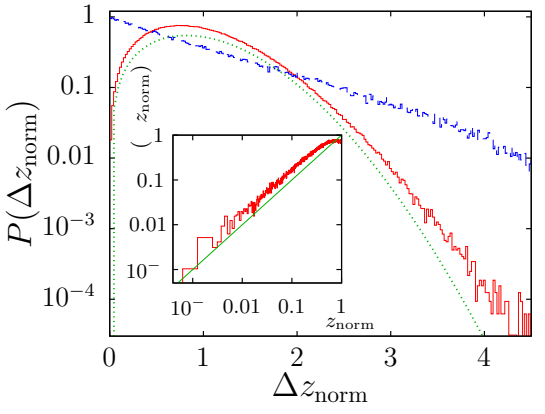

Fig. 25. (Color online) Distribution of normalized level spacings in the spectrum of random cubic graph with disorder strength $\eta = 2$ and size $N = 1000$. The levels analyzed are restricted to intervals $z \in [-0.1, 0.1]$ (solid line) and $z \in [-7, -6]$ (dashed line). The dotted line is the dependence $\propto \Delta z_{\rm norm} \exp\big(-a(\Delta z_{\rm norm})^2\big)$, with $a = 0.75$, which corresponds to the Gaussian orthogonal ensemble. In the inset we show the detail of the distribution at $z \in [-0.1, 0.1]$ for very small spacings. The straight line is the linear dependence $\propto \Delta z_{\rm norm}$.

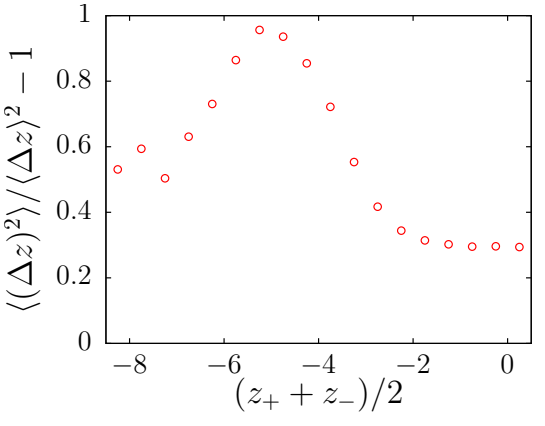

Fig. 26. (Color online) Relative variance of the level spacing distribution, depending on the center of the interval over which the distribution is calculated. The disorder strength is $\eta = 2$ and the size of the system $N = 1000$.

5 Conclusions

Numerically diagonalizing matrices up to size $10\,000 \times 10\,000$, we investigated localization transition in Erdős-Rényi and random cubic graphs. In ER graphs, the free parameter was the average degree, while in random cubic graphs, the parameter was the strength of disorder in the diagonal matrix elements. The quantity to discriminate between localized and extended regimes was the inverse participation ratio. We averaged IPR over large number of realizations and using finite-size scaling, we extracted the mobility edge. The benchmark for the position of the mobility edge was the band edge found in the effective medium approximation.

The localization properties in ER and random cubic graphs are much different. In the former, the mobility edge goes more or less in parallel with the EMA band edge, when we change the average degree, and the fraction of localized states decreases when the average degree grows. In the latter, the EMA band edge is significantly farther than the mobility edge, or else, much of the localized states are actually present within the range of EMA spectrum. The results are consistent with analytical findings which predicted that a critical disorder strength exists, beyond which all states are localized.

The inverse participation ratio exhibits rather strong fluctuations. In the extended phase, the relative width of the IPR distribution decreases with increasing system size, while in the localized phase the width of the distribution approaches a finite value. Moreover, the distribution contains non-trivial structures of several peaks. We interpret these structures as corresponding to states localized around one, two, three, etc. sites.

For the random cubic graphs, we analyzed also the level spacing statistics confirming the expectation that in the localized region the statistics is close to Poissonian, while in the extended region it is close to the statistics of Gaussian orthogonal ensemble.

I wish to thank to J. Mašek for numerous useful comments. This work was carried out within the project AV0Z10100520 of the Academy of Sciences of the Czech Republic and was supported by the MŠMT of the Czech Republic, grant no. OC09078.

References

1. P.W. Anderson, Phys. Rev. **109**, 1492 (1958)
2. A. Amir et al., *50 Years of Anderson Localization*, edited by E. Abrahams (World Scientific Publishing Co., Singapore, 2010)
3. P.A. Lee, T.V. Ramakrishnan, Rev. Mod. Phys. **57**, 287 (1985)
4. B. Kramer, A. MacKinnon, Rep. Prog. Phys. **56**, 1469 (1993)
5. F. Evers, A.D. Mirlin, Rev. Mod. Phys. **80**, 1355 (2008)
6. R. del Rio, S. Jitomirskaya, Y. Last, B. Simon, Phys. Rev. Lett. **75**, 117 (1995)
7. E. Abrahams, P.W. Anderson, D.C. Licciardello, T.V. Ramakrishnan, Phys. Rev. Lett. **42**, 673 (1979)
8. D. Vollhardt, P. Wölfle, Phys. Rev. B **22**, 4666 (1980)
9. D. Vollhardt, P. Wölfle, in *Electronic Phase Transitions*, edited by W. Hanke, Y.V. Kopaev (North-Holland, Amsterdam, 1992), p. 1
10. I.M. Suslov, Sov. Phys. JETP **81**, 925 (1995)
11. V. Janiš, J. Kolorenč, Phys. Rev. B **71**, 033103 (2005)
12. F.J. Wegner, Phys. Rev. B **19**, 783 (1979)
13. K.B. Efetov, Adv. Phys. **32**, 53 (1983)
14. R. Abou-Chacra, P.W. Anderson, D.J. Thouless, J. Phys. C: Solid State Phys. **6**, 1734 (1973)
15. R. Abou-Chacra, D.J. Thouless, J. Phys. C: Solid State Phys. **7**, 65 (1974)
16. D.E. Logan, P.G. Wolynes, Phys. Rev. B **31**, 2437 (1985)
17. P.D. Antoniou, E.N. Economou, Phys. Rev. B **16**, 3768 (1977)
18. S.M. Girvin, M. Jonson, Phys. Rev. B **22**, 3583 (1980)
19. K.B. Efetov, Physica A **167**, 119 (1990)

20. A.D. Mirlin, Y.V. Fyodorov, Nucl. Phys. B **366**, 507 (1991)
21. H. Kunz, B. Souillard, J. Phys. Lett. **44**, L-411 (1983)
22. P. Stollmann, *Caught by Disorder. Bound States in Random Media* (Birkhäuser, Boston, 2001)
23. M. Aizenman, S. Warzel, Phys. Rev. Lett. **106**, 136804 (2011)
24. P. Markoš, Acta Physica Slovaca **56**, 561 (2006)
25. C. Monthus, T. Garel, Phys. Rev. B **81**, 224208 (2010)
26. P. Cizeau, J.-P. Bouchaud, Phys. Rev. E **50**, 1810 (1994)
27. A. Cavagna, I. Giardina, G. Parisi, Phys. Rev. Lett. **83**, 108 (1999)
28. S. Ciliberti, T.S. Grigera, V. Martín-Mayor, G. Parisi, P. Verrocchio, Phys. Rev. B **71**, 153104 (2005)
29. R. Kühn, J. Phys. A: Math. Theor. **41**, 295002 (2008)
30. F.L. Metz, I. Neri, D. Bollé, Phys. Rev. E **82**, 031135 (2010)
31. G. Biroli, G. Semerjian, M. Tarzia, Prog. Theor. Phys. Suppl. **184**, 187 (2010)
32. C. Monthus, T. Garel, J. Phys. A: Math. Theor. **44**, 145001 (2011)
33. F.R.K. Chung, *Spectral Graph Theory* (American Mathematical Society, 1997)
34. B. Bollobás, *Random Graphs* (Academic Press, London, 1985)
35. G.J. Rodgers, A.J. Bray, Phys. Rev. B **37**, 3557 (1988)
36. G.J. Rodgers, C. De Dominicis, J. Phys. A: Math. Gen. **23**, 1567 (1990)
37. Y.V. Fyodorov, A.D. Mirlin, J. Phys. A: Math. Gen. **24**, 2219 (1991)
38. Y.V. Fyodorov, A.D. Mirlin, Phys. Rev. Lett. **67**, 2049 (1991)
39. A. Khorunzhy, G.J. Rodgers, J. Math. Phys. **38**, 3300 (1997)
40. G. Biroli, R. Monasson, J. Phys. A: Math. Gen. **32**, L255 (1999)
41. M. Bauer, O. Golinelli, J. Stat. Phys. **103**, 301 (2001)
42. G. Semerjian, L.F. Cugliandolo, J. Phys. A: Math. Gen. **35**, 4837 (2002)
43. T. Rogers, I. Pérez Castillo, R. Kühn, K. Takeda, Phys. Rev. E **78**, 031116 (2008)
44. S.N. Evangelou, Phys. Rev. B **27**, 1397 (1983)
45. S.N. Evangelou, J. Stat. Phys. **69**, 361 (1992)
46. S.N. Evangelou, E.N. Economou, Phys. Rev. Lett. **68**, 361 (1992)
47. S.N. Dorogovtsev, A.V. Goltsev, J.F.F. Mendes, A.N. Samukhin, Phys. Rev. E **68**, 046109 (2003)
48. M. Sade, T. Kalisky, S. Havlin, R. Berkovits, Phys. Rev. E **72**, 066123 (2005)
49. A.L. Cardoso, R.F.S. Andrade, A.M.C. Souza, Phys. Rev. B **78**, 214202 (2008)
50. G. Zhu, H. Yang, C. Yin, B. Li, Phys. Rev. E **77**, 066113 (2008)
51. S. Jalan, N. Solymosi, G. Vattay, B. Li, Phys. Rev. E **81**, 046118 (2010)
52. O. Giraud, B. Georgeot, D.L. Shepelyansky, Phys. Rev. E **80**, 026107 (2009)
53. F. Slanina, Z. Konopásek, Adv. Compl. Syst. **13**, 699 (2010)
54. C. Bordenave, M. Lelarge, Random Struct. Algorithms **37**, 332 (2010)
55. F. Slanina, Phys. Rev. E **83**, 011118 (2011)
56. E.N. Economou, M.H. Cohen, Phys. Rev. B **5**, 2931 (1972)
57. R. Kühn, J. van Mourik, J. Phys. A: Math. Theor. **44**, 165205 (2011)
58. Z. Burda, J. Duda, J.M. Luck, B. Waclaw, Phys. Rev. Lett. **102**, 160602 (2009)
59. F. Delyon, B. Simon, B. Souillard, Phys. Rev. Lett. **52**, 2187 (1984)
60. F. Delyon, B. Simon, B. Souillard, Ann. Inst. H Poincaré, Phys. Theor. **42**, 283 (1985)
61. Y.V. Fyodorov, A.D. Mirlin, H.-J. Sommers, J. Phys. I France **2**, 1571 (1992)
62. M. Kolář, F. Slanina, Eur. Phys. J. B **31**, 379 (2003)
63. L. Erdős, A. Knowles, H.-T. Yau, J. Yin, `arXiv:1103.1919 [math.PR]` (2011)
64. M.L. Mehta, *Random Matrices* (Academic Press, San Diego, 1991)

[Slanina01]

ELSEVIER

Physica A 299 (2001) 334–343

PHYSICA A

www.elsevier.com/locate/physa

Harms and benefits from social imitation

František Slanina*

Institute of Physics, Academy of Sciences of the Czech Republic, Na Slovance 2, CZ-18221 Praha, Czech Republic

Abstract

We study the role of imitation within a model of economics with adaptive agents. The basic ingredients are those of the minority game. We add the possibility of local information exchange and imitation of the neighbour's strategy. Imitators should pay a fee to the imitated. Connected groups are formed, which act as if they were single players. Coherent spatial areas of rich and poor agents result, leading to the decrease of local social tensions. Size and stability of these areas depends on the parameters of the model. Global performance measured by the attendance volatility is optimised at certain value of the imitation probability. The social tensions are suppressed for large imitation probability, but due to the price paid by the imitators the requirements of high global effectivity and low social tensions are in conflict, as well as the requirements of low global and low local wealth differences.

PACS: 05.65.+b; 02.50.Le; 87.23.Ge

Keywords: Minority game; Self-organisation; Economics

1. Introduction

The minority game introduced by Challet and Zhang [1,2] following the earlier ideas of Arthur [3] became in recent years a playing ground for studying various aspects of the economic systems.

In the minority game (MG) we have N players who choose repeatedly between two options and compete to be in the minority group. This is the idealisation of various situations, where the competition for limited resources leads to intrinsic frustration. One can think, for example, of cars choosing between two alternative routes or a speculator who tries to earn money by buying and selling shares in such a manner that the majority takes the opposite action than herself.

* Fax: +420-2-8689-0527.
E-mail address: slanina@fzu.cz (F. Slanina).

0378-4371/01/$ - see front matter
PII: S0378-4371(01)00314-4

[Slanina01]

Let us recall some well-known facts about the MG. The players share a public information, saying what were the outcomes of the game in past M rounds. The players interact only through this information. Therefore, the system has a "mean-field" character, in the sense that no short-range interactions exist.

The self-organization is achieved by allowing players to have several strategies and choose among them the strategy which seems to be the best one. This feature leads to decrease of the fluctuations of attendance below its random coin-tossing value, thus increasing the global effectivity of the system. It was found that the relevant parameter is $\alpha = 2^M/N$ and the maximum effectivity is reached for $\alpha = \alpha_c \simeq 0.34$ [2,4,5] and the properties of this phase transition are thoroughly studied using the methods developed in the theory of neural networks [6–8].

More complete account of the current state of the standard MG and its ramifications is given in other contributions in these proceedings [9,10]. We would like to stress especially the attempts to go back to the economic motivations of MG and model the market mechanisms [11–14].

The observation that the crowded (low α) phase exhibits low global effectivity bears an important hint. Indeed, if we start with the crowded phase, we can improve the performance by grouping the agents together. This mechanism may bring about the condensation of individual investors around consulting companies and investment funds, which is the behaviour found in real life.

Indeed, an individual investor who sees that she is all the time behind her neighbours may feel tempted to refrain from her own initiative and transfer the burden of decisions to more successful (more wealthy) individuals. That is what we will call imitation. The temptation for imitation in the population will be quantified by a parameter $p \in [0,1]$. Of course, an agent, who is otherwise prone to imitation, will *not* imitate, if she has larger wealth and therefore is better off than her neighbours. So, there may be two questions to be positively answered if the imitation is to occur: Has the agent natural tendency to imitation? Has any of her neighbours larger wealth?

It is also natural to suppose that the decision maker, or the imitated individual, will use (or misuse) her position to require a fee from those on which behalf her acts. Therefore, the imitators will pay a commission ε to the imitated. As we will see, the value of the commission has important consequences for the behaviour of the agents.

We introduced recently [15] the possibility of local interactions into the standard MG. In this contribution, we further analyse the properties of social structures emerging from the local information exchange. When doing so we go beyond the mean-field character of the usual MG. Related works were already done, either assuming that the global information is fully replaced by a local one [16] or using the MG scheme for evolving the Kauffmans's Boolean networks [17] to the critical state [18].

In our variant of the MG the local information is used to enable the players to decide, whether they want to use their own strategies or imitate their neighbours. Indeed, it is quite common that people do not invest individually, but rely on an advice from

specialised agencies, or simply follow the trend they perceive in their information neighbourhood. In so doing, the individuals coalesce into groups, which act as single players. In the framework of minority game, we will study the social structure induced by the occurrence of these groups. It should be expected that this will lead to increase in the global performance in the crowded (small α) phase. This is indeed confirmed by the simulations.

2. Minority game on a chain with allowed imitation

We introduce the possibility of local information exchange in our variant of the minority game. In analogy to the metabolic pathways in living organisms, we can imagine a kind of "information metabolism" in work within the economic system. Information flow along the edges of certain information network. The study of the geometry of graphs describing these information networks is now a scientific field on its own [19–21]. Within the framework of MG a linear chain [16] and random network with fixed connectivity K [18] was already investigated in different contexts.

Here, we take the simplest possible choice of a linear chain with one-directional nearest-neighbour connections. Each player can obtain the information only from her left-hand neighbour, namely about her neighbour's wealth.

There will be two conditions needed for a player to imitate her neighbour. First, the player should have internal disposition for being an imitator. We simplify the variety of risk-aversion levels by postulating only two types of players. Each player has a label $\tilde{l} \in \{1,0\}$ indicating, whether the player is a potential imitator ($\tilde{l}=1$) or always a leader ($\tilde{l}=0$). At the beginning we take each of the players and attribute her label 1 with probability p and label 0 with probability $1-p$. We also allow swapping between the two types of behaviour, at a constant rate. The labels can change at each step with probabilities p_1 $(1 \to 0)$ and p_2 $(0 \to 1)$. We choose always $p = p_2/(p_1 + p_2)$, so that the average density of potential imitators does not change in time.

The second condition for the player of type 1 to actually imitate in the current step is that her neighbour has larger accumulated wealth than the player itself. We suppose that the player does not know what are the strategies of her neighbour, but if she observes that the neighbour's behaviour is more profitable than her own strategy, she relegates the decision to the neighbour and takes the same action. The player of type 0 will never imitate. Therefore, she will always look only at her S strategies and choose the best estimate from them.

The above rules are formalized as follows. We have an odd number N of players. Each player has $S=2$ strategies, denoted $s_j \in \{1,2\}$. The two possible actions a player can take are 0 and 1. The winning action is 1 if most players took 0 and vice versa. The members of the winning side receive 1 point, the loosing side 0 points. The players know the last M outcomes of the game. This information is arranged into the M-bit string $\mu \in \{0,1\}^M$. The strategies are tables attributing to each of 2^M possible strings μ the action a^{μ}_{j,s_j} the player j takes, if she chooses the strategy s_j. The scores $U_{j,s}$ of

the strategies are updated according to the minority rule

$$U_{j,s}(t+1) = U_{j,s}(t) + 1 - \delta\left(a_{j,s}^{\mu(t)} - \theta\left(\sum_i a_i(t) - N/2\right)\right), \tag{1}$$

where $a_j(t)$ is the action the player j takes at time t.

The potential imitators will copy the action from their more successful neighbours. Let W_j be the wealth of the jth player and the variables l_j describe the actual state of imitation, in analogy with the labels $\tilde{l}_j$ describing potential state of imitation. We can write $l_j = \tilde{l}_j\,\theta(W_{j-1} - W_j)$, with $\theta(x) = 1$ for $x > 0$ and 0 otherwise. The actions of the players are

$$a_j = l_j a_{j-1} + (1 - l_j) a_{j,s_M}\,. \tag{2}$$

We also suppose that the imitation is not for free. The player who imitates passes a small fraction ε of its wealth increase to the imitated player. This rule accounts for the price of information. Then, we update the wealth of players iteratively,

$$\Delta W_j(t) = (1 - \varepsilon l_j)(\varepsilon l_{j+1}\,\Delta W_{j+1}(t) + 1 - \delta\left(a_j - \theta\left(\sum_i a_i(t) - \frac{N}{2}\right)\right), \tag{3}$$

where $\Delta W_j(t) = W_j(t+1) - W_j(t)$.

3. Imitation structures

In our simulations we observe that the time evolution of the number of actually imitating players, $N_i = \sum_j l_j$, depends on p_1. The time dependence of the fraction of imitators N_i/N for several values of p_1 is shown in Fig. 1. For $p_1 = 0$ it increases

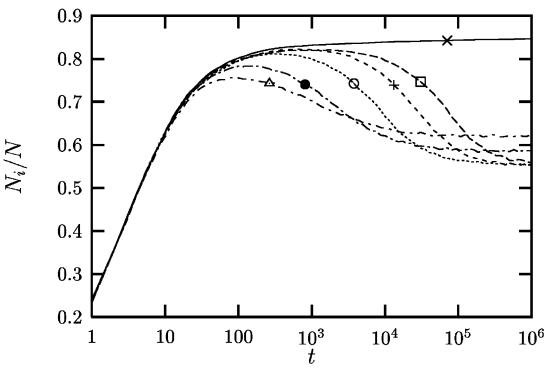

Fig. 1. Time dependence of the fraction of imitators, for $N = 1001$, $M = 6$, $S = 2$, and $p = 0.95$, averaged over 10 independent runs. Different curves (marked by symbols) correspond to different probability $p_1 = 0$ (×), 5×10^{-6} (□), 1.5×10^{-5} (+), 5×10^{-5} (⊙), 5×10^{-4} (●), 5×10^{-3} (△).

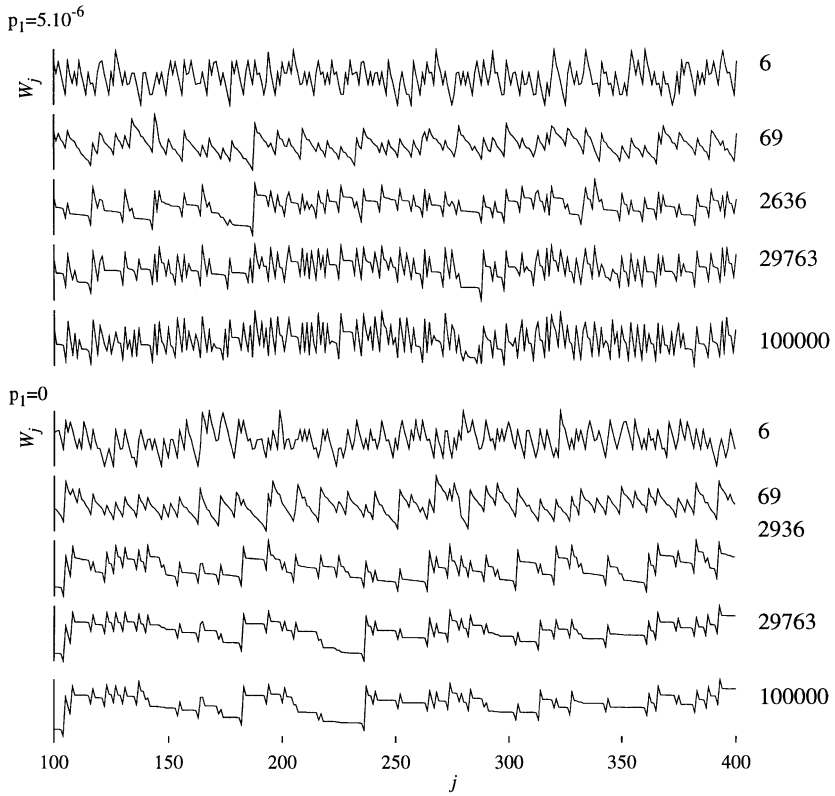

Fig. 2. Example of the evolution of the distribution of wealth among players, for $N = 1001$, $M = 6$, $S = 2$, $\varepsilon = 0.05$, and $p = 0.95$. The upper 5 curves correspond to $p_1 = 5 \times 10^{-6}$, while the lower 5 curves have $p_1 = 0$. The time step at which the snapshot is taken is indicated on the right. For each time, the vertical axis indicates the wealth W_j of the jth player.

monotonously until saturation, while for $p_1 \neq 0$ it grows toward a local maximum and then decreases and saturates at a value weakly dependent on p_1, but significantly below the $p_1 = 0$ value.

An example of the time evolution of the spatial wealth distribution is given in Fig. 2 for $p = 0.95$ and two values of $p_1 = 5 \times 10^{-6}$ and 0. The initially random distribution of wealth among players changes qualitatively during the evolution of the system. Coherent groups of poor and wealthy players are formed. Again, the situation is qualitatively different if we allow the players to switch between potential imitator and leaders. We have shown in the previous work [15] that for $p_1 = 0$ the poor groups persist forever. We can see the same behaviour also in Fig. 2 for $p_1 = 0$. On the other hand, for $p_1 \neq 0$ we observe that large poor groups are unstable and split again into smaller clusters. This leads to lowering of the global wealth differences, as will be analysed in the next section.

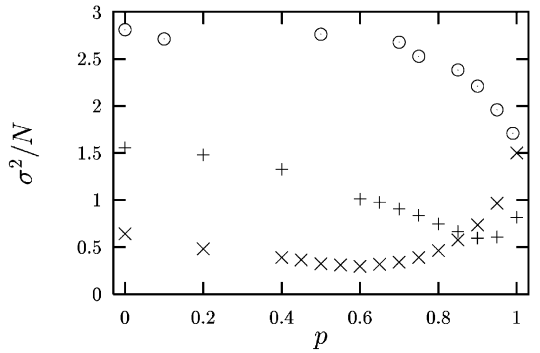

Fig. 3. Dependence of the attendance fluctuations on the imitation probability for $p_1 = 0$. The number of players is $N = 1001$ and memory length $M = 5$ ($\odot$), $M = 6$ ($+$), and $M = 7$ ($\times$).

4. Globally uniform wealth versus small social tensions

The time averaged attendance fluctuations $\sigma^2 = \langle (A - N/2)^2 \rangle$ measure the distance from the global optimum. The global effectivity is higher for smaller σ^2. We investigated the influence of the imitation on the global effectivity.

We found that in the crowded phase the system becomes more efficient if imitation is allowed ($p > 0$), but there is a local minimum in the dependence of σ^2/N on p, indicating that there is an optimal level of imitation, beyond which the system starts to perform worse. The results for $N = 1001$ are shown in Fig. 3. We can see that the minimum occurs at smaller values for larger M. We can also observe that for longer memories ($M = 7$ in our case) the value of the fluctuations for $p = 1$ is significantly above the value without imitation ($p = 0$), while the value at the minimum still lies below the $p = 0$ value. This implies that moderate imitation can be beneficiary, while exaggerated one can be harmful.

The increase of spatial coherence by creation of poor and wealthy groups can result in decrease of local social tension. To quantify it, we introduce a kind of "utility function" [22] $U(\Delta W)$, which indicates, how much the wealth difference ΔW is subjectively perceived. We will use the utility function in the form $U(x) = x^{1/2}$. Then, the average measure of the local social tension is

$$d_{0.5} = \frac{1}{\langle W \rangle} \left(\sum_{j=1}^{N-1} |W_j - W_{j+1}|^{1/2} \right)^2 , \tag{4}$$

where we denoted the average wealth $\langle W \rangle = \frac{1}{N} \sum_{j=1}^{N} W_j$.

The stationary values of the tension for various values of the commission ε are shown in Fig. 4, for $p_1 = 0$. An important feature of the p-dependence is the maximum at certain imitation probability. The maximum becomes more pronounced for larger commission ε, while for $\varepsilon = 0.01$ it disappears.

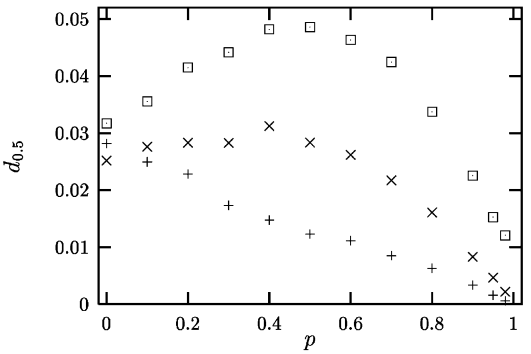

Fig. 4. Relative local tension for $N = 1001$, $M = 6$, $p_1 = 0$ measured by utility function $(\Delta W)^{1/2}$ for commission $\varepsilon = 0.05$ (⊡), 0.03 (×), and 0.01 (+).

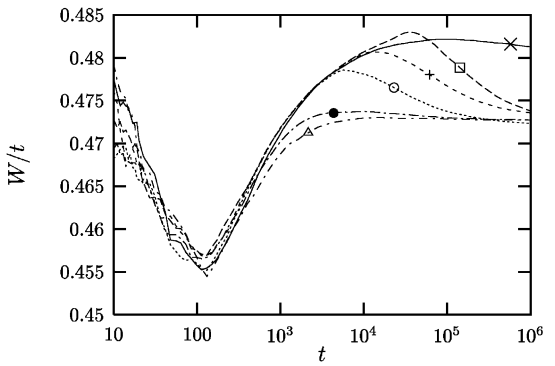

Fig. 5. Growth of the average wealth of agents, for $N = 1001$, $M = 6$, $S = 2$, $p = 0.95$, sample averaged over 10 independent runs. Different curves (marked by symbols) correspond to different probability $p_1 = 0$ (×), 5×10^{-6} (□), 1.5×10^{-5} (+), 5×10^{-5} (⊙), 5×10^{-4} (●), 5×10^{-3} (△).

This observation has an important consequence. Imagine, we are social experimentalists starting with a system with no information exchange and no imitation. Let us try to lower the social tensions by gradually encouraging the people to buy information from the neighbours and imitate each other. If the cost of the information (ε) is too high, this social strategy would fail, because small increase in imitation would *enhance* the social tension. Lower social tension must have been achieved by a macroscopic change in the social behaviour: by jumping over the maximum in the function $d_{0.5}(p)$. This may serve as a toy example of how too greedy environment (too costly information) can prevent the system to find a global optimum.

By comparing Figs. 3 and 4 we can also see that for high ε optimal performance (minimum σ^2/N) can be close to maximum in social tensions. Therefore, in greedy environment the requirements of effectivity and social peace are in conflict.

Fig. 5 shows, the growth rate of the average wealth for several values of the switching probability p_1. We can see that the growth rate converges to a constant value,

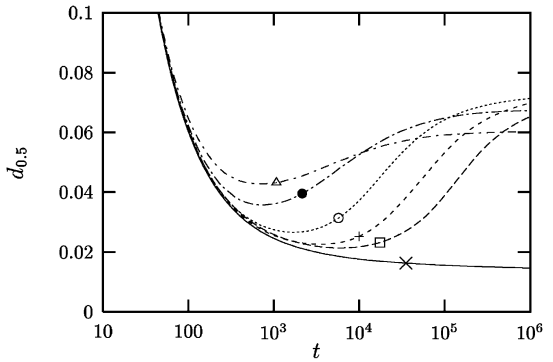

Fig. 6. Time evolution of the local tensions, for $N = 1001$, $M = 6$, $S = 2$, $p = 0.95$, sample averaged over 10 independent runs. Different curves (marked by symbols) correspond to different probability $p_1 = 0$ (×), 5×10^{-6} (□), 1.5×10^{-5} (+), 5×10^{-5} (⊙), 5×10^{-4} (●), 5×10^{-3} (△).

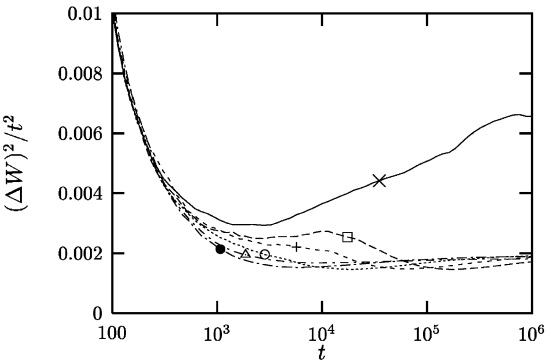

Fig. 7. Time evolution of the wealth dispersion, for $N = 1001$, $M = 6$, $S = 2$, $p = 0.95$, averaged over 10 independent runs. Different curves (marked by symbols) correspond to different probability $p_1 = 0$ (×), 5×10^{-6} (□), 1.5×10^{-5} (+), 5×10^{-5} (⊙), 5×10^{-4} (●), 5×10^{-3} (△).

which is higher for $p_1 = 0$ and nearly independent of p_1 for $p_1 \neq 1$. In all cases, we confirm that the average wealth grows linearly with time.

In Fig. 6 we can see the time evolution of the local tensions for several values of the switching probability p_1. We observe that the switching enhances the local tensions. On the other hand, in Fig. 7, we can see the time dependence of the growth rate in the global wealth dispersion, $\langle W^2 \rangle - \langle W \rangle^2$ (by angle brackets we denote the average over all players). There is a clear difference between the cases of $p_1 = 0$, where the wealth dispersion grows much more rapidly than t^2 and $p_1 \neq 0$, where the dispersion grows as t^2, at a rate nearly independent of p_1.

This means that, if we allow switching between potential imitation and leader states, the wealth distribution only re-scales linearly in time (this observation together with the linear growth if the average wealth suggests that the probability density at time t converge as $P(W,t) = \Phi(W/t)$ where the function $\Phi(x)$ does not depend on time). On

the contrary, if we forbid the switching, the poor imitators are frozen forever in their poverty and in the wealth distribution the rich and poor diverge steadily.

However, recalling the discussion of Figs. 6 and 5 we can see that the requirement of low global wealth dispersion (a "just" world, achieved by enabling the poor imitators switch to leaders and thus become richer) deteriorates both global efficiency (measured now by the wealth growth rate) and, more surprisingly, the local social tensions.

5. Conclusions

We investigated the creation of rich and poor spatial domains due to local information exchange, within the framework of the minority game (MG). Coherent spatial areas of rich and poor agents emerge. Several macroscopic conflicts of interest are observed in our model:

(1) We found that the effect of imitation leads to increased effectivity in the crowded phase of MG. The price paid for the information needed to imitation leads to the conflict between effectivity and local social tensions. High information cost also prevents the system from coming to the state of lower social tensions by gradual increase of the imitation probability.

(2) We allow for switching between imitation and non-imitation (leader) states. Such a switching makes the global wealth differences smaller, but increases the local social tensions.

The creation of coherent areas of poor and rich agents leads to decrease in the local social tensions, but only if p is sufficiently close to 1. The lowest value of the social tension is reached at $p=1$, but for such a value the global effectivity is significantly lower than its optimum value. Therefore, we observe a conflict of local interests (maximisation of social tension) with global performance (maximisation of attendance fluctuations).

Acknowledgements

I wish to thank to Yi-Cheng Zhang for numerous useful discussions. This work was supported by the Grant Agency of the Czech Republic, Grant Project No. 202/01/1091. I acknowledge the financial support from the University of Fribourg, Switzerland, where part of this work was done.

References

[1] D. Challet, Y.-C. Zhang, Physica A 246 (1997) 407.
[2] D. Challet, Y.-C. Zhang, Physica A 256 (1998) 514.
[3] W.B. Arthur, Am. Econom. Rev. (Papers Proc.) 84 (1994) 406.
[4] R. Savit, R. Manuca, R. Riolo, Phys. Rev. Lett. 82 (1999) 2203.
[5] N.F. Johnson, S. Jarvis, R. Jonson, P. Cheung, Y.R. Kwong, P.M. Hui, Physica A 258 (1998) 230.

[Slanina01]

[6] D. Challet, M. Marsili, Phys. Rev. E 60 (1999) R6271.
[7] D. Challet, M. Marsili, R. Zecchina, Phys. Rev. Lett. 84 (2000) 1824.
[8] A. De Martino, M. Marsili, cond-mat/0007397.
[9] M. Marsili, Physica A 299 (2001) 93–103 [these proceedings].
[10] D. Challet, M. Marsili, Y.-C. Zhang, Physica A 299 (2001) 228–233 [these proceedings].
[11] D. Challet, M. Marsili, Y.-C. Zhang, Physica A 276 (2000) 284.
[12] F. Slanina, Y.-C. Zhang, Physica A 272 (1999) 257.
[13] N.F. Johnson, M. Hart, P.M. Hui, D. Zheng, cond-mat/9910072.
[14] D. Challet, A. Chessa, M. Marsili, Y.-C. Zhang, cond-mat/0011042.
[15] F. Slanina, Physica A 286 (2000) 367.
[16] T. Kalinowski, H.-J. Schulz, M. Briese, Physica A 277 (2000) 502.
[17] S.A. Kauffman, The Origins of Order: Self-organization and Selection in Evolution, Oxford University Press, Oxford, 1993.
[18] M. Paczuski, K.E. Bassler, Phys. Rev. Lett. 84 (2000) 3185.
[19] D.J. Watts, S.H. Strogatz, Nature 393 (1998) 440.
[20] A.-L. Barabási, R. Albert, Science 286 (1999) 509.
[21] F. Slanina, M. Kotrla, Phys. Rev. E 62 (2000) 6170.
[22] R.C. Merton, Continuous-Time Finance, Blackwell Publishers, Cambridge, 1990.

[SlaLav03]

Eur. Phys. J. B **35**, 279–288 (2003)
DOI: 10.1140/epjb/e2003-00278-0

THE EUROPEAN PHYSICAL JOURNAL B

Analytical results for the Sznajd model of opinion formation

F. Slanina[1,a] and H. Lavička[2]

[1] Institute of Physics, Academy of Sciences of the Czech Republic, Na Slovance 2, 18221 Praha, Czech Republic
[2] Faculty of Nuclear Sciences and Physical Engineering, Czech Technical University in Prague, Břehová 7, 11519 Praha 1, Czech Republic

Received 17 April 2003 / Received in final form 21 July 2003
Published online 2 October 2003 –

Abstract. The Sznajd model, which describes opinion formation and social influence, is treated analytically on a complete graph. We prove the existence of the phase transition in the original formulation of the model, while for the Ochrombel modification we find smooth behaviour without transition. We calculate the average time to reach the stationary state as well as the exponential tail of its probability distribution. An analytical argument for the observed $1/n$ dependence in the distribution of votes in Brazilian elections is provided.

PACS. 89.65.-s Social and economic systems – 05.40.-a Fluctuation phenomena, random processes, noise, and Brownian motion – 02.50.-r Probability theory, stochastic processes, and statistics

1 Introduction

There is significant convergence between statistical physics and mathematical sociology in approaches to their respective fields [1]. Ising model, the single most studied statistical physics model, finds its numerous applications in sociophysics simulations. Conversely, sociologically inspired models pose new challenges to statistical physics. We believe this is the case of the Sznajd model we are studying here.

The model of Sznajd-Weron and Sznajd [2] was designed to explain certain features of opinion dynamics. The slogan "United we stand, divided we fall" lead to simple dynamics, in which individuals placed on a lattice (one-dimensional in the first version) can choose between two opinions (political parties, products etc.) and in each update step a pair of neighbours sharing common opinion persuade their neighbours to join their opinion. Therefore, it was noted that contrary to the Ising or voter [3] models, information does not flow from the neighbourhood to the selected spin, but conversely, it flows out from the selected cluster to its neighbours.

The model initiated a surge of immediate interest [4–25] and the results of numerical simulations can be briefly summarised as follows. The results do not depend much on the spatial dimensionality or on the type of the neighbourhood selected [11]. In the case of q choices of opinion, the system has q obvious homogeneous stationary (absorbing) states, where all individuals choose the same opinion. There is no way to go out of the homogeneous state, so it is an attractor of the dynamics. This is reminiscent of a zero-temperature dynamics, which in Ising model leads to rich behaviour [26]. However, in the Sznajd model, the possible metastable states, like the "antiferromagnetic" configuration have negligible probability to occur, unless we introduce explicitly also an "antiferromagnetic" dynamic rule as it was used in the very first formulation [2].

The case $q = 2$ was studied mostly, denoting the opinions by Ising variables $+1$ and -1. The probability of hitting the stationary state of all $+1$ (or, complementary, all -1) was studied, depending on the initial fraction p of the individuals choosing $+1$. Sharp transition was observed at value $p = 0.5$ [11]; for $p > 0.5$ the probability to reach eventually the state of all opinions $+1$ is close to one, while for $p < 0.5$ it is negligible, which can be interpreted as a dynamical phase transition. The distribution of times needed to reach the stationary state was measured, revealing a peak followed by relatively fast decay. This means that the average hitting time is a well-defined quantity [11].

It was also found in one and two-dimensional lattices that the fraction of individuals who never changed opinion decays as a power with time, similarly to Ising model. While the exponent in one dimension agrees with the Ising case, the two-dimensional Sznajd model gives different exponent than Ising model, indicating different dynamical universality class [13]. Also the waiting time between two subsequent opinion changes is distributed according to a power-law [2].

[a] e-mail: slanina@fzu.cz

Among other studies, let us mention the influence of advertising effects [18,19] and price formation [20]. Long-range interactions were studied in [21].

In a very short but intriguing note [22] Ochrombel suggested a drastic simplification of the Sznajd model. In the Ochrombel version it is not necessary to have a cluster of identical opinions. Any individual is capable to convince her neighbours to select the same opinion. This model was reported to share all essential features of the original Sznajd model, only the phase transition in the probability of hitting the state of all $+1$ at $p = 0.5$ is absent.

The Sznajd model was also used to model the election process. There is recent empirical evidence from Brazilian elections [27–29] that the distribution of votes per candidate follows a power-law, more specifically $P(n) \sim 1/n$, where n is the number of votes. This result was reproduced in a study [4] based on Sznajd model on a scale-free network [30–32].

The dynamics of elections was thoroughly investigated by Galam [33–36], showing that majority rule applied on sufficiently many hierarchical levels leads to a homogeneous "totalitarian" state with one opinion pervading the whole system.

Other approaches to physical modelling of opinion dynamics were also investigated [37,38] and among them especially the Axelrod model, which was found to have rich behaviour from the statistical physics point of view [39–41].

We should also mention the well studied voter model [3,42–44], which is very similar in spirit to the Sznajd model. Indeed, the relation of the two models was studied *e.g.* in [45] and it seems that Sznajd model reduces to the voter model at least for certain setups (especially using the Ochrombel simplification on a complete graph) while for others the voter model can be generalised so that it includes the rules of Sznajd model as a special case. In fact, similar analysis to that presented here was performed for voter model, contact process and related processes in [46]. The persistence properties of the voter model on complete graph were studied in [42].

Very recently a "Majority rule" model, sharing some features with Sznajd model, was introduced and studied in [47] and its generalisation to the Majority-Minority model [48] gives in the mean-field approximation results closely related to ours.

2 Formulation of the model and its simplifications

2.1 General scheme

In the original formulation of the Sznajd model, the "united we stand" principle is often stressed [2,11]. It means that only a cluster of identical opinions can spread the same opinion toward its neighbours. However, this principle was relaxed in the Ochrombel simplification [22] without qualitatively affecting many of the results (except the presence of the phase transition). We will propose some other simplifications here, supposing the results remain robust.

Let us have N agents, each of which can be in one of q states (opinions) $\sigma \in S$. We may for example think of a q-state Potts model variables. Each agent sits on a node of a social network, and they can interact along the edges with their nearest neighbours.

The opinion of the agent i is denoted σ_i. The state of the system is described by the set of opinions of all the agents, $\Sigma = [\sigma_1, \sigma_2, ..., \sigma_N]$.

The variable $\Sigma(t)$ performs a discrete-time Markov process, whose transition probabilities from time t to $t+1$ differ in various cases, which will be specified in the following.

2.2 Case I: two against one

The first case investigated, which we will sometimes call "two against one", generalises and simultaneously simplifies the various versions introduced in [11]. The main difference is in the fact that we will change at maximum *one* agent at each time step. This may not significantly change the behaviour, as the various choices of neighbourhood in [11] exhibit only little difference.

Our algorithm will iterate the following three steps. First, choose randomly an agent i. Then, choose randomly one of its neighbours, say j. If $\sigma_i(t) \neq \sigma_j(t)$, nothing happens. However, if $\sigma_i(t) = \sigma_j(t)$, we will choose randomly one of the common neighbours of both i and j, say k, and set $\sigma_k(t+1) = \sigma_i(t)$. We may also write it schematically as reactions AAB $\rightarrow$ AAA, BBA $\rightarrow$ BBB.

2.3 Case II: Ochrombel simplification

In this case, we do not need to have two neighbours in the same state. Everybody can influence each of its neighbours. We choose an agent i at random. Then, choose j randomly among neighbours and set $\sigma_j(t+1) = \sigma_i(t)$. Therefore, the process may be written as AB $\rightarrow$ AA, BA $\rightarrow$ BB. In fact, on fully connected network the Ochrombel simplification is equivalent to voter model, whose dynamical properties were studied *e.g.* in [42].

As an obvious observation we can note that both in case I and case II the uniform states, with all σ_i equal, are stable under the dynamics. However, we can expect variety of metastable states in the case I, in which there are no pairs of neighbours in the same state, therefore the dynamics does not proceed any further.

3 On a fully-connected network

We will approximate the complex social network by the fully-connected network (the complete graph) of N nodes. Here, any two agents are neighbours; in the case I we simply choose three agents i, j, k at random and in the case II two agents i, j at random. Note that the order in which

they are chosen matters. This makes our process different *e.g.* from the majority [47] or majority-minority [48] models, although on fully connected network the difference may consist only in rescaling certain variables.

We will call this setup a mean-field approximation in the same sense as the Ising model on the complete graph can be considered as an approximation for Ising model on hypercubic lattice of high dimensionality. Of course this is not a good approximation to the original one-dimensional formulation of the Sznajd model [2], but we believe it is appropriate for much more realistic studies of Sznajd model on complex networks [4,16,23]. We refer the reader to Appendix A for a more formal definition of the Sznajd model on an arbitrary graph.

In fully-connected network the state of the system is fully described by the occupation numbers $N_\sigma = \sum_{i=1}^{N} \delta_{\sigma_i \sigma}$, or equivalently the densities $n_\sigma = N_\sigma/N$, for each opinion $\sigma \in S$. The dynamics of these occupation numbers fully describes the evolution of the system. As the total number of nodes is conserved, there are $q-1$ independent dynamical variables.

Let us start with the case II (Ochrombel simplification) with only two opinions, $q = 2$. The variable σ can assume only two values, denoted $\sigma = \pm 1$ for convenience. Indeed, we are effectively working with Ising spins. The state is described by one dynamical variable only, which will be taken as a "magnetisation",

$$m = \frac{N_+ - N_-}{N}. \tag{1}$$

In one step of the dynamics, three events can happen. The magnetisation may remain constant or it can change by $\pm 2/N$. The probabilities of these three events can be easily calculated

$$\begin{aligned}
\mathrm{Prob}\left\{ m \to m + \frac{2}{N} \right\} &= \frac{1}{4}\left(1-m^2\right)\left(1 + \frac{1}{N-1}\right) \\
\mathrm{Prob}\left\{ m \to m - \frac{2}{N} \right\} &= \frac{1}{4}\left(1-m^2\right)\left(1 + \frac{1}{N-1}\right) \\
\mathrm{Prob}\left\{ m \to m \right\} &= \left(\frac{1}{2}\left(1+m^2\right) - \frac{1}{N}\right) \\
&\quad \times \left(1 + \frac{1}{N-1}\right).
\end{aligned} \tag{2}$$

Our objective is writing the master equation for the probability density of the random variable $m(t)$, which we denote P_m. It can be found easily in the thermodynamic limit $N \to \infty$. Indeed, we find that the time should be rescaled as

$$t = N^2 \tau \tag{3}$$

in the thermodynamic limit. Then the probability density evolves according to the partial differential equation

$$\frac{\partial}{\partial \tau} P_m(m,\tau) = \frac{\partial^2}{\partial m^2}\left[\left(1-m^2\right) P_m(m,\tau)\right]. \tag{4}$$

The latter equation describes in principle fully the evolution of the Sznajd model in Ochrombel simplification on a complete graph. It has the form of a diffusion equation with position-dependent diffusion constant.

Let us turn now to the case I (original Sznajd model), again with $q = 2$. We may repeat step by step the considerations made above for the case II. Namely, our dynamical variable will be again the magnetisation m which may either remain unchanged or change by $\pm 2/N$ in one step. For the probabilities of these events we can find formulae analogous to (2)

$$\begin{aligned}
\mathrm{Prob}\left\{ m \to m + \frac{2}{N} \right\} &= \frac{\left(1-m^2\right)}{8}\left(1 + m + \frac{1+3\,m}{N}\right) \\
\mathrm{Prob}\left\{ m \to m - \frac{2}{N} \right\} &= \frac{\left(1-m^2\right)}{8}\left(1 - m + \frac{1-3\,m}{N}\right) \\
\mathrm{Prob}\left\{ m \to m \right\} &= 1 - \frac{\left(1-m^2\right)}{4}\left(1 + \frac{1}{N}\right)
\end{aligned} \tag{5}$$

where the terms of order $1/N^2$ are neglected. Note that the probabilities of changes $\pm 2/N$ are not symmetric, contrary to the previous case (II). This fact has all-important consequences. We will see later that it is responsible for the fact that the original Sznajd model exhibits phase transition, while in Ochrombel simplification the transition is absent.

A more immediate consequence is that the time must be rescaled differently, in order to get sensible thermodynamic limit, namely

$$t = 2N\,\tau. \tag{6}$$

The second consequence is that the equation for $P_m(m,\tau)$ contains *first* derivative with respect to m, representing a pure drift in magnetisation:

$$\frac{\partial}{\partial \tau} P_m(m,\tau) = -\frac{\partial}{\partial m}\left[(1-m^2) m\, P_m(m,\tau)\right]. \tag{7}$$

Contrary to the previous case (4) the diffusion term, containing the second derivative in m, represents only the finite-size correction to the drift term. However, this correction may dominate close to points $m = \pm 1$ and $m = 0$ where the drift velocity becomes zero.

Next case investigated will be the case II with arbitrary value of q. Moreover, we will assume that the number of opinions is large, $q \gg 1$. Let us define the distribution of occupation numbers

$$D(n) = \frac{N}{q} \sum_{\sigma=1}^{q} \delta\left(n - n_\sigma\right) \tag{8}$$

where $\delta(x) = 1$ for $x = 0$ and zero elsewhere. It would be much more difficult to write the full dynamic equation for $D(n)$. Therefore, we use the approximation which replaces the distribution $D(n)$ by its configuration average $P_n(n) = \langle D(n) \rangle$. In the limit $N \to \infty$ and $q \to \infty$ and substituting the variable $x = 2n - 1$ we arrive at the equation

$$\frac{\partial}{\partial \tau} P_n(x,\tau) = \frac{\partial^2}{\partial x^2}\left[\left(1-x^2\right) P_n(x,\tau)\right]. \tag{9}$$

The time is rescaled again according to the equation (3). We can see that the equations (4) and (9) have identical form, although the interpretation of variables is different. We can therefore solve the two cases simultaneously. This will be performed in the next section.

4 Solution of the dynamics

4.1 Two against one: case I

The case I, $q = 2$ is described by the equation

$$\frac{\partial}{\partial \tau} P(x,\tau) = -\frac{\partial}{\partial x}\left[(1-x^2)x\, P(x,\tau)\right]. \qquad (10)$$

It can be easily verified that the solution has the following general form

$$P(x,\tau) = [(1-x^2)x]^{-1}\, f\left(\mathrm{e}^{-\tau}\, \frac{x}{\sqrt{1-x^2}}\right) \qquad (11)$$

for arbitrary function $f(y)$. The form of the function $f(y)$ is given by initial conditions. For example if the initial condition is a δ-function, it keeps the same form during the evolution, only the location shifts in time. This way we could in principle calculate, how long it takes to reach the edges of the interval from given initial position. This would be the time to reach the stationary state. However, it comes out that the time needed blows up. The reason comes from the infinite-size limit $N \to \infty$. Indeed, very close to the points $x = \pm 1$ the finite-size effects take over.

We can estimate the average time needed to reach the stationary state in finite system by the following consideration. In fact, the equation (10) describes the drift which pushes the system toward the stationary state, but neglects the effect of diffusion, which becomes important at a distance $\sim 1/N$ from the points $x = \pm 1$. Therefore, we must calculate the time necessary for the drift to drive the system to the point $\pm(1 - 1/N)$. The initial fraction p of opinions $+1$ corresponds to the initial condition $x_0 = 2p - 1$ and from the formula (11) we have the following estimate for the average time $\langle \tau_{\mathrm{st}} \rangle$ to reach the stationary state

$$\langle \tau_{\mathrm{st}} \rangle \simeq -\ln\left(\frac{|2p-1|}{\sqrt{p(1-p)}}\, \frac{1}{\sqrt{N}}\right). \qquad (12)$$

It is also possible to include the correction terms of order $O(1/N)$ into equation (10) and deduce the equation for the average time to reach the absorbing state $\langle \tau_{\mathrm{st}} \rangle(x_0)$ on condition that the process started at initial position x_0. Following the general scheme [49] we obtain a second-order ordinary differential equation

$$\left(1+\frac{3}{N}\right)\left(1-{x_0}^2\right) x_0\, \frac{\mathrm{d}}{\mathrm{d}x_0}\langle \tau_{\mathrm{st}} \rangle (x_0) + \frac{1}{N}\left(1-{x_0}^2\right)\, \frac{\mathrm{d}^2}{\mathrm{d}{x_0}^2}\langle \tau_{\mathrm{st}} \rangle (x_0) = -1. \qquad (13)$$

The solution of (13) is

$$\langle \tau_{\mathrm{st}} \rangle (x_0) = N \int_{-1}^{x_0} \int_{y}^{0} \frac{\mathrm{e}^{\frac{N+3}{2} z^2}}{1-z^2} \mathrm{d}z\; \mathrm{e}^{-\frac{N+3}{2} y^2}\, \mathrm{d}y. \qquad (14)$$

Indeed, for x_0 not too close to either of the points $x_0 = -1, 0, 1$ (the distance must be large compared to $1/N$) we obtain from the formula (14) an approximate expression of the form given in (12). Another way to obtain the same p dependence as in (12) is to omit the $O(1/N)$ terms in the equation (13) and solve the first-order differential equation. In this case, however, we lose any information about the dependence on N. We should also note that a result essentially equivalent to equation (12) was obtained also in [47].

It is rather interesting to observe that the deterministic dynamics of Galam model [34,36] leads to a formula very similar to (12), while the interpretation of the time variable is totally different: in Galam model it represents the number of hierarchical levels on which the majority rule is iterated.

It would be desirable to calculate the full probability distribution for the time to reach the stationary state τ_{st} and not only the average. That is possible using again the formalism of adjoint equation [49], when we introduce the $1/N$ corrections to equation (10) but the resulting partial differential equation is difficult to solve explicitly. Instead, we estimate the exponential tail of the distribution by a simple consideration.

Indeed, after the drift had pushed the system to the state in which there is only single spin -1 immersed in a sea of all $+1$-s it finally comes into uniform stationary state if the first pair of spins chosen is both $+1$ and the third one is the single -1. This choice has probability $\simeq 1/N$. Therefore, the relaxation time toward the uniform state is $t_{\mathrm{relax}} \simeq N$ and using the scaling (6) we have for the tail of the distribution

$$P(\tau_{\mathrm{st}}) \sim \exp(-\frac{\tau_{\mathrm{st}}}{\tau_{\mathrm{relax}}}), \quad \tau_{\mathrm{st}} \to \infty \qquad (15)$$

with

$$\tau_{\mathrm{relax}} \simeq \frac{1}{2}. \qquad (16)$$

The most important observation we can draw from the solution (11) is the presence of the dynamic phase transition, as observed in numerical simulations. Indeed, starting with any fixed positive magnetisation, we have initial condition $P(x,0) = \delta(x - x_0)$, $x_0 > 0$, and the drift expressed by equation (11) always take us to the state with all agents having opinion $+1$, while from any state with negative magnetisation the drift leads the system eventually to the state with all agents having opinion -1 and the probability of ending in the state of all $+1$ is therefore $P_+ = \theta(p - 1/2)$. The possible deviations from this rule close to the zero magnetisation (*i.e.* $p = 0.5$) are due to the finite size effects, which are neglected in (10). The presence of the phase transition is also indicated by the divergence of the average time to reach the stationary state (12) for $p \to 1/2$.

4.2 Ochrombel simplification: case II

The equation

$$\frac{\partial}{\partial\tau}P(x,\tau)=\frac{\partial^2}{\partial x^2}\left[(1-x^2)\,P(x,\tau)\right] \qquad (17)$$

describes both the case II, $q=2$ and II, $q\gg 1$, only the interpretation of the variable x differ: in the former case it corresponds to the magnetisation, while in the latter case it is shifted percentage of votes. By solving equation (17) we treat simultaneously both cases.

The equation of the form (17) was already studied in variety of contexts, *e.g.* population genetics [50,51] or reaction kinetics [52] and can be tackled by standard methods developed for Fokker-Planck equation.

Indeed, we look for the solution using the expansion in eigenvectors. We can write (17) it in the form $\frac{\partial}{\partial\tau}P(x,\tau)=\mathcal{L}P(x,\tau)$ where the linear operator $\mathcal{L}$ acts as $(\mathcal{L}f)(x)=\frac{\partial^2}{\partial x^2}\left[(1-x^2)\,f(x)\right]$. We therefore need to find the set of eigenvectors of $\mathcal{L}$. Denoting $\Phi_c(x)$ the eigenvector corresponding to the eigenvalue $-c$, we have the following equation

$$(1-x^2)\,\Phi_c''(x)-4x\,\Phi_c'(x)+(c-2)\,\Phi_c(x)=0. \qquad (18)$$

The full solution of (17) can be then expanded as

$$P(x,\tau)=\sum_c A_c\mathrm{e}^{-c\tau}\,\Phi_c(x) \qquad (19)$$

with coefficients A_c determined from the initial condition.

Important question to be settled prior to the attempt for solution is, what is the appropriate space of functions $\Phi(x)$. First, the interpretation of these functions as probability densities sets the requirement that it must be normalisable: $\int\Phi(x)\,\mathrm{d}x<\infty$. Second, only the interval $x\in[-1,1]$ is relevant, so $\Phi(x)=0$ outside this interval. Finally, we should anticipate the possibility that δ-functions appear in the solution, namely located at $x=\pm1$, because the uniform states, with all sites carrying the same spin value, are stable under the dynamics.

We therefore look for the solution of (18) in the space of distributions (*i.e.* linear functionals on sufficiently differentiable functions) with support restricted to the interval $[-1,1]$.

It is straightforward to find the eigenvectors corresponding to eigenvalue $c=0$, *i.e.* the stationary solutions of equation (17). They are composed of δ-functions only. In fact, the corresponding eigensubspace is two-dimensional and the base vectors can be chosen as

$$\Phi_{01}=\delta(x-1),\quad \Phi_{02}=\delta(x+1). \qquad (20)$$

For $c\neq0$ we first decompose the solution in ordinary function of x plus a pair of δ-functions, namely

$$\Phi_c=\phi_{c+}\,\delta(x-1)+\phi_{c-}\,\delta(x+1)+\phi_c(x)\,\theta(x-1)\,\theta(x+1) \qquad (21)$$

where ϕ_{c+} and ϕ_{c-} are real numbers and $\phi_c(x)$ is a real doubly differentiable function. Then, equation (18) translates into equation for $\phi_c(x)$

$$(1-x^2)\,\phi_c''(x)-4x\,\phi_c'(x)+(c-2)\,\phi_c(x)=0 \qquad (22)$$

accompanied by two other conditions

$$\lim_{x\to\pm1}\phi_c(x)=-\frac{c}{2}\,\phi_{c\pm}. \qquad (23)$$

The general solution of equation (22) exhibits behaviour $\phi_c(x)\sim(1\mp x)^\alpha$ at $x\to\pm1$, where either $\alpha=0$ or $\alpha=-1$. However, the latter case should be excluded, as it gives non-normalisable probability distribution. In fact it is the condition of normalisability that determines all possible eigenvalues c. The solution of (22) with correct behaviour at $x\to\pm1$ can be expressed in Gegenbauer polynomials [52–54]. The eigenvalues are $c=c_l\equiv(l+1)(l+2)$ for $l=0,1,2,...$ An elementary solution and the table of several lowest polynomials is presented in Appendix B.

It is important to note that for any eigenvalue $c>0$ we have

$$\int\Phi_c(x)\,\mathrm{d}x=0\qquad\int x\,\Phi_c(x)\,\mathrm{d}x=0. \qquad (24)$$

The consequence is that both $\int P(x,\tau)\mathrm{d}x$ and $\int xP(x,\tau)\mathrm{d}x$ are independent of time. While the first conservation law expresses simply the conservation of probability, the second one is a non-trivial consequence of the model dynamics. Mathematically it is related to the fact that the eigenspace corresponding to zero eigenvalue is two-dimensional.

Thus, we found the set of *right* eigenvectors of the operator $\mathcal{L}$. For practical solution we still need to establish the coefficients A_c in equation (19). To this end we need also the set of *left* eigenvectors of $\mathcal{L}$, checking simultaneously that the set of left and right eigenvalues coincide. First, we need to establish the adjoint operator to $\mathcal{L}$, defined by usual relation $(\mathcal{L}f|g)=(f|\mathcal{L}^Tg)$. While $\mathcal{L}$ acts on the space of distributions, its adjoint $\mathcal{L}^T$ acts on the corresponding dual space, which is the space of sufficiently differentiable functions. Straightforward algebra gives $(\mathcal{L}^Tg)(x)=(1-x^2)\,g''(x)$ which implies the following equation for the left eigenvectors

$$(1-x^2)\,\psi_c''(x)+c\,\psi_c(x)=0. \qquad (25)$$

We find again that for $c=0$ the eigensubspace is two-dimensional. We can choose the basis vectors so that they are mutually ortho-normal to the pair of right eigenvectors (20), namely

$$\psi_{01}=\frac{1}{2}(1+x),\quad \psi_{02}=\frac{1}{2}(1-x). \qquad (26)$$

The solutions of (25) for $c>0$ with proper boundary conditions are again polynomials presented in more detail in Appendix B.

The coefficients in the solution (19) with initial condition $P(x,0)=P_0(x)$ are then calculated as

$$A_c=\frac{\int P_0(x)\psi_c(x)\,\mathrm{d}x}{\int\phi_c(x)\psi_c(x)\,\mathrm{d}x}. \qquad (27)$$

From the solution (19) we can deduce an important feature for the distribution of waiting times needed to reach the stationary state. Indeed, if $P_{\rm st}(\tau)$ is the probability density for ending at time τ in the stationary frozen configuration with all agents in the same state, we can express the probability that the stationary configuration was not reached before time τ as

$$P_{\rm st}^{>}(\tau) \equiv \int_{\tau}^{\infty} P_{\rm st}(\tau')\mathrm{d}\tau' = 1 - \lim_{\epsilon\to 0^+}\left(\int_{-1-\epsilon}^{-1+\epsilon} + \int_{1-\epsilon}^{1+\epsilon}\right) P(x,\tau)\mathrm{d}x. \quad (28)$$

We can see that only the δ-function components of the eigenvectors $\Phi_c(x)$ in the expansion (19) contribute to $P_{\rm st}^{>}(\tau_{\rm st})$. More explicitly, we find

$$P_{\rm st}^{>}(\tau) = \sum_{c>0} 2A_c\,\frac{\phi_c(-1)+\phi_c(1)}{c}\,\mathrm{e}^{-c\tau}. \quad (29)$$

As the spectrum of eigenvalues is discrete, for long times only the lowest non-zero c (equal to $c_0 = 2$) is relevant. Therefore, the distribution of waiting times will have an exponential tail $P_{\rm st}^{>}(\tau) \sim \mathrm{e}^{-2\tau},\ \tau\to\infty$. For initial condition $P_0(x) = \delta(x - x_0)$ we can easily compute also the prefactor in the leading term for large τ. Indeed, from (27) we get A_2 and finally obtain

$$P_{\rm st}^{>}(\tau) \simeq \frac{6}{4}(1-x_0^2)\,\mathrm{e}^{-2\tau},\ \tau\to\infty. \quad (30)$$

As the functions $\phi_c(x)$ are odd for $c = c_l$ with odd l, we should expect that the corrections to the formula (30) will be governed by the second next eigenvalue $c_2 = 12$. We will see later how it can be checked in numerical simulations.

As in the case I the average time $\langle\tau_{\rm st}\rangle(x_0)$ to reach the absorbing state when starting at position x_0 can be obtained, using the general formalism [49], from the equation

$$\left(1-{x_0}^2\right)\frac{\mathrm{d}^2}{\mathrm{d}{x_0}^2}\langle\tau_{\rm st}\rangle(x_0) = -1 \quad (31)$$

which can be solved easily

$$\langle\tau_{\rm st}\rangle(x_0) = -\frac{x_0}{2}\ln\frac{1+x_0}{1-x_0} - \frac{1}{2}\ln\frac{1-{x_0}^2}{4} \quad (32)$$

(see also [52,53]). The method of adjoint equation [49,53] can be used to calculate the distribution of times to reach the absorbing state, when starting from initial position at $x = x_0$, yielding results equivalent to our direct calculation. Indeed, inserting the initial condition $P_0(x) = \delta(x - x_0)$ into (27) we can see that the expression (29) represents an expansion in the eigenvectors $\psi_c(x_0)$ of the adjoint operator $\mathcal{L}^T$ taken at point x_0.

Contrary to the case I, we do not observe any phase transition here. This is due to the conservation of average magnetisation in the dynamics [47]. From this fact it follows immediately that $P_+ = p$. This result can be confirmed by an explicit calculation. Starting with fixed magnetisation $x_0 = 2p - 1$, the initial condition $P(x,0) = \delta(x - x_0)$ broadens under the diffusive dynamics (17) and leaves always non-zero probability of ending in either of the possible stationary states. We already noted that $\int x\,P(x,\tau)\,\mathrm{d}x$ is independent of time under the dynamics (17). Therefore, the asymptotic state is the following combination of the eigenvectors (20) with $c = 0$

$$\lim_{\tau\to\infty} P(x,\tau) = \frac{1-x_0}{2}\,\delta(x+1) + \frac{1+x_0}{2}\,\delta(x-1) \quad (33)$$

and the probability of ending in the state of all $+1$ is therefore simply $P_+ = p$.

4.3 Distribution of votes

As already stressed in Section 3, equation (17) describes also the evolution of the distribution of votes in the case of $q \gg 1$ parties. We will present an argument how our results may explain the empirical data, suggesting the $1/n$ law for the distribution of votes.

As stressed in the discussion following equation (23), the time-independent solutions of equation (17) can behave either as $1 + x$ or $(1 + x)^{-1}$ in the limit $x \to -1$. However, the latter case was excluded by the requirement of normalisability of the probability density. On the other hand, relaxing the normalisability condition, the functions

$$\tilde{\phi}_{01}(x) = \frac{1}{1+x} \quad (34)$$

$$\tilde{\phi}_{02}(x) = \frac{1}{1-x} \quad (35)$$

are solutions of (22) with eigenvalue $c = 0$. (Of course, any linear combination of them is also solution with $c = 0$.)

How should be any of these additional solutions interpreted? The zero eigenvalue suggest that the function is stationary in time. However, it is not normalisable, therefore this solution cannot be reached from any initial condition. But if the distribution $P_n(x,\tau)$ is close to $\tilde{\phi}_{01}(x)$ (or $\tilde{\phi}_{02}(x)$) in some interval I of x, it is probable that it $P_n(x,\tau)$ will remain close to (34) (or (35), respectively) for certain period of time, while the interval I will gradually shrink and eventually disappear. Therefore, we may suggest (34) and (35) as a metastable states, or long-lived transient states.

This may explain the observation from simulations performed in [4]. In this work, the distribution of the type $1/n$ is obtained in a suitably chosen transient regime, in certain range of n. As $x = 2n - 1$, the behaviour of (34) at $x \to -1$ corresponds precisely to $1/n$ behaviour for small n.

A slightly more rigorous variant of the above argument is also possible. Imagine now that the political system represented by the set of opinions S is not closed, but new opinions may appear, replacing other ones which vanish.

Indeed, the current induced by the dynamics of case II can be read off from equation (17)

$$j = -\frac{\partial}{\partial x}[(1-x^2)P(x,\tau)] \quad (36)$$

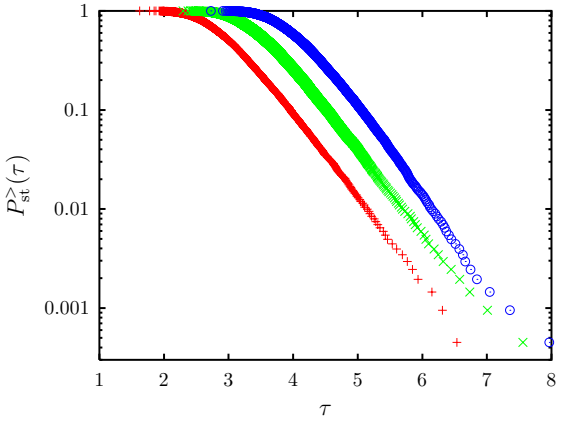

Fig. 1. Probability of reaching the stationary state in time larger than τ, for case I, $q = 2$, $N = 2000$. The values of initial fraction p of opinions $+1$ are 0.1 (+) 0.2 (×) and 0.7 (⊙).

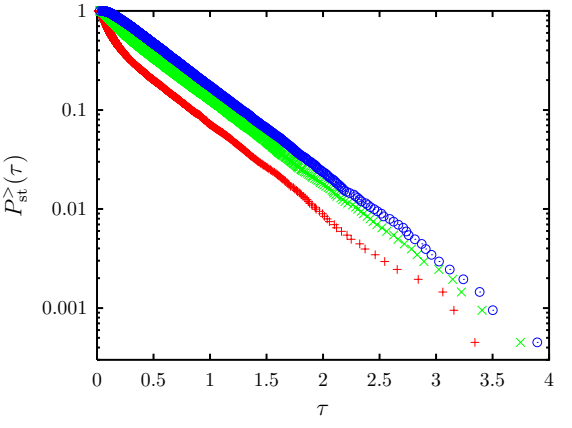

Fig. 2. Probability of reaching the stationary state in time larger than τ, for case II, $q = 2$, $N = 2000$. The values of initial fraction p of opinions $+1$ are 0.1 (+) 0.2 (×) and 0.7 (⊙).

and by insertion of the solution (34) we deduce that there is homogeneous flow $j = +1$ outward the value $x = -1$, *i.e.* $n = 0$. We may interpret this flow as a consequence of an external source placed somewhere close to the point $x = -1$, *i.e.* $n = 0$. Such a source accounts for the influx of new opinions, or new parties, into the system. It is very reasonable to assume that the source is placed at very small values of n, as new subjects are likely to gain little support initially.

5 Comparison with numerical simulations

We performed numerical simulations of the Sznajd model on fully connected network according to algorithms described in Sections 2.2 (case I) and 2.3 (case II). The main focus was on the dynamical properties, namely the distribution of times needed to reach the homogeneous stationary state. We show in Figures 1 and 2 the probabilities $P^{>}_{\rm st}(\tau)$ that the time $\tau_{\rm st}$ to reach the stationary state is larger that τ. We can clearly see that the probability decays exponentially with τ in both cases I and II.

Let us discuss the case I first. Following the analytical expectation (15) we can fit the exponential tail of the distribution as

$$P^{>}_{\rm st}(\tau) \simeq \exp\left(-\frac{\tau - \langle\tau_{\rm st}\rangle}{\tau_{\rm relax}}\right), \quad \tau \to \infty. \qquad (37)$$

The results for $\langle\tau_{\rm st}\rangle$ can be seen in Figure 3, compared with the analytical prediction of equation (12). Similarly in Figure 4 we can compare the fitted relaxation time with the analytical result. Both $\langle\tau_{\rm st}\rangle$ and $\tau_{\rm relax}$ agree satisfactorily with the analytical predictions. The deviations around the value $p = 0.5$ are due to finite size effects; the comparison of the results for system sizes $N = 2000$ and $N = 4000$ supports this interpretation. From equation (12) we can see that $\langle\tau_{\rm st}\rangle$ diverges logarithmically for $N \to \infty$. This is confirmed by the simulation data which fall onto single curve in Figure 3 for different system sizes.

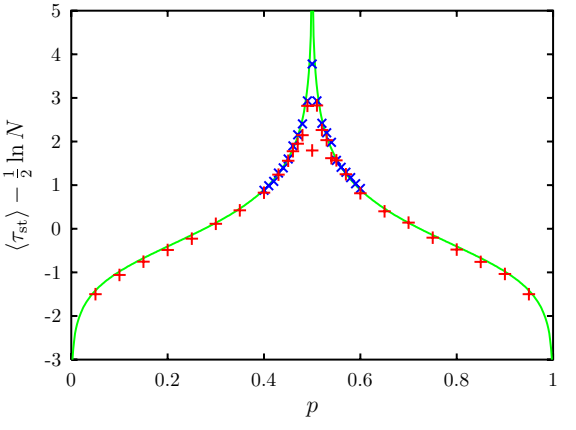

Fig. 3. Average time of reaching the stationary state in dynamics of case I, $q = 2$. The system size is $N = 2000$ (+) and $N = 4000$ (×). The line is the analytic prediction of equation (12)

Now let us turn to the case II. The equation (29) yields the leading term in the tail of the distribution $P^{>}_{\rm st}(\tau)$ and in principle also the corrections to it. As the functions $\phi_c(x)$ are odd for $c = c_l$ with odd l, the next non-zero correction will come from the eigenvalue $c_2 = 12$. Therefore, we expect the behaviour

$$P^{>}_{\rm st}(\tau) \simeq \exp\left(-\frac{\tau - \tau_0}{\tau_{\rm r0}}\right) + a_1 \exp(-\frac{\tau}{\tau_{\rm r1}}),\ \tau \to \infty \qquad (38)$$

with

$$\tau_{\rm r0} = \frac{1}{2}, \quad \tau_{\rm r1} = \frac{1}{12}. \qquad (39)$$

As in the initial condition $P_0(x) = \delta(x - x_0)$ we have $x_0 = 2p - 1$, we can deduce from equation (30) the following estimate

$$\tau_0 \simeq \ln\sqrt{6\,p\,(1-p)}. \qquad (40)$$

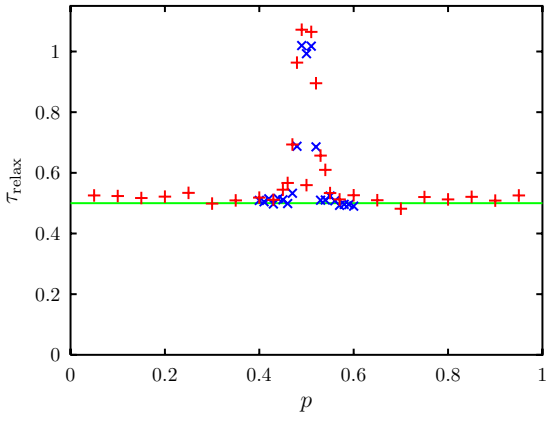

Fig. 4. Relaxation time toward the stationary state in dynamics of case I, $q = 2$. The system size is $N = 2000$ (+) and $N = 4000$ (×). The horizontal line is the analytic prediction of equation (16).

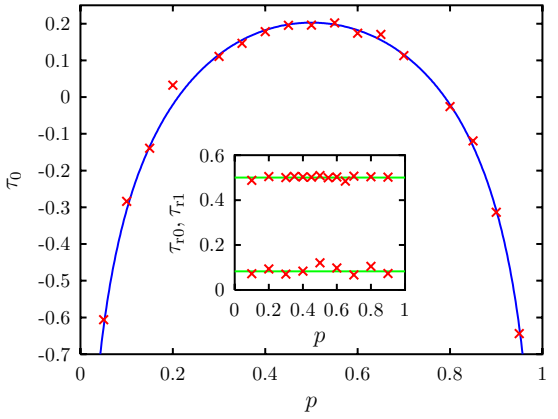

Fig. 5. The fitted parameter τ_0 for reaching the stationary state in dynamics of case II, $q = 2$. The system size is $N = 2000$. The line represents the formula (40). In the inset, the fitted first two relaxation times $\tau_{\rm r0}$ and $\tau_{\rm r1}$ are shown. The horizontal lines are corresponding analytical predictions from equation (39).

We can see from Figure 5 that it corresponds well to the numerical data. In the inset of Figure 5 we can also see the fitted relaxation times $\tau_{\rm r0}$ and $\tau_{\rm r1}$. Also here the correspondence with analytical prediction (39) is good.

6 Conclusions

We formulated a mean-field version of the Sznajd model of opinion formation by putting it on a complete graph. Solving the underlying diffusion equations we found analytical results for several dynamical properties, as well as exact long-time asymptotics. The results differ substantially in the two cases studied: first, the original Sznajd model, where a cluster of identical opinions is necessary to persuade others to join them, and second, the Ochrombel simplification, where also isolated agent can persuade others. Dynamical phase transition was found analytically in the original Sznajd model, while in the Ochrombel version it is absent. This finding agrees with previous numerical results.

The approach to stationary state was the main concern of our calculations. We found that the distribution of times to reach the stationary state has an exponential tail which we were able to calculate analytically. In the case of Ochrombel simplification, we obtained also the corrections and a formula which gives in principle the whole distribution. We compared the analytical results for the tail (and in the Ochrombel case also for the first correction) with numerical simulations and we found good agreement. The method of adjoint equation enabled us to find analytically the average time to reach the stationary state, in both cases.

We found also another signature of the phase transition in the original Sznajd model, expressed by the divergence of the average time to reach the stationary state. Contrary to the Ochrombel case, in the original Sznajd model the average time needed for reaching the stationary state blows up logarithmically with increasing system size. This finding was also confirmed in our numerical simulations.

The analytical treatment provided an explanation of the $1/n$ distribution of votes, documented in Brazilian elections. We found that this behaviour corresponds to long-lived transient state of the dynamics of the Sznajd model with large number of possible opinions, or alternatively to the dynamics of an open version of the Sznajd model, where new opinions may continuously emerge.

This work was supported by the project No. 202/01/1091 of the Grant Agency of the Czech Republic.

Appendix A: Sznajd model on an arbitrary social network

Our system is composed of N agents placed on nodes of a social network, represented by the graph $\Lambda = (\Gamma, E)$ where Γ is the set of nodes and E set of edges, *i.e.* unordered pairs of nodes. For a node $i \in \Gamma$ we denote $\Gamma_i = \{j \in \Gamma | (i,j) \in E\}$ the set of neighbours of i.

The opinion of the agent i s denoted σ_i. The state of the system is described by the set of opinions of all the agents, $\Sigma = [\sigma_1, \sigma_2, ..., \sigma_N] \in S^\Gamma$. The variable $\Sigma(t)$ performs a discrete-time Markov process, defined as follows.

In the case I we iterate the following three steps. First, choose $i \in \Gamma$ at random. Then, choose $j \in \Gamma_i$ randomly among neighbours of i. If $\sigma_i(t) \neq \sigma_j(t)$, nothing happens. However, if $\sigma_i(t) = \sigma_j(t)$, we will choose randomly one of the common neighbours $k \in \Gamma_i \cap \Gamma_j \setminus \{i,j\}$ and set $\sigma_k(t+1) = \sigma_i(t)$.

In the case II we choose $i \in \Gamma$ at random. Then, choose $j \in \Gamma_i$ randomly among neighbours and set $\sigma_j(t+1) = \sigma_i(t)$.

If the graph is random and densely connected, we may approximate it by the complete graph with N nodes, *i.e.* for each pair of nodes $i, j \in \Gamma$ there is an edge connecting them, $(i, j) \in E$. It means that the set of neighbours of a node $i \in \Gamma$ is $\Gamma_i = \Gamma \setminus \{i\}$. This is a kind of a mean-field approximation.

Appendix B: Finding the eigenvectors

We can look for the solution of the equation (22) in the form of power series

$$\phi_c(x) = \sum_{l=0}^{\infty} b_l \, x^l \tag{B.1}$$

and find the recurrence relation for the coefficients

$$b_{l+2} = \left(1 - \frac{c}{(l+1)(l+2)}\right) b_l. \tag{B.2}$$

We should distinguish two cases. Either the sequence of coefficients b_l contains non-zero values for arbitrarily large l, or it is truncated at some order and (B.1) becomes a polynomial. In the former case the solution behaves as $\phi_c(x) \sim (1-x^2)^{-1}$ at $x \to \pm 1$ and must be excluded. The latter case is possible only if

$$c = c_l \equiv (l+1)(l+2) \tag{B.3}$$

for some $l \geq 0$. Moreover, in order to have a solution in the form of a polynomial, we require that $b_1 = 0$ if l in the equation (B.3) is even, and $b_0 = 0$ if l in the equation (B.3) is odd. The following table lists the solution for several lowest eigenvalues (taking $b_0 = 1$ for even l and $b_1 = 1$ for odd l).

l	c_l	$\phi_c(x)$
0	2	1
1	6	x
2	12	$1 - 5x^2$
3	20	$x - \frac{7}{3}x^3$
4	30	$1 - 14x^2 + 21x^4$
$\vdots$	$\vdots$	$\vdots$

(B.4)

In fact, up to a multiplicative constant, the functions $\phi_c(x)$ are Gegenbauer polynomials [53,54].

The same procedure can be used for finding the eigenvectors of the adjoint operator, solving equation (25). We expand the function $\psi_c(x)$ in power series

$$\psi_c(x) = \sum_{l=0}^{\infty} d_l \, x^l \tag{B.5}$$

and find the recurrence relation for the coefficients

$$d_{l+2} = \frac{(l-1)l - c}{(l+1)(l+2)} \, d_l. \tag{B.6}$$

Again we conclude that the only acceptable values of c are given by condition $c = c_l \equiv (l+1)(l+2)$ for $l = 0, 1, 2, ...$ and in this case the eigenvectors are polynomials of order $l+2$ in the variable x. The following table lists the solution for lowest eigenvalues (taking $d_0 = 1$ for even l and $d_1 = 1$ for odd l).

l	c_l	$\psi_c(x)$
0	2	$1 - x^2$
1	6	$x - x^3$
2	12	$1 - 6x^2 + 5x^4$
3	20	$x - \frac{10}{3}x^3 + \frac{7}{3}x^5$
4	30	$1 - 15x^2 + 35x^4 - 21x^6$
$\vdots$	$\vdots$	$\vdots$

(B.7)

It is important to note that the set of right eigenvalues coincides with the set of left eigenvalues, which proves consistency of our approach.

Note that neither $\phi_c(x)$ nor $\psi_c(x)$ are orthogonal polynomials. Instead, they are mutually orthogonal, *i.e.* $\int_{-1}^{1} \phi_c(x)\psi_{c'}(x)\mathrm{d}x = 0$ for $c \neq c'$. This is due to the fact that the operator $\mathcal{L}$ is not self-adjoint.

References

1. *Modeling Complexity in Economic and Social Systems*, edited by F. Schweitzer (World Scientific, Singapore, 2002)
2. K. Sznajd-Weron, J. Sznajd, Int. J. Mod. Phys. C **11**, 1157 (2000)
3. T.M. Liggett, *Stochastic Interacting Systems: Contact, Voter, and Exclusion Processes* (Springer, Berlin, 1999)
4. A.T. Bernardes, D. Stauffer, J. Kertesz, Eur. Phys. J. B **25**, 123 (2002)
5. A.T. Bernardes, U.M.S. Costa, A.D. Araujo, D. Stauffer, Int. J. Mod. Phys. C **12**, 159 (2001)
6. D. Stauffer, Int. J. Mod. Phys. C **13**, 315 (2002)
7. D. Stauffer, `cond-mat/0207598`
8. D. Stauffer, Adv. Complex Systems **5**, 97 (2002)
9. D. Stauffer, Comput. Sci. Engineering **5**, 71 (2003)
10. A.A. Moreira, J.S. Andrade Jr., D. Stauffer, Int. J. Mod. Phys. C **12**, 39 (2001)
11. D. Stauffer, A.O. Sousa, S. Moss de Oliveira, Int. J. Mod. Phys. C **11**, 1239 (2000)
12. D. Stauffer, P.M.C. de Oliveira, `cond-mat/0208296`
13. D. Stauffer, P.M.C. de Oliveira, Eur. Phys. J. B **30**, 587 (2002)
14. D. Stauffer, J. Artificial Soc. Social Simulation **5**, `http://www.soc.surrey.ac.uk/JASSS/5/1/4.html`(2001)
15. A.S. Elgazzar, Int. J. Mod. Phys. C **12**, 1537 (2001)
16. A.S. Elgazzar, Physica A **324**, 402 (2003)
17. K. Sznajd-Weron, Phys. Rev. E **66**, 046131 (2002)
18. K. Sznajd-Weron, R. Weron, Physica A **324**, 437 (2003)
19. C. Schulze, Int. J. Mod. Phys. C **14**, 95 (2003)
20. K. Sznajd-Weron, R. Weron, Int. J. Mod. Phys. C **13**, 115 (2002)

21. C. Schulze, Physica A **324**, 717 (2003)
22. R. Ochrombel, Int. J. Mod. Phys. C **12**, 1091 (2001)
23. J. Bonnekoh, `cond-mat/0305125`
24. L. Sabatelli, P. Richmond, `cond-mat/0305015`
25. D. Stauffer, `cond-mat/0307133`
26. V. Spirin, P.L. Krapivsky, S. Redner, Phys. Rev. E **65**, 016119 (2001)
27. R.N. Costa Filho, M.P. Almeida, J.S. Andrade, Jr., J.E. Moreira, Phys. Rev. E **60**, 1067 (1999)
28. M.L. Lyra, U.M.S. Costa, R.N. Costa Filho, J.S. Andrade Jr., `cond-mat/0211560`
29. R.N. Costa Filho, M.P. Almeida, J.E. Moreira, J.S. Andrade Jr., Physica A **322**, 698 (2003)
30. A.-L. Barabási, R. Albert, Science **286**, 509 (1999)
31. R. Albert, A.-L. Barabási, Rev. Mod. Phys. **74**, 47 (2002)
32. S.N. Dorogovtsev, J.F.F. Mendes, Adv. Phys. **51**, 1079 (2002)
33. S. Galam, Physica A **274**, 132 (1999)
34. S. Galam, Physica A **285**, 66 (2000)
35. S. Galam, Eur. Phys. J. B **25**, 403 (2002)
36. S. Galam, `cond-mat/0307404`
37. E. Ben-Naim, P.L. Krapivsky, S. Redner, Physica D **183**, 190 (2003)
38. F. Vazquez, P.L. Krapivsky, S. Redner, J. Phys. A **36**, L61 (2003)
39. C. Castellano, M. Marsili, A. Vespignani, Phys. Rev. Lett. **85**, 3536 (2000)
40. D. Vilone, A. Vespignani, C. Castellano, Eur. Phys. J. B **30**, 399 (2002)
41. K. Klemm, V.M. Eguíluz, R. Toral, M. San Miguel, Phys. Rev. E **67**, 026120 (2003)
42. E. Ben-Naim, L. Frachebourg, P.L. Krapivsky, Phys. Rev. E **53**, 3078 (1996)
43. I. Dornic, H. Chaté, J. Chave, H. Hinrichsen, Phys. Rev. Lett. **87**, 045701 (2001)
44. M. Mobilia, Phys. Rev. Lett. **91**, 028701 (2003)
45. L. Behera, F. Schweitzer, `cond-mat/0306576`
46. R. Dickman, R. Vidigal, J. Phys. A: Math. Gen. **35**, 1147 (2002)
47. P.L. Krapivsky, S. Redner, Phys. Rev. Lett. **90**, 238701 (2003)
48. M. Mobilia, S. Redner, `cond-mat/0306061`
49. C.W. Gardiner, *Handbook of stochastic methods* (Springer, Berlin, 1985)
50. S. Wright, Proc. Natl. Acad. Sci. USA **31**, 382 (1945)
51. D. Dorninger, H. Langer, Discrete Appl. Math. **6**, 209 (1983)
52. D. ben-Avraham, D. Considine, P. Meakin, S. Redner, H. Takayasu, J. Phys. A: Math. Gen. **23**, 4297 (1990)
53. S. Redner, *A guide to first-passage processes* (Cambridge University Press, Cambridge, 2001)
54. I.S. Gradshteyn, I.M. Ryzhik, *Table of Integrals, Series, and Products*, 5th edn. (Academic Press, 1994)

[SlaSznPrz08]

A Letters Journal Exploring the Frontiers of Physics

April 2008

EPL, **82** (2008) 18006 www.epljournal.org
doi: 10.1209/0295-5075/82/18006

Some new results on one-dimensional outflow dynamics

F. Slanina[1,2], K. Sznajd-Weron[3(a)] and P. Przybyła[3]

[1] *Institute of Physics, Academy of Sciences of the Czech Republic - Na Slovance 2, CZ-18221 Praha, Czech Republic, EU*
[2] *Center for Theoretical Study - Jilská 1, Praha, Czech Republic, EU*
[3] *Institute of Theoretical Physics, University of Wrocław - pl. Maxa Borna 9, 50-204 Wrocław, Poland, EU*

received 12 December 2007; accepted in final form 13 February 2008
published online 26 March 2008

PACS 89.65.-s – Social and economic systems
PACS 05.40.-a – Fluctuation phenomena, random processes, noise, and Brownian motion
PACS 02.50.-r – Probability theory, stochastic processes, and statistics

Abstract – In this paper we introduce a modified version of the one-dimensional outflow dynamics in the spirit of the Sznajd model, which simplifies the analytical treatment. The equivalence between original and modified versions is demonstrated in simulations. Using the Kirkwood approximation, we obtain an analytical formula for the exit probability and we show that it agrees very well with computer simulations in the case of random initial conditions. Moreover, we compare our results with earlier analytical calculations obtained from the renormalization group method and from the general sequential probabilistic frame introduced by Galam and show that our result is superior to the others. Using computer simulations we investigate the time evolution of several correlation functions in order to check the validity of the Kirkwood approximation. Surprisingly, it turns out that the Kirkwood approximation gives correct results even for such initial conditions for which it cannot be easily justified.

Introduction. – Opinion-dynamics models are among the most studied topics in the field of sociophysics [1]. The two-state, or "Ising-like" models have been used since the very beginning [2]. The interest in opinion dynamics was triggered by the works of Galam [3,4] and a large amount of works was produced, including the study of the voter [5,6], Sznajd [7] and majority rule [3,4,8] models. These models have two features in common. First, the complexity of real-world opinions is reduced to the minimum set of two options, $\sigma = +1$ or -1. Second, the individuals bearing these opinions are immobile; they are attached to the sites of a lattice, which may be linear chain, hypercubic lattice, random graph or any of other possibilities. The basic questions asked when studying these models are: what is the probability to reach consensus in opinions, say, all individuals having $\sigma = +1$? and what is the time necessary to reach such consensus?

More specifically, the Sznajd model can be characterised by the outflow dynamics. Contrary to the kinetic Ising model, the information does not spread from the neighbourhood of a chosen site towards that site but, conversely, from a cluster of sites to the neighbourhood of that cluster. In one dimension, the dynamics is defined as follows. If a pair of neighbours at sites x, $x+1$ agree in opinion, $\sigma(x) = \sigma(x+1)$, the two neighbours of the pair adopt the same opinion, *i.e.* $\sigma(x-1) \to \sigma(x)$ and $\sigma(x+2) \to \sigma(x)$. Otherwise the two neighbouring states are unchanged. In higher dimensions and on other lattices the rule is defined analogously.

By now, quite a few results have been accumulated (an interested reader may resort to reviews [1,9–12]). In this letter, we shall address the question: what is the probability P_+ that all of the individuals eventually reach consensus in state, say, +, provided that at the beginning the fraction of + opinions was p? This quantity is commonly called exit probability [13,14]. From the simulations [15], as well as from the exact solution on a complete graph [16] and a renormalisation-group calculation [17] it is known that it is a step function with discontinuity at $p = 0.5$, unless the lattice is a one-dimensional chain. In this case it is a continuous function [18]. Therefore, the one-dimensional case is singular and poses a problem of fundamental interest.

Several analytical approaches have been proposed. We have already mentioned the mean-field solution [16], which, however, is inapplicable in 1D. Later, Galam in [19] presented a general sequential probabilistic frame (GSPF), which extended a series of earlier opinion dynamics

(a) E-mail: kweron@ift.uni.wroc.pl

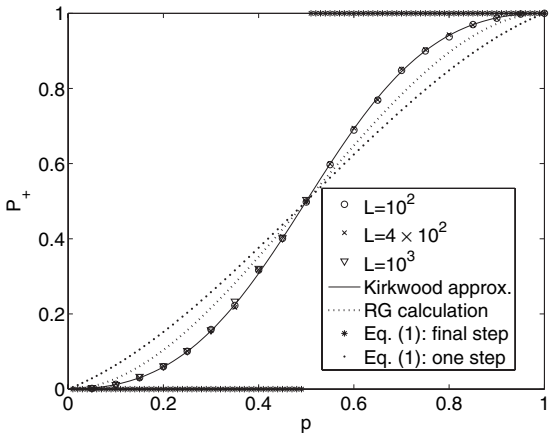

Fig. 1: Exit probability P_+ from the random initial state consisting of the fraction p of up-spins for the modified original outflow dynamics in one dimension for several lattice sizes L. It may be seen that results agree very well with the analytical formula given by eq. (22) obtained from the Kirkwood approximation (solid line). The renormalization group (RG) results obtained in [17] for growing networks and calculations made by Galam within his general sequential probabilistic frame (GSPF) given by eq. (1) agree with simulation results much worse. However, it should be noticed that a one-step update yields much more reasonable results than the final step function obtained by successive iterations of eq. (1). Results obtained for a modified version of the outflow dynamics in which only one neighbour of the central pair is changed are exactly the same. Results are averaged over 10^4 samples.

models. Within his frame, he was able to find analytic formulae for the probability $p(t+1)$ that a randomly chosen agent shares opinion $+$ at time $t+1$ in terms of the same probability $p(t)$ at time t. Among several models, he considered also the same one-dimensional rule as we are about to study here and within the GSPF he found the following dynamical rule [19]:

$$p(t+1) = p(t)^4 + \frac{7}{2}p(t)^3[1-p(t)] + 3p(t)^2[1-p(t)]^2 + \frac{1}{2}p(t)[1-p(t)]^3. \quad (1)$$

Iterating this formula until the absorbing state is reached, one can find that the exit probability P_+ is a step function (see fig. 1).

In the paper [17] the real-space renormalization-group approach has been proposed to calculate the probability $P_+(p)$ for the outflow dynamics on a network. In the case of a growing network, either hierarchical or of Barabási-Albert type, the resulting formula was $P_+ = 3p^2 - 2p^3$, while in the case of a fixed network they have found that P_+ is a step function, just the same as for the complete graph [16].

In fig. 1 we can compare the exit probability obtained in our simulations of the 1D outflow dynamics with the results of Galam's GSPF and RG calculation of ref. [17] for growing networks. None of them are satisfactory. Note also that if we limited the process of Galam's GSPF to one iteration only, the agreement would be at least qualitatively correct.

So, we can see that currently there is no analytic argument which would satisfactorily explain the behaviour of the outflow dynamics in the Sznajd model in one dimension. Our intention is to fill this gap. In the rest of this paper we present analytical results obtained using the Kirkwood approximation following the method developed in [13] for the majority rule model. Anticipating the conclusions, we can see in fig. 1 that the agreement with simulations is very good.

Approximate solution in 1D. – We consider individuals having opinions represented as spins ± 1 occupying sites on a linear chain of length L. We use the following notation: $\sigma \in \{-1,+1\}^L$ denotes the state of the system and $\sigma(y)$ the state of the individual at site y if the system is in state σ. We also denote by σ^x the state which differs from σ by flipping the spin at site x. Therefore, $\sigma^x(y) = (1-2\delta_{xy})\sigma(y)$.

We introduce here a slight modification of the original outflow rule: we choose a pair of neighbours and if they both are in the same state, then we adjust one (instead of two) of its neighbours (chosen randomly with equal probability 1/2) to the common state. At most one spin is flipped in one step, while in the original formulation two can be flipped simultaneously. Therefore, the time must be rescaled by factor $\frac{1}{2}$. We measure the time so that the speed of all processes remains constant when $L \to \infty$, and thus normally one update takes time $\frac{1}{L}$. Here, instead, we consider also the factor $\frac{1}{2}$, so a single update takes time $\Delta t = \frac{1}{2L}$. Our modification eliminates some correlations due to simultaneous flip of opinions at distance 3. However, if we look at later stages of the evolution, where typically the domains are larger than 2, simultaneous flips occur very rarely. Therefore, we do not expect any substantial difference. Indeed, computer simulations confirm our expectations —only time has to be rescaled (see fig. 2).

On the other hand, the modification simplifies the analytical treatment. Indeed, the update rule can be equivalently formulated as follows: Choose randomly a spin x and side s ($s=1$ for right, $s=-1$ for left). The updated state is $\sigma(x;t+\Delta t) = \sigma(x+s;t)$ if $\sigma(x+s;t) = \sigma(x+2s;t)$, otherwise $\sigma(x;t+\Delta t) = \sigma(x;t)$.

Within such a formulation the probability of the flip $\sigma \to \sigma^x$ in one update is

$$W(\sigma \to \sigma^x) = \frac{1}{8L}[\sigma(x+2)\sigma(x+1) + \sigma(x-1)\sigma(x-2) - \sigma(x)(\sigma(x+2) + \sigma(x+1) + \sigma(x-1) + \sigma(x-2)) + 2]. \quad (2)$$

These flip probabilities are then inserted into the master equation:

$$P(\sigma;t+\Delta t) = \sum_{\sigma'} W(\sigma' \to \sigma)P(\sigma';t), \quad (3)$$

fully describing the evolution of the system.

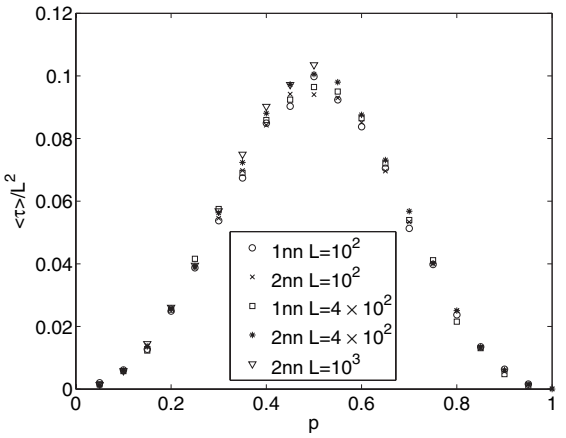

Fig. 2: The mean relaxation times from the random initial state consisting of p up-spins for the modified (1 nn) and original (2 nn) outflow dynamics in one dimension for several lattice sizes L. In the modified version at most one spin is flipped in one elementary step, while in original formulation two can be flipped simultaneously. Therefore, in the case of a modified version the time was rescaled by a factor $\frac{1}{2}$. It should be noticed that in computer simulations time is measured in Monte Carlo steps (MCS). As usual, one MCS consists of L elementary updating, *i.e.* in one MCS L times the pair of spins is randomly and independently selected with probability $1/L$, *i.e.* it may happen that one pair will be chosen several times in one MCS. Since we investigate the relaxation process we simulate the system as long as it reaches the final state with all spins up or down. The average number of MCSs needed to reach the final state depends on the initial concentration of up-spins and is proportional to L^2 analogously to the voter model [5,6,20]. The results presented here are averaged over 10^4 samples.

Now, we make the limit $L \to \infty$, which also implies the continuous time limit, as $\Delta t \to 0$. We also note that most of the transition probabilities $W(\sigma' \to \sigma)$ are zero, since only one spin flip is allowed in one step. Finally we end with

$$\frac{\mathrm{d}}{\mathrm{d}t}P(\sigma;t) = \sum_x \Big[w(\sigma^x \to \sigma)P(\sigma^x;t) - w(\sigma \to \sigma^x)P(\sigma;t)\Big], \tag{4}$$

where the transition rates are trivially related to transition probabilities (2) by a proportionality factor

$$w(\sigma^x \to \sigma) = 2NW(\sigma^x \to \sigma)\,. \tag{5}$$

(The sum is now over an infinite set of sites.)

It is hopeless to solve the master equation as it is. Instead, we write evolution equations for some correlation functions derived from it. We define:

$$\begin{aligned} C_0(t) &= \langle\sigma(y)\rangle \equiv \sum_\sigma \sigma(y)P(\sigma;t), \\ C_1(n;t) &= \langle\sigma(y)\sigma(y+n)\rangle, \\ C_2(n,m;t) &= \langle\sigma(y-n)\sigma(y)\sigma(y+m)\rangle, \\ C_3(n,m,l;t) &= \langle\sigma(y-n)\sigma(y)\sigma(y+m)\sigma(y+m+l)\rangle, \\ &\vdots \end{aligned} \tag{6}$$

Only two equations are relevant for us. The first is

$$\frac{\mathrm{d}}{\mathrm{d}t}C_0(t) = -C_2(1,1;t) + C_0(t) \tag{7}$$

and the second

$$\frac{\mathrm{d}}{\mathrm{d}t}C_1(1;t) = -C_3(1,1,1;t) - C_1(1;t) + C_1(3;t) + 1. \tag{8}$$

These two become a closed set of equations, if we apply the approximations described in the next section. Before going to it, it is perhaps instructive to show the intermediate results which lead to equations (7), (8), and analogically to others, for more complicated correlation functions.

Thus, for example, for the lowest correlation function —the average of one spin— we have

$$\frac{\mathrm{d}}{\mathrm{d}t}\langle\sigma(y)\rangle = -2\langle w(\sigma \to \sigma^y)\sigma(y)\rangle \tag{9}$$

and for the next one in the level of complexity

$$\begin{aligned} \frac{\mathrm{d}}{\mathrm{d}t}\langle\sigma(y)\sigma(y+1)\rangle = &-2\langle w(\sigma \to \sigma^y)\sigma(y)\sigma(y+1)\rangle \\ &-2\langle w(\sigma \to \sigma^{y+1})\sigma(y)\sigma(y+1)\rangle. \end{aligned} \tag{10}$$

The pattern is transparent. When computing the correlation function of spins at sites x_1, x_2, x_3, ..., on the RHS we have the sum of terms, in which we average the product of spins at sites x_1, x_2, x_3, ... with transition rate, which is derived from the spin configuration according to (2) and (5) for flip at positions x_1, x_2, x_3, ... As a formula, this sentence means

$$\frac{\mathrm{d}}{\mathrm{d}t}\left\langle\prod_i \sigma(x_i)\right\rangle = -2\sum_j \left\langle w(\sigma \to \sigma^{x_j})\prod_i \sigma(x_i)\right\rangle. \tag{11}$$

Kirkwood approximation. Now we shall discuss the approximations used for solving eqs. (7) and (8).

The first one is the usual Kirkwood approximation, or decoupling, which is used in various contexts and accordingly it assumes different names. For example in the classical quantum many-body theory of electrons and phonons in solids, it is nothing else than the Hartree-Fock approximation (but contrary to this theory, which may be improved systematically using diagrammatic techniques, here the systematic expansions are not developed). We use the name Kirkwood approximation, following the work [13].

In our case, the Kirkwood approximation amounts to

$$C_3(1,1,1;t) \simeq \big(C_1(1;t)\big)^2 \tag{12}$$

in eq. (8) and

$$C_2(1,1;t) \simeq C_1(1;t)C_0(t) \tag{13}$$

in eq. (7). While the latter assumption (13) enables us to relate equation (7) directly to (8) and therefore to

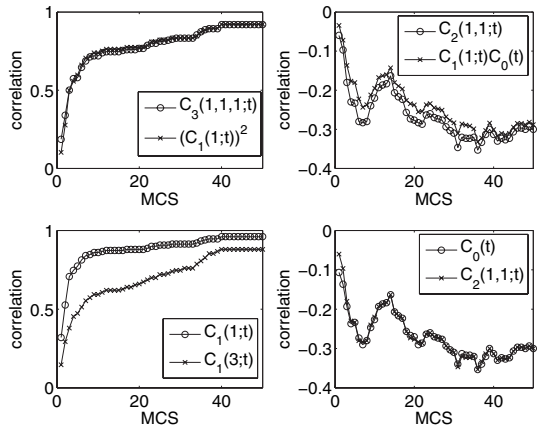

Fig. 3: Sample time evolution of several correlation functions given by eq. (6) for random initial conditions with fraction p of up-spins. The Kirkwood approximation given eqs. (12), (13) and assumption (14) are valid for later stages, although the assumption (12) agrees very well with simulation results from the very beginning (left upper panel). The data come from one single run (not averaged).

solve it as soon as we have the solution of (8), the approximation (12) does not make of (8) a closed equation yet. The point is that there is also the function $C_1(3;t)$ measuring the correlation at distance 3. So, we make also an additional approximation, which is also made in [13]. We suppose that $C_1(n;t)$ only weakly depends on the distance n, or else, that the decay of the correlations is relatively slow. If the spins are correlated to a certain extent on distance 1 (the neighbours), they are correlated to essentially the same extent also on distance 3 (next-next neighbours). This is also justified if the domains are large enough, *i.e.* at later stages of the evolution. So, we assume

$$C_1(3;t) \simeq C_1(1;t)\,. \tag{14}$$

In fig. 3 we present a sample (not averaged) time evolution of several correlation functions. The first assumption (12) agrees very well with simulation results from the very beginning and the second condition (13) agrees with simulations also quite well. On the other hand, the assumption (14) that the decay of the correlations is relatively slow is valid only at later stages of the evolution.

To sum it up, the approximations (12), (13), and (14) say that approximately

$$\begin{aligned} C_0(t) &\simeq \psi(t), \\ C_1(n;t) &\simeq \phi(t), \end{aligned} \tag{15}$$

where $\psi(t)$ and $\phi(t)$ satisfy the equations (the dot denotes the time derivative)

$$\begin{aligned} \dot\psi &= (1-\phi)\psi, \\ \dot\phi &= 1-\phi^2\,. \end{aligned} \tag{16}$$

The solution is straightforward. We assume initial conditions $\phi(0)=m_1$ and $\psi(0)=m_0$. First we solve the second equation from the set (16). This gives

$$\phi(t) = \frac{\sinh t + m_1 \cosh t}{\cosh t + m_1 \sinh t} \tag{17}$$

and inserting that into the first of the set (16) we have

$$\psi(t) = \frac{2m_0}{1+m_1+(1-m_1)\,\mathrm{e}^{-2t}}\,. \tag{18}$$

The most important result is the asymptotics

$$\psi(\infty) = \frac{2m_0}{1+m_1}\,. \tag{19}$$

How to interpret this finding? The average $C_0(t)$ is the average magnetisation. In other terms, it determines the probability that a randomly chosen spin will have state $+1$ at time t. This probability is $p_+(t)=(C_0(t)+1)/2$. Therefore, $m_0=C_0(0)$ is the initial magnetisation. When we go to the limit $t\to\infty$, we know that ultimately the homogeneous state is reached. The asymptotic magnetisation $C_0(\infty)$ therefore says what the probability that the final state will have all spins $+1$ is. It is $(C_0(\infty)+1)/2$. So, (19) means that

$$C_0(\infty) \simeq \frac{2C_0(0)}{1+C_1(1;0)}\,. \tag{20}$$

If the initial state is completely uncorrelated, *i.e.* we set the spins at random, with the only condition that the average magnetisation is m_0, we have $C_1(1;0)=m_0^2$ and

$$C_0(\infty) \simeq \frac{2m_0}{1+m_0^2}\,. \tag{21}$$

Finally, we express this result in terms of the probability $p=(C_0(0)+1)/2$ to have a randomly chosen spin in state $+1$ at the beginning and the probability $P_+=(C_0(\infty)+1)/2$ that all spins are in state $+1$ at the end. We have

$$P_+ \simeq \frac{p^2}{2p^2-2p+1}\,. \tag{22}$$

Computer simulations for random initial conditions, in which assumption $C_1(1;0)=m_0^2$ can be done, show very good agreement with analytical formula (22). In the next section we show how the results will change if we allow correlations in the initial conditions.

Correlated initial conditions. – Here we consider two examples of correlated initial conditions with the fraction p of up-spins:

1) Ordered initial state that consists of two clusters: pL-length of up-spins and $(1-p)L$-length of down-spins, for example in case of $L=10$:

$$\begin{aligned} &p=0.5 : \uparrow\uparrow\uparrow\uparrow\uparrow\downarrow\downarrow\downarrow\downarrow\downarrow \\ &p=0.4 : \uparrow\uparrow\uparrow\uparrow\downarrow\downarrow\downarrow\downarrow\downarrow\downarrow \\ &p=0.3 : \uparrow\uparrow\uparrow\downarrow\downarrow\downarrow\downarrow\downarrow\downarrow\downarrow \\ &\quad\cdots\,. \end{aligned} \tag{23}$$

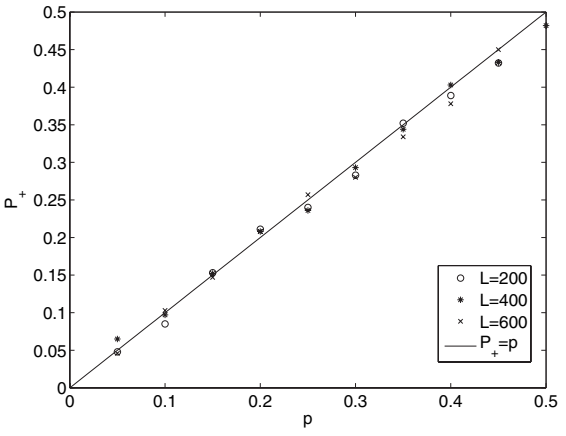

Fig. 4: Exit probability P_+ from the ordered initial state consisting of the fraction p of up-spins for the outflow dynamics in one dimension for several lattice sizes L. The initial state consists of two clusters: pL-length of up-spins and $(1-p)L$-length of down-spins. The results for original and modified rules are the same. The dependence between the initial ratio of up-spins p and the exit probability is given by the simplest linear function $P_+ = p$ as in the case of the voter model. An analytical result in this case can be obtained from eq. (26). Results are averaged over 10^3 samples.

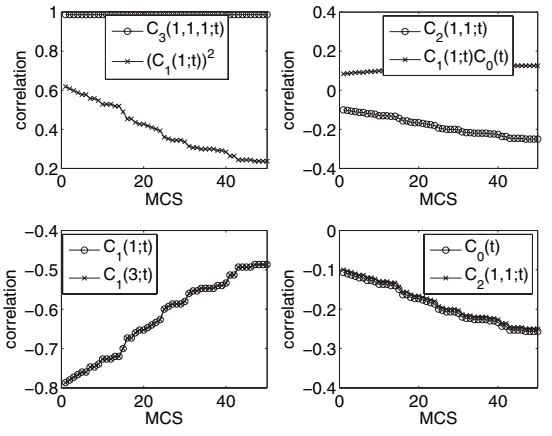

Fig. 5: Sample time evolution of several correlation functions given by eq. (6) for random ordered initial conditions with fraction p of up-spins. The initial state consists of two clusters: pL-length of up-spins and $(1-p)L$-length of down-spins. The Kirkwood approximation given eqs. (12) and (13) are not valid. The data come from one single run (not averaged).

2) Correlated, completely homogeneous, initial state. For such p that $1/p$ is an integer, we set $\sigma(n/p) = 1$ for $n = 0, 1, 2, 3, \ldots$ and $\sigma(x) = -1$ otherwise. For example, in the case of $L = 8$:

$$\begin{aligned} p = 0.5 &: \uparrow\downarrow\uparrow\downarrow\uparrow\downarrow\uparrow\downarrow \\ p = 0.25 &: \downarrow\downarrow\downarrow\uparrow\downarrow\downarrow\downarrow\uparrow \\ &\ldots \ . \end{aligned} \tag{24}$$

In both cases it is easy to calculate exactly the correlation function $C_1(1;0)$. In the first case of ordered initial conditions we obtain

$$C_1(1;0) = 1 - \frac{1}{L} \approx 1. \tag{25}$$

Thus, from eq. (20):

$$C_0(\infty) \simeq \frac{2C_0(0)}{1 + C_1(1;0)} = \frac{2m_0}{1+1} = m_0 \Rightarrow P_+ = p. \tag{26}$$

Computer simulations show that indeed for such initial conditions $P_+ = p$ (see fig. 4).

As we can see, the Kirkwood approximation gives, surprisingly, correct results also in this case. At the same time, fig. 5 shows that eqs. (12) and (13) defining the Kirkwood approximation are not justified by computer simulations.

We have checked also the mean relaxation time in case of ordered initial conditions (fig. 6). It occurs that like for the random initial conditions the mean relaxation time scales with the system size as $\langle\tau\rangle \sim L^2$ (see figs. 2 and 6). The same scaling has been found in the voter model [5,6,20].

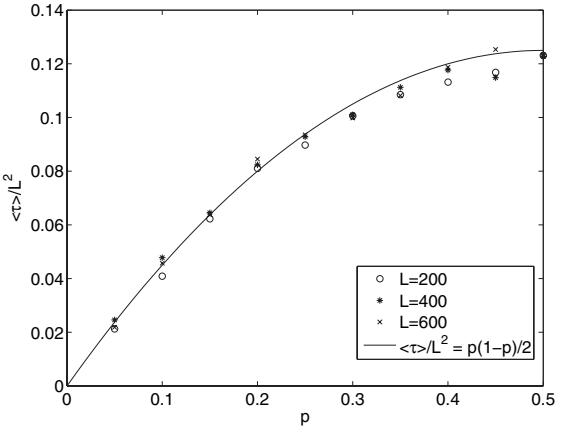

Fig. 6: The mean relaxation times for the outflow dynamics in one dimension for several lattice sizes L. The initial state consists of two clusters: pL-length of up-spins and $(1-p)L$-length of down-spins. The results for original and modified rules are the same. It is clearly visible that in the case of such an ordered initial state the dependence between the initial ratio of up-spins p and the mean relaxation time $\langle\tau\rangle$ is given by a simple parabola rather than by a bell-shaped curve. The data presented in the figure are averaged over 10^4 samples.

However, contrary to the random initial conditions for which a bell-shaped curve is observed, here the mean relaxation times is well described by simple parabola:

$$\frac{\langle\tau\rangle}{L^2} = \frac{1}{2}p(1-p). \tag{27}$$

It is quite easy to understand this result. In fact, in the initial condition there is only one domain wall, where $+1$ and -1 sites come into contact. During the evolution this domain wall performs a random walk and cannot disappear, unless it hits the left or right edge

of the one-dimensional chain. The mean exit time for a random walker among two absorbing walls is well known and depends on the initial position of the walker, which is determined by the proportion p, exactly as indicated in formula (27). The same consideration of a random walker with two absorbing walls also explains the linear dependence of P_+ observed in fig. 4.

For the second case of correlated initial conditions, which are completely homogeneous, we observed in computer simulations that the exit probability is a step function with an unstable fixed point at $p = 0.5$, *i.e.*

$$\begin{aligned} P_+ &= 0, \quad \text{for } p < 0.5, \\ P_+ &= 1, \quad \text{for } p > 0.5, \\ &\text{antiferromagnetic state}, \quad \text{for } p = 0.5. \end{aligned} \tag{28}$$

In this case the two-spins correlation function can be also calculated easily. For $p = \frac{1}{n} < 0.5$, $n = 3, 4, \ldots, L$ we obtain

$$C_1(1;0) = p\left(1 \times \left(\frac{1}{p} - 2\right) + (-1) \times 2\right) = 1 - 4p. \tag{29}$$

Thus, from eq. (20)

$$C_0(\infty) \simeq \frac{2C_0(0)}{1 + C_1(1;0)} = \frac{4p-2}{2-4p} = -1 \Rightarrow P_+ = 0, \tag{30}$$

which again agrees very well with computer simulations, although the Kirkwood approximation cannot be easily justified.

Conclusions. – We introduced a modified version of the one-dimensional outflow dynamics in which we choose a pair of neighbours and if they both are in the same state, then we adjust *one* (in the original version both) of its neighbours to the common state. We checked in computer simulations that in accord with our expectations the results in the case of a modified rule are the same as in the case of the original outflow dynamics, only the time must be rescaled by a factor $\frac{1}{2}$. In the modified version the analytical treatment is greatly simplified and allows to derive the master equation involving only single-flip events. Following the method proposed in [13] we wrote evolution equations for some correlation functions and used the Kirkwood approximation. This approach allowed us to derive the analytical formula for the final magnetisation and, equivalently, for the exit probability. In fact, just before finishing this paper, the same result was published by Lambiotte and Redner as a special case in the work [21] where a model interpolating the voter, the majority rule (or Sznajd) and the so-called vacillating voter dynamics was investigated, using also the Kirkwood approximation.

In the case of random initial conditions the Kirkwood approximation can be justified looking at the time evolution of simulated correlation functions. In this case our analytical results can be simplified to eq. (22) and agree very well with simulations, in contrast to earlier approaches [17,19]. We have checked also how the Kirkwood approximation works in the case of two types of correlated initial conditions. Although in both cases the Kirkwood approximation cannot be easily justified, surprisingly we obtained very good agreement of our formula (20) with computer simulations. The validity of the formula is much wider than the validity of the Kirkwood approximation used in its derivation.

* * *

This work was supported by the MŠMT of the Czech Republic, grant No. 1P04OCP10.001, and by the Research Program CTS MSM 0021620845. KS-W gratefully acknowledges the financial support in the period 2007–2009 of the Polish Ministry of Science and Higher Education through the scientific grant No. N N202 0194 33.

REFERENCES

[1] Castellano C., Fortunato S. and Loreto V., arXiv:0710.3256 (2007).
[2] Callen E. and Shapero D., *Phys. Today*, **27**, July issue (1974) 23.
[3] Galam S., *J. Math. Psychol.*, **30** (1986) 426.
[4] Galam S., *J. Stat. Phys*, **61** (1990) 943.
[5] Liggett T. M., *Stochastic Interacting Systems: Contact Voter, and Exclusion Processes* (Springer-Verlag, New York) 1999.
[6] Krapivsky P. L., *Phys. Rev. A*, **45** (1992) 1067.
[7] Sznajd-Weron K. and Sznajd J., *Int. J. Mod. Phys. C*, **11** (2000) 1157.
[8] Krapivsky P. L. and Redner S., *Phys. Rev. Lett.*, **90** (2003) 238701.
[9] Stauffer D., *Comput. Phys. Commun.*, **146** (2002) 93.
[10] Schechter B., *New Sci.*, **175** (2002) 42.
[11] Fortunato S. and Stauffer D., in *Extreme Events in Nature and Society*, edited by Albeverio S., Jentsch V. and Kantz H. (Springer, Berlin) 2005.
[12] Sznajd-Weron K., *Acta Phys. Pol. B*, **36** (2005) 2537.
[13] Mobilia M. and Redner S., *Phys. Rev. E*, **68** (2003) 046106.
[14] Lambiotte R. and Redner S., *J. Stat. Mech.* (2007) L10001.
[15] Stauffer D., Sousa A. O. and De Oliveira M., *Int. J. Mod. Phys. C*, **11** (2000) 1239.
[16] Slanina F. and Lavička H., *Eur. Phys. J. B*, **35** (2003) 279.
[17] Gonzalez M. C., Sousa A. O. and Herrmann H. J., *Eur. Phys. J. B*, **49** (2006) 253.
[18] Sznajd-Weron K. and Krupa S., *Phys. Rev. E*, **74** (2006) 031109.
[19] Galam S., *Europhys. Lett.*, **70** (2005) 705.
[20] Mobilia M., Petersen A. and Redner S., *J. Stat. Mech.* (2007) P08029.
[21] Lambiotte R. and Redner S., *EPL*, **82** (2008) 18007 (this issue).

[Slanina11a]

Eur. Phys. J. B **79**, 99–106 (2011)
DOI: 10.1140/epjb/e2010-10568-y

THE EUROPEAN PHYSICAL JOURNAL B

Regular Article

Dynamical phase transitions in Hegselmann-Krause model of opinion dynamics and consensus

F. Slanina[1,2,a]

[1] Institute of Physics, Academy of Sciences of the Czech Republic, Na Slovance 2, 18221 Praha, Czech Republic
[2] Center for Theoretical Study, Charles University in Prague, Academy of Sciences of the Czech Republic, Jilská 1, 11000 Praha, Czech Republic

Received 22 July 2010 / Received in final form 19 November 2010
Published online 23 December 2010 –

Abstract. The dynamics of the model of agents with limited confidence introduced by Hegselmann and Krause exhibits multiple well-separated regimes characterised by the number of distinct clusters in the stationary state. We present indications that there are genuine dynamical phase transitions between these regimes. The main indicator is the divergence of the average evolution time required to reach the stationary state. The slowdown close to the transition is connected with the emergence of the groups of mediator agents which are very small but have decisive role in the process of social convergence. More detailed study shows that the histogram of the evolution times is composed of several peaks. These peaks are unambiguously interpreted as corresponding to mediator groups consisting of one, two, three etc. agents. Detailed study reveals that each transition possesses also an internal fine structure.

1 Introduction

Formation of consensus is one of the most studied topics in the field of sociophysics. It was the subject of the early paper by Callen and Shapero [1] (which was originally intended as a contribution to the Moscow seminar banned by the Communist authorities [2]). The early attempts to apply the ideas of synergetics to social phenomena were driven by similar ideas [3]. Consensus was in the centre of the papers of Galam [4–6], who revived the term "sociophysics" and made it known to general audience [7]. For recent reviews, see e.g. [8,9].

The consensus models can be divided into two well-defined groups. The models of the first type assume that the agents can choose among a small number of discrete opinions. The simplest case is the binary choice, studied in the voter [10], Galam [5,11–13], Sznajd [14–20], and majority-rule models [21,22].

The second type of models acknowledges that the opinion of the agents may stretch on a continuous line (or a space of any dimensionality and structure). The opinions evolve in time by attraction, i.e. the agents shift their position in the opinion space towards areas where other agents are already concentrated. Assuming that this dynamics is linear, DeGroot [23] introduced the model of opinion convergence in which the opinions in the next time step are linear combinations of the original opinions. The conditions required for reaching consensus were clarified in stabilization theorems [23,24]. Essentially, the statement is that if the agents form a network of interactions which is a single connected cluster, the system always reaches full consensus. The only case in which different opinions survive in the stationary state is the trivial one, when the agents split into several clusters with no communication whatsoever. This is certainly an exaggerated view of the society as we know it.

The fundamental ingredient missing in the model of DeGroot was the limited (or bounded) confidence. It is based on a rather trivial observation that people who differ too much in their opinions are unable to force the partner shift her opinion and unwilling to make themselves a tiniest step towards the opponent. The opinions are frozen, if they are incompatible. Within discrete-opinion models this idea was excellently implemented in the Axelrod model [25–37], while for continuous opinions, bounded confidence was introduced within the model of Deffuant et al. [38,39]. Contrary to the parallel and linear dynamics of DeGroot, the dynamics in Deffuant et al. model is stochastic. In each step, a pair of agents is chosen at random and their opinions are shifted towards each other, on condition that they do not differ more than the confidence threshold ε. This model was investigated very thoroughly [40–51] both by simulations of finite systems and by numerical solution of the partial integro-differential equation corresponding to infinite-size limit. It was found that the ultimate stationary regime is a combination of δ-peaks in the distribution of opinions. A single peak means full consensus, while multiple peaks imply breaking the

[a] e-mail: slanina@fzu.cz

society into several non-communicating groups. There is a sequence of sharp transitions between regimes of one, two, three, etc. peaks, at critical values of the confidence threshold. Numerical estimates suggest that the transition from full consensus to multiple peaks occurs at $\varepsilon_{c1} \simeq 0.5$. However, the side peaks only gain macroscopic weight at another critical value $\varepsilon_{c2} \simeq 0.27$ [41,49,52].

While the model of Deffuant et al. uses sequential stochastic dynamics, the model of Hegselmann and Krause (HK) [53] is more close to the original DeGroot model. The randomness enters only in the initial condition and further evolution is deterministic. In each step, the new values of the opinion variable are linear combinations of those opinions, which are not farther than the confidence threshold. From the uniformly random initial condition, one or several groups of identical opinions evolve. Contrary to the Deffuant et al. model, the absorbing state (i.e. such that none of the opinions can change any more) is reached after finite number of steps, provided the number of agents is finite. The HK model was investigated both by simulations and by solution of corresponding partial integro-differential equation [52,54–64]. Numerically, it was found that the transition to full consensus appears around the critical value $\varepsilon_c \simeq 0.2$ [57]. A smart way of discretization the integro-differential equation, called interactive Markov chain [62–66], provides two conflicting results for the consensus transition. For odd number of discretization intervals, the answer is $\varepsilon_c \simeq 0.19$ [52,62], while for even number of intervals one gets $\varepsilon_c \simeq 0.22$ [60,62]. Later, we shall mention arguments indicating that the correct discretization is with odd number of intervals. The advantage of the approach using interactive Markov chains is that in enables proving stabilization theorems on the HK dynamics [67–69].

Various modifications of Deffuant et al. and HK models were investigated. For example, a model which interpolates between Deffuant et al. and HK was introduced [70]. Heterogeneous confidence thresholds [63,71], influence of extremists [40,72] and presence of a "true truth" [61,73] were studied. Introduction of multi-dimensional opinion space [39,60,65,74] is also a natural generalization. Interestingly, introduction of noise into the dynamics alters the behaviour profoundly [75]. This might be interpreted so that HK and Deffuant et al. models follow a strictly zero-temperature dynamics, which is unstable with respect to noise.

The aim of this paper is to investigate in detail the transitions from full consensus to state with two groups, to state with three, four etc. groups. Especially, we show in detail the phenomenon of critical slowdown, already hinted in [60,65,70] and show how it is related to the presence of mediators, introduced on an intuitive level in [66].

2 Phases in the Hegselmann-Krause model

2.1 Definitions

Let us first recall the definition of the HK model. The system consists of N agents. The opinion of agent i at time t is a number $x_i(t) \in (0,1)$. Thus, the state of the system is described by the N-component vector $x(t)$. The evolution of the state vector in discrete time $t = 0, 1, 2, \ldots$ is deterministic and seemingly linear

$$x_i(t+1) = \sum_{j=1}^{N} M_{ij}[x(t)]\, x_j(t) \tag{1}$$

but the mixing matrix M is not constant, but depends on the actual state x. The dependence $M[x]$ is dictated by the principle of bounded confidence. If $\varepsilon \in (0,1)$ is the confidence threshold, then

$$M_{ij}[x] = \begin{cases} 0 & \text{for } |x_i - x_j| > \varepsilon \\ \frac{1}{N_{ij}} & \text{for } |x_i - x_j| \le \varepsilon \end{cases} \tag{2}$$

where the normalization factor N_{ij} is the number of agents not farther than ε from the agent i, $N_{ij} = |\{j : |x_i - x_j| \le \varepsilon\}|$. As the initial condition, we choose set of independent random values $x_i(0)$, uniformly distributed in the interval $(0,1)$.

The dynamics (1), (2) has infinite number of absorbing states. They can be classified according to the number of non-communicating clusters. The state with ν clusters is characterised by numbers $f_1 < f_2 < \ldots < f_\nu$ such that $f_{l+1} - f_l > \varepsilon$ and $\forall i\, \exists l : x_i = f_l$. The smallest t for which $x(t)$ is an absorbing state will be called consensus time and denoted τ.

As the initial condition is random, the time τ to reach an absorbing state as well as the number ν of clusters in that state are also random variables. We shall be mainly interested in the mean values $\langle\tau\rangle$ and $\langle\nu\rangle$, averaged over initial conditions.

2.2 Which absorbing state?

The number of clusters in the absorbing state depends mainly on the confidence threshold ε, but also on the initial condition. We show in Figure 1 three typical examples. For large enough ϵ the evolution ends in a state with single cluster, while for smaller ε the resulting ν differs according to the configuration of opinions at the beginning. If we average the final number of clusters, we observe a decreasing function of ε, as shown in Figure 2. A more detailed look (see the inset in Fig. 2) shows that for increasing number of agents, well-defined plateaus develop at integer values of $\langle\nu\rangle$, separated by steps which become sharper for increasing N and we may conjecture that discontinuities emerge for $N \to \infty$ at critical values $\varepsilon = \varepsilon_{c1}$, ε_{c2}, etc. From Figure 2 we can estimate the first two of them as $\varepsilon_{c1} \simeq 0.2$, $\varepsilon_{c2} \simeq 0.14$.

2.3 Critical slowing down

The critical values ε_{ck} mark dynamical phase transitions from regime with k clusters in absorbing state to $k+1$ clusters. It is very questionable if the notions of first-order versus continuous phase transitions can be transferred from

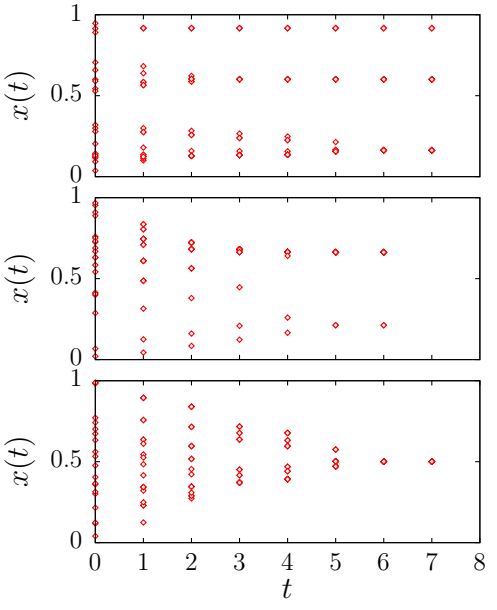

Fig. 1. (Color online) Examples of the evolution of opinions of $N = 20$ agents. The confidence threshold is $\varepsilon = 0.1$ (upper panel) and $\varepsilon = 0.25$ (middle and lower panel). The evolution is stopped as soon as the clusters stop changing.

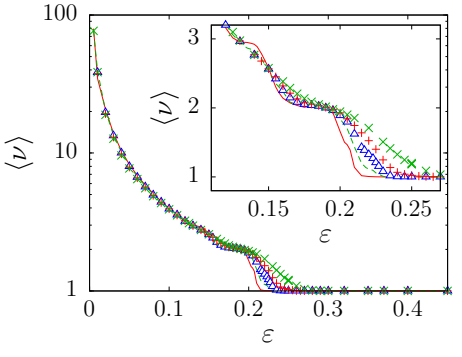

Fig. 2. (Color online) Dependence of the average number of clusters on the confidence threshold. The number of agents is $N = 5000$ (solid line), 2000 (dashed line), 1000 (△), 500 (+), and 200 (×). In the inset, detail of the same data.

equilibrium to non-equilibrium transitions. However, we can study certain features, which are distinctive in equilibrium, also in non-equilibrium case. One of them is the slowdown of the dynamics close to the critical point. This is a signature of continuous transition. In HK model, we can measure the average time to reach an absorbing state as a function of ε, and indeed, we observe peaks located at the transition regions, as seen in Figure 3. The height of the peaks increases with the number of agents, which suggests diverging time at the transition points. The overall picture emerging from these results seems to be the following. In HK model in the limit $N \to \infty$, we have a sequence of phases characterised by one, two, three. etc. clusters in the absorbing state which is the result of the dynamics. The phase transitions occur at confidence thresholds ε_{c1}, ε_{c2} etc., where the average number of clusters jumps

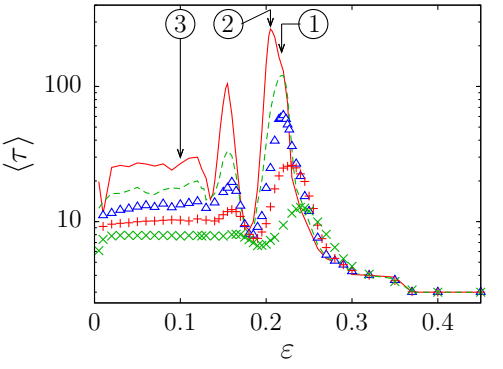

Fig. 3. (Color online) Dependence of the average time to reach an absorbing state on the confidence threshold. The number of agents is $N = 5000$ (solid line), 2000 (dashed line), 1000 (△), 500 (+), and 200 (×). The arrows with circled numbers indicate the values of ε used in Figures 6–8.

discontinuously between two integer values, and where the average consensus time diverges. Having this in mind, we can consider the phase transitions second-order. In the following sections we shall see that the phase transitions in HK model are even more subtle than that.

3 How the absorbing state is reached

From now on, we shall concentrate on the first of the sequence of transitions, where the full consensus ends. We show in Figures 4 and 5 details of the ε-dependence of average number of clusters and average time to reach an absorbing state, respectively.

We can see in Figure 4 that increasing N results in decrease of $\langle\nu\rangle$ in the transition region. (We shall defer the sociological perspective of this phenomenon to the Conclusions). The transition becomes steeper, but the inflexion point is shifted leftwards. Similarly, in Figure 5 we observe that the peak not only grows when number of agents increases, but shifts quite markedly to lower values of ε. The vales of ε_{c1} inferred from the finite-N results must be considered as upper bounds to the true critical value valid in the thermodynamic limit.

We can gain further insight into the divergence of consensus time at the transition, if we plot the histogram of times to reach an absorbing state for values of ε close to the maximum of the peak in $\langle\tau\rangle$. We show the results for $N = 2000$ at $\varepsilon = 0.218$ and for $N = 5000$ at $\varepsilon = 2.05$, in Figures 6 and 7, respectively. The characteristic feature of the histograms is a sequence of peaks. The height of the peaks is nearly the same, especially for larger N. For comparison, we plot in Figure 8 the histogram of consensus times for $\varepsilon = 1$, far from any major peak in $\langle\tau\rangle$. There are barely visible traces of peaks, but as the system size increases, the histogram becomes flat, contrary to the transition region, where the peaks in the histogram become more pronounced. Therefore, the peaks in the histogram are tightly related to the divergence of consensus time at the transition.

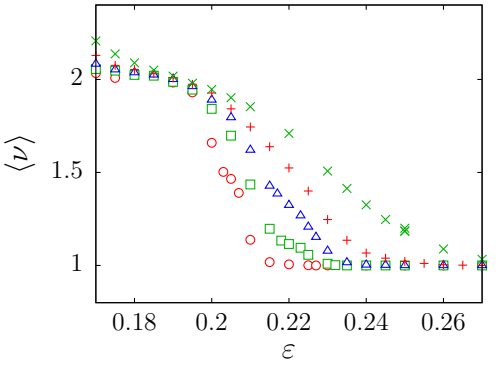

Fig. 4. (Color online) Detail of the dependence of the average number of clusters on the confidence threshold. The number of agents is $N = 5000$ (○), 2000 (□), 1000 (△), 500 (+), and 200 (×).

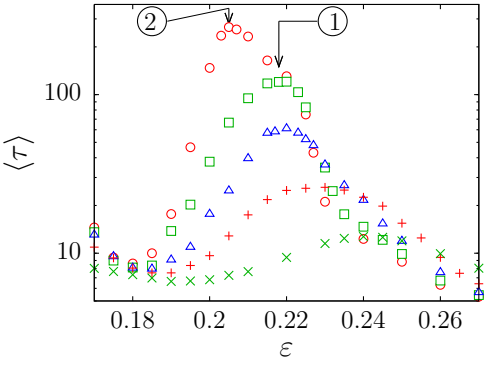

Fig. 5. (Color online) Detail of the dependence of the average time to reach an absorbing state on the confidence threshold. The number of agents is $N = 5000$ (○), 2000 (□), 1000 (△), 500 (+), and 200 (×). The arrows with circled numbers indicate the values of ε used in Figures 6 and 7.

As a next step, we must ask what is the origin of the peaks. The emergence of the peaks implies that there are certain typical lengths of the evolution from the initial condition to the absorbing state. We naturally expect that the typical lengths correspond to typical structural features of the evolution. To see that, we show in Figure 9 spatio-temporal diagrams of the evolution of the system for five principal peaks in the histogram. The consensus times are indicated by letters A to E in Figure 6 and the corresponding panels in Figure 9 are denoted by the same letters. We can see immediately a common feature of all these five samples. After a very short transient period, three clusters are formed, one of them close to the exact middle and two of them on the wings. The latter are slowly attracted to the central cluster, until their distance falls below ε. Then, all three collapse into a single cluster and an absorbing state with full consensus is reached.

Neglecting the very short transient, the consensus time is given by the time needed to attract the wing clusters to the distance ε. We assume that the middle cluster contains N_{med} "mediator" agents and is located at $x(0) = 1/2$, while the other groups are equal in size $N_+ = N_- = (N - N_{\mathrm{med}})/2$ and are located initially at $x_\pm(0) = 1/2 \pm \Delta x$.

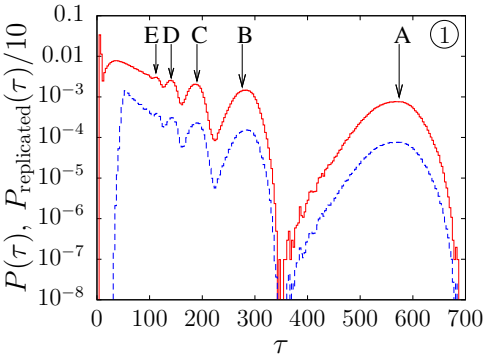

Fig. 6. (Color online) Histogram of times to reach an absorbing state, for $N = 2000$ and $\varepsilon = 0.218$ (full line). The arrows marked by capital letters A to E indicate the length of consensus time realised in the evolution samples shown in Figure 9. The circled "1" refers to the arrow in Figures 3 and 5. We draw also the distribution found by replication of the longest peak, according to (6), with $k_{\max} = 11$ (dashed line). For better visibility, it is scaled down by the factor 10.

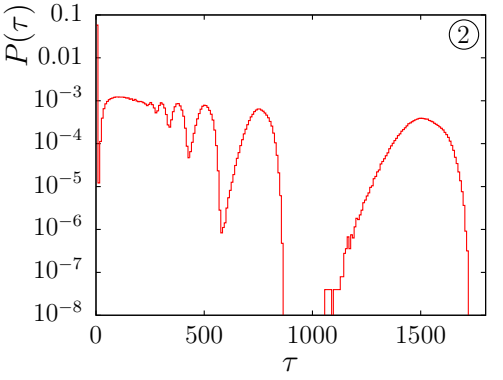

Fig. 7. (Color online) Histogram of times to reach an absorbing state, for $N = 5000$ and $\varepsilon = 0.205$.

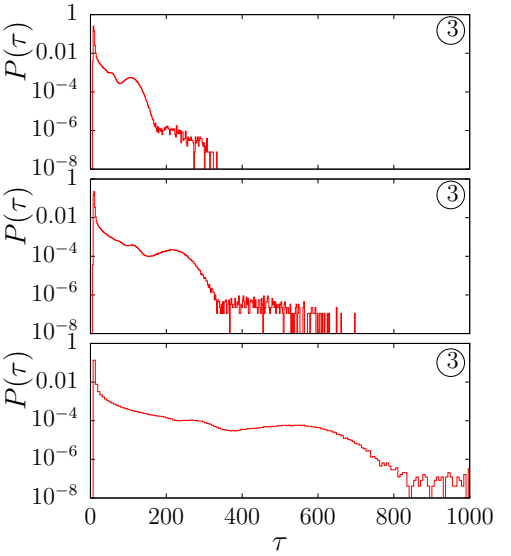

Fig. 8. (Color online) Histogram of times to reach an absorbing state, for $\varepsilon = 0.1$ and $N = 1000$ (upper panel), $N = 2000$ (middle panel), and $N = 5000$ (lower panel).

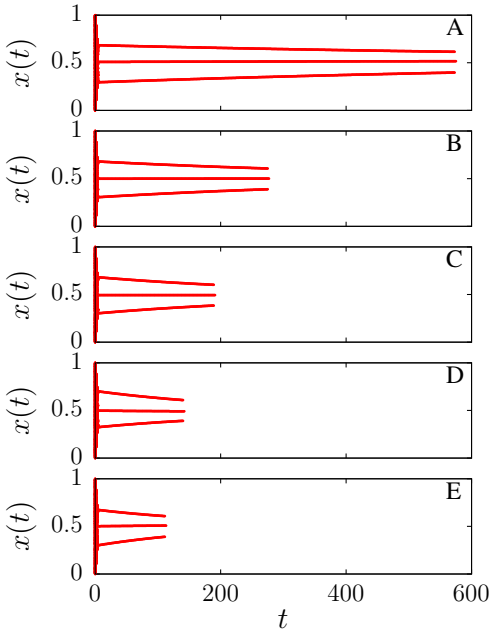

Fig. 9. (Color online) Examples of the evolution with different size of the central mediator group, from top to bottom $N_{\rm med} = 1, 2, 3, 4,$ and 5. The capital letters in the top right corners relate to the arrows in Figure 6.

The middle cluster does not move and the wing clusters evolve according to the difference equation

$$x_\pm(t+1) - x_\pm(t) = -\frac{N_{\rm med}}{N_\pm + N_{\rm med}}\left(x_\pm - \frac{1}{2}\right). \qquad (3)$$

For $N_{\rm med}/N \ll 1$ the dynamics is very slow and we can replace the difference in (3) by derivative. Hence, the consensus time is estimated as

$$\tau = \frac{N}{2N_{\rm med}} \ln\frac{2\Delta x}{\varepsilon}. \qquad (4)$$

Since the initial condition must be $\Delta x < \varepsilon$, otherwise the clusters would never coalesce, and $N_{\rm med} \geq 1$, we get a strict upper bound to the consensus time, provided the mechanism of three clusters is in force

$$\tau \leq N \ln\sqrt{2}. \qquad (5)$$

Indeed, we can see that the histograms in Figures 6 and 7 obey the bound (5).

The width of the peaks in the histogram is due to the fluctuations in the initial positions of the wing clusters. The peaks differ only in the number of mediators. Indeed, the evolution patterns A to E in Figure 9 are observed for number of mediators $1, 2, \ldots, 5$. Comparing that with Figure 6, where the peaks are denoted by corresponding letters A to E, we clearly see that the peak at longest consensus has $N_{\rm med} = 1$, the second has $N_{\rm med} = 2$ etc. This fact suggests, that the peaks for $N_{\rm med} = 2, 3, \ldots$ can be obtained by replication the peak at $N_{\rm med} = 1$. Denoting $P_1(\tau)$ the latter peak only, we approximate the full distribution of consensus times by

$$P(\tau) \simeq P_{\rm replicated}(\tau) = \sum_{k=1}^{k_{\rm max}} k\, P_1(k\,\tau). \qquad (6)$$

This approximation assumes that all sizes of the mediator group up to $N_{\rm med} = k_{\rm max}$ have the same probability and neglect the influence of the initial short transient. Therefore, it is reasonably accurate for a few highest peaks, but fails at short τ, as it is confirmed in Figure 6.

Let us also note that the mechanism of mediators located in the middle explains why, in the numerical solution of the partial differential equation for HK model, the discretization into even number of equally-sized intervals is wrong. Indeed, in this case the mediator cluster is located just at the border of two intervals, however fine the discretization is, and this induces numerical artifacts into the results.

4 Fine structure of the transitions

We already noted that the dependence of $\langle\nu\rangle$ on ε is not like the dependence of average magnetization on temperature, as seen in simulations of finite-size Ising model. The transition region is not only squeezed into more narrow region, but is also shifted to lower ε. The same is observed also in $\langle\tau\rangle$. When the system size grows, the peaks do not simply grow and get thinner, but are also shifted to lower ε, consistently with the behaviour of $\langle\nu\rangle$. Let us look at this shifting of peaks in more detail.

To this end, we performed simulations of fairly large systems (up to $N = 2\times10^5$) in the range of ε which covers the transition from the full consensus phase ($\langle\nu\rangle = 1$) to the phase with two clusters ($\langle\nu\rangle = 2$). The picture which emerges, is demonstrated in Figures 10 and 11. It is somewhat surprising that the peaks in $\langle\tau\rangle$ only apparently move. Closer look at Figure 10 reveals that a peak at certain value of ε remains at the same position when N grows, but a new peak starts growing at somewhat smaller ε. When this second peak reaches some height, it saturates and another peak is born and grows at even smaller ε. In this way, older peaks do not depend on N any more, but rather are overgrown by new ones. To our knowledge, this effect has no analogy in equilibrium phase transitions and is entirely related to dynamical nature of the transition in HK model.

Similar fine structure of the transition region is observed on the dependence of average number of clusters on ε. In the transition region, it drops from $\langle\nu\rangle = 2$ to $\langle\nu\rangle = 1$. To make the details more visible, we plot the quantity $(\langle\nu\rangle - 1)/(2 - \langle\nu\rangle)$, instead of $\langle\nu\rangle$, in logarithmic scale. In Figure 11 we can see that $\langle\nu\rangle$ drops from 2 to 1 in step-wise manner. For $N = 10^4$ we observe plateaus, or regions of ε, where the average number of clusters is nearly constant somewhere between 1 and 2. When the system size grows, these steps, or plateaus, diminish in the value of $\langle\nu\rangle$ but keep their width. Moreover, the edges of the steps decrease more slowly, so that the dependence of $\langle\nu\rangle$ on

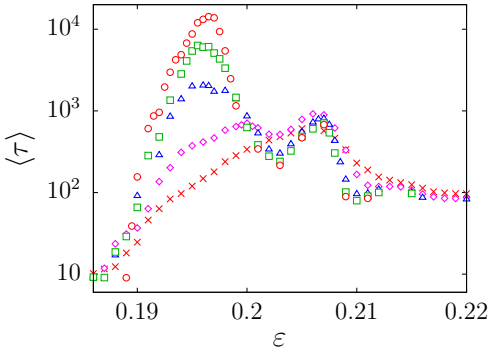

Fig. 10. (Color online) Fine structure of the average time to reach an absorbing state, at the transition from full consensus to phase with two clusters. The system size is $N = 2\times10^5$ (○), 10^5 (□), 5×10^4 (△), 2×10^4 (◇), 10^4 (×).

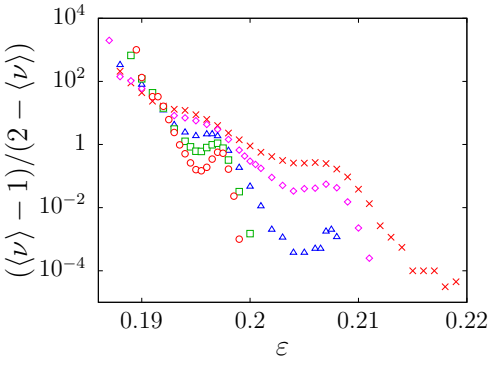

Fig. 11. (Color online) Fine structure of the average number of clusters in absorbing state, at the transition from full consensus to phase with two clusters. The system size is $N = 2\times10^5$ (○), 10^5 (□), 5×10^4 (△), 2×10^4 (◇), 10^4 (×).

ε becomes non-monotonous and the "plateaus" have depression in the middle. Interestingly, the peaks in $\langle\tau\rangle$ are located just next to the right edges of these "plateaus". We assume that the sequence of the peaks in $\langle\tau\rangle$ and plateaus in $\langle\nu\rangle$ tends to a point $\varepsilon = \varepsilon_{c1}$, which is the location of the true phase transition in the limit $N \to \infty$. Form the data in Figures 10 and 11 we can estimate $\varepsilon_{c1} \simeq 0.19$.

Comparing Figures 10 and 11 we can see that the non-monotonous dependence of $\langle\nu\rangle$ on ε goes hand in hand with the multiple-peak dependence of $\langle\tau\rangle$ on ε. We do not have a detailed account for this phenomenon, but the following scenario seems plausible.

The behaviour in the transition region is dominated by the slow evolution of three-cluster system, as described above. The existence of full consensus depends on emergence of the mediator group. In other words, the average number of clusters is related to the probability $P_{\rm med}(\varepsilon;0)$ that the mediator group is empty, as $\langle\nu\rangle = 1 + P_{\rm med}(\varepsilon;0)$, as long as more than two clusters in the absorbing state occur with negligible probability. We suppose that for given ε and very large N the fraction of agents in the mediator group approaches a limit $\mu(\varepsilon) = \lim_{N\to\infty} N_{\rm med}/N$. As the full consensus is only possible if $\mu(\varepsilon) > 0$, we may consider $\mu(\varepsilon)$ as order parameter of the non-equilibrium phase transition in HK model. The location ε_{c1} of the transition is determined by $\mu(\varepsilon_{c1}) = 0$.

We also assume that a "master" probability distribution exists $F(\rho, n)$, independent of ε and N, so that the probability distribution for $N_{\rm med}$ is

$$P_{\rm med}(\varepsilon; N_{\rm med}) = F(\mu(\varepsilon)\, N; N_{\rm med}). \tag{7}$$

The parameter ρ stands for the average size of the mediator group, so $\rho = \sum_{n=1}^{\infty} nF(\rho, n)$. We do not have direct access to the distribution $F(\rho, n)$ in simulations. In absence of any other information we hay hypothesise that the distribution might be Poissonian, $F(\rho, n) = e^{-\rho}\,\rho^n/n!$. According to (4) and assuming that Δx is proportional to ε, we have the estimate

$$\langle\tau\rangle \propto \sum_{N_{\rm med}=1}^{N_{\rm med,max}} \frac{N}{N_{\rm med}} F(\mu(\varepsilon)\, N; N_{\rm med}). \tag{8}$$

The upper bound $N_{\rm med,\,max}$ for the size of the mediator group can be safely extended to infinity. For fixed ε (and therefore fixed $\mu(\varepsilon)$) and $N \to \infty$ the average consensus time approaches a limit which is proportional to $\langle\tau\rangle \propto 1/\mu(\varepsilon)$. On the other hand, for N fixed and variable ε, the dependence of $\langle\tau\rangle$ according to (8) develops a maximum as a function of μ. The location of the maximum shifts when N grows as $\mu_{\rm max} \propto 1/N$. This way, the location of the peak in $\langle\tau\rangle(\varepsilon)$ approaches ε_{c1} as $N \to \infty$.

If the fraction μ of agents in the mediator cluster was a monotonous function of ε, with $\mu = 0$ at the critical point $\varepsilon = \varepsilon_{c1}$, we would see a peak in $\langle\tau\rangle$ growing and shifting gradually to lower values of ε, up to its asymptotic position at the critical point. Then, also $\langle\nu\rangle = 1 + F(\mu(\varepsilon)\, N; 0)$ would be a monotonously decreasing function of ε. However, we can see violation of this monotonicity in Figure 11. Therefore, μ is not a monotonous function of ε, which explains both the non-monotonicity of $\langle\nu\rangle$ and the fact that multiple peaks appear in $\langle\tau\rangle$, instead of observing smooth shift and growth of a single peak. The non-monotonicity imposes a deformation on the otherwise smooth growth and shift of the peak in $\langle\tau\rangle$. This deformation results in apparent emergence of new peaks next to the older ones. In fact, as long as the approximation $\lim_{N\to\infty}\langle\tau\rangle \propto 1/\mu(\varepsilon)$ is justified, the non-monotonicity in $\mu(\varepsilon)$ is directly visible in non-monotonicity, i.e. multiple-peak structure, of $\langle\tau\rangle$, close to the critical point.

However, the key ingredient of the whole phenomenon of fine structure of the transition, which is the non-monotonicity of $\mu(\varepsilon)$ remains unexplained. Clearly, it relies on the processes happening within the relatively short transient period. The three-cluster structure, i.e. two wings plus mediators, is formed in this period and the distribution of the number of mediators is established, which we assumed, for simplicity, to have the form $F(\mu(\varepsilon)\, N; N_{\rm med})$, but actually can be more complex.

5 Conclusions

We investigated in detail phase structure of the Hegselmann-Krause model of consensus formation. The

only parameters of the model are confidence threshold and number of agents. The dynamics is deterministic, but the initial condition is random. We found that, depending on the value of the confidence threshold, well-defined phases exist, characterised by the number of non-communicating clusters in the absorbing state. This number is one in full consensus phase, while it is two, three, etc. in phases lacking full consensus among all agents, but exhibiting consensus within the clusters. The phases are separated by dynamical phase transitions, characterised by divergence of the time needed to reach the absorbing state, reminiscent of critical slowing down known from second order equilibrium phase transitions.

The mechanism which leads to the divergence of characteristic time at the phase transition is related to the emergence of a group of mediators, i.e. a small cluster in the middle of the opinions, which is able to attract the two clusters on the left and right wings from the mediators. The mediator cluster can be arbitrarily small, but non-empty. One single mediator is able to attract arbitrarily large wing clusters, if they are located initially within the confidence threshold. The attraction is the slower the larger the wing clusters are, but typically close to the transition the wing clusters contain nearly all the agents, while the fraction contained in the mediator cluster is tiny. Hence the divergence of the time needed to reach the absorbing state, when the system size grows. This mechanism is reflected also in the histogram of times to reach consensus, which exhibits a characteristic series of peaks. Each of the peaks corresponds to a specific number of agents in the mediator group, which is one for the farthest peak, two for the next one, etc.

The most surprising feature of the dynamical phase transition in HK model is its fine structure. In the transition region, the average time to reach absorbing state, as a function of the confidence threshold, exhibits not just a growing peak when system size grows. The peak is also shifted towards lower values, in a complex manner. Apparently, the peak grows with system size until saturation, and then a new peak starts growing at a lower value of the confidence threshold. Thus, a series of peaks, overgrowing each other, emerges. We assume that the positions of the peaks tend to a limit which is the location of the phase transition in the infinite-size limit.

If we interpret the results obtained in terms of the (hypothetical) average fraction of agents in the mediator cluster, we come to conclusion that this quantity must be a non-monotonous function of the confidence threshold in the transition region. If it were monotonous, the peak in the average time to reach absorbing state would continuously shift towards lower values when system size grows. But non-monotonicity of the average size of the mediator cluster imposes a deformation on this shift, which looks like new peaks were born next to older ones. However, we must admit that the non-monotonicity of the average fraction of agents in the mediator cluster remains unexplained.

Finally, let us make one sociological observation. In the transition region from full consensus phase, the average number of clusters in the absorbing state reflects the probability to reach consensus. When the system size grows, with confidence threshold fixed, the probability of consensus increases. More agents are more likely to reach consensus at the end. It is easy to understand this phenomenon in terms of the mediators. In a larger system of agents the probability to get non-empty mediator group is larger. Because this tiny mediator group is vital for consensus, it is easier to reach consensus in larger society. It is a challenge to experimental sociologists to test this prediction in reality.

This work was carried out within the project AV0Z10100520 of the Academy of Sciences of the Czech republic and was supported by the MŠMT of the Czech Republic, grant No. OC09078 and by the Research Program CTS MSM 0021620845.

References

1. E. Callen, D. Shapero, Phys. Today **27**, 23 (1974)
2. *Collective phenomena and the applicatios of physics to other fields of science*, edited by N.A. Chigier, E.A. Stern (Brain Research Publications, Fayetteville, 1975)
3. W. Weidlich, Phys. Rep. **204**, 1 (1991)
4. S. Galam, Y. Gefen, Y. Shapir, J. Math. Sociol. **9**, 1 (1982)
5. S. Galam, J. Math. Psychol. **30**, 426 (1986)
6. S. Galam, S. Moscovici, Eur. J. Soc. Psychol. **21**, 49 (1991)
7. S. Galam, Physica A **336**, 49 (2004)
8. C. Castellano, S. Fortunato, V. Loreto, Rev. Mod. Phys. **81**, 591 (2009)
9. F. Slanina, in *Encyclopedia of Complexity and Systems Science* (Springer, New York, 2009), Vol. 8379
10. T.M. Liggett, *Stochastic Interacting Systems: Contact, Voter, and Exclusion Processes* (Springer, Berlin, 1999)
11. S. Galam, J. Stat. Phys. **61**, 943 (1990)
12. S. Galam, Physica A **274**, 132 (1999)
13. S. Galam, Physica A **285**, 66 (2000)
14. K. Sznajd-Weron, J. Sznajd, Int. J. Mod. Phys. C **11**, 1157 (2000)
15. D. Stauffer, P.M.C. de Oliveira, arXiv:cond-mat/0208296
16. L. Behera, F. Schweitzer, Int. J. Mod. Phys. C **14**, 1331 (2003)
17. F. Slanina, H. Lavička, Eur. Phys. J. B **35**, 279 (2003)
18. S. Krupa, K. Sznajd-Weron, Int. J. Mod. Phys. C **16**, 177 (2005)
19. F. Slanina, K. Sznajd-Weron, P. Przybyła, Europhys. Lett. **82**, 18006 (2008)
20. R. Lambiotte, S. Redner, Europhys. Lett. **82**, 18007 (2008)
21. P.L. Krapivsky, S. Redner, Phys. Rev. Lett. **90**, 238701 (2003)
22. M. Mobilia, S. Redner, Phys. Rev. E **68**, 046106 (2003)
23. M.H. DeGroot, J. Am. Stat. Assoc. **69**, 118 (1974)
24. R.L. Berger, J. Am. Stat. Assoc. **76**, 415 (1981)
25. R. Axelrod, J. Confl. Resolut. **41**, 203 (1997)
26. C. Castellano, M. Marsili, A. Vespignani, Phys. Rev. Lett. **85**, 3536 (2000)
27. K. Klemm, V.M. Eguíluz, R. Toral, M. San Miguel, arXiv:cond-mat/0210173
28. F. Vazquez, P.L. Krapivsky, S. Redner, J. Phys. A: Math. Gen. **36**, L61 (2003)

29. K. Klemm, V.M. Eguíluz, R. Toral, M. San Miguel, Physica A **327**, 1 (2003)
30. K. Klemm, V.M. Eguíluz, R. Toral, M. San Miguel, Phys. Rev. E **67**, 045101 (2003)
31. F. Vazquez, S. Redner, J. Phys. A: Math. Gen. **37**, 8479 (2004)
32. D. Jacobmeier, Int. J. Mod. Phys. C **16**, 633 (2005)
33. K. Klemm, V.M. Eguíluz, R. Toral, M. San Miguel, J. Econ. Dyn. Control **29**, 321 (2005)
34. J.C. González-Avella, M.G. Cosenza, K. Tucci, Phys. Rev. E **72**, 065102 (2005)
35. M.N. Kuperman, Phys. Rev. E **73**, 046139 (2006)
36. J.C. González-Avella, V.M. Eguíluz, M.G. Cosenza, K. Klemm, J.L. Herrera, M. San Miguel, Phys. Rev. E **73**, 046119 (2006)
37. F. Vazquez, S. Redner, Europhys. Lett. **78**, 18002 (2007)
38. G. Deffuant, D. Neau, F. Amblard, G. Weisbuch, Adv. Compl. Syst. **3**, 87 (2000)
39. G. Weisbuch, G. Deffuant, F. Amblard, J.P. Nadal, arXiv:cond-mat/0111494
40. G. Deffuant, F. Amblard, G. Weisbuch, T. Faure, J. Artif. Soc. Soc. Simulation **5**, 4 (2002) http://jasss.soc.surrey.ac.uk/5/4/1.html
41. E. Ben-Naim, P.L. Krapivsky, S. Redner, Physica D **183**, 190 (2003)
42. D. Stauffer, Int. J. Mod. Phys. C **13**, 315 (2002)
43. D. Stauffer, A.O. Sousa, C. Schulze, arXiv:cond-mat/0310243
44. G. Weisbuch, Eur. Phys. J. B **38**, 339 (2004)
45. D. Stauffer, H. Meyer-Ortmanns, J. Mod. Phys. C **15**, 241 (2004)
46. G. Deffuant, F. Amblard, G. Weisbuch, arXiv:cond-mat/0410199
47. F. Amblard, G. Deffuant, Physica A **343**, 725 (2004)
48. P. Assmann, Int. J. Mod. Phys. C **15**, 1439 (2004)
49. S. Fortunato, Int. J. Mod. Phys. C **15**, 1301 (2004)
50. S. Fortunato, Int. J. Mod. Phys. C **16**, 17 (2005)
51. G. Weisbuch, G. Deffuant, F. Amblard, Physica A **353**, 555 (2005)
52. J. Lorenz, Int. J. Mod. Phys. C **18**, 1819 (2007)
53. R. Hegselmann, U. Krause, J. Artif. Soc. Soc. Simulation **5** (2002), http://jasss.soc.surrey.ac.uk/5/3/2.html
54. A. Pluchino, V. Latora, A. Rapisarda, Eur. Phys. J. B **50**, 169 (2006)
55. S. Fortunato, Int. J. Mod. Phys. C **15**, 1021 (2004)
56. S. Fortunato, Physica A **348**, 683 (2005)
57. S. Fortunato, Int. J. Mod. Phys. C **16**, 259 (2005)
58. S. Fortunato, arXiv:cond-mat/0501105
59. S. Fortunato, D. Stauffer, in *Extreme Events in Nature and Society*, edited by S. Albeverio, V. Jentsch, H. Kantz (Springer, Berlin, 2006), p. 233
60. S. Fortunato, V. Latora, A. Pluchino, A. Rapisarda, Int. J. Mod. Phys. C **16**, 1535 (2005)
61. R. Hegselmann, U. Krause, J. Artif. Soc. Soc. Simulation **9** (2006), http://jasss.soc.surrey.ac.uk/9/3/10.html
62. J. Lorenz, arXiv:0708.3293 (2007)
63. J. Lorenz, Complexity **15**, 43 (2010)
64. J. Lorenz, arXiv:0806.1587 (2008)
65. J. Lorenz, EJESS **19**, 213 (2006)
66. J. Lorenz, Thesis, Universität Bremen, 2007
67. J. Lorenz, Physica A **355**, 217 (2005)
68. J. Lorenz, in *Positive Systems, Lecture Notes in Control and Information Sciences* (Springer, Berlin, 2006), Vol. 341, p. 209
69. J. Lorenz, D.A. Lorenz, IEEE Trans. Automat. Contr. **55**, 1651 (2010)
70. D. Urbig, J. Lorenz, in *Proceedings of the Second Conference of the European Social Simulation Association* (2004), ISBN 84-688-7964-9
71. M.F. Laguna, G. Abramson, D.H. Zanette, Complexity **9**, 31 (2004)
72. M. Porfiri, E.M. Bollt, D.J. Stilwell, Eur. Phys. J. B **57**, 481 (2007)
73. K. Malarz, Int. J. Mod. Phys. C **17**, 1521 (2006)
74. M.F. Laguna, G. Abramson, D.H. Zanette, Physica A **329**, 459 (2003)
75. M. Pineda, R. Toral, E. Hernández-García, J. Stat. Mech. P08001 (2009)

[Slanina04]

PHYSICAL REVIEW E **69**, 046102 (2004)

Inelastically scattering particles and wealth distribution in an open economy

František Slanina*
Institute of Physics, Academy of Sciences of the Czech Republic, Na Slovance 2, CZ-18221 Praha, Czech Republic
(Received 10 November 2003; published 14 April 2004)

Using the analogy with inelastic granular gases we introduce a model for wealth exchange in society. The dynamics is governed by a kinetic equation, which allows for self-similar solutions. The scaling function has a power-law tail, the exponent being given by a transcendental equation. In the limit of continuous trading, a closed form of the wealth distribution is calculated analytically.

DOI: 10.1103/PhysRevE.69.046102 PACS number(s): 89.65.−s, 05.40.−a, 02.50.−r

I. INTRODUCTION

The distribution of wealth among individuals within a society was one of the first ''natural laws'' of economics [1]. Indeed, its study was motivated by the desire to bring the accuracy attributed to natural sciences, namely physics, to economic sciences. The celebrated Pareto law states that the higher end of the wealth distribution follows a power-law $P(W) \sim W^{-1-\alpha}$ with exponent α robust in time.

The validity of the Pareto law was questioned and reexamined many times but the core message, stating that the tail of the distribution is a power law remains in force. There are recent investigations, e.g., Refs. [2–5], giving reasonable empirical evidence for it. In fact, it is not so much the functional form itself but its spatial and temporal stability that is intriguing. Indeed, while the value of the exponent α may slightly vary from one society to another, the very fact of the power-law tail in the distribution is valid almost everywhere. Recent investigations suggest that the range of validity of the Pareto law may extend as far in the past as to the ancient Egypt of the Pharaohs [6].

The universality of the power-law tail is surely a phenomenon asking for explanation. Recently, there was a lot of effort establishing finally the multiplicative random processes repelled from zero as a mathematical source of the power-law distributions [7–20]. Alternatively, the killed multiplicative processes as sources of power laws were studied in Ref. [4]. However, there are plenty of possible ways how the multiplicative random processes of this type come onto scene. One of the most studied implementations were the generalized Lotka-Volterra equations [10–13] and the analogy with directed polymers in random media [21–23]. Both of these schemes are formalized by a kinetic equation describing the exchange of wealth between agents and global redistribution of wealth which plays the role of repelling from zero. Related approaches were subsequently pursued by a number of studies and simulations [24–40].

More recently, empirical studies of the lower end of the wealth axis showed that the distribution of wealth is rather exponential than a power law, while the high-wealth tail still remains a power law [3,41,42]. This finding was interpreted as a result of a conservation law for total wealth, leading to the robust Boltzmann-like exponential distribution, whatever the random wealth exchange be, in full analogy with the energy distribution in a gas of elastically scattering molecules.

This, together with older studies within the same spirit [43], lead to the view of economic activity as a scattering process of agents, analogous to inelastically scattering particles [29–31,44–47]. Indeed, the inelasticity is indispensable to explain the power-law tail and it is also reasonable to suppose that the total wealth increases on average.

The numerical simulations performed to date confirm the emergence of power-law tail in agent-scattering processes with great reliability. However, analytic insight is lacking in most of the studies available today. The main concern of our work is to fill this gap, providing analytical results at least for a simplified model of wealth exchange. To comply with the task we will be guided by existing analytical approaches for models of inelastically scattering particles.

Inelastic scattering of particles was studied thoroughly in the context of granular materials [48]. The simplest one of the models used is the Maxwell model, whose inelastic variant was investigated in detail [49–61]. More realistic models of granular gases were also introduced [62,63] but their full account goes beyond the topic of this work. The most important conclusion of these studies is that a self-similar solution of the kinetic equations exist, which is not stationary in time, but assumes time-independent form after proper rescaling of the energy. The tail of the scaling function becomes a power law under certain condition.

The formalism developed for granular gases can be readily adapted for binary wealth exchange of agents. Indeed, within the mean-field version of the Maxwell model the particles scatter randomly one with another irrespectively of their positions. This corresponds to randomly picking pairs of agents for interaction, with no care of the (possibly complex) structure of their relationships. In reality the economic activity goes along links in a complex social network [64,65]. Indeed, recently there were investigations of the role of network topology in wealth distribution [34,66]. We may consider the present model as an approximation of that network by a complete graph.

The main difference from the mean-field Maxwell model is that the energy of the granular gas decreases by dissipation, while the average total wealth of the agents increases due to the economic activity. The sign of the nonconservation is therefore opposite in the two cases. While the form of the equations may remain the same, the solution cannot be

*Electronic address: slanina@fzu.cz

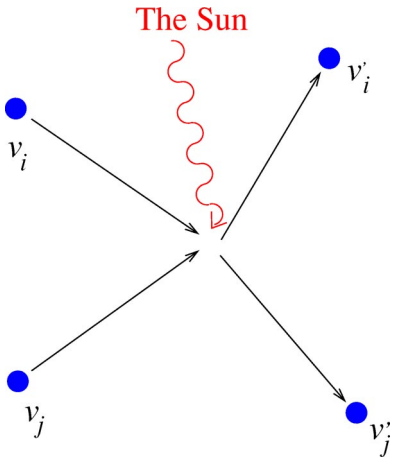

FIG. 1. Schematic picture of the scattering process, where the wealth is exchanged and produced.

directly continued from one domain to another. Therefore, while the case of dissipation is relatively well understood, new approaches are needed in the case of production. That is the aim of the present work.

II. INTERACTING AGENTS AS SCATTERING PARTICLES

A. Description of the process

Imagine a society of N agents, each of which possess certain wealth v_i, $i=1,2,...,N$. From time to time the agents interact in essentially instantaneous ''collision'' events, when a certain fraction of the wealth can be exchanged. Moreover, we suppose the system is open and the interaction can catalyze an increase of the total wealth of the two interacting agents. Indeed, the source of the human wealth lies beyond our society and the ultimate cause is the energy poured to the Earth from the Sun. Nonetheless, the external energy is utilized only through a human activity and we simplify the problem by assuming that the net increase of wealth happens at the very moments of agents' interaction.

We also assume that only pairwise interaction occurs. This may be a very crude assumption, as corporate decisions affect many agents simultaneously. However, we expect the presence of multilateral interactions does not affect the essential mechanisms in work here.

The dynamics of our model is described as follows. In each time step t a pair of agents (i, j) is chosen randomly. They interact and exchange wealth according to the symmetric rule

$$\begin{pmatrix} v_i(t+1) \\ v_j(t+1) \end{pmatrix} = \begin{pmatrix} 1+\epsilon-\beta & \beta \\ \beta & 1+\epsilon-\beta \end{pmatrix} \begin{pmatrix} v_i(t) \\ v_j(t) \end{pmatrix}. \quad (1)$$

All other agents leave their wealth unchanged, $v_k(t+1)=v_k(t)$ for all k different from both i and j. The parameter $\beta \in (0,1)$ quantifies the wealth exchanged, while $\epsilon>0$ measures the flow of wealth from the outside. The process is sketched schematically in Fig. 1.

This rule is similar to those studied in Refs. [43,53,56] and simulated numerically in Refs. [29,31,44,47] but we consider it slightly more realistic as it treats the agents in *a priori* symmetric manner. It also embraces various sources of wealth nonconservation within a single effective parameter ϵ. In fact, also the formulation based on the similarity with the problem of directed polymers [21,22] can be reduced to a rule of the form similar to Eq. (1). Therefore, we are studying a representative of a whole class of related models and we expect the analytical results we will present have rather broad relevance.

B. Kinetic equation

Equation (1) describes a matrix multiplicative stochastic process of vector variable $v(t)$ in discrete time t. Processes of this type are thoroughly studied, e.g., in the context of granular gases. Indeed, if the variables v_i are interpreted as energies corresponding to ith granular particle, we can map the process to the mean-field limit of the Maxwell model of inelastic particles. However, the energy dissipation conventionally quantified by the restitution coefficient implies now the negative value $\epsilon<0$, contrary to our assumption $\epsilon>0$. We will see later that this apparently small variation makes big difference in the analytical treatment of the process.

The full information about the process in time t is contained in the N-particle joint probability distribution $P_N(t;v_1,v_2,...,v_N)$. However, we can write a kinetic equation involving only one- and two-particle distribution functions

$$P_1(t+1;v)-P_1(t;v) = \frac{2}{N}\left[-P_1(t;v)+\int P_2(t;v_i,v_j) \times \delta((1-\beta+\epsilon)v_i+\beta v_j-v)dv_i dv_j\right] \quad (2)$$

which may be continued to give eventually an infinite hierarchy of equations of BBGKY type. As a standard approximation we use the factorization

$$P_2(t;v_i,v_j)=P_1(t;v_i)P_1(t;v_j) \quad (3)$$

which breaks the hierarchy on the lowest level, neglecting the correlations between the wealth of the agents, induced by the scattering. In fact, this approximation becomes exact for $N\to\infty$. Therefore, in thermodynamic limit the one-particle distribution function bears all information.

Rescaling the time as $\tau=2t/N$ in the thermodynamic limit $N\to\infty$, we obtain for the one-particle distribution function $P(\tau;v)=P_1(t,v)$ a Boltzmann-like kinetic equation

$$\frac{\partial P(v)}{\partial \tau}+P(v)=\int P(v_i)P(v_j) \times \delta((1-\beta+\epsilon)v_i+\beta v_j-v)dv_i dv_j \quad (4)$$

which describes exactly the process (1) in the limit $N\to\infty$. This equation has the same form as the mean-field version for the well-studied Maxwell model of inelastically scattering particles [54,56,57]. The main difference consists in the

fact that here the wealth increases, while in inelastic gas the energy decreases. This seemingly little difference has, however, deep consequences for the solution of Eq. (4). Note also that within the framework of Maxwell model the distributions are expressed in terms of velocities, while our dynamical variables correspond rather to energies of the particles.

III. SOLUTION OF THE KINETIC EQUATION

A. Self-similar solutions

Note first that the average wealth $\overline{v}=\int vP(v)dv$ in the process described by the kinetic equation (4) grows exponentially

$$\overline{v}(\tau)=\overline{v}(0)e^{\epsilon\tau} \tag{5}$$

and therefore Eq. (4) has no stationary solution. However, we may look for a quasistationary self-similar solution in the form [50,54,56,57]

$$P(\tau;v)=\frac{1}{\overline{v}(\tau)}\Phi\left(\frac{v}{\overline{v}(\tau)}\right). \tag{6}$$

Using the Laplace transform $\hat{\Phi}(x)=\int_0^\infty \Phi(w)e^{-xw}dw$ we can write a nonlocal differential equation for the scaling function in the form

$$\epsilon x\hat{\Phi}'(x)+\hat{\Phi}(x)=\hat{\Phi}((1-\beta+\epsilon)x)\hat{\Phi}(\beta x). \tag{7}$$

A hint about possible solutions can be obtained from a special exactly solvable case $\epsilon=-2\sqrt{\beta}+2\beta$. It can be easily verified [54] that the function $\hat{\Phi}_1(x)=(1+\sqrt{2x})e^{-\sqrt{2x}}$ is a solution of Eq. (7). Inverting the Laplace transform we obtain the corresponding wealth distribution $\Phi_1(w)=(1/\sqrt{2\pi})w^{-5/2}\exp(-1/2w)$ which has a similar form as obtained in previous studies [13,21,22]. However, in this case the value of ϵ is negative, which contradicts our assumption of wealth increase, while for $\epsilon>0$ the above idea leading to the function $\hat{\Phi}_1(x)$ does not work. Therefore, we must look for alternative ways. The leading idea of our approach is that Eq. (7) is nearly local for small values of ϵ and β. Therefore, we will expand the factors on the right-hand side (RHS) of Eq. (7) in Taylor series in ϵ and β and perform the limit ϵ, $\beta\to 0$. As the parameters ϵ and β quantify the amount of wealth increase and exchange in a single trade event, we interpret the latter limit as the limit of continuous trading. In fact, such a limit should also involve a rescaling of time τ, but because we are interested only in the stationary regime, the explicit time dependence does not enter our considerations.

It should be also stressed that an important feature can be inferred from the observation that the system behaves differently for positive and negative ϵ. Indeed, it suggests a singularity at the point of precise conservation of wealth $\epsilon=0$.

B. Power-law tails

The main concern in empirical studies of wealth distribution is about the shape of tails, which assumes a power-law

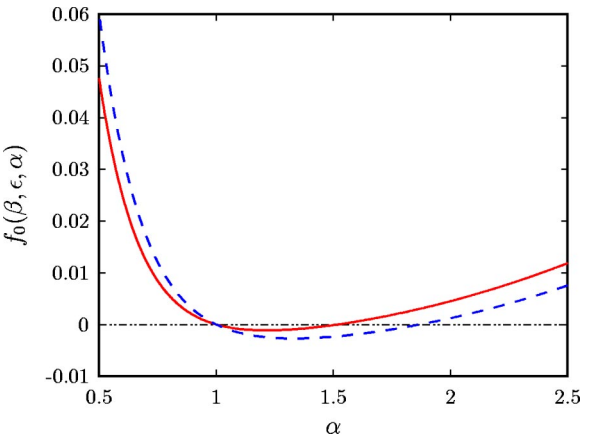

FIG. 2. Solution of the equation $f_0(\beta,\epsilon,\alpha)\equiv(1+\epsilon-\beta)^\alpha+\beta^\alpha-1-\epsilon\alpha=0$ for $\epsilon=0.1$ and $\beta=0.0025$ (full line) and $\beta=0.004$ (dashed line).

form. The behavior of the distribution $\Phi(w)$ for $w\to\infty$ can be deduced from the singularity of the Laplace transform $\hat{\Phi}(x)$ at $x\to 0$. Therefore, we assume the following behavior [54,57]:

$$\hat{\Phi}(x)=1-x+A|x|^\alpha+\cdots \quad \text{for} \quad x\to 0, \tag{8}$$

where $\alpha\in(1,2)$. This type of singularity results in the power-law tail as $\Phi(w)\sim w^{-\alpha-1}$ for $w\to\infty$. Insertion of Eq. (8) into Eq. (7) leads to a transcendental equation for the exponent α

$$(1+\varepsilon-\beta)^\alpha+\beta^\alpha-1-\varepsilon\alpha=0 \tag{9}$$

the solution of which is illustrated in Fig. 2. Obviously, there is always a trivial solution $\alpha=1$. The power-law tail is due to another, nontrivial solution, which falls into the desired interval (1, 2) only for certain values of the parameters β and ϵ. We can see the allowed region in Fig. 3; a solution in the range $\alpha\in(1,2)$ exists within the shaded region. We can also see that fixed value of α defines a line in the β-ϵ plane. We can approach the limit $\epsilon\to 0$, $\beta\to 0$ while keeping α constant.

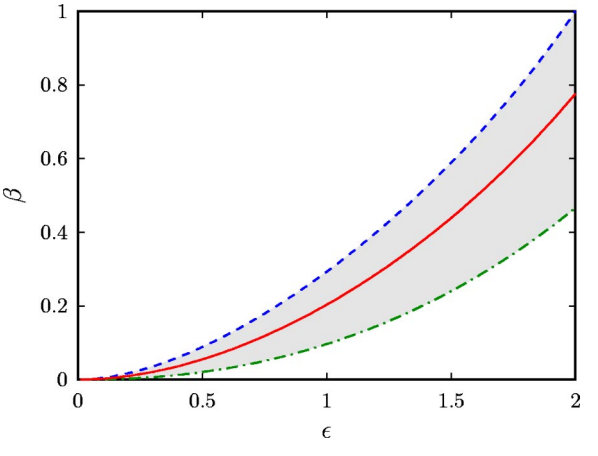

FIG. 3. Solution in the range $\alpha\in(1,2)$ exists within the shaded region. The dashed line corresponds to $\alpha=2$, the dash-dotted line to $\alpha=1$, and the full line to the solution $\alpha=3/2$.

This is to be interpreted as continuous trading, as the amount of wealth exchange and increase in a single trading step is infinitesimally small. Making this, the nonlocal terms in Eq. (7) become local and we can expect to obtain an ordinary differential equation, soluble by standard methods.

C. Continuous trading limit

Indeed, expanding Eq. (9) we obtain the following formula relating β and ϵ for fixed α in the limit of continuous trading $\beta\to 0$, $\epsilon\to 0$:

$$\beta=\frac{\alpha-1}{2}\epsilon^2+O(\epsilon^3)+O(\epsilon^{2\alpha}). \tag{10}$$

The leading correction term to Eq. (10) depends on the value of α; for $1<\alpha<3/2$ it is of order $O(\epsilon^{2\alpha})$, for $3/2<\alpha<2$ it is of order $O(\epsilon^3)$, while in the special point $\alpha=3/2$ we should include both correction terms, as they are of the same order $O(\epsilon^3)$. Systematic expansion in ϵ is developed in the Appendix.

Taking the same limit with fixed α in Eq. (7) we obtain, using Eq. (10), the following equation:

$$-\frac{1}{2}x\hat{\Phi}''(x)+\frac{\alpha-1}{2}(\hat{\Phi}'(x)+\hat{\Phi}(x))=0. \tag{11}$$

Of the two independent solutions of Eq. (11) only one has correct asymptotics $\hat{\Phi}(x)\to 0$ for $x\to+\infty$. It can be expressed using modified Bessel function

$$\hat{\Phi}(x)=C'x^{\alpha/2}K_\alpha(2\sqrt{\alpha-1}\sqrt{x}), \tag{12}$$

where the constant C' is fixed by the normalization $\hat{\Phi}(0)=1$. Inverting the Laplace transform we finally obtain the wealth distribution

$$\Phi(w)=Cw^{-\alpha-1}\exp\left(-\frac{\alpha-1}{w}\right) \tag{13}$$

with $C=(\alpha-1)^\alpha/\Gamma(\alpha)$.

We can see that the distribution obtained exhibits the desired power-law behavior for large wealth. Moreover, it has a maximum at a finite value of $w=w_{\max}\equiv(\alpha-1)/(\alpha+1)$ and depression for low wealth values. The size of the depletion is determined by the exponential term in Eq. (13), i.e., by the same value of α which determines the power in the power law. This corresponds to the idea presented, e.g., in Ref. [11] stating that it is the value of the lower bound for the allowed wealth which determines the value of the exponent. Here, however, this result comes purely formally as a result of the analytic computation. In our approach it is the interplay between wealth increase (parameter ϵ) and wealth exchange (parameter β) that dictates the value of the exponent α.

D. Corrections for finite trading in one step

Expanding Eq. (7) in powers of ϵ and β it is possible to include systematic corrections to Eq. (11) and therefore corrections to wealth distribution (13) for a finite amount of wealth increase and exchange in single trading step. Details of the calculations are given in the Appendix; here we only summarize the results.

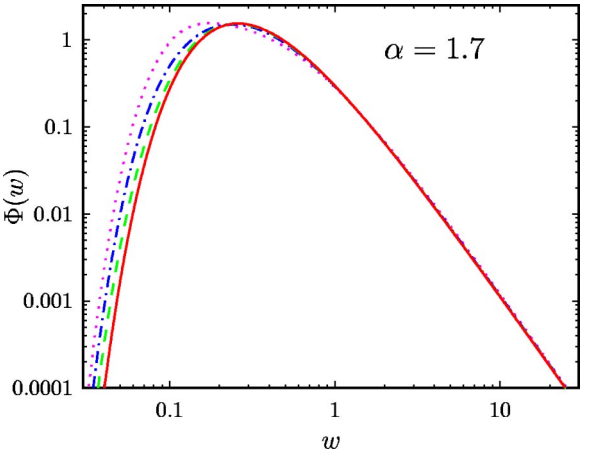

FIG. 4. Wealth distribution according to Eq. (15) for $\epsilon\to 0$ (full line), $\epsilon=0.03$ (dashed line), $\epsilon=0.1$ (dash-dotted line), and $\epsilon=0.3$ (dotted line).

The expansion (10) of the parameter β in powers of ϵ can be continued as

$$\beta=\frac{\alpha-1}{2}\epsilon^2+\frac{1}{\alpha}\left(\frac{\alpha-1}{2}\right)^\alpha\epsilon^{2\alpha}-\frac{(\alpha-1)(2\alpha-1)}{6}\epsilon^3+O(\epsilon^4)+O(\epsilon^{4\alpha-2}). \tag{14}$$

Correspondingly, the wealth distribution, expanded in powers of ϵ is

$$\Phi(w)=\frac{(\alpha-1)^\alpha}{\Gamma(\alpha)}w^{-1-\alpha}\exp\left(\frac{1-\alpha}{w}\right)\times\left[1+\frac{\alpha-1}{3}\left(\frac{2\alpha}{w}-\frac{\alpha-1}{w^2}-\nu_{10}\right)\epsilon-\frac{2}{\alpha}\left(\frac{\alpha-1}{2}\right)^\alpha\left(\ln w+\frac{1}{w}-\nu_{01}\right)\epsilon^{2(\alpha-1)}\right]+O(\epsilon^4)+O(\epsilon^{4\alpha-2}), \tag{15}$$

where the constants ν_{01} and ν_{10} are given in the Appendix. We show in Fig. 4 the wealth distribution according to Eq. (15) for $\alpha=1.7$ and several positive values of ϵ, namely for $\epsilon=0.03$, 0.1, and 0.3. We can see that the distribution is affected mainly at small values of wealth, shifting the maximum toward smaller w when ϵ increases. On the contrary, the tail of the distribution is nearly unaffected, showing universal and robust power-law behavior.

Let us stress again that the solution known for $\epsilon<0$ cannot be properly continued to the region of $\epsilon>0$, due to the presence of singularity at $\epsilon=0$. The singularity can be seen, e.g., in the behavior of the solution of Eq. (9), as shown in Fig. 5. However, for $\alpha=3/2$ the formula (13) describes the solution of Eq. (7) on both limits $\epsilon\to 0^+$ and $\epsilon\to 0^-$. This implies that the singularity is rather weak, because the solution of

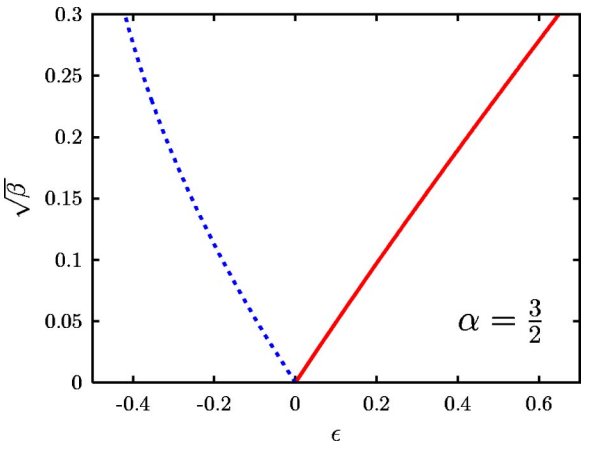

FIG. 5. Solution of Eq. (9) for $\alpha=3/2$ in the ranges $\epsilon>0$ (full line) and $\epsilon<0$ (dashed line). Note the singularity at $\epsilon=0$ which means that we must skip from one of the three solutions of Eq. (9) to another one.

Eq. (7) is continuous in ϵ, and only the derivative with respect of ϵ has a jump at $\epsilon=0$. One may speculate about the fate of the singularity if we allowed ϵ and β not fixed parameters but random processes themselves. Most probably the singularity would vanish but final answer is left for future work.

IV. CONCLUSIONS

We formulated a model of wealth production and exchange, where agents randomly interact pairwise. Using the analogy with the mean-field version of the Maxwell model for inelastic scattering of granular particles we obtain analytical results for the wealth distribution.

The dynamics of the model is governed by a kinetic equation for one-particle distribution function. We look for self-similar scaling solutions, corresponding to redefining the unit of wealth after each wealth increase. The form of these solutions is given by a nonlocal differential equation, exactly soluble only in the practically irrelevant case of net wealth decrease. Therefore we turned to approximation schemes.

First, we looked at the behavior for large wealth. The tail of the wealth distribution has a power-law form, and its exponent α is determined by the interplay between the intensity of the wealth exchange and the amount of wealth produced. The form line in the β-ϵ plane with fixed α is found, depending quadratically on ϵ for $\epsilon\to 0$. The physically allowed values $\alpha\in(1,2)$ determine a horn-shaped region in the β-ϵ plane.

The second approximation consisted in taking the limit of continuous trading, meaning small wealth production and small exchange within a single trading operation, while keeping the exponent α constant. Here we obtained closed formula for the entire wealth distribution, which has a power-law tail as expected and a maximum at certain (low) wealth value. The form of the wealth distribution corresponds to those found in previous studies [13,21,22]. It is interesting to note that this general form has one-to-one correspondence between the position $w_{\max}$ of the maximum of the distribution and the value of the exponent. There are few agents having wealth below $w_{\max}$. This suggests that the intuition formalized, e.g., in Refs. [11,13], that the exponent is ''tuned'' by the low-wealth behavior of the distribution, may be in work quite generally. Here, the free parameters are apparently the wealth production and exchange, but in reality these parameters may be themselves tuned by a mechanism which fixes the position of the maximum of the wealth distribution, i.e., the lowest wealth compatible with survival.

However, there is still open question of the specific values of the exponent, which are quite robust in different societies. It seems, also on the basis of our results, that it cannot be explained by the bare mechanism of economic exchange and some other ingredient, possibly of sociological origin, is required.

ACKNOWLEDGMENTS

I wish to thank Paul Krapivsky and Eli Ben-Naim for stimulating comments and discussions. This work was supported by Project No. 202/01/1091 of the Grant Agency of the Czech Republic.

APPENDIX: SYSTEMATIC EXPANSION FOR SMALL ϵ AND β

Let us start with the special value $\alpha=3/2$. Here, Eq. (9) has an explicit solution in the form

$$\epsilon=\frac{1}{8}\frac{-3\sqrt{\beta}+17\beta-29\beta^{3/2}+15\beta^2+4\beta^{5/2}-4\beta^3+\sqrt{3}\sqrt{(3-2\sqrt{\beta})\beta(2\sqrt{\beta}+1)^3(\sqrt{\beta}-1)^6}}{\sqrt{\beta}-3\beta+3\beta^{3/2}-\beta^2}. \quad \text{(A1)}$$

However, the nonlocal differential equation (7) still does not yield explicit solution. Inverting the expression (A1) we get the following series expansion:

$$\beta=\frac{1}{4}\epsilon^2-\frac{1}{12}\epsilon^3+\frac{1}{16}\epsilon^4-\frac{7}{144}\epsilon^5+\frac{113}{2592}\epsilon^6+O(\epsilon^7). \quad \text{(A2)}$$

For general value of α the variable β is expressed as a series in two small parameters ϵ and $\eta=\epsilon^{2(\alpha-1)}$, which coincide only if $\alpha=3/2$. Therefore, we can write

$$\beta=\epsilon^2\sum_{m,n=0}^{\infty}\beta_{mn}\epsilon^{m+2(\alpha-1)n} \quad \text{(A3)}$$

and the various terms take variable precedence in the order of smallness when $\epsilon \to 0$, depending on the value of α. For the first several coefficients we have

$$\beta_{00} = \frac{\alpha - 1}{2}, \tag{A4}$$

$$\beta_{10} = -\frac{(\alpha - 1)(2\alpha - 1)}{6}, \tag{A5}$$

$$\beta_{01} = \frac{1}{\alpha}\left(\frac{\alpha - 1}{2}\right)^{\alpha}. \tag{A6}$$

Starting from the expansion (A3) we can convert the first order nonlocal differential equation (7) for $\hat{\Phi}(x)$ into infinite-order local differential equation for $\Phi(w)$. The price to pay for it is that the coefficients in the latter equation contain the moments $\mu_k = \int \Phi(w) w^k dw$ of the solution itself. Indeed, we can write

$$\hat{\Phi}((1 - \nu + \epsilon)x) = \lim_{y \to x} \exp\left((\epsilon - \beta)x \frac{d}{dy}\right)\hat{\Phi}(y), \tag{A7}$$

$$\hat{\Phi}(\beta x) = \lim_{y \to 0} \exp\left(\beta x \frac{d}{dy}\right)\hat{\Phi}(y). \tag{A8}$$

Therefore, we obtain a linear combination of terms of the following form:

$$x^{m+n} \frac{d^m \hat{\Phi}(x)}{dx^m} \frac{d^n \hat{\Phi}(0)}{dx^n} \tag{A9}$$

which, after inverse Laplace transform, give rise to terms

$$(-1)^{m+n} \mu_n \frac{d^{m+n}}{dw^{m+n}}[w^m \Phi(w)]. \tag{A10}$$

However, the first two moments are fixed by definition. Indeed, the normalization of the probability distribution fixes the zeroth moment and the fixed average wealth, imposed by the scaling condition (6) fixes the first moment, so that $\mu_0 = \mu_1 = 1$. This consideration leads to the equations for lowest correction to the solution (13) , which are free of unknown higher moments.

Generally, the solution can be then expressed in the form of the series in powers of ϵ and $\epsilon^{2(\alpha-1)}$

$$\Phi(w) = \Phi_0(w) \sum_{m,n=0}^{\infty} \phi_{mn}(w) \epsilon^{m + 2(\alpha - 1)n}. \tag{A11}$$

We assume $\phi_{00}(w) = 1$. The normalization must be independent of ϵ, which can be written as

$$\int_0^{\infty} \Phi_0(w) \phi_{mn}(w) dw = \delta_{m0} \delta_{n0}. \tag{A12}$$

Therefore, the lowest term obeys the equation

$$\frac{w^2}{2} \Phi_0'(w) + \left(\frac{\alpha - 1}{2} w - \frac{\alpha - 1}{2}\right)\Phi_0(w) = 0 \tag{A13}$$

which has the following solution satisfying the normalization (A12):

$$\Phi_0(w) = \frac{(\alpha - 1)^{\alpha}}{\Gamma(\alpha)} w^{-1-\alpha} \exp\left(\frac{1 - \alpha}{w}\right). \tag{A14}$$

Indeed, it coincides with the result of Eq. (13).

The next two terms satisfy the following equations:

$$\frac{w^2}{2} \phi_{10}'(w) = \frac{\alpha - 1}{3}\left(\alpha - \frac{\alpha - 1}{w}\right), \tag{A15}$$

$$\frac{w^2}{2} \phi_{01}'(w) = -\frac{1}{\alpha}\left(\frac{\alpha - 1}{2}\right)^{\alpha}(w - 1) \tag{A16}$$

which can be easily solved. We obtain

$$\phi_{10}(w) = -\frac{\alpha - 1}{3}\left(\frac{2\alpha}{3} - \frac{\alpha - 1}{w^2} - \nu_{10}\right), \tag{A17}$$

$$\phi_{01}(w) = -\frac{2}{\alpha}\left(\frac{\alpha - 1}{2}\right)^{\alpha}\left(\ln w + \frac{1}{w} - \nu_{01}\right) \tag{A18}$$

and the constants ν_{01}, ν_{10} are fixed by the normalization condition (A12). We find explicitly

$$\nu_{10} = \alpha, \tag{A19}$$

$$\nu_{01} = \ln(\alpha - 1) - \Psi(\alpha) + \frac{\alpha}{\alpha - 1}, \tag{A20}$$

where $\Psi(x) = \Gamma'(x)/\Gamma(x)$ is the logarithmic derivative of the gamma function.

[1] V. Pareto, *Cours d'economie Politique* (F. Rouge, Lausanne, 1897).
[2] M. Levy and S. Solomon, Physica A **242**, 90 (1997).
[3] A. Drăgulescu and V. M. Yakovenko, Physica A **299**, 213 (2001).
[4] W. J. Reed and B. D. Hughes, Phys. Rev. E **66**, 067103 (2002).
[5] H. Aoyama, W. Souma, and Y. Fujiwara, Physica A **324**, 352 (2003).
[6] A. Y. Abul-Magd, Phys. Rev. E **66**, 057104 (2002).
[7] M. Levy and S. Solomon, Int. J. Mod. Phys. C **7**, 595 (1996).
[8] M. Levy and S. Solomon, Int. J. Mod. Phys. C **7**, 65 (1996).
[9] O. Biham, O. Malcai, M. Levy, and S. Solomon, Phys. Rev. E **58**, 1352 (1998).
[10] S. Solomon, in *Decision Technologies for Computational Finance*, edited by A.-P. Refenes, A. N. Burgess, and J. E. Moody (Kluwer Academic Publishers, Dordrecht, 1998).

[Slanina04]

[11] S. Solomon, in *Application of Simulation to Social Sciences*, edited by G. Ballot and G. Weisbuch (Hermes Science Publications, 2000).
[12] Z.-F. Huang and S. Solomon, Eur. Phys. J. B **20**, 601 (2001).
[13] S. Solomon and P. Richmond, Physica A **299**, 188 (2001).
[14] A. Blank and S. Solomon, Physica A **287**, 279 (2000).
[15] S. Solomon and M. Levy, e-print cond-mat/0005416.
[16] Z.-F. Huang and S. Solomon, Physica A **294**, 503 (2001).
[17] D. Sornette and R. Cont, J. Phys. I **7**, 431 (1997).
[18] D. Sornette, Physica A **250**, 295 (1998).
[19] D. Sornette, Phys. Rev. E **57**, 4811 (1998).
[20] H. Takayasu, A.-H. Sato, and M. Takayasu, Phys. Rev. Lett. **79**, 966 (1997).
[21] M. Marsili, S. Maslov, and Y.-C. Zhang, Physica A **253**, 403 (1998).
[22] J.-P. Bouchaud and M. Mézard, Physica A **282**, 536 (2000).
[23] Z. Burda, D. Johnston, J. Jurkiewicz, M. Kamiński, M. A. Nowak, G. Papp, and I. Zahed, e-print cond-mat/0101068.
[24] W. Souma, e-print cond-mat/0011373.
[25] H. Aoyama, Y. Nagahara, M. P. Okazaki, W. Souma, H. Takayasu, and M. Takayasu, e-print cond-mat/0006038.
[26] W. Souma, e-print cond-mat/0202388.
[27] W. Souma, Y. Fujiwara, and H. Aoyama, Phys. Rev. E **65**, 026102 (2002).
[28] Y. Fujiwara, W. Souma, H. Aoyama, T. Kaizoji, and M. Aoki, e-print cond-mat/0208398.
[29] A. Chakraborti and B. K. Chakrabarti, Eur. Phys. J. B **17**, 167 (2000).
[30] B. K. Chakrabarti and A. Chatterjee, in *Applications of Econophysics*, Conference Proceedings of the Second Nikkei Symposium on Econophysics, Tokyo, Japan, 2002 (Springer-Verlag, Tokyo, 2003) pp. 280–285; e-print cond-mat/0302147.
[31] A. Chatterjee, B. K. Chakrabarti, and S. S. Manna, e-print cond-mat/0301289; Phys. Scr. **T106**, 36 (2003); e-print cond-mat/0311227.
[32] A. Das and S. Yarlagadda, e-print cond-mat/0304685.
[33] S. Pianegonda, J. R. Iglesias, G. Abramson, and J. L. Vega, Physica A **322**, 667 (2003).
[34] J. R. Iglesias, S. Gonçalves, S. Pianegonda, J. L. Vega, and G. Abramson, Physica A **327**, 12 (2003).
[35] S. Pianegonda and J. R. Iglesias, e-print cond-mat/0311113.
[36] J. R. Iglesias, S. Gonçalves, G. Abramson, and J. L. Vega, e-print cond-mat/0311127.
[37] M. Anazawa, A. Ishikawa, T. Suzuki, and M. Tomoyose, e-print cond-mat/0307116.
[38] T. Mizuno, M. Katori, H. Takayasu, and M. Takayasu, e-print cond-mat/0308365.
[39] T. Mizuno, M. Takayasu, and H. Takayasu, e-print cond-mat/0307270.
[40] Y. Fujiwara, C. Di Guilmi, H. Aoyama, M. Gallegati, and W. Souma, e-print cond-mat/0310061.
[41] A. Drăgulescu and V. M. Yakovenko, Eur. Phys. J. B **17**, 723 (2000); **20**, 585 (2001); in *Modeling of Complex Systems: Seventh Granada Lectures*, AIP Conf. Proc. No. 661 (AIP, New York, 2003), p. 180.
[42] V. M. Yakovenko, e-print cond-mat/0302270.
[43] S. Ispolatov, P. L. Krapivsky, and S. Redner, Eur. Phys. J. B **2**, 267 (1998).
[44] N. Scafetta, S. Picozzi, and B. J. West, e-print cond-mat/0209373.
[45] N. Scafetta and B. J. West, e-print cond-mat/0306579.
[46] M. Gligor and M. Ignat, Eur. Phys. J. B **30**, 125 (2002).
[47] S. Sinha, Phys. Scr., T **T106**, 59 (2003).
[48] H. M. Jaeger, S. R. Nagel, and R. P. Behringer, Rev. Mod. Phys. **68**, 1259 (1996).
[49] A. V. Bobylev, J. A. Carillo, and I. M. Gamba, J. Stat. Phys. **98**, 743 (2000).
[50] A. V. Bobylev and C. Cercignani, J. Stat. Phys. **106**, 547 (2002); **110**, 333 (2003).
[51] A. Baldassarri, U. Marini Bettolo Marconi, and A. Puglisi, Europhys. Lett. **58**, 14 (2002).
[52] I. Ispolatov and P. L. Krapivsky, Phys. Rev. E **61**, R2163 (2000).
[53] E. Ben-Naim and P. L. Krapivsky, Phys. Rev. E **61**, R5 (2000).
[54] P. L. Krapivsky and E. Ben-Naim, J. Phys. A **35**, L147 (2002).
[55] E. Ben-Naim and P. L. Krapivsky, Phys. Rev. E **66**, 011309 (2002).
[56] D. Ben-Avraham, E. Ben-Naim, K. Lindenberg, and A. Rosas, Phys. Rev. E **68**, 050103 (2003).
[57] M. H. Ernst and R. Brito, Europhys. Lett. **58**, 182 (2002).
[58] M. H. Ernst and R. Brito, e-print cond-mat/0111093; Phys. Rev. E **65**, 040301 (2002); J. Stat. Phys. **109**, 407 (2002); Europhys. Lett. **58**, 182 (2002); cond-mat/0304608.
[59] E. Ben-Naim and P. L. Krapivsky, Lect. Notes. Phys. **624**, 65 (2003).
[60] T. Antal, M. Droz, and A. Lipowski, Phys. Rev. E **66**, 062301 (2002).
[61] E. Barkai, Phys. Rev. E **68**, 055104 (2003).
[62] A. Baldassarri, U. Marini Bettolo Marconi, and A. Puglisi e-print cond-mat/0105299.
[63] A. Baldassarri, U. Marini Bettolo Marconi, A. Puglisi, and A. Vulpiani, Phys. Rev. E **64**, 011301 (2001).
[64] D. J. Watts and S. H. Strogatz, Nature (London) **393**, 440 (1998).
[65] A.-L. Barabási and R. Albert, Science **286**, 509 (1999).
[66] T. Di Matteo, T. Aste, and S. T. Hyde, cond-mat/0310544.

[Slanina01a]

PHYSICAL REVIEW E, VOLUME 64, 056136

Mean-field approximation for a limit order driven market model

František Slanina*
Institute of Physics, Academy of Sciences of the Czech Republic, Na Slovance 2, CZ-18221 Praha, Czech Republic
(Received 27 April 2001; published 30 October 2001)

A mean-field variant of the model of limit order driven market introduced recently by Maslov is formulated and solved. The agents do not have any strategies and the memory of the system is kept within the order book. We show that the evolution of the order book is governed by a matrix multiplicative process. The resulting stationary distribution of step-to-step price changes is calculated. It exhibits a power-law tail with exponent 2. We obtain also the price autocorrelation function, which agrees qualitatively with the experimentally observed negative autocorrelation for short times.

DOI: 10.1103/PhysRevE.64.056136 PACS number(s): 05.40.−a, 89.90.+n

I. INTRODUCTION

The complexity of market behavior, seen as a particular example of a natural phenomenon, has fascinated physicists for many years [1]. The main source of interest comes from a kind of critical behavior, made explicit by the power-law distribution and scaling in the economic time series, first observed by Mandelbrot (see Ref. [2], and references therein) and studied in detail by Mantegna and Stanley [3–5] and subsequently by many others (see, e.g., Refs. [6–11]).

Scaling and multifractal properties call for an explanation in terms of a model mimicking the behavior of individual agents in the market. The physicist's optimism in looking for such a model might be strengthened by recent successes in modeling other social phenomena, e.g., in the cellular-automata models of traffic [12]. The idea consists in assuming that the overwhelming complexity of a human being is irrelevant in certain special conditions: when driving a car, only a very basic set of behaviors is at work. Similarly, it is assumed that a trading agent, when put on the floor, follows only a limited set of instincts or acquired patterns. Therefore, in this approach, the economic complexity is not due to the intrinsic complexity of each agent (as usual hand-waving arguments by liberal opponents of ''reductionism'' state), but an emergent property of a large set of nonlinearly interacting simple units.

Many microscopic stock market models have emerged during the last several years. One of the first ones was the model introduced by Levy, Levy, and Solomon [13–15], which captures essential features of the price fluctuations and explains also the power-law distribution of investor's wealth, which is the famous Pareto law.

Another approach was used in the model of Bak, Paczuski, and Shubik [16]: buyers and sellers are represented by particles subject to a reaction-diffusion process. The introduction of a nontrivial strategy of the agents leads to a realistic value of the Hurst exponent for the price fluctuations. A simpler version of the model was then solved analytically [17]. A variety of other approaches were investigated [18–34].

The above mentioned models mainly do not take into account the realistic details of the price formation through the book of orders. This mechanism was implemented in the model set up by Maslov [35] and a similar perspective was then used in a recent series of papers by Matassini and Franci [36–38]. The book of orders perspective to market modeling was empirically investigated in Refs. [39,40].

With such a diversity of models, most of which give a plausible explanation of observed facts, a question arises: whether there is a common mechanism behind various approaches, making them essentially equivalent. Indeed, it was found that such a mechanism may be the multiplicative stochastic process repelled from zero, or the multiplicative-additive process. It was studied thoroughly by various authors and in diverse contexts [15,41–52]. The goal we pose in this work is to show that essentially the same mechanism is responsible for the power-law distribution of price changes also in the limit order model.

II. LIMIT ORDER DRIVEN MARKET MODEL

Recently, Maslov and co-workers [35,39] proposed a model, based on the assumption that there are two kinds of market participants. Prudent investors place their orders at a prescribed price and a trade occurs as soon as there is anyone accepting that price. On the other hand, speculators buy and sell at any moment at the price which is available in the market. The price signal $p(t)$ was found to have a power-law spectrum, with Hurst exponent $H=1/4$. The price changes during a unit time interval $x=p(t+1)-p(t)$ have probability distribution that follows clear power law $P(x) \sim x^{-(1+\alpha)}$ in two regimes. For small x the exponent is $1+\alpha_1=0.6\pm0.1$, while in the regime of large price changes the exponent is $1+\alpha_2=3\pm0.2$. These values are to be compared to the experimentally found values $1+\alpha_1\simeq2.5$ and $1+\alpha_2\simeq4$, respectively [6,9–11].

The presented model [35] can be described as follows. There are orders to buy and sell placed on a straight line, which is the axis of the price x. In a stable situation, all buy orders are lower than all sell orders, so that we can describe the state by single function $\rho(x)$, density of the orders, and a number ξ, which is the last realized price. Then, all $x<\xi$ correspond to buy, all $x>\xi$ to sell orders.

Two events can change the state. First, new limit orders may be dropped, such that $\rho(x)\to\rho(x)+\eta(x-\xi)$. We sup-

*Email address: slanina@fzu.cz

pose the function $\eta(x)$ is equal in all events and is symmetric, $\eta(x)=\eta(-x)$. Second, a market-price order can arrive. An order to buy an amount s results in clearing all sell orders up to the price $\xi+x_+$, where

$$\int_{\xi}^{\xi+x_+}\rho(x)\mathrm{d}x=s. \tag{1}$$

The new price is then $\xi\to\xi+x_+$, so that x_+ is the price increment, while the new density is $\rho(x)\to[1-\theta(x-\xi)\theta(\xi+x_+-x)]\rho(x)$. Analogical formulas will hold for the sell order.

As we can see, there are no strategies that would lead the agents to perform specific actions. The model is barely stochastic. The long-term memory of the system and thus a possible power-law behavior stems from the order book, or the time-dependent density function $\rho(x)$ that may keep arbitrarily old orders.

III. MATRIX FORMULATION

Our essential approximation to this model will consist in supposing a uniform density of orders on each side from the current price level ξ. In reality, both dropping new limit orders and clearing them by market orders make the density of states uneven and fluctuating. When supposing that after an event the uniform density of states is restored, we make a kind of ''mean-field'' approximation: the actual position of each limit order is not important, as if they were freely moving particles making an effective medium, within which the price fluctuates. A high density of the medium will result in smaller price fluctuations and vice versa.

The density on the upper side will be denoted ρ_+, on the lower side ρ_-. It is convenient to describe the densities in terms of the potential price changes, which would occur if a market-price order arrives. They are simply $x_+=s/\rho_+$ for buy and $x_-=s/\rho_-$ for sell order. The numbers $x_\pm$ form a vector

$$X=\begin{pmatrix}x_+\\x_-\end{pmatrix},$$

which performs a stochastic process, as the densities $\rho_\pm$ and, therefore, the numbers $x_\pm$ are updated after arrival of each order. The dynamical rules of the process represent a simplified version of the limit order driven dynamics.

There are three types of events: (i) dropping of limit orders, (ii) market-price order to buy, and (iii) market-price order to sell. We suppose that all market-price orders have the same volume s and all limit order events the same volume v. Further, we assume that market orders to buy and sell occur with the same probability. In order to keep the total number of limit orders constant on an average, we should suppose that at a given moment there is a probability $p=s/(s+v)$ to drop a limit order. Each of the market-price events (ii) and (iii) have then an equal probability $(1-p)/2$. (Here we tacitly assume that the limit orders that are not met last forever. One can also investigate some realistic variants, where the limit orders slowly die out.)

Let us investigate first the consequence of an arrival of a market-price order to buy. By definition, the price level increases by x_+. As the density of orders is constant, average density on the right-hand side from the new price is unchanged. If now another buy order arrives, it finds the same density and the price change is the same too. Therefore, the new value of x_+ is equal to the old one, $x_+\to x_+$. On the other hand, if now a new market order to sell arrives, there are no limit orders in the interval of width x_+ below the current price level, and when we go further down, there is a constant density s/x_-. As a result, the price decreases by x_++x_-. Hence, the new value of x_- is $x_-\to x_++x_-$.

To sum it up, the effect of the buy order consists in the replacement

$$\begin{aligned}x_+&\to x_+\\ x_-&\to x_++x_-.\end{aligned} \tag{2}$$

It can be expressed in matrix form

$$X\to X'=T_+X \tag{3}$$

where

$$T_+=\begin{pmatrix}1&0\\1&1\end{pmatrix}. \tag{4}$$

Similarly, for the action of a sell order we get

$$X\to X'=T_-X, \tag{5}$$

where

$$T_-=\begin{pmatrix}1&1\\0&1\end{pmatrix}. \tag{6}$$

Now we turn to the changes due to dropping limit orders. It is necessary to specify the function $\eta(x)$, representing the average volume of orders set at distance x from the current price. As we already mentioned, we suppose it to be an even function. Moreover, the volume was supposed to be fixed, $\int\eta(x)\mathrm{d}x=v$. We apply here the simplest choice $\eta(x)=v/2(\delta(x-d)+\delta(x+d))$, which means that all new orders are placed at the same distance d from the current price, either below (buy) or above (sell). This distribution reflects the fact that the limit orders are not typically set arbitrarily close to the current price but there is a certain minimum offset d.

Dropping limit orders affects the vector X according to the formula

$$x_\pm\to\frac{1}{2}(3-1/p)\,x_\pm. \tag{7}$$

Indeed, a buy (or sell) order will annihilate the amount $v/2$ from the just deposited limit order and amount $s-v/2$ from the original density of old limit orders. The shift is, therefore, $x_\pm=(s-v/2)/\rho_\pm$. Writing v in terms of the probability p, i.e., $v=(1/p-1)s$, we obtain the formula (7). So, in matrix form we have

$$X \to X' = SX, \tag{8}$$

where

$$S = \frac{1}{2}\left(3 - \frac{1}{p}\right)\begin{pmatrix} 1 & 0 \\ 0 & 1 \end{pmatrix}. \tag{9}$$

The price changes only after a market order is issued, while dropping limit orders leaves the price unchanged. So, between two subsequent shifts of the price, $m \geqslant 0$ limit orders can arrive, with probability $P_m(m) = (1-p)p^m$. The change of the vector X due to one market order and m limit orders is $X \to S^m T_\pm X$. When calculating the evolution of the probability distribution for X, we should sum over all possible realizations. Hence, the probability distribution for the vector X should satisfy the equation

$$P_X(X) = \frac{1}{2}\sum_{\sigma=\pm}\sum_{m=0}^{\infty}\int \mathrm{d}X'\, P_m(m) P_X(X')\,\delta(X - S^m T_\sigma X') \tag{10}$$

in the stationary state.

IV. DISTRIBUTION OF PRICE CHANGES

We will make a further approximation at this stage. The matrix S is simply a unit matrix multiplied by a constant. If the same were true also for the matrices $T_\pm$, the process would be reduced to a simple multiplicative random walk, whose properties are well known and their relevance in modeling price fluctuations is testified by a series of models, as mentioned in the Introduction.

Our approximation will consist first in replacing the matrices $T_\pm$ by the average $\overline{T} = \frac{1}{2}(T_+ + T_-)$ and furthermore, we will take only the highest eigenvalue of the matrix $\overline{T}$, which is 3/2. Then, instead of a pair of price changes x_+ and x_- we have a single scalar quantity x, describing the absolute value of the price change.

Note that the same results can be obtained by assuming from beginning, that $x_+ = x_-$, i.e., that the density of states is equal on both sides of the price level. This means, that we make a further ''mean-field'' approximation, suppressing not only the fluctuations along the price axis, but also fluctuations from one side to the other of the already averaged density of states.

This way we define our multiplicative random process. The fact that there is a small but finite offset d in placing the limit orders ensures that the values of $x_\pm$ (therefore, also of x) cannot be smaller than d. This feature plays the role of ''repulsion from zero,'' which was found essential for establishing the power-law tails [42,45] and is usually guaranteed by the additive term [43,46].

For the probability distribution of the price changes we obtain

$$P(x) = \sum_{m=0}^{\infty}(1-p)p^m \int \mathrm{d}x' P(x') \times \delta\left(x - \frac{3}{2}x'\left(\frac{3-\frac{1}{p}}{2}\right)^m\right) \tag{11}$$

and assuming a power-law tail of the probability distribution in the form $P(x) \sim x^{-1-\alpha}$, we obtain the following equation for the exponent:

$$\sum_{m=0}^{\infty}(1-p)p^m\left[\frac{3}{2}\left(\frac{3-\frac{1}{p}}{2}\right)^m\right]^\alpha = 1. \tag{12}$$

As can be easily checked, apart from the trivial solution $\alpha = 0$, it has a nontrivial solution $\alpha = 1$, independent of p. Therefore, the distribution of price changes has a power-law tail

$$P(x) \simeq x^{-2}. \tag{13}$$

Note that the calculation could be further simplified by writing the equation analogical to Eq. (11), relating the probability distribution just after single step. Then, instead of the sequence of steps consisting of one market order followed by m limit orders we have one step being either limit or market order. This equation gives precisely the same power-law tail. However, such an approach is slightly inconsistent, because setting a limit order does not imply any trade, thus the price change at this moment is zero.

V. PRICE AUTOCORRELATION FUNCTION

One of the well-known facts about financial data series is the negative short-time autocorrelation of price changes [6]. Here, we will show how this effect naturally emerges from the matrix nature of our stochastic process.

We will compute the autocorrelation function defined as

$$C(t, t+\tau) = \frac{\langle x(t)x(t+\tau)\rangle}{\sqrt{\langle x^2(t)\rangle\langle x^2(t+\tau)\rangle}}, \tag{14}$$

where $x(t)$ is the actual price change at time t and $\tau \geqslant 1$. We will denote $M(t) \in \{S, T_+, T_-\}$ the matrix describing the action performed at time t and $P_M(M)$ its probability distribution. Of course, we introduced already $P_M(T_-) = P_M(T_+) = (1-p)/2$ and $P_M(S) = p$.

Now we introduce the function of taking the price change from the vector $X = \binom{x_-}{x_+}$

$$\begin{aligned} \mathcal{X}(X;M) &= x_+ \quad \text{if} \quad M = T_+ \\ &= 0 \quad \text{if} \quad M = S \\ &= x_- \quad \text{if} \quad M = T_- \quad . \end{aligned} \tag{15}$$

Note that the operator $\mathcal{X}$ is linear in the argument X. Then

$$\langle x(t)x(t+\tau)\rangle = \int dX\, P_X(X)\tilde{C}(X), \tag{16}$$

where

$$\tilde{C}(X) = \sum_{M(t)} \cdots \sum_{M(t+\tau)} \prod_{i=0}^{\tau} P_M(M(t+i)) \times \mathcal{X}(X;M(t))\, \mathcal{X}(M(t+\tau-1)\cdots M(t)X;M(t+\tau)). \tag{17}$$

We find easily, using the linearity of the operator $\mathcal{X}$ and introducing the sign vector $E=(1,-1)$

$$\tilde{C}(X) = \frac{1-p}{2} E \left(\sum_M P_M(M) M \right)^{\tau-1} (x_+ T_+ - x_- T_-) X. \tag{18}$$

The multiplication by E extracts only the lower one of the two eigenvalues of the averaged matrix

$$\sum_M P_M(M) M = \frac{1}{2} \begin{pmatrix} 1+p & 1-p \\ 1-p & 1+p \end{pmatrix}. \tag{19}$$

The lower eigenvalue is p, hence

$$\tilde{C}(X) = -(1-p)p^{\tau-1} x_+ x_- . \tag{20}$$

We can calculate similarly the corresponding expression for the denominator of Eq. (15). We obtain at the end

$$C(t,t+\tau) = -p^{\tau-1} \frac{2\langle x_+ x_- \rangle}{\langle x_+^2 \rangle + \langle x_-^2 \rangle}. \tag{21}$$

We can clearly observe the negative autocorrelation that decays with characteristic time that depends on the relative frequency of putting the limit and market orders, measured by the probability p. The result obtained suffers from the divergence of second moments of the variables x_+, x_-, resulting from the power-law tail calculated in the last section. However, only the ratio of the moments enter the formula (21). Moreover, if we suppose as an initial condition a distribution for x_+, x_- with finite moments, the moments will remain finite for any finite time and we naturally expect that the ratio of the second moments will converge to a finite value even if the second moments themselves diverge.

VI. CONCLUSIONS

In conclusion, we solved in the mean-field approximation the Maslov model of stock market fluctuations. We found a stationary distribution of price changes with a power-law tail with the exponent $1+\alpha=2$, which is within the Lévy stable region. We found negative short-time autocorrelation of the price changes, decaying exponentially with time. The relaxation time depends on the relative frequency of putting market orders and limit orders: the decay is slower if a market order comes only after more limit orders. This is intuitively clear, because it is the market order that ensures the liquidity.

Our result differs in two important points from the simulations of Maslov [35]. First, the numerical value of the power-law tail exponent is different. This can be attributed to the approximation we made in the form of the density of orders $\rho(x)$. Indeed, we assumed, as a zero approximation, constant density. On the other hand, it is known from the solution of the reaction-diffusion model of market [17] that the density may have complicated nontrivial form. Another source of the difference may be the neglect of fluctuations.

Another difference consist in lacking the second power-law regime for small price changes. However, as discussed in Ref. [35], this second and different power law comes from the fact, that the new limit orders may be placed farther than the reach of the price change. As we implicitly supposed that the new orders are put to very small distance d from the current price, we can observe only the distribution for price changes larger than d.

ACKNOWLEDGMENTS

I am indebted to Y.-C. Zhang and the University of Fribourg, Switzerland, for financial support and kind hospitality. I wish to thank Sergei Maslov for stimulating discussions and many claryfying remarks. This work was supported by the grant agency of the Czech Republic, Grant No. 202/01/1091.

[1] *The Economy as an Evolving Complex System*, edited by P.W. Anderson, K.J. Arrow, and D. Pines (Addison Wesley, Reading, MA, 1988).
[2] B.B. Mandelbrot, Physica A **263**, 477 (1999).
[3] R.N. Mantegna, Physica A **179**, 232 (1991).
[4] R.N. Mantegna and H.E. Stanley, Nature (London) **376**, 46 (1995).
[5] R.N. Mantegna and H.E. Stanley, *Introduction to Econophysics: Correlations and Complexity in Finance* (Cambridge University Press, Cambridge, 1999).
[6] J.-P. Bouchaud and M. Potters, *Theory of Financial Risks* (Cambridge University Press, Cambridge, 2000).
[7] S. Galluccio, G. Caldarelli, M. Marsili, and Y.-C. Zhang, Physica A **245**, 423 (1997).
[8] N. Vandewalle and M. Ausloos, Eur. Phys. J. B **4**, 257 (1998).
[9] P. Gopikrishnan, M. Meyer, L.A.N. Amaral, and H.E. Stanley, Eur. Phys. J. B **3**, 139 (1998).
[10] V. Plerou, P. Gopikrishnan, L.A.N. Amaral, M. Meyer, and H.E. Stanley, Phys. Rev. E **60**, 6519 (1999).
[11] P. Gopikrishnan, V. Plerou, L.A.N. Amaral, M. Meyer, and H.E. Stanley, Phys. Rev. E **60**, 5305 (1999).
[12] K. Nagel and M. Schreckenberg, J. Phys. I **2**, 2221 (1992).
[13] M. Levy, H. Levy, and S. Solomon, Econ. Lett. **45**, 103 (1994).
[14] M. Levy, H. Levy, and S. Solomon, J. Phys. I **5**, 1087 (1995).
[15] M. Levy and S. Solomon, Int. J. Mod. Phys. C **7**, 65 (1996).
[16] P. Bak, M. Paczuski, and M. Shubik, Physica A **246**, 430 (1997).

[Slanina01a]

[17] L.-H. Tang and G.-S. Tian, Physica A **264**, 543 (1999).
[18] H. Takayasu, H. Miura, T. Hirabayashi, and K. Hamada, Physica A **184**, 127 (1992).
[19] A.-H. Sato and H. Takayasu, Physica A **250**, 231 (1998).
[20] T. Lux and M. Marchesi, Nature (London) **397**, 498 (1999).
[21] R. Cont and J.-P. Bouchaud, Macroecon. Dyn. **4**, 170 (2000).
[22] G. Caldarelli, M. Marsili, and Y.-C. Zhang, Europhys. Lett. **40**, 479 (1997).
[23] D. Chowdhury and D. Stauffer, Eur. Phys. J. B **8**, 477 (1999).
[24] D. Sornette, D. Stauffer, and H. Takayasu, e-print cond-mat/9909439.
[25] J.-P. Bouchaud and R. Cont, Eur. Phys. J. B **6**, 543 (1998).
[26] G. Iori, e-print adap-org/9905005.
[27] G. Iori, Int. J. Theor. Appl. Finance **3**, 467 (2000).
[28] F. Slanina and Y.-C. Zhang, Physica A **272**, 257 (1999).
[29] F. Slanina and Y.-C. Zhang, Physica A **289**, 290 (2001).
[30] L. Kullmann and J. Kertész, e-print cond-mat/0105473.
[31] D. Challet and Y.-C. Zhang, Physica A **246**, 407 (1997).
[32] D. Challet, M. Marsili, and Y.-C. Zhang, Physica A **276**, 284 (2000).
[33] N.F. Johnson, M. Hart, P.M. Hui, and D. Zheng, Int. J. Theor. Appl. Finance **3**, 443 (2000).
[34] D. Challet, M. Marsili, and Y.-C. Zhang, e-print cond-mat/0101326.
[35] S. Maslov, Physica A **278**, 571 (2000).
[36] F. Franci and L. Matassini, e-print cond-mat/0008466.
[37] L. Matassini and F. Franci, e-print cond-mat/0103106.
[38] L. Matassini and F. Franci, Physica A **289**, 526 (2001).
[39] S. Maslov and M. Mills, e-print cond-mat/0102518.
[40] D. Challet and R. Stinchcombe, e-print cond-mat/0106114.
[41] J.M. Deutsch, Physica A **208**, 433 (1994).
[42] M. Levy and S. Solomon, Int. J. Mod. Phys. C **7**, 595 (1996).
[43] H. Takayasu, A.-H. Sato, and M. Takayasu, Phys. Rev. Lett. **79**, 966 (1997).
[44] D. Sornette, Physica A **250**, 295 (1998).
[45] D. Sornette and R. Cont, J. Phys. I **7**, 431 (1997).
[46] D. Sornette, Phys. Rev. E **57**, 4811 (1998).
[47] O. Biham, O. Malcai, M. Levy, and S. Solomon, Phys. Rev. E **58**, 1352 (1998).
[48] M. Marsili, S. Maslov, and Y.-C. Zhang, Physica A **253**, 403 (1998).
[49] S. Solomon, in *Application of Simulation to Social Sciences*, edited by G. Ballot and G. Weisbuch (Hermes Science, Paris, 2000).
[50] Z.-F. Huang and S. Solomon, Eur. Phys. J. B **20**, 601 (2001).
[51] S. Solomon and M. Levy, e-print cond-mat/0005416.
[52] J.-P. Bouchaud and M. Mézard, Physica A **282**, 536 (2000).

[Slanina08]

Eur. Phys. J. B **61**, 225–240 (2008)
DOI: 10.1140/epjb/e2008-00059-3

THE EUROPEAN PHYSICAL JOURNAL B

Critical comparison of several order-book models for stock-market fluctuations

F. Slanina[a]

Institute of Physics, Academy of Sciences of the Czech Republic, Na Slovance 2, 18221 Praha, Czech Republic and Center for Theoretical Study, Jilská 1, Prague, Czech Republic

Received 19 July 2007 / Received in final form 4 January 2008
Published online 16 February 2008 –

Abstract. Far-from-equilibrium models of interacting particles in one dimension are used as a basis for modelling the stock-market fluctuations. Particle types and their positions are interpreted as buy and sel orders placed on a price axis in the order book. We revisit some modifications of well-known models, starting with the Bak-Paczuski-Shubik model. We look at the four decades old Stigler model and investigate its variants. One of them is the simplified version of the Genoa artificial market. The list of studied models is completed by the models of Maslov and Daniels et al. Generically, in all cases we compare the return distribution, absolute return autocorrelation and the value of the Hurst exponent. It turns out that none of the models reproduces satisfactorily all the empirical data, but the most promising candidates for further development are the Genoa artificial market and the Maslov model with moderate order evaporation.

PACS. 89.65.-s Social and economic systems – 05.40.-a Fluctuation phenomena, random processes, noise, and Brownian motion – 02.50.-r Probability theory, stochastic processes, and statistics

1 Introduction

The order book is the central notion in the stock market. People willing to buy or sell express their desire in well-specified orders and the authority of the stock exchange logs all the orders in a list, where they wait until they are either satisfied (executed) or cancelled. The visible part of the stock market dynamics, i.e. the complex movement of the price, is rooted in the detailed and mostly invisible processes happening within the order book. Anyone who wants to study seriously the stock market fluctuations, must pay attention to the dynamics of the order book.

There are several reasons why physicists may and should embark on such study. First, the discipline of Econophysics is now established and accepted with decent respect within the Physics community [1–4]. But even if the study of economic phenomena by the tools of physics were a bare empty bubble (which is *not!*, the author believes) to be broken into pieces, the study of the order book itself may remain one of the shards of value. (Another one may be the Minority Game [5].) Indeed, the second motivation to spend some effort here is that the order book is a genuinely one-dimensional non-equilibrium system with complex dynamics. It abounds with rich phenomena and poses a serious intellectual challenge, which may provoke development of new tools in one-dimensional non-equilibrium physics.

The most simplified view of an order book may be the following. The orders are immobile particles of two kinds, A (for asks, i.e. orders to sell), and B (for bids, i.e. orders to buy), residing on a line of price (or logarithm of price, if more convenient). All bids are always on the left of all asks. The actual price lies somewhere between (and included) the highest bid and the lowest ask. The interval between the two is the spread and it is one of the key quantities observed in the order book. Besides these limit orders, waiting for the future in the order book, also market orders arrive, which buy or sell immediately at any price available in the market. Thus, the market orders provide liquidity.

As we already said, the tip of the order-book iceberg is the price. All order-book models must be confronted with what is known about the price fluctuations. These *stylised facts* are now very well established [6–9]. To quote here only those which we shall be faced later, the price movements are generically characterised by a power-law tail in return distribution, with exponent $1 + \alpha \simeq 4$, power-law autocorrelation of volatility, with exponent ranging between 0.3 to 0.5, anomalous Hurst exponent $H \simeq 2/3$, measured either directly in the so-called Hurst plot, or as a by-product of another essential feature of the price fluctuations, which is the scaling. It must be noted, though, that the scaling holds satisfactorily only for not too long time separations. At larger times, the gradual crossover to Gaussian shape of return distribution is observed. This feature is well reproduced in multifractal

[a] e-mail: slanina@fzu.cz

stochastic models (from many works in this direction see e.g. [10–13]). However, we must state from the beginning, that explanation of multifractality and other subtle features of the stock-market fluctuations [14,15], goes beyond the scope of this paper.

Let us mention at least some of the special features found empirically in order books. The literature is indeed very ample [16–41]. The first thing we may ask is the average order book profile, i.e. the average number of orders existing in given moment at given distance form the current price. It was found that it has sharp maximum very close to, but away from, the price [18,26,27]. The decrease at large distances seems to be a power law with exponent $\simeq 2$ [26,27], but the form of the increase between the price and the peak is not so clear.

Related information is contained in the price impact function, which says how much the price moves when an order of a specific volume arrives. In first approximation, we consider the virtual impact function, obtained by simple integration of the order book profile from the current price to the new, shifted price. Beyond the maximum, the profile decreases and therefore the virtual impact is a convex function [17,18,24]. The striking surprise in the empirical study of order books is, that the actual price impact is much smaller, and moreover, it is a concave, rather than convex, function of volume [24]. The form of the price impact was studied intensively [20,32–38], yet a controversy persist, whether it can be better fitted on a square root (a qualitative theoretical argument for this fit can be found in [42]), a power with exponent <0.5 or on a logarithm.

The incoming orders have various volumes and it turns out that they are power-law distributed [17]. For the market orders, the exponent is $\simeq 1.4$, while for the limit orders it has higher value $\simeq 2$. The limit orders are deposited at various distances from the current price and also here the distribution follows a power law [26,27,31,39], although the value of the exponent reported differs rather widely ($\simeq 1.5$ to $\simeq 2.5$) from one study to another. The limit orders are eventually either satisfied or cancelled. The time they spend within the order book is again power-law distributed [18,19,43] with exponent $\simeq 2.1$ for cancellations and $\simeq 1.5$ for satisfactions.

There were attempts to explain some of the properties of price fluctuations as direct consequences of the empirically found statistics of order books. In references [20,44] the power-law tail in return distribution is related to the specific square-root form of the impact function combined with power-law distribution of order volumes. On the other hand, reference [34] shows that the distribution of returns copies the distribution of first gap (the distance between best and second best order – where "best" means "lowest" for asks and "highest" for bids). It was also found that the width of the spread is distributed as power law, with exponent $\simeq 4$ [22], which is essentially the same value as the exponent for the distribution of returns. The discussion remained somewhat open [21,41], but we believe that the properties of the price fluctuations cannot be deduced entirely from the statistics of the order book. For example the difference between the virtual and actual price impact suggests that the order book reacts quickly to incoming orders and reorganises itself accordingly. Therefore, without detailed *dynamical* information on the movements deep inside the book we cannot hope for explanation of the *dynamics* of the price.

2 Existing models

There is no space here for an exhaustive review of the order-book modelling, not to speak of other types of stock-market models. We select here only a few models we shall build upon in the later sections and quote only a part of the literature. We apologise for unavoidable omissions, not due to underestimation of the work of others, but dictated by reasonable brevity of this study.

2.1 Stigler

To our best knowledge, the first numerical model of the order book and the first computer simulation ever in economics was the work of Stigler [45]. The model is strikingly simple. There are only limit orders of unit volume and they are supplied randomly into the book within a fixed allowed interval of price. If the new order is e.g. a bid and there is an ask at lower price, then the bid is matched with the lowest ask and both of them are removed. If the bid falls lower than the lowest ask, it is stored in the book and waits there.

From this example we understand, why the order-book models are often called "zero-intelligence" models. Indeed, there is no space for strategic choice of the agents and the people may be very well replaced by random number generators. It is interesting to note that experiments with human versus machine trading were performed [46], which found as much efficiency in "zero-intelligence" machines as in "rational" people (graduate students of business).

2.2 Bak, Paczuski, and Shubik

Another model, very simple to formulate but difficult to solve, was introduced by Bak, Paczuski, and Shubik (BPS) [47]. On a line representing the price axis, two kinds of particles are placed. The first kind, denoted A (ask), corresponds to sell orders, while the second, B (bid), corresponds to buy orders. The position of the particle is the price at which the order is to be satisfied. A trade can occur only when two particles of opposite type meet. If that happens, the orders are satisfied and the particles are removed from the system. This can be described as annihilation reaction $A + B \to \emptyset$. It is evident that all B particles must lie on the left with respect to all A particles. The particles diffuse freely and in order to keep their concentration constant on average, new orders are inserted from the left (B type) and from the right (A type). The whole picture of this order-book model is therefore identical to the two-species diffusion-annihilation process. The

changes in the price are mapped on the movement of the reaction front.

Many analytical results are known for this model. Most importantly, the Hurst exponent can be calculated exactly [48–51] and the result is $H = 1/4$. This value is well below the empirically established value $H \simeq 2/3$.

Several modifications of the bare reaction-diffusion process were introduced [47] to remedy some of the shortcomings of the model. The simplest one is to postulate a drift of articles towards the current price. This feature mimics the fact that in real order books the orders are placed close to the current price. It also suppresses the rather unnatural assumption of free diffusion of orders. However, the measured Hurst exponent remains to be $H = 1/4$ as before.

More important modification consists in a kind of "urn" process. The new orders are placed close to already existing ones, thus mimicking certain level of "copying" or "herding" mechanism, which is surely present in the real-world price dynamics. In this case the Hurst exponent is higher and in fact very close to the random walk value, $H \simeq 1/2$.

The diffusion constant of the orders can also be coupled to the past volatility, introducing a positive feedback effect. This way the Hurst exponent can be enhanced up to the level consistent with the empirical value. In this case, scaling was observed in the distribution of returns with Hurst exponent $H \simeq 0.65$.

2.3 Genoa market model

The diffusion of orders contradicts reality. Indeed, orders can be placed into the order book, and later either cancelled or satisfied, but change in price is very uncommon. It is therefore wise to return back to Stigler's immobile orders but to make his model more realistic.

Rather involved modification of the Stigler model appeared much later under the name of Genoa artificial market [52–57]. The model contains many ingredients and is therefore very plastic.

Again, there are only limit orders and the liquidity is assured by non-empty intersection of intervals, where the bids and asks, respectively, are deposited. In practical implementation, the probability of order placement was Gaussian, with the centre shifted slightly above the current price for asks and slightly below for the bids. The width of the Gaussians was also related to the past volatility, thus introducing a feedback. Note that essentially the same feedback was introduced already in the BPS model. The price of the contract was calculated according to demand-offer balance. There was also a herding of agents in play, in the spirit of the Cont-Bouchaud model [58]. The main result to interest us here was the power-law tail of the return distribution, with very realistic value of the exponent. However, it was not at all clear which of the many ingredients of the model is responsible for the appearance of the power-law tail.

2.4 Maslov model

To appreciate the crucial role of the market orders, Maslov introduced a model [59], in which the bids are deposited always on the left and asks on the right from the current price. The limit orders never meet each other. The execution of the orders is mediated by the market orders, annihilating the highest bid or lowest ask, depending on the type of the market order.

The Maslov model has several appealing features. Especially, the return distribution characterised by exponent $1+\alpha \simeq 3$ seems to be close to the empirically found power law. The scaling in return distribution is clearly seen as well as the volatility clustering manifested by power-law decay of the autocorrelation of absolute returns. However, the Hurst exponent is $1/4$ as in the BPS model, which is bad news. Maslov model was treated analytically in a kind of mean-field approximation [60]. Unfortunately, the exponent $\alpha = 1$ found there disagrees with the simulations. Later, the reason for this difference was identified in the assumption of uniform density of orders on either of the sides of the price. Taking the density zero at the current price and linearly increasing on both the ask and bid side, the exponent becomes $\alpha = 2$, in agreement with the numerics [61].

2.5 Models with uniform deposition

The Maslov model is still very idealised. The most important difference from real situation is the absence of cancellations. In real order books the orders can be scratched, if their owners think that they waited too long for their patience. The group of Farmer and others introduced several variants of models with cancellation ("evaporation") of orders [62–65]. Another fundamental feature which makes these models different from the Maslov model is that the orders are deposited uniformly within their allowed range, i.e. bids from the current price downwards up to a prescribed lower bound and equivalently for the asks.

The order book profile, price impact and many related properties were studied very thoroughly and their dependence on the rates of thee processes involved was clarified. An important step forward was the analytical study performed in [62]. Two complementary "mean-field" approaches were applied, achieving quite good agreement with the simulations. The first approach calculates the average density of orders as a continuous function, neglecting the fluctuations. The other approach represents the state of the order book by intervals between individual orders, assuming that at most one order can be present on one site (a kind of exclusion principle). The approximation consists in neglecting the correlations between the lengths of the intervals.

This line of research was recently pushed forward in and important paper by Mike and Farmer [66]. A scheme, which was given very fitting name "empirical model" was proposed, which incorporates several basic empirical facts on the order flow dynamics, namely the distribution of distances, from the best price, where the orders are placed;

the long memory in the signs of the orders; the cancellation probability, depending on the position of the order. Including these empirical ingredients into the Farmer model, an excellent agreement with other empirical findings was observed, including the return and spread distributions. The importance of that work, at least from our point of view, consists in observation that the most tangible feature of the price fluctuation, the return distribution, is in fact a secondary manifestation of more basic and yet unexplained features. These are the features which enter the model of [66] as empirical input.

In our work, we address a less ambitious but more fundamental question. What will be the fluctuation properties of these models without assuming anything special about order flow? We shall see that in many aspects the answer is disappointing in the sense that the results are often far from reality. This means that the inputs of [66] are essential. On the other hand, we can hardly be satisfied until we detect the causes behind the empirical ingredients of [66].

2.6 Other approaches

A rather phenomenological model was simulated in [26]. The profile of the order book was successfully explained assuming power-law distribution of placement distances from the current price.

In fact, the crucial role of the evaporation of orders was first noticed in the work of Challet and Stinchcombe [18]. The new limit orders were deposited close to the price, with standard deviation which was linearly coupled with the width of the spread. The evaporation caused a clearly visible crossover from Hurst exponent $H = 1/4$ at short time distances to the random-walk value $H = 1/2$ at larger times. This class of models was investigated in depth subsequently [19,67,68]. In a related development, a version of asymmetric exclusion model [69] was adapted as an order-book model [70]. The two crucial ingredients are the (biased) diffusion of particles (orders), returning somewhat back to the BPS model, and the exclusion principle, allowing at most one order at one site. It also forbids "skipping" of particles, so each order represents an obstacle for the diffusion of others. Price is represented by the particle of a special type. Mapping to the exactly soluble asymmetric exclusion model gives the precise value of the Hurst exponent $H = 2/3$, nicely coinciding with reality. One must remember, though, that the price for this result is the unrealistic assumption of diffusing orders. Moreover, even if we accepted the view that removal and immediate placement of an order not far from the original position may be effectively described as diffusion, why then the particles are not allowed to overtake each other? We consider that feature very far from reality.

Let us only list some other works we consider relevant for order-book modelling [71–76]. Schematic models, like the Interacting Gaps model [77,78], may also bring some, however limited, insight. Despite continuing effort of many groups performing empirical analyses as well as theoretical studies, the true dynamics of the order book is far from being fully understood. On one side, the trading in the stock market is much more intricate than mere play of limit and market orders. There are many more types of them, sometimes rather complicated. At the same time, it becomes more and more evident that assuming "zero-intelligence" players misses some substantial processes under way in the stock market. Strategic thinking cannot be avoided without essential loss. This brings us close to our last remark. All the models mentioned in this section are appropriate only to those markets, which operate without an official market maker. In presence of a market maker, the orders do not interact individually, but in smaller or larger chunks. One is tempted to devise a "zero-intelligence" model with a market maker, but there is perhaps a wiser path to follow. We have in mind a combination of order-book models with Minority Game. The latter represents an antipole to "zero-intelligence" order-book models and amalgamating the two opposites may prove fruitful.

In this work we shall not go thus far. Our aim is rather to clarify the dark places in the ensemble of existing order-book models. Performing new simulations for several of these models in parallel, we hope to shed some light on the the usefulness and the limitations of them.

3 New simulations

Here we present our new results of numerical simulations of the models sketched above. Some of the data aim at improving the results already present in the literature, but mostly we try to clarify aspects not studied before. We also used the same methodology in analysing the simulations for all models, in order to make comparable statements for each of the models under scrutiny.

3.1 Bak-Paczuski-Shubik model

The first model to study is the Bak-Paczuski-Shubik (BPS) model. As we already explained, we have two types of diffusing particles, called A and B. There are N particles of each type, i.e. total $2N$ particles placed at the segment of length L. The particles can occupy integer positions from the set $\{1, 2, \ldots, L\}$. In one update step we choose one particle and change its position as $c_i' = c_i \pm 1$ (there is no bias, so both signs of the change have the same probability), on condition that the new position stays within the allowed interval, $1 \leq c_i' \leq L$. We use the convention that the time advances by $1/(2N)$ in one step. If the new site was empty or there was already another particle of the same type at the new position, nothing more happens an the update is completed. We set $c_i(t + 1/(2N)) = c_i'$ and $c_k(t + 1/(2N)) = c_k(t)$, $k \neq i$ On the other hand, if the new site is occupied by a particle of opposite type, say, particle j, so that $c_j(t) = c_i'$, then the two particles annihilate. To keep the number of particles constant, we immediately supply two new particles at opposite edges of the allowed segment. E.g. if i was type

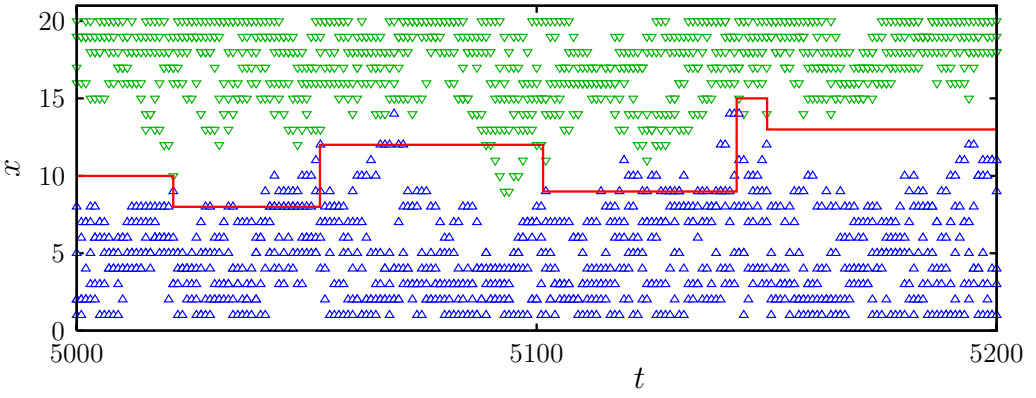

Fig. 1. Example of the evolution of the Bak-Paczuski-Shubik model. Triangles up (△) denote positions of bids, triangles down (▽) mark the asks. The full line traces the evolution of the price, showing jumps where transactions occurred. There are $N = 5$ particles of each type on the segment of length $L = 20$.

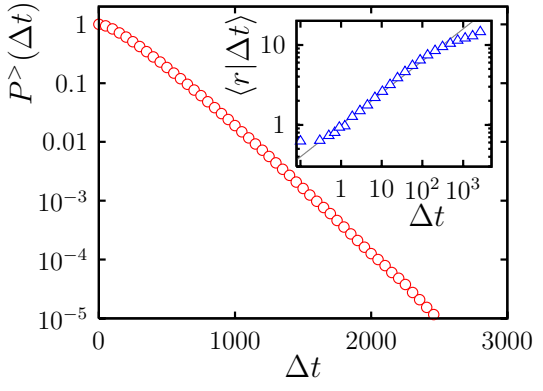

Fig. 2. Distribution of inter-event times in BPS model. On the segment of length $L = 500$, there are $N = 200$ particles of each kind. In the inset, average return occurring after waiting time Δt, for the same values of L and N. The line is the power $\propto (\Delta t)^{0.4}$.

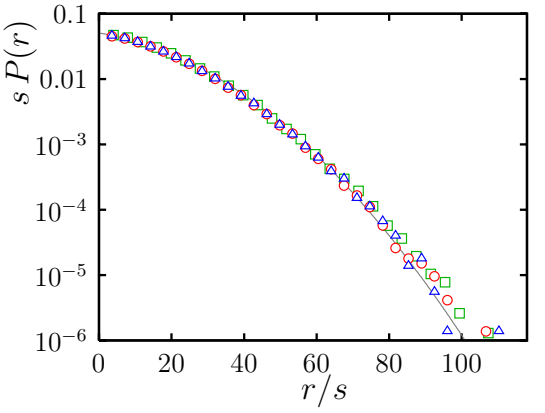

Fig. 3. Distribution of one-transaction returns in BPS model, rescaled by the factor $s = N^{1/2}L^{-1/4}$. The parameters are $L = 250$, $N = 50$ (△); $L = 500$, $N = 200$ (○); $L = 250$, $N = 250$ (□). The line is the dependence $\propto \exp\left(-r/(50s) - (r/(34s))^2\right)$.

B and j was type A, the update is $c_i(t + 1/(2N)) = 1$, $c_j(t + 1/(2N)) = L$ and $c_k(t + 1/(2N)) = c_k(t)$, $k \neq i, j$.

The annihilation corresponds to an elementary transaction. The price set in this deal is just the position where the annihilation took place, $x(t + 1/(2N)) = c'_i$. If the transaction did not occur, the price stays unchanged, $x(t+1/(2N)) = x(t)$. This completes the definition of the variant of the BPS model simulated here.

In Figure 1 we can see how the typical configuration of orders evolves in time. There are rather long periods where the price does not change, but the positions of orders are mixed substantially. We shall first look at these waiting times between consecutive trades. In Figure 2 we can see the (cumulative) probability distribution of them. It is evident that the distribution is exponential, or very close to it, so we can consider the sequence of trade times at least approximately as Poisson point process.

The most desired quantity is the one-trade return distribution. If t_i is the time of ith trade, we define $r(t_i) = x(t_{i+1}) - x(t_i)$ and in Figure 3 we plot the distribution of the absolute returns $P(r) = \langle \delta(r - |r(t_i)|)\rangle$ in stationary state, for several sizes L and particle numbers N. We find that the distribution collapses onto a single curve when we rescale the data by the factor

$$s = N^{1/2}L^{-1/4}\,. \tag{1}$$

We then find

$$P(r) = \frac{1}{s}\,F\left(\frac{r}{s}\right) \tag{2}$$

and the scaling function decays faster than an exponential. The fit of the type $F(x) \simeq A\exp(-ax - bx^2)$ seems to be fairly satisfactory. Evidently, this distribution is very far from the fat tails observed empirically. It is also interesting to see how the one-trade return depends on the waiting time before the trade. We measure the conditional average of the return

$$\langle r|\Delta t\rangle = \frac{\sum_i |r(t_i)|\,\delta(t_i - t_{i-1} - \Delta t)}{\sum_i \delta(t_i - t_{i-1} - \Delta t)} \tag{3}$$

and find (see the inset in Fig. 2) that it increases slowly as a power law $\langle r|\Delta t\rangle \sim (\Delta t)^{0.4}$.

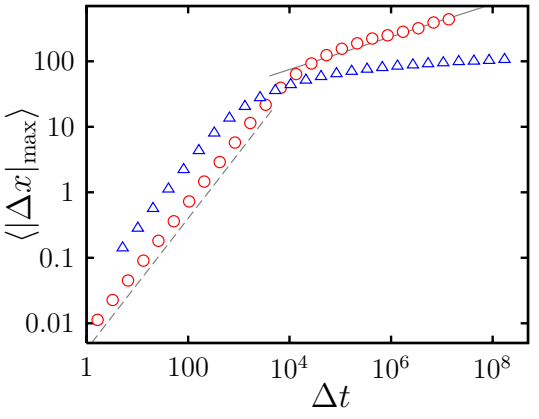

Fig. 4. Hurst plot for BPS model. The parameters are $L = 2\times10^4$, $N = 2\times10^4$ (○), and $L = 250$, $N = 50$ (△). The dashed line is the dependence $\propto \Delta t$, while solid line is $\propto (\Delta t)^{1/4}$.

Diffusion of the price is quantified by the Hurst plot. Usually we calculate the quantity

$$R(\Delta t) = \left\langle \frac{\max_{t',t''\in(t,t+\Delta t)} \left|x(t') - x(t'')\right|}{\sqrt{\left\langle r^2(t')\right\rangle_{t'} - \left\langle r(t)\right\rangle_{t'}^2}} \right\rangle_t \qquad (4)$$

where the average $\langle \ldots \rangle_{t'}$ is taken over interval $t' \in (t, t+\Delta t)$ while the average $\langle \ldots \rangle_t$ extends over all times. The time-dependent normalisation in the denominator of (4) accounts for temporal variations of the volatility.

However, especially in BPS model the measure (4) is inconvenient as it does not cover properly the time scales below the typical waiting time. We use instead a simplified and also frequently used quantity

$$\left\langle |\Delta x|_{\max} \right\rangle = \left\langle \max_{t',t''\in(t,t+\Delta t)} \left|x(t') - x(t'')\right| \right\rangle_t . \qquad (5)$$

Both (4) and (5) are expected to share the same asymptotic behaviour for $\Delta t \to \infty$, i.e. $R(\Delta t) \sim \left\langle |\Delta x|_{\max} \right\rangle \sim (\Delta t)^H$ with Hurst exponent H.

The results for BPS model are shown in Figure 4. We can appreciate there how difficult it is to actually observe the value $H = 1/4$ predicted by the theory. Relatively long "short-time" regime seen in Figure 4 is characterised by $H = 1$, which corresponds to ballistic, rather than diffusive, movement of the price. In this regime, the time scale is shorter than the average inter-event time, so there is typically at most one transaction. The transaction times follow approximately the Poisson point process, so the probability that one transaction occur during time Δt is, for short times, proportional to Δt. Assuming that the price change, if it occurs, has certain typical size, the scale of the average price change should be also proportional to Δt. Hence the ballistic behaviour $H = 1$ seen in the Hurst plot. Note, however, that this argument needs some refinement, because, as we have seen in Figure 2, longer waiting times imply larger price jumps afterwards. Nevertheless, we believe that the general line of the argument is true.

The behaviour changes when Δt becomes comparable to the average inter-event time. The most often encountered result is represented by triangles in Figure 4. At scales larger than the average inter-event time the quantity $\left\langle |\Delta x|_{\max} \right\rangle$ saturates, yielding $H = 0$. It is easy to understand why it must be so. If the density of particles is large enough, the configuration of the order book can be described by average concentrations $\rho_A(y)$ and $\rho_B(y)$ of particles A and B, respectively. The variable $y \in (0, L)$ measures the position on the price axis. It is easy to find that neglecting the fluctuations in the order density the solution of the BPS model trivialises into $\rho_B(y) = \frac{8N}{L^2}(L/2 - y)\theta(L/2 - y)$, $\rho_A(y) = \frac{8N}{L^2}(y - L/2)\theta(y - L/2)$. So, in absence of fluctuations the price is pinned in the exact middle of the allowed interval. This is just the saturation regime $H = 0$.

To see the theoretically predicted Hurst exponent $H = 1/4$ we must find a time window between the ballistic and pinned regime. This is often very narrow, if it exists at all, as testified in Figure 4 by the data for $L = 250$ and $N = 50$. Only for large enough size with small enough density of orders the fluctuation regime $H = 1/4$ is observable. (Note that in the finite-size analysis the number of orders must scale as $N \propto L^2$ with the length of the allowed interval.) In Figure 4 we can see an example for $L = N = 2 \times 10^4$, where such time window is visible.

The difficulty to observe the desired regime in BPS model contrasts with the way the exponent $H = 1/4$ was derived analytically [48,49]. In these works the two reactants occupy initially the positive and negative half-lines, respectively. Then, they are let to diffuse and react. Annihilated particles are not replaced. Therefore, the reaction front spreads out indefinitely and we can observe a well defined long-time regime characterised by the exponent $H = 1/4$. (There is also a logarithmic factor there, but we neglect it in this discussion.) On the contrary, in BPS the long-time regime has always $H = 0$.

3.2 Stigler model and its free variant

In Stigler model, we have again the allowed price range $\{1, 2, \ldots, L\}$, where the orders can be placed. There can be at most N orders total. If, at time t, there is still the order deposited at time $t - N$, it is removed. Then, we deposit a new order. We decide whether it will be a bid or an ask (with equal probability) and choose randomly, with uniform distribution, its position within the allowed price range. A transaction may follow. If the new order is e.g. a bid placed at position c_t and the lowest ask is at position $c_A \le c_t$, then the new price is set to $x_t = c_A$ and both the new bid at c_t and the old lowest ask at c_A are removed. If $c_A > c_t$, the price does not change, $x_t = x_{t-1}$ and the new bid stays in the order book. (Symmetrically it holds for depositing an ask.)

In Figure 5 we show an example of the typical time sequence of price x_t and one-step returns $r_t = x_t - x_{t-1}$. Qualitatively, we can guess that the fluctuations are far from Gaussian, i.e. returns will not obey the normal distribution. Indeed, we can see in Figure 6 that for several decades the distribution falls off slowly as a power with small exponent, $P(r) \sim r^{-0.3}$ and then it is sharply cut off. Indeed, the cutoff comes from the natural bound $|r_t| < L$.

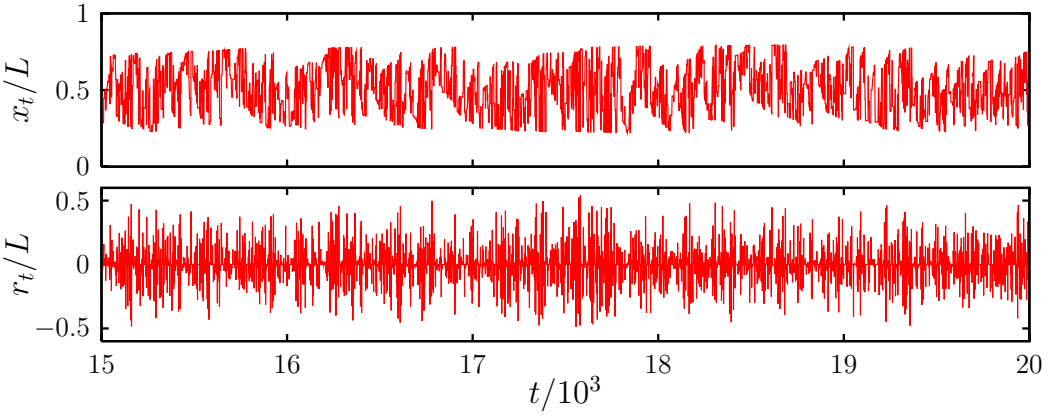

Fig. 5. Example of the evolution of the Stigler model. In the upper panel, time dependence of the actual price; in the lower panel, one-step returns. On the segment of length $L = 5000$ there are at most $N = 5000$ orders.

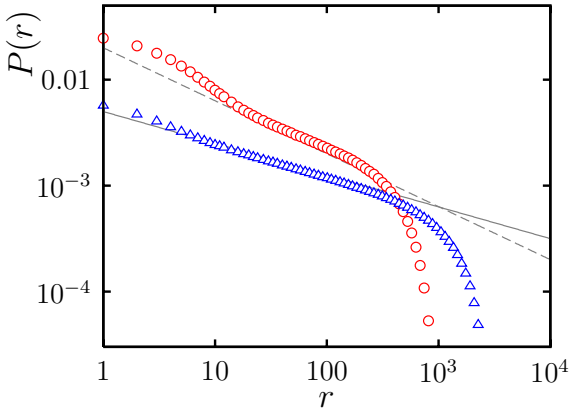

Fig. 6. Distribution of one-step returns for Stigler model with $L = 5000$ and $N = 5000$ (△) and for the free Stigler model with $N = 5000$, $s = 4000$, and $d = 10^4$ (○). The lines are power laws $\propto r^{-0.3}$ (solid) and $\propto r^{-0.5}$ (dashed).

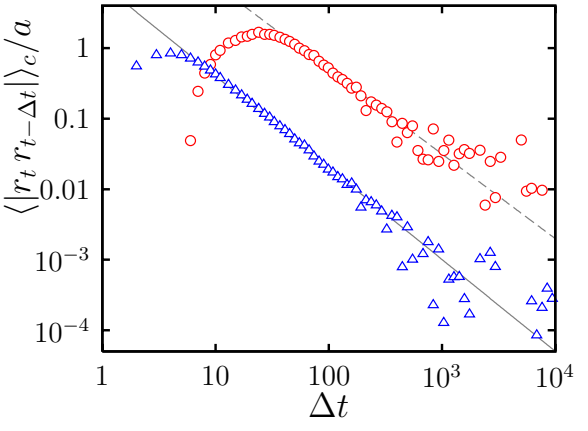

Fig. 7. Autocorrelation of absolute returns for the Stigler model with $L = 5000$ and $N = 5000$ (△) and for the free Stigler model with $N = 5000$, $s = 4000$, and $d = 10^4$ (○). The lines are power laws $\propto (\Delta t)^{-1.3}$ (solid) and $\propto (\Delta t)^{-1.2}$ (dashed). In order to have all data in the same frame, we introduced an auxiliary factor $a = 10$ (○) and $a = 10^4$ (△).

In the time series in Figure 5 we can also glimpse the volatility clustering. To measure it quantitatively, we plot in Figure 7 the autocorrelation of absolute returns

$$\langle|r_t\, r_{t-\Delta t}|\rangle_c = \langle|r_t\, r_{t-\Delta t}|\rangle - \langle|r_t|\rangle\langle|r_{t-\Delta t}|\rangle\ . \qquad (6)$$

It decays as a power, but with rather large exponent, $\langle|r_t\, r_{t-\Delta t}|\rangle_c \sim (\Delta t)^{-1.3}$. On the other hand, the returns themselves are only short-time negatively correlated with exponential decay, as can be seen in Figure 8.

These findings show that Stigler model is not a very good candidate model for explaining the empirical facts. However, it may well serve as a starting point for successful construction of better models. The first limitation we must remove is the fixed range of prices from 1 to L. A severe consequence of this limitation is the saturation seen in the Hurst plot (Fig. 13). In long time regime, the Hurst exponent is obviously $H = 0$. To cure this problem we introduce a "free" variant of the Stigler model. It may be also considered as a precursor of the Genoa market model, to be studied in the next section.

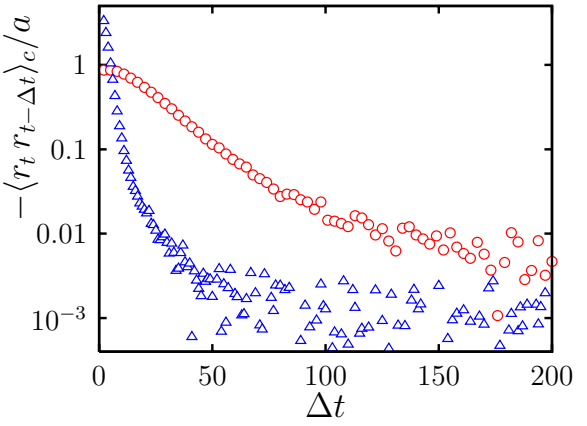

Fig. 8. Autocorrelation of returns for the Stigler model with $L = 5000$ and $N = 5000$ (△) and for the free Stigler model with $N = 5000$, $s = 4000$, and $d = 10^4$ (○). In order to have all data in the same frame, we introduced an auxiliary factor $a = 100$ (○) and $a = 10^4$ (△).

The price axis is now extended to all integer numbers. Of course, the position on this axis must be now interpreted as logarithm of price, rather than price itself. Nonetheless, for brevity we shall speak of "price" also in this case. The orders are again deposited randomly within an allowed range, but now the range depends on the actual position of the price x_t. We introduce two integer parameters, the width of the allowed interval d and the shift s of the interval's centre with respect to the current price. Denote c_t the order issued at time t. If it is a bid, it is deposited uniformly within the range $x_t - s - d/2 < c_t \leq x_t - s + d/2$, while for an ask the range is $x_t + s - d/2 \leq c_t < x_t + s + d/2$. Of course, in order to have any transactions at all, we must have $d \geq 2s$. As with the Stigler model, the orders older than N steps are removed.

In spite of the change in the deposition rules, the basic features of the free Stigler model remain very similar to those of the original variant. In Figure 6 we can see that the return distribution exhibits slow power-law decay $P(r) \sim r^{-0.5}$ with a sharp cutoff at large returns. The exponent $\simeq 0.5$ is larger than in the Stigler model, but still remains very much below the empirical value $\simeq 4$. The autocorrelation of absolute returns (see Fig. 7) decays as a similar power law $\langle |r_t\, r_{t-\Delta t}| \rangle_c \sim (\Delta t)^{-1.2}$. In addition, a peak in the autocorrelation function, merely visible in Stigler model, becomes quite pronounced here and is shifted to larger times, about $(\Delta t)_{\mathrm{peak}} \simeq 20$. This indicates some quasi-periodic pattern in the time series of the volatility, related probably to a typical waiting time between subsequent trades. Indeed, we found that the waiting times are exponentially distributed, and for the parameters of Figure 7 the average waiting time is about $\simeq 11$. As for the autocorrelation of returns, it decays exponentially again, albeit more slowly, as shown in Figure 8.

The main difference observed, compared to the original Stigler model, is shown in the Hurst plot, Figure 13. At shorter times, there is a tendency to saturation, as in the Stigler model, but at larger times the purely diffusive regime with $H = 1/2$ prevails. We can attribute these results the following interpretation. The orders present in the order book form a "bunch" located somewhere around the current price. Orders too far from the price are usually cancelled after their lifetime (equal to N) expires. Hence the localisation around the price. Now, while in the Stigler model the bunch of orders is imprisoned between 1 and L, in the free Stigler model the bunch can wander around, following the price changes. The value $H = 1/2$ shows that the movements of the bunch as a whole can be described as an ordinary random walk.

3.3 Genoa market model

Both in original and free Stigler model, the agents behind the scene have truly zero intelligence. At most, they look at the price in this instant and place orders at some distance from it, but the distance is not affected neither by the present nor the past sequence of prices. However, it is reasonable to expect that the agents react to the fluctuations observed in the past. The simplest feedback mechanism may be that the distance to place an order is proportional to the volatility measured during some time period in the past. This idea was already applied in one of the variants of the BPS model [47] and lies in the basis of the Genoa artificial market [52]. What we shall call "Genoa market model" from now on, is in fact very reduced version of the complex simulation scheme of reference [52]. We believe, however, that we retain the most significant ingredients.

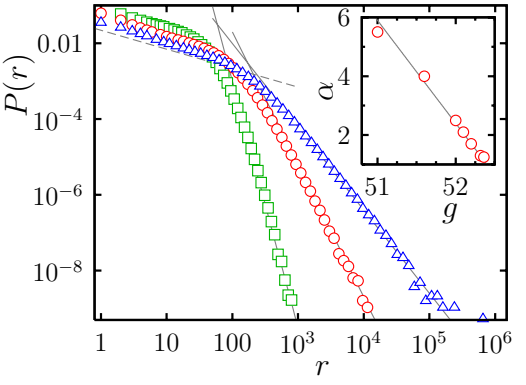

Fig. 9. Return distribution in the Genoa market model. Maximum number of orders is $N = 1000$, width to shift ratio is $b = 7$. The feedback factor is $g = 51$ (□), 52 (○), and 52.36 (△). The three solid lines are power laws $\propto r^{-1-\alpha}$ with the exponents (from left to right) $\alpha = 5.5$, 2.5, and 1.2. The dashed line is the power $\propto r^{-0.5}$. In the inset, the dependence of the tail exponent α on the feedback factor g. The line is the dependence $(\alpha - 1) \propto (52.4 - g)$ indicating that the critical value lies at $g_c \simeq 52.4$.

We must first define a convenient measure of instantaneous volatility. Averaging absolute price changes with an exponentially decaying kernel

$$v_t = \lambda \sum_{t'=0}^{\infty} (1-\lambda)^{t'} |x_{t-t'} - x_{t-t'-1}| \,. \tag{7}$$

turns out to be a good choice. We use the value $\lambda = 10^{-3}$ throughout the simulations. The orders will be placed on integer positions within an interval determined by the width and the shift from actual price, as in the free Stigler model, but now these two parameters are time-dependent. Their ratio will be held constant and both will expand as the volatility v_t will grow. So, the prescription will be

$$\begin{aligned} d_t &= \lceil g\, v_t \rceil \\ s_t &= \left\lfloor \frac{d_t}{b} \right\rfloor \end{aligned} \tag{8}$$

and the constants b and g, besides the maximum number of orders (i.e. maximum lifetime of an order) N constitute the parameters of the model. In order that we have any transactions at all, we impose the bound $b > 2$.

The feedback mechanism we apply makes significant difference in all aspects of the model. Let us look first at the return distribution. In Figure 9 we can see how

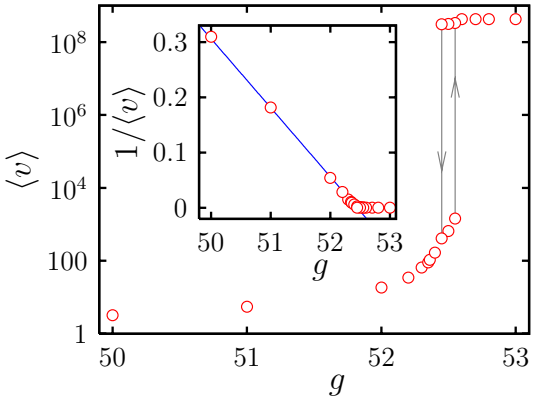

Fig. 10. Genoa market model. Dependence of the average volatility on the feedback factor g. The parameters are $N = 1000$, $b = 7$. The lines with arrows indicate the hysteresis curve, the false signature of an apparent first-order transition. In the inset, the same data but plotted differently. The line is the dependence $\propto (52.4 - g)$, suggesting the critical value $g_c \simeq 52.4$.

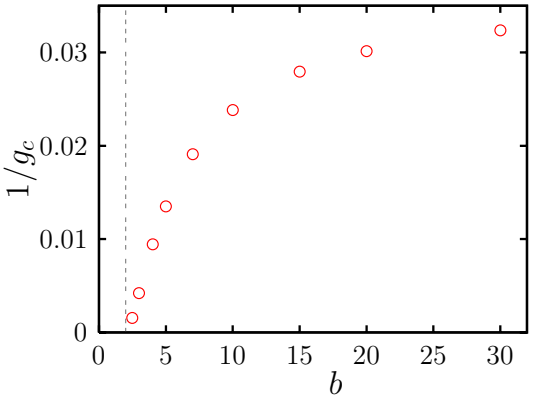

Fig. 11. Phase diagram of the Genoa market model for $N = 1000$. Inverse of the critical value g_c of the feedback factor, deduced from the simulations, depends on the width to shift ratio b. The phase transition is absent in the (trivial) region $b < 2$, indicated by dashed line.

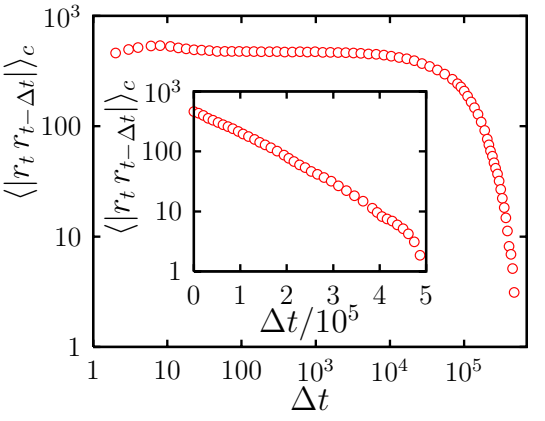

Fig. 12. Autocorrelation of absolute returns in the Genoa market model, for parameters $N = 1000$, $b = 7$, $g = 52$. In the inset, the same data are plotted in linear-logarithmic scale.

it changes when we tune the parameter g. Generically, a power-law tail $P(r) \sim r^{-1-\alpha}$ develops, with an exponent strongly depending on g. The larger g, the smaller the exponent, until for some critical value $g = g_c$ it approaches the limit $\alpha = 1$. Beyond that point, the average return, i.e. also the stationary value of the average volatility v_t diverges. This may be regarded as a kind of phase transition. It is also worth noting that for low returns there is an interval where another power law holds, with $1 + \alpha \simeq 0.5$. This is the remainder of the behaviour characteristic for the free Stigler model, the parent of the Genoa stock market.

We can look at this behaviour from another aspect when we directly calculate the time average $\langle v \rangle = \lim_{T\to\infty} \frac{1}{T} \sum_{t=0}^{T} v_t$. Its dependence on g is shown in Figure 10. This plot requires some explanation. The actual implementation of the algorithm prevents the average volatility from diverging. Instead, it reaches a relatively large value above 10^8. So, all points beyond this level should be considered as effectively infinite. Moreover, in Figure 10 we can see a sign of bistability, or hysteresis, which is at first sight a signature of a first-order phase transition. However, a more careful analysis with varying N shows that the presence of an apparent hysteresis curve is misleading. Actually, it is a subtle finite-size effect and the phase transition is continuous (i.e. second order).

We can see that the transition points found independently in Figures 9 and 10 are consistent, so it is indeed a single transition with two aspects. In fact, the coincidence between Figures 9 and 10 means equality of time and "ensemble" averages, i.e. ergodicity of the model dynamics.

In Figure 11 we show a phase diagram of the model, indicating the dependence of the critical point g_c on the parameter b. When b approaches its lower limit equal to 2 (note that there are no trades for $b < 2$), the critical value g_c diverges. It comes as no big surprise, because trades became more rare when $b \to 2$ and therefore the volatility diminishes. This allows the feedback measured by g to be stronger without divergence in the realised average volatility. The phase diagram depends on the maximum number of orders N, but we found that the dependence is very weak and never changes the qualitative look of the phase diagram. The reason for this is that for large N the actual number of orders present in the system is maintained mainly by the annihilation by other orders and the fraction of orders which live long enough to be discarded at the end of their lifetime is very small. In other words, the average number of orders in the system $\langle N_{\mathrm{present}} \rangle$ grows extremely slowly with N.

To complete the study of the Genoa market model, we show in Figure 12 the autocorrelations and in Figure 13 the Hurst plot. Contrary to both the Stigler model and its free variant, the autocorrelation of absolute returns decays as a clear exponential, although the characteristic time is extremely long. As for the Hurst exponent, is is equal to $H = 1/2$, in accord with the behaviour of the free Stigler model. In both Genoa and free Stigler models the long-time behaviour of $R(\Delta t)$ is dominated by the diffusion of the bunch of orders as a whole. What makes difference between the two is the dynamics within the bunch, but

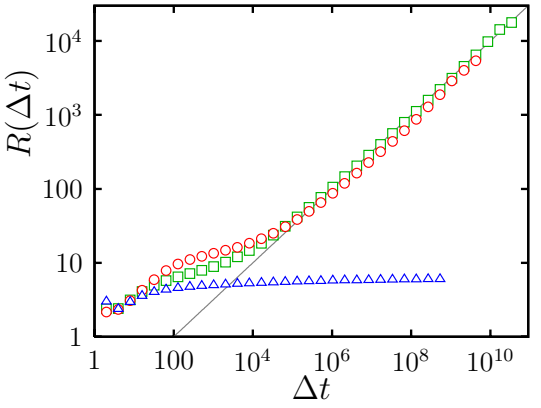

Fig. 13. Comparison of Hurst plots for Stigler model with parameters $L = 5000$, $N = 5000$ (△), free Stigler model with $N = 5000$, $s = 4000$, $d = 10^4$ (○), and Genoa market model with $N = 1000$, $b = 7$, $g = 51.6$ (□). The line is the power $\propto (\Delta t)^{1/2}$.

this is not visible in the Hurst plot. Note also that for the parameters used in Figure 13 the regime with $H = 1/2$ starts at times $\simeq 10^5$. At such time scale the autocorrelations are already damped out, regardless the power-law decay in free Stigler or the slow exponential decay in Genoa models (compare Figs. 7 and 12).

3.4 Maslov model

So far, the models investigated did not distinguish between limit orders and market orders. The distinction was only implicit. All bids placed below the lowest ask acted effectively as limit orders, as well as the asks placed above the highest bid. In the model of Maslov [59] the orders of unit volume were issued at each step, being limit orders or market orders with equal probability 1/2. The limit orders were placed at close vicinity of the current price. Here we add also the feature of order evaporation, as in [18]. Each order present in the book will have the same probability of being cancelled (evaporated). Therefore, we do not take into account the age of the order, as we did in various variants of the Stigler model.

We tune the speed of the evaporation by a parameter q. For simpler terminology, we shall call it evaporation probability. Actually, the probabilities of deposition, satisfaction and evaporation event in one step of the evolution, at time t, will be defined as, respectively,

$$W_t^{+\mathrm{dep}} = \frac{1}{2 + q\left(\frac{N_t}{\overline{N}} - 1\right)}$$
$$W_t^{-\mathrm{sat}} = \frac{1-q}{2 + q\left(\frac{N_t}{\overline{N}} - 1\right)}$$
$$W_t^{-\mathrm{eva}} = \frac{q\,\frac{N_t}{\overline{N}}}{2 + q\left(\frac{N_t}{\overline{N}} - 1\right)} \qquad (9)$$

where N_t is the actual number of orders in the book. The parameter $\overline{N}$ controls the number of orders in the book and again, to simplify the terminology, it will be called average number of orders, although the actual value of the average number of orders is slightly different (due to the effect of fluctuations). If the evaporation probability is zero, the parameter $\overline{N}$ becomes irrelevant for the dynamics. Note that the three probabilities (9) change in time, as the total number of orders N_t fluctuates.

The orders are placed at integer positions denoting the (logarithm of the) price. Let x_t be the price at time t and N_{At}, N_{Bt} actual number of asks and bids, respectively, with the total number of orders $N_t = N_{At} + N_{Bt}$.

In case deposition is selected to happen, according to probabilities (9), we add an ask ($N_{At+1} = N_{At}+1$) or a bid ($N_{Bt+1} = N_{Bt} + 1$) with equal probability. The position of the new order is $c_t = x_t + 1$, for the ask and $c_t = x_t - 1$ sign for the bid. The price remains unchanged, $x_{t+1} = x_t$ because no transaction occurred.

The execution, or satisfaction, of an order happens always when a market order is issued, and there is a limit order to match it. Again, sell and buy side are equivalent, so they are selected with equal probability 1/2. Suppose a sell order is issued and there is at least one bid, $N_{Bt} > 0$, and c_B is the position of the highest bid. Then, the new price is $x_{t+1} = c_B$, we update $N_{Bt+1} = N_{Bt} - 1$ and remove the order at c_B from the book. Symmetrically it holds for the buy order.

When the evaporation of an order is about to happen, we select any of the existing orders with uniform probability and remove it from the system. Note that removals of a bid and an ask are not equiprobable, as we evaporate a bid with probability N_{Bt}/N_t and an ask with probability N_{At}/N_t.

We can see in Figure 14 the space-time diagram of a typical evolution of the order book. The price "sows" new orders along its fluctuating path, which are either satisfied, as the price returns next to its original position, or they vanish by evaporation. Longer price jumps occur when the density of orders is low. Conversely, the price becomes temporarily pinned, when it enters a region with large density of orders.

Let us first revisit the results for the original Maslov model without evaporation ($q = 0$). In Figure 15 we show the distribution of returns at several time lags

$$P_{\Delta t}(r) = \langle \delta(r - |x_t - x_{t-\Delta t}|) \rangle \, . \qquad (10)$$

We can see clearly the power-law tail $P_{\Delta t}(r) \sim r^{-3}$, observed first in [59]. The results can be also rescaled to fall onto a single curve, $P_{\Delta t}(r) = \frac{1}{s} F\left(\frac{r}{s}\right)$ as shown in Figure 16. The dependence of the scaling factor s on the time lag Δt is shown in the inset of Figure 16 and we can clearly see the power-law dependence $s \propto (\Delta t)^{1/4}$. Hence we deduce the Hurst exponent of the price fluctuation process $H = 1/4$. The same value of the Hurst exponent is confirmed independently by drawing the Hurst plot, Figure 20.

The volatility clustering, measured by the autocorrelation of absolute returns, is shown in Figure 17. The autocorrelations decay as a power law, similarly as in the Stigler model, but now the exponent is significantly lower,

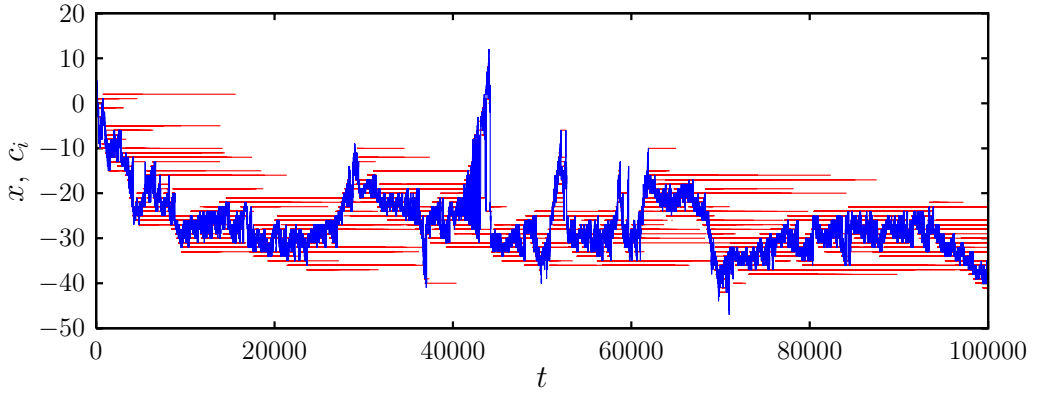

Fig. 14. Example of the evolution of the Maslov model with evaporation. Each segment of a horizontal line corresponds to one order, placed where the segment starts and executed or evaporated where the segment ends. The rugged line is the time dependence of the actual price. Average number of orders is $\overline{N} = 100$ and the probability of evaporation $q = 0.05$.

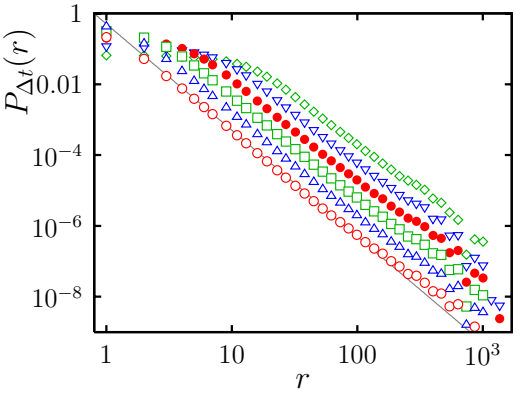

Fig. 15. Distribution of returns in the Maslov model without evaporation, at time lags $\Delta t = 1$ (○), 10 (△), 100 (□), 10^3 (●), 10^4 (▽), and 10^5 (◇). The line is the power $\propto r^{-3}$.

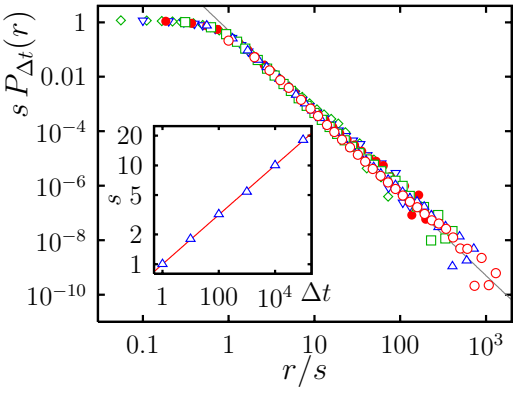

Fig. 16. Rescaled distribution of returns in the Maslov model without evaporation. The meaning of the symbols is the same as in Figure 15. The line is the power $\propto r^{-3}$. In the inset we plot the dependence of the scaling constant on the time lag. The line is the power $\propto (\Delta t)^{1/4}$.

$\langle |r_t\, r_{t-\Delta t}| \rangle_c \sim (\Delta t)^{-0.5}$, which makes the behaviour much more similar to empirical price sequences.

Now we investigate the effect of finite evaporation probability, $q > 0$. In the distribution of one-step returns, Figure 18, it leads to deformation of the original power-

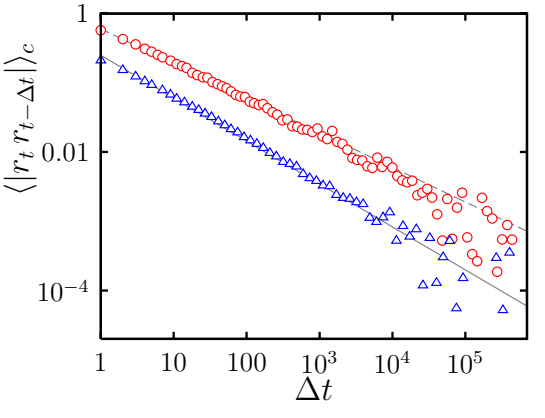

Fig. 17. Autocorrelation of absolute returns for the Maslov model without evaporation (○) and with evaporation probability $q = 0.01$ (△). Average number of orders is $\overline{N} = 1000$. The dashed line is the power $\propto (\Delta t)^{-0.5}$ and the solid line is $\propto (\Delta t)^{-0.62}$.

law dependence. At very small values of q, we observe an effective increase of the power-law exponent, to values $1 + \alpha = 4$ and even more. This would sound fine, as this is just the value reported in empirical studies. However, a cutoff starts developing as well and when we increase q further, the cutoff prevails and the power-law regime vanishes completely. Since the evaporation destroys the power law, it is not surprising that the scaling also breaks down. In Figure 19 we can see that no scaling can be seen, because at each time lag the shape of the graph is different.

While the return distribution changes substantially, the absolute return autocorrelation remains nearly the same. The decay follows again a power law, but the exponent is somewhat larger, $\langle |r_t\, r_{t-\Delta t}| \rangle_c \sim (\Delta t)^{-0.62}$. The long-time correlations are caused by the immobile orders who sit within the book until the price finds its path back to them. Evaporation removes some of the orders, thus eroding the correlations. Quantitatively it results in suppression of the correlation function.

Finally, we look at the Hurst plot, Figure 20. As mentioned already in [18], evaporation of orders induces the

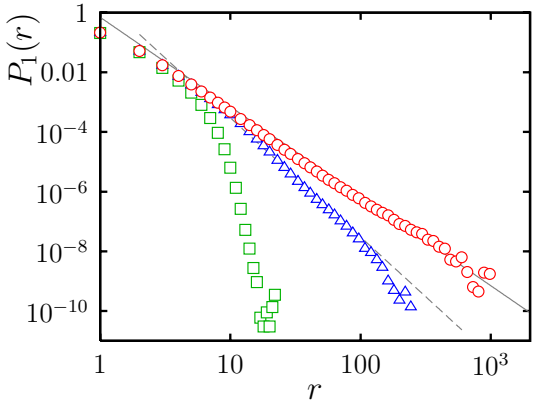

Fig. 18. Distribution of one-step returns in the Maslov model with (△, □) and without (○) evaporation. The evaporation probability is $q = 0.01$ (△), 0.05 (□); the average number of orders is $\overline{N} = 1000$. The solid line is the power $\propto r^{-3}$, the dashed line is $\propto r^{-4}$.

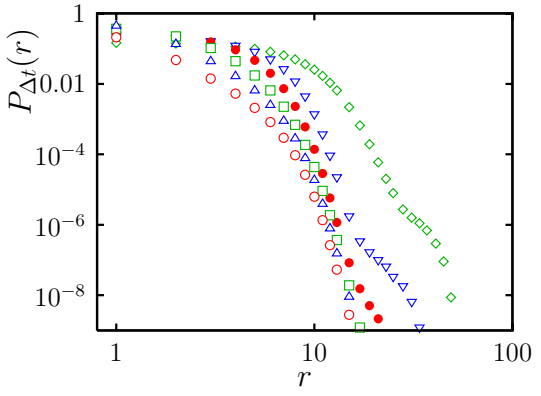

Fig. 19. Distribution of returns in the Maslov model with evaporation. The parameters are $q = 0.05$, $\overline{N} = 1000$. The lime lags are $\Delta t = 1$ (○), 10 (△), 100 (□), 10^3 (●), 10^4 (▽), and 10^5 (◇).

crossover to purely diffusive behaviour, $H = 1/2$ at large times. Interestingly, when we compare the quantity $R(\Delta t)$ at equal time difference for different values of q we can see that larger evaporation probability actually suppresses the diffusion. The Hurst exponent $H = 1/2$ remains universal, but the diffusion constant is lower for larger q. The possible explanation is that the evaporation events go at the expense of satisfaction events. Therefore, there are less trades per unit of time, hence the slower diffusion of the price.

We studied also another modification of the Maslov model, where the evaporation of orders was implemented in the sense of Stigler model. Instead of removing an arbitrarily chosen order with fixed probability, we track the age of the orders and remove them if the age exceeds certain fixed lifetime. We did not observe much difference compared to the variant with usual evaporation. The Hurst plot looks much like that of Figure 20, showing clear crossover from the short time $H = 1/4$ to long-time $H = 1/2$ behaviour. Absolute returns autocorrelation decays as a power with similar (slightly larger) exponent.

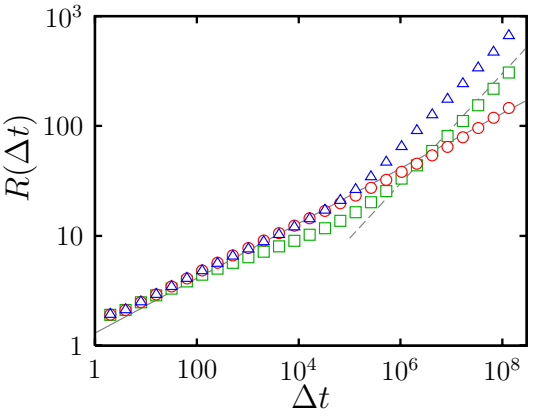

Fig. 20. Hurst plot for the Maslov model without evaporation (○) and with evaporation probability $q = 0.01$ (△) and 0.05 (□). Average number of orders is $\overline{N} = 1000$. The solid line is the power $\propto (\Delta t)^{1/4}$, the dashed line is $\propto (\Delta t)^{1/2}$.

Somewhat larger difference can be seen in the return distribution. The finite lifetime of the orders leads to decrease in the exponent of the power-law part, while the evaporation causes its increase. Qualitatively, the cutoff at larger returns seems more severe than in the case of evaporation, although quantitative comparison is hardly possible. To sum up, we consider the variant with finite lifetime farther from the reality than the variant with simple evaporation.

3.5 Uniform deposition model

In Maslov model, the new orders are placed locally, at distance 1 from the actual price. It could be possible to fix another limit for the maximum distance, and indeed, in the original work [59] this number was 5. There is little, if any, effect of the precise value of this parameter. The important thing is that the orders are never placed farther than certain predefined limit.

In reality, however, the distribution of distances at which the orders are placed is rather broad and decays as a power law [26]. The mechanism responsible for this power law is probably related to the optimisation of investments performed by agents working at widely dispersed time horizons [39]. Actually it is reasonable to expect that the distribution of time horizons and (related to it) distribution of distances is maintained by equilibration, so that all agents expect just the same average gain, irrespectively of the time horizon on which they act. This idea would certainly deserve better formalisation.

Instead of taking the empirical distribution of placements as granted without deeper theoretical understanding, we prefer to compare the localised deposition in Maslov model with a complementary strategy applied in the set of models investigated by Daniels, Farmer and others [62–65]. Instead of keeping short distance from the price, the orders are deposited with equal probability at arbitrary distance. In this work, we adopt one of the variants studied in [62] and within this paper we shall call it Uniform Deposition Model (UDM).

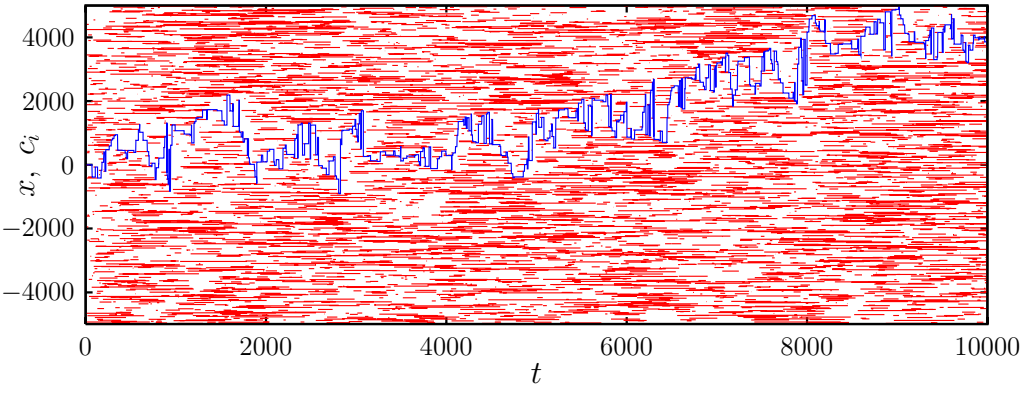

Fig. 21. Example of the evolution of the Uniform Deposition Model. Each segment of a horizontal line corresponds to one order. The rugged line is the time dependence of the actual price. The width of the segment of allowed prices is $L = 10^4$. Average number of orders is $\overline{N} = 100$ and the evaporation probability $q = 0.9$.

In fact, the only difference with respect to the Maslov model with evaporation, defined in Section 3.4 is that we limit the price to a segment of length L and orders are deposited uniformly on this segment. So, the orders and price can assume integer position from the set $S = \{-L/2, -L/2+1, \ldots, L/2-2, L/2-1\}$. As in the Maslov model, there are three classes of events, deposition, order satisfaction, and evaporation. Their probabilities are defined by the same formulae (9) as in the Maslov model. When an order is to be deposited, we first look where is the price x_t. Then, select randomly a point c_t from the set $S\backslash\{x_t\}$ and deposit an order there. If $c_t > x_t$ the order becomes an ask, if $c_t < x_t$ it is a bid. (We forbid depositing exactly at the price position.) Although the probabilities (9) look the same as in the Maslov model, we should note that there is a big difference in the typical values of the evaporation probability q. In Maslov model the orders are clustered around the price and the evaporation is somehow a complement or correction to the natural satisfaction of the limit orders by incoming market orders. So, q is typically a small number compared to 1. On the contrary, in UDM the evaporation is essential, because orders are deposited in the whole allowed segment and ought to be removed also from areas where the price rarely wanders. Therefore, q is comparable to, although smaller than, one. Very often, the simulations were performed in the regime where $1 - q$ was much smaller than 1.

To see a typical situation, we plot in Figure 21 the space-time chart of orders and price. We can see how the price "crawls" through a see of orders and the configuration of the orders changes substantially also very far from the price and without being affected by its movement. Of course, this is to be expected due to uniform deposition rule. On the other hand, this is certainly not a realistic feature.

We found fairly interesting, although absolutely unrealistic, the distribution of one-step returns, as shown in Figures 22 and 23. The tail is characterised by power-law decay $P_1(r) \sim r^{-0.75}$ and the exponent, close to the fraction 3/4, seems to be universal, irrespectively of the parameters q and $\overline{N}$. The value of the exponent is far

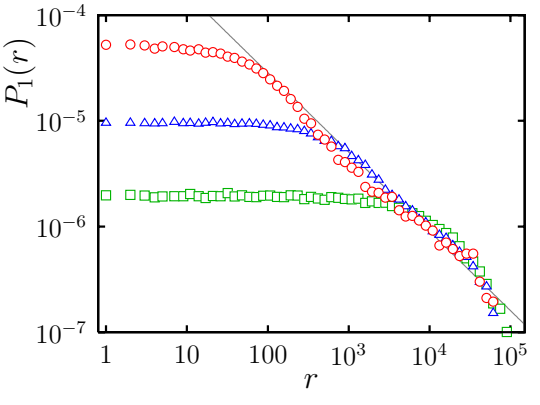

Fig. 22. Distribution of one-step returns in UDM. The parameters are $L = 10^6$, $q = 0.9$, and $\overline{N} = 10^4$ (○), 10^3 (△), and 100 (□). The line is the power $\propto r^{-0.75}$.

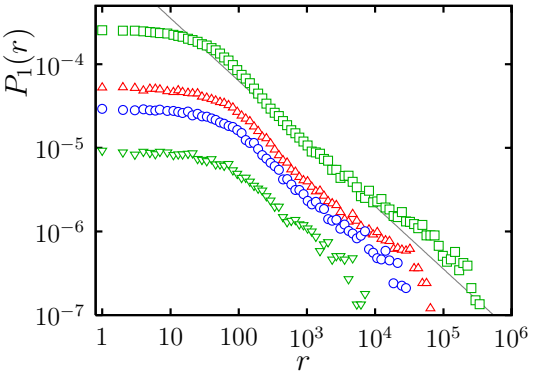

Fig. 23. Distribution of one-step returns in UDM. The parameters are $L = 10^6$, $\overline{N} = 10^4$, and $q = 0.5$ (□), 0.9 (△), 0.95 (○), and 0.99 (▽). The line is the power $\propto r^{-0.75}$.

below the empirical value, but the very fact of universal behaviour in such reaction-deposition model calls for explanation. We do not have any yet.

While the power law in the return distribution indicates some scale-free behaviour at single time, we find no sign of scaling when we compare the returns at different time scales. We can see that in Figure 24. At longer lags the power-law tail vanishes and the distribution becomes

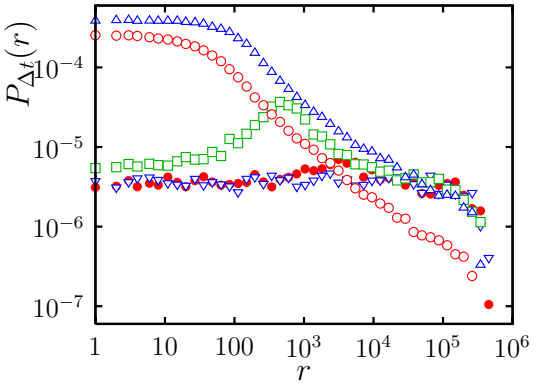

Fig. 24. Distribution of returns in UDM at different time lags. The parameters are $L = 10^6$, $\overline{N} = 10^4$, and $q = 0.5$. The time lags are $\Delta t = 1$ (○), 10 (△), 100 (□), 10^3 (●), and 10^4 (▽).

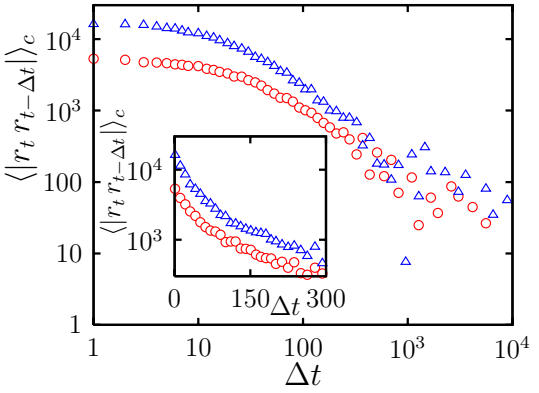

Fig. 25. Autocorrelation of absolute returns in UDM. The parameters are $L = 10^5$, $q = 0.9$; $\overline{N} = 10^3$ (○), and 100 (△).

uniform. This means that after long enough time the price can jump arbitrarily from one position to another within nearly all the allowed range, except the vicinity of the extremal points. In fact, the same behaviour was observed also for long enough time lags in the Stigler model. Certainly, the origin of such behaviour is the very existence of the limited price range, both in UDM and the Stigler model.

Let us look on the volatility clustering now. In Figure 25 we show the autocorrelation of absolute returns. the decay is rather slow, i.e. slower than exponential, but at the same time it is faster than a power law. This behaviour is special to the Uniform Deposition Model.

Finally, in Figure 26 we show the Hurst plot. Again, there is close similarity to the Stigler model in the sense that there is no long-time diffusive regime but saturation is observed instead. Only in the very short initial transient we observe ordinary diffusion-like behaviour characterised by $H = 1/2$. It is unclear from our simulations whether there is an intermediate time window in which a non-trivial Hurst exponent (like the notorious $H = 1/4$) would be observed.

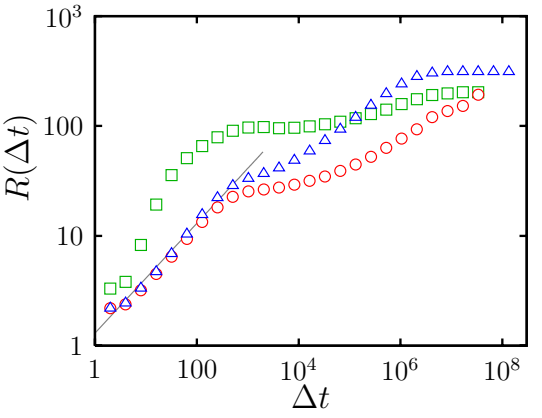

Fig. 26. Hurst plot for UDM. The parameters are $L = 10^6$; $q = 0.9$ (○, △), and 0.5 (□); $\overline{N} = 10^4$ (○, □) and 1000 (△). The line is the power $\propto (\Delta t)^{1/2}$.

4 Conclusions

It is not easy to make a synoptic comparison of the whole ensemble of models studied here. However, one easy conclusion can be drawn, that none of them reproduces satisfactorily the reality. Most importantly, the empirically observed Hurst exponent $H \simeq 0.6$ is not found anywhere. We can classify the diffusion behaviour into three main types. The first and most trivial one is dominated by the saturation, $H = 0$ and happens always when the price is restricted by definition to an interval, like in the Stigler and Uniform Deposition models. The same holds also for the asymptotic regime of the BPS model, although in the latter the interesting things happen at the intermediate time scale, where $H = 1/4$. We do not exclude the possibility that also in UDM the intermediate times have $H = 1/4$, but we were not able to make any conclusive statement about that. The second type is characterised by asymptotic sub-diffusion, with $H = 1/4$. Strictly speaking this holds only for the Maslov model without evaporation. The third and most frequent type of behaviour can be described as ordinary diffusion ($H = 1/2$) at long times. The initial transient regime may exhibit either $H = 1/4$, as in the Maslov model with evaporation or with fixed finite lifetime of orders, or it may instead show the tendency to saturation, as in the free Stigler model and Genoa artificial market model. It seems really difficult to design an order-book model where super-diffusive behaviour ($H > 1/2$) would arise naturally, without being put in by hand. We cannot resist the temptation to compare this difficulty with the situation in stochastic modelling by continuous-time random walks [79]. There also, the sub-diffusive behaviour can be found easily, but the super-diffusive one should be essentially forced.

The power-law tails in the return distribution seem to work slightly better. When we set apart the BPS model, where the tail decays even faster than exponentially, we can distinguish the models where the exponent in the power-law decay is far too low ($\alpha < 0$), which comprises Stigler model, free Stigler model and UDM, from the models, where the exponent lies close, although not always

precisely at the empirical value. The latter group contains the Genoa market model and the Maslov model with and without evaporation. The best chance for success when matched with the real data has the Genoa model, where the exponent can be tuned by variation of the model parameters. On the other hand, it is a priori unclear, why the parameter values should be this and not that. In the Maslov model proper, the exponent is universal, $\alpha = 2$. Adding evaporation increases this value, so the agreement with the data can be again tuned, in this case by changing the evaporation speed. However, evaporation induces not only effective increase of the exponent, but also emergence of a cutoff. In fact, we think that the change in exponent is only an illusion brought about by combination of the power law and a weak cutoff. This contrasts with the Genoa model, where, below the phase transition, the power-law tails are genuine for all values of the parameter $g < g_c$.

The very existence of the phase transition in the Genoa market model is a remarkable fact. It is intimately related to the dependence of the tail exponent on g. When the exponent drops to the value $\alpha = 1$ the average return diverges and the transition occurs. One could speculate, how the picture would change if the feedback between volatility and order placement was defined differently. For example, the volatility can be defined through squares of returns, instead of absolute returns. This would also sound more natural, we think. We expect that in this case the transition would be related to the divergence of the second moment of the return distribution, i.e. it would be located at such parameter values which would imply the exponent $\alpha = 2$. Otherwise, the picture would be most probably the same.

There is one feature, not so much important as such, but showing that the free Stigler model, Genoa stock market and Maslov model are members of the same family. If we look at the return distribution at small returns, we find that Genoa stock market and Maslov model (see Ref. [59]) exhibit another power-law regime, with very small exponent $1 + \alpha \simeq 0.5$. Clearly it is the sign that deep within the bunch of orders surrounding the price the two models behave just like the free Stigler model, which shows the same power law in entire range of returns.

The return distribution in the Maslov model without evaporation has a very important and appealing feature. Its is the scaling property. The returns at different time lags scale with Hurst exponent equal to $H = 1/4$. Qualitatively it agrees with the empirically found scaling, but, unfortunately, quantitatively it is completely off. An important finding is that the evaporation of orders destroys the scaling, which is also absent in the UDM model. On the contrary, we also observed scaling in the Genoa market model, but not a perfect one. The difference between different lags is in the (not so much important, after all) low-return range, where the power-law tail is not yet developed.

When we want to compare the volatility clustering measured through the autocorrelation of absolute returns, we exclude the BPS model. Due to rather long waiting times, the measurement of the autocorrelation was impractical. In all remaining models, we found slow decay of the autocorrelations, but the functional form was not always a power. In fact, there are two exceptions. In the Genoa market model, the decay is exponential, although very slow. In UDM, the decay is faster than any power-law but slower than an exponential. A stretched exponential may be perhaps the candidate. In the remaining models, the power-law decay is observed. The difference lies in the exponent. While in the Stigler and free Stigler model, the exponent is above 1, in the Maslov model, both with and without evaporation, the value lies at or close to 1/2.

A crucial conclusion from the above is, that we cannot simply pick a model ("the best one") from those studied here and apply it directly for a stock-market practice, e.g. for option pricing. All the models need some extensions or modifications to serve well as a realistic description. In this work we had no intent to amend the models by gluing together ad hoc parts with the only scope to get exponents right. We consider that counter-productive. If a simple, bare model is not satisfactory, one should look for another one, preferably as simple as the first one. That is why we strove to compare "bare" models here. To express our feeling, the models which passed the tests with highest scores were the Genoa market model and the Maslov model, with some (but not too much) evaporation of orders. We must also note that the empirical model of reference [66] reproduces the data for return distribution by far the best accuracy. At the same time, though, it makes use of several empirical inputs, rather than clear microscopic mechanisms, and therefore follows somewhat different modelling philosophy than ours. That is why we leave this model aside, without neglecting its merits and importance.

To sum up, we compared several order-book models of stock-market fluctuations. None of them is fully satisfactory yet. Calculating the return distribution, volatility autocorrelation and the Hurst plot, we were able to identify which of the models are promising candidates for future development. To tell the names, they are the Genoa market model and the Maslov model.

This work was supported by the MŠMT of the Czech Republic, grant no. 1P04OCP10.001, and by the Research Program CTS MSM 0021620845.

References

1. *The Economy as an Evolving Complex System*, edited by P.W. Anderson, K.J. Arrow, D. Pines (Addison Wesley, Reading, 1988)
2. R.N. Mantegna, H.E. Stanley, *Introduction to Econophysics: Correlations and Complexity in Finance* (Cambridge University Press, Cambridge, 1999)
3. J.-P. Bouchaud, M. Potters, *Theory of Financial Risks* (Cambridge University Press, Cambridge, 2000)
4. F. Schweitzer (editor), *Modeling Complexity in Economic and Social Systems* (World Scientific, Singapore, 2002)

5. D. Challet, Y.-C. Zhang, Physica A **246**, 407 (1997)
6. R.N. Mantegna, H.E. Stanley, Nature **376**, 46 (1995)
7. Y. Liu, P. Cizeau, M. Meyer, C.-K. Peng, H.E. Stanley, Physica A **245**, 437 (1997)
8. P. Gopikrishnan, M. Meyer, L.A.N. Amaral, H.E. Stanley, Eur. Phys. J. B **3**, 139 (1998)
9. V. Plerou, P. Gopikrishnan, L.A.N. Amaral, M. Meyer, H.E. Stanley, Phys. Rev. E **60**, 6519 (1999)
10. N. Vandewalle, M. Ausloos, Eur. Phys. J. B **4**, 257 (1998)
11. E. Bacry, J. Delour, J.F. Muzy, Phys. Rev. E **64**, 026103 (2001)
12. Z. Eisler, J. Kertész, Physica A **343**, 603 (2004)
13. R. Liu, T. Di Matteo, T. Lux, e-print `arXiv:0704.1338` (2007)
14. J.-P. Bouchaud, A. Matacz, M. Potters, Phys. Rev. Lett. **87**, 228701 (2001)
15. F. Lillo, S. Mike, J.D. Farmer, Phys. Rev. E **71**, 066122 (2005)
16. B. Biais, P. Hillion, C. Spatt, J. Finance **50**, 1655 (1995)
17. S. Maslov, M. Mills, Physica A **299**, 234 (2001)
18. D. Challet, R. Stinchcombe, Physica A **300**, 285 (2001)
19. D. Challet , R. Stinchcombe, Physica A **324**, 141 (2003)
20. X. Gabaix, P. Gopikrishnan, V. Plerou, H.E. Stanley, Nature **423**, 267 (2003)
21. V. Plerou, P. Gopikrishnan, X. Gabaix, H.E. Stanley, Quant. Finance **4**, C11 (2004)
22. V. Plerou, P. Gopikrishnan, H.E. Stanley, Phys. Rev. E **71**, 046131 (2005)
23. B. Rosenow, Int. J. Mod. Phys. C **13**, 419 (2002)
24. P. Weber, B. Rosenow, Quant. Finance **5**, 357 (2005)
25. P. Weber, B. Rosenow, Quant. Finance **6**, 7 (2006)
26. J.-P. Bouchaud, M. Mézard, M. Potters, Quantitative Finance **2**, 251 (2002)
27. M. Potters, J.-P. Bouchaud, Physica A **324**, 133 (2003)
28. J.-P. Bouchaud, Y. Gefen, M. Potters, M. Wyart, Quant. Finance **4**, 176 (2004)
29. J.-P. Bouchaud, J. Kockelkoren, M. Potters, Quant. Finance **6**, 115 (2006)
30. M. Wyart, J.-P. Bouchaud, J. Kockelkoren, M. Potters, M. Vettorazzo, e-print `physics/0603084` (2006)
31. I. Zovko, J.D. Farmer, Quant. Finance **2**, 387 (2002)
32. F. Lillo, J.D. Farmer, R.N. Mantegna, e-print `cond-mat/0207428`
33. F. Lillo, J.D. Farmer, R.N. Mantegna, Nature **421**, 129 (2003)
34. J.D. Farmer, L. Gillemot, F. Lillo, S. Mike, A. Sen, Quant. Finance **4**, 383 (2004)
35. J.D. Farmer, P. Patelli, I.I. Zovko, Proc. Natl. Acad. Sci. U.S.A. **102**, 2254 (2005)
36. A. Ponzi, F. Lillo, R.N. Mantegna, e-print `physics/0608032` (2006)
37. J.D. Farmer, N. Zamani, Eur. Phys. J. B **55**, 189 (2007)
38. J.D. Farmer, A. Gerig, F. Lillo, S. Mike, Quant. Finance **6**, 107 (2006)
39. F. Lillo, Eur. Phys. J. B **55**, 453 (2007)
40. E. Scalas, T. Kaizoji, M. Kirchler, J. Huber, A. Tedeschi, Physica A **366**, 463 (2006)
41. J.D. Farmer, F. Lillo, Quant. Finance **4**, C7 (2004)
42. Y.-C. Zhang, Physica A **269**, 30 (1999)
43. A.W. Lo, A.C. MacKinlay, J. Zhang, J. Financial Economics **65**, 31 (2002)
44. X. Gabaix, P. Gopikrishnan, V. Plerou, H.E. Stanley, Physica A **324**, 1 (2003)
45. G.J. Stigler, J. Business **37**, 117 (1964)
46. D.K. Gode, S. Sunder, J. Political Economy **101**, 119 (1993)
47. P. Bak, M. Paczuski, M. Shubik, Physica A **246**, 430 (1997)
48. P.L. Krapivsky, Phys. Rev. E **51**, 4774 (1995)
49. G.T. Barkema, M.J. Howard, J.L. Cardy, Phys. Rev. E **53**, 2017 (1996)
50. D. Eliezer, I.I. Kogan, e-print `cond-mat/9808240`
51. L.-H. Tang, G.-S. Tian, Physica A **264**, 543 (1999)
52. M. Raberto, S. Cincitti, S.M. Focardi, M. Marchesi, Physica A **299**, 319 (2001)
53. S. Cincotti, S.M. Focardi, M. Marchesi, M. Raberto, Physica A **324**, 227 (2003)
54. M. Raberto, S. Cincotti, Physica A **355**, 34 (2005)
55. M. Raberto, S. Cincotti, S.M. Focardi, M. Marchesi, Computational Economics **22**, 255 (2003)
56. M. Raberto, S. Cincotti, C. Dose, S.M. Focardi, M. Marchesi, in *Nonlinear Dynamics and Heterogeneous Interacting Agents*, edited by T. Lux, S. Reitz, E. Samanidou 305 (Springer, Berlin, 2005)
57. S. Cincotti, S.M. Focardi, L. Ponta, M. Raberto, E. Scalas, in *The Complex Network of Economic Interactions*, edited by A. Namatame, T. Kaizouji, Y. Aruka, 239 (Springer, Berlin, 2006)
58. R. Cont, J.-P. Bouchaud, Macroeconomic Dynamics **4**, 170 (2000)
59. S. Maslov, Physica A **278**, 571 (2000)
60. F. Slanina, Phys. Rev. E **64**, 0561136 (2001)
61. S. Maslov, private communication
62. E. Smith, J.D. Farmer, L. Gillemot, S. Krishnamurthy, Quant. Finance **3**, 481 (2003)
63. M.G. Daniels, J.D. Farmer, G. Iori, E. Smith, e-print `cond-mat/0112422`
64. M.G. Daniels, J.D. Farmer, L. Gillemot, G. Iori, E. Smith, Phys. Rev. Lett. **90**, 108102 (2003)
65. G. Iori, M.G. Daniels, J.D. Farmer, L. Gillemot, S. Krishnamurthy, E. Smith, Physica A **324**, 146 (2003)
66. S. Mike, J.D. Farmer, J. Economic Dynamics and Control **32**, 200 (2008)
67. D. Challet, R. Stinchcombe, e-print `cond-mat/0208025`
68. R. Stinchcombe, in *Econophysics and Sociophysics: Trends and Perspectives*, edited by B.K. Chakrabarti, A. Chakraborti, A. Chatterjee (Wiley-VCH, Weinheim, 2006) pp. 35–63
69. T. Halpin-Healy, Y.-C. Zhang, Phys. Rep. **254**, 215 (1995)
70. R.D. Willmann, G.M. Schütz, D. Challet, Physica A **316**, 430 (2002)
71. M.F.M. Osborne, Econometrica **33**, 88 (1965)
72. L. Kullmann, J. Kertész, Physica A **299**, 234 (2001)
73. F. Franci, R. Marschinski, L. Matassini, Physica A **294**, 213 (2001)
74. L. Matassini, F. Franci, Physica A **289**, 526 (2001)
75. J.D. Farmer, S. Joshi, J. Economic Behavior and Organization **49**, 149 (2002)
76. D. Challet, e-print `physics/0608013` (2006)
77. L. Muchnik, F. Slanina, S. Solomon, Physica A **330**, 232 (2003)
78. A. Svorenčík, F. Slanina, Eur. Phys. J. B **57**, 453 (2007)
79. E. Scalas, in *The Complex Network of Economic Interactions*, edited by A. Namatame, T. Kaizouji, Y. Aruka (Springer, Berlin, 2006)